Imperial College London
Department of Aeronautics

Miniaturized IoT-based Systems for Structural Integrity and Health Monitoring

Fatih Dagsever

Submitted in part fulfilment of the requirements
for the degree of Doctor of Philosophy at
Department of Aeronautics
Faculty of Engineering
Imperial College London
March 2025



I hereby declare that this thesis and the work reported herein was composed by and originated entirely from me. Information derived from the published and unpublished work of others has been acknowledged in the text and references are given in the list of sources.

Fatih Dagsever (2025)

The copyright of this thesis rests with the author. Unless otherwise indicated, its contents are licensed under a Creative Commons Attribution-Non Commercial-No Derivatives 4.0 International Licence (CC BY-NC-ND).

Under this licence, you may copy and redistribute the material in any medium or format on the condition that; you credit the author, do not use it for commercial purposes and do not distribute modified versions of the work.

When reusing or sharing this work, ensure you make the licence terms clear to others by naming the licence and linking to the licence text.

Please seek permission from the copyright holder for uses of this work that are not included in this licence or permitted under UK Copyright Law.

Abstract

This PhD research presents the design, development, and validation of miniaturized IoT-based Structural Health Monitoring (SHM) systems to improve the reliability and safety of composite structures. Conventional SHM approaches are often constrained by extensive cabling, limited scalability, and bulky data acquisition units, posing significant challenges in weight-sensitive aerospace applications. To overcome these limitations, this work introduces novel miniaturized wireless SHM platforms.

The first proposed system integrates a multi-layer Printed Circuit Board (PCB), a Wireless Sensor Network (WSN), and a Graphical User Interface (GUI), providing real-time data acquisition while significantly reducing wiring complexity through ZigBee-based communication. The second system, a Passive Sensing Node, is designed for impact detection and localization, operating with a coin-cell battery-powered event-triggered comparator. Using Bluetooth Low Energy (LE) and a shared clock for time synchronization, it enables ultra-low-power operation with immediate response to impact events.

Building upon these developments, the third system is a multi-sensor platform that unifies a piezoelectric transducer, a strain gauge, an accelerometer, and an environmental sensor on a compact 3×3 cm flexible PCB. Designed for low-power Bluetooth LE communication, it enables multi-modal data acquisition for comprehensive condition monitoring. Finally, the fourth system integrates active and passive sensing within a single platform, combining an external Analog-to-Digital Converter (ADC) and a Digital-to-Analog Converter (DAC) to facilitate both guided wave-based inspections and spontaneous impact detection. In passive mode, impact-induced signals are captured and transmitted wirelessly, while in active mode, the system successfully generates actuation signals such as tone bursts for structural evaluation.

Collectively, these proposed systems offer a comprehensive solution to on-board SHM, focusing on miniaturization, wireless data transmission, light-weight, and energy efficiency along with a user interface. Experimental tests on composite panels confirm their capability for real-time SHM and highlight their potential to protect the structural integrity of composite structures.

Acknowledgements

This PhD was supported by Republic of Türkiye Ministry of National Education.

I dedicate this thesis to all those who offered their constant support throughout my doctoral journey. To my family, whose belief in my abilities never diminished and whose guidance shaped my ambitions; to my supervisors and colleagues, who shared their expertise and kept me motivated; and to my friends, who reminded me to persevere even in challenging moments. Your collective encouragement and faith in my work made this achievement possible. Thank you for walking beside me in this endeavour.

Contents

Abstract **3**

Acknowledgements **4**

Nomenclature **13**

1 Introduction **15**
1.1 Overview . . . 15
1.2 Problem Statement . . . 18
1.3 Aim and Objectives . . . 19
1.4 Thesis Organization . . . 21

2 Literature Review **23**
2.1 SHM Systems . . . 23
2.2 Sensors Used in SHM . . . 30
2.3 WSNs in SHM . . . 36
2.3.1 IoT, Wireless Systems, and WSN Architecture in SHM . . . 36
2.3.2 Applications, Case Studies, and Challenges in SHM . . . 41

3 SHM System Design Principles and Development Strategies **50**
3.1 System Goals and Design Philosophy . . . 50
3.2 Overview of the Proposed SHM Systems . . . 54
3.3 Design and Development of a ZigBee-based SHM System for Composite Structures 55
3.3.1 Introduction . . . 55
3.3.2 ZigBee-based SHM System Design . . . 57
3.3.3 Conclusions . . . 74

4 Passive Sensing Node **76**
4.1 Introduction . . . 76
4.2 The Proposed System . . . 80
4.2.1 Time Synchronization among Multiple PSNs . . . 83
4.2.2 Low-Power Operation (Sleep Mode & Triggered Wake-Up, Battery-Powered) 85
4.2.3 Wireless Data Transmission . . . 87
4.2.4 Lightweight and Miniaturized Design . . . 89
4.2.5 Processing Capability (Decision-Making, Detection, Localization) . . . 90
4.2.6 GUI for Data Processing . . . 91
4.3 System Implementation . . . 92
4.4 PSN Performance Evaluation . . . 101
4.4.1 Integrated GUI for PSN . . . 102

4.4.2 Acquisition and Digital Conversion of Passive Sensing Signals with GUI-Based Visualization . . . 102
4.4.3 Comparative Validation of PSN Measurements Against Digital Oscilloscope Data . . . 106
4.4.4 Timestamp Acquisition and TDoA Analysis in Impact Testing . . . 108
4.4.5 Power Consumption . . . 108
4.4.6 Range Testing . . . 110
4.5 Impact Localization . . . 111
4.6 Conclusions . . . 119

5 Multi-Sensor SHM System 122
5.1 Introduction . . . 122
5.2 Principle of Multi-Sensor System for SHM . . . 126
5.3 Multi-Sensor SHM System . . . 128
5.3.1 RF MCU . . . 128
5.3.2 Power Management . . . 129
5.3.3 Sensors and DAQ . . . 131
5.3.4 Wireless Communication in MSS . . . 134
5.4 MSS System Implementation . . . 136
5.4.1 Function Modules in MSS . . . 136
5.4.2 Wireless Network Implementation in MSS . . . 138
5.4.3 Experimental Setups for Different SHM applications . . . 141
5.5 Results and System Performance of MSS . . . 148
5.5.1 Application 1: Event-triggered experiment to acquire all types of sensor data . . . 148
5.5.2 Application 2: Real-time continuous strain and acceleration DAQ . . . 148
5.5.3 Application 3: Timestamp experiment for impacts . . . 149
5.5.4 PZT signal acquisition performance . . . 151
5.5.5 Continuous strain and acceleration data acquisition performance . . . 153
5.5.6 Power Consumption . . . 159
5.5.7 Range Testing . . . 160
5.6 Conclusions . . . 161

6 Integrated Active-Passive Sensing System 164
6.1 Introduction . . . 165
6.2 Development of Integrated Active-Passive Sensing System . . . 168
6.2.1 Modes of IAPS System . . . 172
6.2.2 Hardware Design of IAPS System . . . 175
6.3 System Implementation . . . 178
6.4 Experimental Setup and Results . . . 182
6.4.1 Passive Sensing Mode Verification . . . 184
6.4.2 Active Sensing Mode . . . 187
6.5 Conclusions . . . 191

7 Conclusions and Future Work 193
7.1 System Enhancements and Future Research Directions for Advanced Wireless SHM 197
7.1.1 System Enhancements . . . 197
7.1.2 Future Research Directions . . . 198

7.2 List of Publications 200

A Reproducing Permissions **215**

List of Tables

2.1 Comparison of common sensor types Used in SHM 34

3.1 Comparison of the wireless sensor prototypes for WSN-based SHM 56

4.1 Time to generate interrupt event in the different modes of the comparator . . . 86
4.2 The specifications of PSN 93
4.3 Timestamps and TDoA in the event of impact around each sensor 108
4.4 Measured current consumption under different operating conditions 109
4.5 Power consumption under different operating conditions 110
4.6 Effective Communication Range for Different TX Powers and Modulation Schemes 111

5.1 TDoA in the event of impact around each MSS 151
5.2 Characterized current draw across multiple operating states 160
5.3 Power consumption across multiple operating states 160
5.4 Achieved Communication Range under Various TX Power Levels and Modulation Strategies 161

List of Figures

2.1 Sensor examples used in SHM (a) PZT (b) Strain gauge sensor 24
2.2 Main components of an SHM system 27
2.3 Wi-Act, top and bottom sides respectively [34]. Image reproduced with permission of the rights holder, Elsevier Science & Technology Journals [A.1]. 41
2.4 Wi-Pass [35]. © 2019 IEEE 42
2.5 WISAN Coordinator and sensor node [84]. Image reproduced with permission of the rights holder, Sage Publications [A.2] 43
2.6 Fabricated hardware by Sidibe et al. [89]. Creative Commons CC BY 4.0 licence. 44
2.7 Fabricated hardware by Le et al. [59]. Creative Commons CC BY 4.0 licence. . . 45
2.8 Fabricated hardware by Fort et al. [33]. Creative Commons CC BY 4.0 licence. . 46
2.9 Wireless sensor node prototypes: (a) Narada wireless sensing platform [53]. Image reproduced with permission of the rights holder, American Society of Civil Engineers [A.3], (b) WSNG2 Prototype [45]. Image reproduced with permission of the rights holder, Elsevier Science & Technology Journals [A.4], (c) AEPod Prototype [61]. Image reproduced with permission of the rights holder, Springer Nature BV [A.5], (d) Xnode smart sensor [115]. Creative Commons CC BY 4.0 licence., (e) Fabricated hardware by Ando et al. [3]. © 2023 IEEE, (f) AUSAM+ system [91]. Creative Commons CC BY 4.0 licence. 49

3.1 The design of the ZigBee-based SHM system, 4-layer PCB with the dimensions of 60x70 cm, (a) top side and (b) bottom side 60
3.2 Experimental setup to monitor the structural health of the composite panel . . . 63
3.3 Example record of the captured sensing signals from the composite structure . . 64
3.4 Active sensing results processed and visualized by the developed GUI 66
3.5 250 kHz tone-burst signal with 5-cycle 67
3.6 Chirp signal varying from 50 to 350 kHz 68
3.7 ZigBee star-topology network including central (C), router (R) and end device (E) 70
3.8 ZigBee-based SHM data flow 72
3.9 The GUI developed for the ZigBee-based SHM system 74

4.1 Composite panel with PZTs and Passive Sensing Nodes (PSNs) 81
4.2 Passive sensing system with PSNs 82
4.3 Antenna pattern design 89
4.4 Comparison of PSN and £2 coin 93
4.5 The system block diagram of the PSN with their functions 94
4.6 The modules of PSN, (a) Top view (b) Bottom view 94
4.7 The installation of a peripheral PSN to the PZT sensor mounted on the composite panel 95
4.8 CR2032 coin-cell battery (3V, 240 mAh) used to supply power to each PSN . . . 96

4.9 The central PSN connected to the PC with USB-TTL converter 96
4.10 Non-synchronous timers of master (central) and slave (peripheral) devices 97
4.11 Synchronous timers of master (central) and slave (peripheral) devices 98
4.12 Time difference between master (central) and slave (peripheral) devices 99
4.13 Bluetooth LE packet created to wirelessly transmit sensing results 99
4.14 PSNs and the distance between the sensors 101
4.15 The developed GUI for PSN 103
4.16 Wirelessly-Transmitted Passive Sensing Results, (a) PSN 1 (b) PSN 2 (c) PSN 3 (d) PSN 4 104
4.17 All PSN Data 105
4.18 Digital oscilloscope result 107
4.19 PSN result 107
4.20 The comparison of the oscilloscope and PSN data 107
4.21 Impact estimation training setup 112
4.22 Visualization of kNN-based impact localization for different k values 113
4.23 Real-time impact location estimation with the GUI 115
4.24 Visualization of true vs estimated impact locations for different number of neighbours (k) values 116
4.25 Effect of number of neighbours (k) on impact localization error 117
4.26 Error metrics for different number of neighbours (k) values 119

5.1 Conceptual block diagram of the miniaturized MSS for SHM 128
5.2 Output voltage vs strain gauge resistance 131
5.3 PZT signal acquisition stages 132
5.4 Serial communication (SPI) between MCU and sensors with digital output (BMA400 and BME280) 135
5.5 Multi-Sensor SHM system in two-layer flexible PCB, (a) Top view (b) Bottom view 136
5.6 The function modules of Multi-Sensor SHM system 138
5.7 Format of ADC data packet 140
5.8 Format of timestamp data packet 141
5.9 Format of environmental data packet 141
5.10 Format of accelerometer data packet 141
5.11 Multi-Sensor SHM system on a composite panel, (a) PZT sensor (b) MSS integration 142
5.12 Multiple MSSs setup on a composite panel 143
5.13 Comparator events with threshold aspect 144
5.14 Multi-Sensor System GUI 145
5.15 Experimental setup for strain measurement with aluminium specimen 146
5.16 GUI modified for strain measurement 147
5.17 Timestamps and sensor data from four MSSs in the wireless network 149
5.18 PZT signals from four MSSs in the wireless network 150
5.19 Real-time strain data display 151
5.20 Real-time acceleration data display for three axes 152
5.21 Digital oscilloscope measurement of the PZT signal 152
5.22 MSS PZT result 153
5.23 The comparison of the oscilloscope and MSS results 153
5.24 Experimental setup to compare acceleration and strain gauge measurements between the proposed MSS and a DAQ system, top view 154

5.25 Experimental setup to compare acceleration and strain gauge measurements between the proposed MSS and a DAQ system, bottom view . . . 155
5.26 Strain gauge measurement with HBK DAQ system . . . 155
5.27 Strain gauge measurement with the proposed MSS system . . . 156
5.28 Comparison of strain gauge measurement between the proposed MSS and HBK DAQ system . . . 157
5.29 Acceleration measurement with HBK DAQ system . . . 157
5.30 Acceleration measurement with the proposed MSS system . . . 158
5.31 Comparison of acceleration measurement between the proposed MSS and HBK DAQ system . . . 159
5.32 A close-up comparison of acceleration measurement between the proposed MSS and HBK DAQ system . . . 159

6.1 PCB layout of IAPS System . . . 170
6.2 Power management block diagram of IAPS System . . . 171
6.3 Passive Sensing illustration in the composite panel area covered by PZTs . . . 172
6.4 Passive sensing signal data flow . . . 173
6.5 Active Sensing illustration in the composite panel area covered by PZTs . . . 174
6.6 The stages of the actuation signal generation . . . 174
6.7 Active Sensing signal stages . . . 175
6.8 IAPS system prototype in a 4-layer PCB, (a) Top view, and (b) Bottom view. . 179
6.9 4-layer PCB stack-up of the prototyped PCB . . . 180
6.10 The function modules of IAPS system in the top layer . . . 181
6.11 The function modules of IAPS system in the bottom layer . . . 182
6.12 IAPS system experimental setup . . . 183
6.13 Comparison of Impact-induced signals and their attenuated forms in the passive mode of the IAPS system. (a) 2 times attenuation, (b) 3 times attenuation. . . . 185
6.14 Digital oscilloscope result . . . 186
6.15 IAPS system result in the passive sensing mode . . . 186
6.16 The comparison of the oscilloscope and IAPS system results . . . 187
6.17 GUI plot for passive sensing results from 4 channels in the IAPS system . . . 188
6.18 Digital form of the 50 kHz tone-burst signal for the DAC with 12-bit resolution and 500 kHz sampling rate . . . 189
6.19 Oscilloscope measurement of the 50 kHz tone-burst signal from the actuator PZT 189
6.20 Active sensing result captured from a PZT channel . . . 190

A.1 Reproducing permission 1 . . . 216
A.2 Reproducing permission 2 . . . 217
A.3 Reproducing permission 3 . . . 218
A.4 Reproducing permission 4 . . . 219
A.5 Reproducing permission 5 . . . 220

Nomenclature

List of Abbreviations

AC Advisory Circular

ADC Analog-to-Digital Converter

API Application Programming Interface

Bluetooth LE Bluetooth Low Energy

CPS Cyber-Physical System

DAC Digital-to-Analog Converter

DAQ Data Acquisition

DC/DC Direct Current to Direct Current

EMI Electromagnetic Interference

FAA Federal Aviation Administration

GATT Generic Attribute Profile

GPIO General-Purpose Input/Output

GPIOTE GPIO Tasks and Events

GSM Global System for Mobile Communications

GUI Graphical User Interface

IAPS Integrated Active-Passive Sensing

ICs Integrated Circuits

kNN k-Nearest Neighbors

LDO Low-Dropout

Li-Po Lithium-Polymer

MAC Media Access Control

MCU Microcontroller Unit

MEE Mean Euclidean Error

MEMS Micro-Electro-Mechanical Systems

MSS Multi-Sensor System

MTU Maximum Transfer Unit

NDI Non-Destructive Inspection

NUS Nordic UART Service

PCB Printed Circuit Board

PPI Programmable Peripheral Interconnect

PSN Passive Sensing Node

PZT Piezoelectric Transducer

RAPID Reconstruction Algorithm for Probabilistic Inspection of Defects

RC Resistor–Capacitor

RF Radio Frequency

RMSE Root Mean Squared Error

SD Standard Deviation

SHM Structural Health Monitoring

SMDs Surface-Mount Devices

SPI Serial Peripheral Interface

TDoA Time Difference of Arrival

TTL Transistor-Transistor Logic

UART Universal Asynchronous Receiver Transmitter

WISAN Wireless Intelligent Sensor and Actuator Network

WSHMS Wireless Structural Health Monitoring System

WSN Wireless Sensor Network

Chapter 1

Introduction

1.1 Overview

Structural Health Monitoring (SHM) is a promising engineering methodology that integrates state-of-the-art sensor technologies, Data Acquisition (DAQ) systems, and signal processing algorithms to enable continuous and real-time monitoring of structural integrity. SHM represents a paradigm shift from traditional Non-Destructive Inspection (NDI) methods, which are often periodic and risk overlooking early-stage damage. SHM has made it possible to promptly detect potential issues by mitigating the risk of catastrophic failures and extending the service life of critical structures.

The advantages of SHM extend beyond damage detection. It offers cost-effective solutions, enhanced reliability, and long-term monitoring capabilities, making it an attractive alternative for industries that prioritize safety and efficiency. The integration of SHM technologies in this field has not only improved safety standards but also reduced operational costs and extended the life of structural components.

The critical aspect of SHM systems is the effective selection and deployment of sensor technologies deployed to specific monitoring needs. Commonly used sensors include fiber optic sensors, ultrasonic transducers, strain gauges, and Piezoelectric Transducers (PZTs). Each sensor type offers unique advantages:

- **Fiber Optic Sensors (FOS):** Known for their high sensitivity and resistance to Electro-

magnetic Interference (EMI), these sensors are ideal for harsh environments.

- **Ultrasonic Sensors:** Particularly effective in identifying subsurface defects, these sensors rely on high-frequency sound waves.
- **Strain Gauges:** Valued for their simplicity and reliability, these devices provide critical data on stress distribution and deformation.
- **PZTs:** Distinguished by their dual functionality as actuators and sensors, PZTs support both passive and active monitoring. Passive sensing enables real-time detection of dynamic events, such as impacts, while active sensing employs controlled excitation to analyze wave propagation and localize damage.
- **Accelerometers:** Utilized to capture vibrational characteristics and dynamic responses, accelerometers provide valuable insights into the properties of structural integrity and stiffness. Their ability to measure low-frequency motions and detect subtle changes in natural frequencies makes them especially suitable for vibration-based damage detection and assessing overall structural health.

PZTs have gained significance due to their compact size, ease of installation, and versatility. These sensors are crucial for SHM applications requiring energy efficiency and real-time diagnostics, particularly in aerospace structures where weight and space constraints are critical.

SHM systems are extensively implemented in various engineering fields, including buildings, bridges, and aircraft, to monitor structural responses to fatigue, environmental degradation, and unexpected impacts. Early detection and mitigation of damage in these applications are vital for ensuring public safety, reducing maintenance costs, and extending service life. Advanced DAQ systems play a critical role in efficiently collecting and transmitting high-fidelity data, enabling accurate structural health assessments even in remote or inaccessible locations.

Recent developments in SHM have underscored the importance of wireless communication technologies, such as Wireless Sensor Networks (WSNs) and Internet of Things (IoT) systems. These innovations address traditional wired system limitations, including high installation costs and scalability issues. WSNs eliminate extensive cabling and facilitate monitoring through

strategically deployed sensor nodes. Similarly, IoT integration enhances real-time monitoring capabilities, providing centralized data processing and improved scalability for large-scale structures.

The application of SHM in aerospace is particularly transformative due to the unique challenges posed by composite materials and the demanding operational constraints. Lightweight and high-strength composite materials are susceptible to complex damage mechanisms such as delamination and fiber breakage. SHM systems equipped with advanced sensors and algorithms enable early detection of such issues, ensuring operational safety and reducing maintenance costs.

Wireless SHM systems used in aerospace often incorporate miniaturized and energy-efficient hardware to meet weight and space limitations. Methods such as Time Difference of Arrival (TDoA) and synchronized wireless networks further enhance the diagnostic accuracy of these systems. Furthermore, protocols like Bluetooth LE and ZigBee support lightweight and energy-efficient communication, making them suitable for on-board applications.

Despite significant advancements, SHM systems face challenges related to scalability, energy efficiency, and data management. Wireless systems must address synchronization issues and ensure reliable multi-node DAQ for complex structures. Moreover, the miniaturization and cost-effectiveness of SHM hardware remains critical for widespread implementation, especially in weight-sensitive aerospace environments.

Future research should focus on integrating advanced sensing technologies with robust data processing to enhance diagnostic precision. Energy-efficient communication protocols and innovative hardware designs will be crucial in overcoming existing limitations and offering practical, scalable, and high-performing SHM solutions. The potential of SHM highlights its growing importance in modern engineering and underscores the need for continued innovation, especially in the aeronautics field.

1.2 Problem Statement

The capability of SHM systems to detect possible problems has motivated significant research, especially in fields such as aerospace, where operational safety, cost-effectiveness, and long-term reliability are crucial. However, despite considerable advances in SHM technologies, several limitations inhibit their practical application, particularly in aerospace environments.

Current SHM methodologies often rely on bulky and energy-intensive wired DAQ systems. These systems, while effective under controlled laboratory conditions, are poorly suited for deployment in real-world aerospace applications where weight, space, and energy efficiency are critical constraints. In addition, the high installation costs, complex cable management, and scalability challenges associated with wired systems make them impractical for large-scale or remote structures such as aircraft. Consequently, there is a need for miniaturized, lightweight, and energy-efficient SHM solutions that can operate reliably in real-world conditions.

WSNs have been proposed as a suitable alternative to traditional wired systems, offering advantages such as reduced weight, simplified installation, and enhanced scalability. However, their implementation introduces several challenges, including the requirement for precise time synchronization among sensor nodes, the need for low-power operation to ensure extended service life, and the demand for robust wireless communication to ensure reliable data transmission. Furthermore, the lack of a commercial solution that fully addresses SHM implementation in aerospace structures requires a specialized approach. For each specific use case, the WSNs must be carefully designed and adapted to the unique operational and environmental conditions of the structure, followed by strict manufacturing and testing to validate their reliability and functionality throughout the service.

Recent advances in IoT technologies have further expanded the potential of SHM systems by enabling real-time condition monitoring through extensive sensor networks. However, many existing IoT-enabled SHM systems often rely on simple peer-to-peer communication between only two nodes (central and peripheral), which is inadequate for the complex monitoring requirements of large aerospace structures. Moreover, the limited miniaturization and integration of SHM systems with lightweight wireless communication technologies, such as Bluetooth LE and ZigBee,

restrict their applicability in weight-sensitive aerospace environments. The use of Bluetooth LE and ZigBee in SHM is feasible particularly in scalable and secure multi-node network configurations.

To address these limitations, there is a critical need for the development of innovative SHM systems used in aerospace applications. Such systems must integrate miniaturized and multifunctional hardware designs, establish robust wireless communication protocols, and implement energy-efficient DAQ units capable of operating under real-world conditions. In addition, these systems must prioritize affordability and ease of implementation to facilitate widespread implementation. Using advances in IoT, WSNs, and low-power wireless communication technologies, it is possible to design SHM solutions that overcome current limitations and meet the requirements of the aerospace sector.

This research aims to address these challenges by proposing novel SHM solutions incorporating miniaturized hardware, energy-efficient wireless networks, and precise time synchronization mechanisms. These advances will enable real-time monitoring and impact detection in composite structures, improving safety, operational efficiency, and maintenance practices in the aerospace industry.

1.3 Aim and Objectives

The aim of this PhD research is to develop smart and miniaturized electronic systems, along with wireless communication, to advance the field of SHM. The focus is on overcoming challenges related to weight, power consumption, wireless communication, and system integration, with the ultimate goal of creating a comprehensive and efficient SHM solution suitable for real-world applications. This includes the development of both active and passive SHM systems, incorporating miniaturized DAQ units with wireless communication modules, computational software, and user-friendly graphical interfaces. In addition, the objectives of the study and how this PhD research has contributed to the progress beyond the state-of-the-art for each objective are listed below:

- **Enhanced Wireless Communication:** Developed a modular wireless network compris-

ing multiple interconnected nodes to facilitate robust and efficient data exchange in SHM systems, easily upscaled to large and complex structures.

- **Miniaturization:** Designed and tested low-cost miniaturized SHM systems suitable for compact and weight-sensitive environments, particularly in aerospace settings, to expand the applicability of SHM solutions.
- **Low Power Consumption:** Designed and implemented energy-efficient SHM systems to address sustainability challenges and extend operational capabilities for longer periods, especially in resource-constrained settings.
- **Time Synchronization for Accurate Impact Localization:** Implemented precise time synchronization mechanisms across distributed wireless sensor nodes to enable accurate calculation of the TDoA for damage localization.
- **Simplified Implementation:** Developed SHM systems that are easy to deploy, requiring fewer resources such as cables, enabling widespread implementation and use.
- **Extended Application to On-Board Scenarios:** Adapted existing WSN-based SHM techniques for on-board applications, particularly in aeronautical environments, meeting low-weight and functionality requirements under real-world service conditions.
- **User-Friendly Interfaces:** Developed user-friendly graphical interfaces for SHM systems to facilitate user interaction, data visualization, and processing.
- **Comprehensive SHM Solution:** Integrated miniaturized DAQ units integrated with wireless communication modules, computational software, and user-friendly interfaces to create a comprehensive and efficient SHM solution suitable for real-world applications.

By systematically addressing the defined objectives, this research has advanced SHM from an early development stage to a set of tested, practical IoT-based systems including both active and passive sensing strategies. Multiple sensor types, such as PZTs, strain gauges, accelerometers, and environmental sensors, were utilized, prototyped, and integrated into lightweight miniaturized platforms. These distributed wireless sensor networks, when implemented in composite structures,

have demonstrated reliable real-time DAQ, continuous monitoring capabilities, and minimal added mass. Furthermore, this research included the development of a dedicated Graphical User Interface (GUI), which receives incoming data, executes processing procedures, generates visual representations, and stores relevant information. Consequently, these accomplishments confirm the feasibility of fully integrated SHM methods for composite aerostructures.

1.4 Thesis Organization

This thesis is presented in several chapters, each addressing a key element of miniaturized, efficient, and wireless SHM in composite aerostructures.

Chapter 1 establishes the motivation for advanced SHM systems, highlighting the shortcomings of traditional wired DAQ approaches and emphasizing the need for lightweight, scalable, and real-time condition assessment in modern composite aerostructures. The chapter concludes by detailing the main research problem, along with the aim and objectives of this work.

Chapter 2 surveys the scope of SHM methodologies, from established NDI to emerging WSN solutions. The chapter discusses various sensor types, such as PZTs, fiber optic sensors, strain gauges, accelerometers, and examines both active and passive sensing strategies. Attention is paid to low-power communication protocols and the role of IoT. The review ends with the identification of knowledge gaps, which is followed by the subsequent system designs in this thesis.

Chapter 3 begins by outlining the essential system goals for compact, wireless, and low-power monitoring in composite aerostructures, highlighting critical needs such as miniaturized PCB design and real-time data handling. It then details a design philosophy focused on multi-functional hardware, event-triggered architectures, user-friendly GUIs, and robust wireless networks. This is followed by brief overviews of four proposed systems in this PhD research. Furthermore, this chapter includes the design and development of a ZigBee-based SHM system for composite structures.

Chapter 4 focuses on impact detection and localization with the proposed system called Passive Sensing Node. Its architecture employs an event-triggered comparator, Bluetooth LE

transmission, and a shared clock for time synchronization in WSN to detect and localize sudden impacts on composite structures.

Chapter 5 extends the scope of SHM by presenting a Multi-Sensor System (MSS) on a flexible, compact PCB that combines a Piezoelectric Transducer (PZT), strain gauge, accelerometer, and environmental sensor. By measuring various parameters in real time, it provides comprehensive information on structural condition and ambient influences.

Chapter 6 covers the concept of active and passive sensing combined on a single, multi-channel platform. The external Analog-to-Digital Converter (ADC) and the Digital-to-Analog Converter (DAC) enable actuation signal generation (for guided wave–based inspections) and DAQ.

Chapter 7 concludes the main findings, emphasizing how the proposed platforms address the crucial demands of composite structure monitoring from multi-modal sensors and low-energy event-triggered acquisition to integrated active–passive sensing. In addition, potential future work and directions are highlighted, such as a unified system architecture to establish an ecosystem that accommodates all developed systems and the incorporation of energy-harvesting approaches for extended service life. These advances would enrich and simplify future SHM deployments in aeronautical engineering.

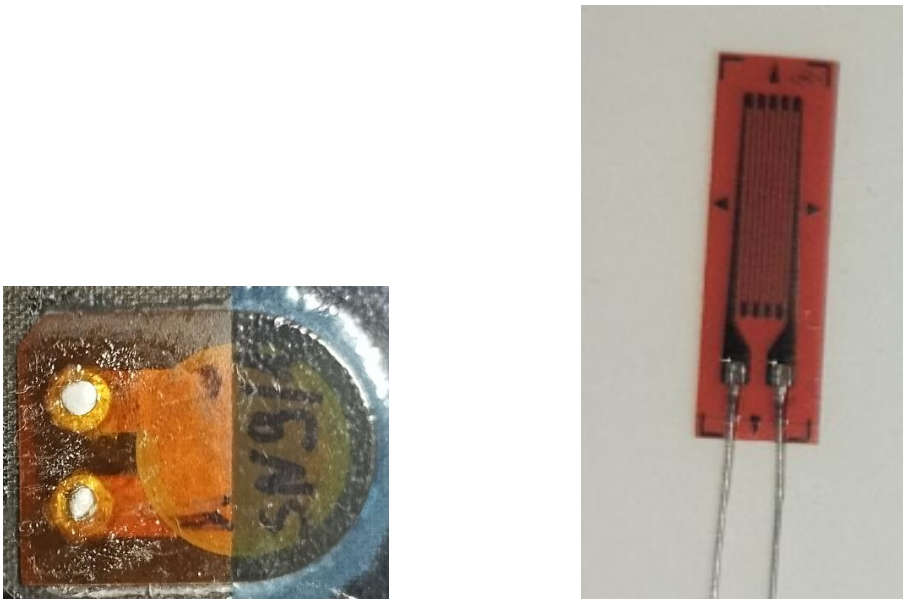
Chapter 2

Literature Review

2.1 SHM Systems

SHM represents a highly promising methodology that incorporates a range of advanced technologies, including sensors, DAQ systems, and signal processing algorithms, to enable continuous monitoring and evaluation of the integrity of various structures [5, 63]. By providing real-time insights into structural conditions, SHM offers a significant advantage over traditional NDI techniques, which are typically employed during scheduled maintenance and repair cycles of critical infrastructures. These traditional methods often rely on periodic checks and may miss early-stage damage, whereas SHM systems are capable of identifying potential problems promptly, thereby reducing the risk of catastrophic failures. This advantage has driven an extensive research interest in SHM, as supported by a number of studies and publications exploring various aspects of its application and development [14, 23, 51, 77, 92, 97].

In addition to its damage detection capabilities, SHM also offers significant benefits such as improved reliability and the ability to provide long-term monitoring solutions. These advantages make it an attractive option for industries seeking to optimize structural maintenance and safety protocols. In particular, SHM has been widely adopted in the aerospace sector, where it is applied to monitor aircraft structures composed of composite materials, which are prone to unique damage mechanisms that require sophisticated monitoring techniques [85, 86]. The integration of SHM into critical applications not only improves safety, but also contributes to



(a) (b)

Figure 2.1: Sensor examples used in SHM (a) PZT (b) Strain gauge sensor

reduced operational costs and extended structural lifespans, underscoring its growing importance in modern engineering practice.

Given the diverse conditions and challenges faced by different structures, the selection of appropriate sensor technologies becomes a key determinant of the effectiveness of the SHM system. Various damage detection methods with a wide range of sensor technologies, such as fiber optic sensors, ultrasonic transducers, strain gauges, and PZTs, are essential for SHM systems [1, 8, 35, 82, 105, 108]. Each sensor type brings unique advantages and characteristics to the monitoring process, enabling the detection and assessment of damage in diverse structural applications. For example, fiber optic sensors offer high sensitivity and immunity to EMI, making them suitable for monitoring in challenging environments, while ultrasonic sensors are highly effective in capturing subsurface defects through high-frequency sound waves. Strain gauges, known for their simplicity and reliability, measure deformations in structures under load, providing valuable information on stress distribution and potential areas of failure. As an example, a PZT and a strain gauge are demonstrated in Fig. 2.1a and Fig. 2.1b, respectively.

Among these technologies, PZTs have gained particular importance because of their versatility, ease of installation, compact size, and dual functionality as actuators and sensors. These transducers can be used in two modes: passive and active. In passive sensing, PZTs function

as receivers, capturing external impacts or vibrations to assess structural responses without directly altering the system. This approach is particularly useful for detecting sudden impacts, such as those caused by collisions or falling debris. In contrast, active sensing involves the PZTs performing dual roles, where they actively excite the structure with controlled input signals and subsequently measure the structural responses to these excitations. This method provides more detailed diagnostic capabilities by enabling analysis of wave propagation characteristics and localized damage within the monitored structure [45, 95, 114]. The ability of PZTs to operate effectively in both passive and active modes enhances their applicability to a broad spectrum of SHM tasks, from real-time impact detection to detailed damage localization. This flexibility, combined with their lightweight and low-power requirements, has made PZTs an essential component in the advancement of SHM technologies, particularly for applications requiring compact and efficient monitoring systems.

The frequency regions associated with detecting local and global structural changes in SHM are distinct due to the nature of the physical changes measured. Global structural changes are captured mainly in the low-frequency range, typically involving the natural frequencies of the structure. These frequencies are sensitive to widespread changes in mass or stiffness but often miss small or localized damage [44, 87]. Local damage is more effectively detected at higher frequencies, particularly in the kilohertz range. Methods like EMI or guided waves operating in this range can detect small cracks and local delaminations [43, 87].

SHM methods are extensively implemented in various engineering applications, including buildings, bridges, and other critical infrastructure, to improve safety and prevent catastrophic failures. These structures are exposed to many harmful influences throughout their service life, including fatigue caused by repetitive loading, corrosion resulting from environmental exposure, and unexpected damage caused by external impacts or natural disasters. Over time, such conditions compromise the structural integrity and reliability of these systems, posing risks to public safety and increasing maintenance costs. Therefore, early detection and monitoring of damage in these structures is critical to extend their service life, improve operational safety, and optimize maintenance schedules [1, 16, 35, 95, 105, 114].

For effective SHM implementation, the use of energy-efficient and reliable DAQ units is

critical. These systems are playing an important role for SHM by collecting, processing, and transmitting data from sensors installed on the structure. Energy efficiency is particularly crucial in remote or inaccessible locations, such as tall buildings, long-span bridges, or airborne systems, where frequent maintenance or battery replacements are impractical. Furthermore, the reliability of DAQ units ensures the consistent capture of high-fidelity data, which is necessary to accurately diagnose structural health and detect even slight signs of damage. Commercial DAQs are designed to integrate various types of sensors and record multiple sensor outputs with high resolution and minimum noise and interference. Hence, they enable real-time monitoring of different structural parameters such as strain, vibration, temperature, and acoustic emissions under a large variation of load scenarios. Consequently, these systems are bulky and expensive [1, 16, 35, 95, 105, 114].

SHM systems have shown significant potential to detect and identify damage in composite structures under controlled laboratory conditions. These environments allow for precise testing of SHM technologies, ensuring their ability to identify structural defects such as cracks and delaminations. However, the true value of SHM systems lies in their deployment on-board operational platforms such as aircraft, where real-time monitoring can enhance safety and maintenance efficiency. To achieve this, SHM systems must meet strict weight requirements and operate reliably in service conditions such as fluctuating temperatures, vibrations, and environmental exposure. Most DAQ systems for SHM have recently been designed for ground-based testing in controlled environments. While essential for validating SHM technologies, these systems are often too bulky and energy-intensive for on-board use. Miniaturized DAQ systems, capable of operating in real-world conditions, have been successfully tested on aircraft structures with only a few examples. These developments highlight the challenges and opportunities to advance SHM technologies for practical in-service applications [16]. The progression of miniaturized and reliable SHM systems is critical to realizing their full potential in aerospace and beyond, enabling safer and more efficient monitoring of composite structures in real-time.

The SHM process involves multiple stages, as shown in Fig. 2.2 to ensure the effective detection and localization of damage within critical structures, ultimately preventing catastrophic failures. SHM systems mainly rely on sensor-equipped DAQ units to collect real-time information

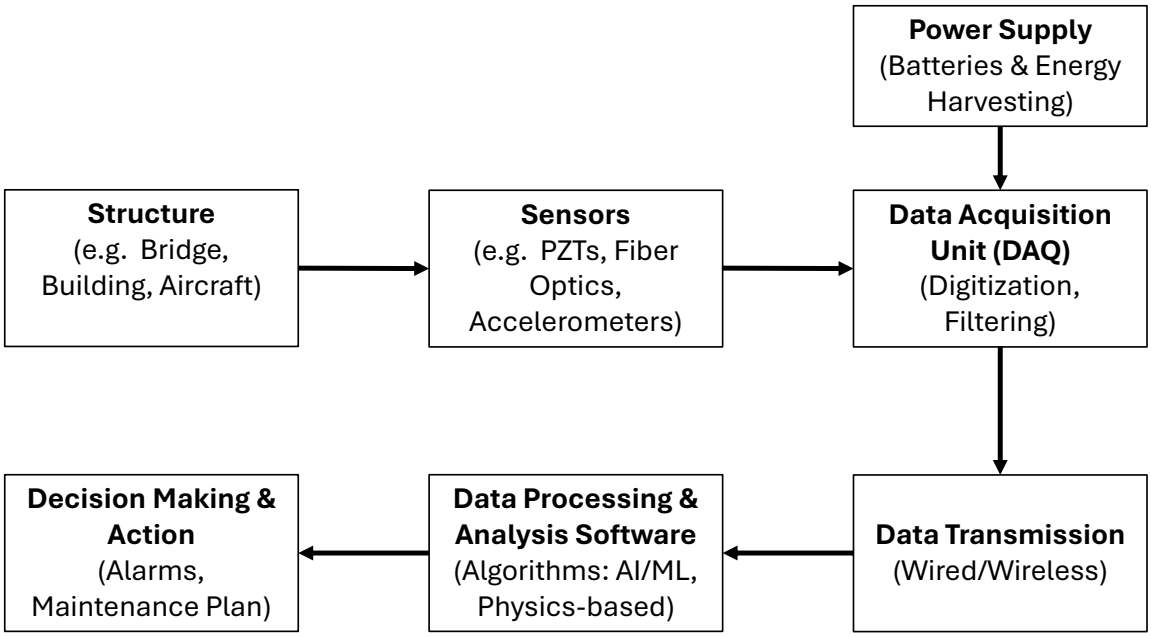


Figure 2.2: Main components of an SHM system

about structural condition. These sensors, which may include PZTs, fiber optics, strain gauges, and ultrasonic devices, capture various physical parameters such as strain, vibration, temperature, and acoustic emissions. The data collected are then processed using advanced algorithms to analyze structural responses, identify anomalies, and pinpoint damage locations with high precision. This systematic approach allows for timely maintenance interventions, extending the useful life of critical infrastructure and improving the safety of critical infrastructure [40].

Recent advances in IoT technology have further revolutionized SHM, introducing new possibilities for DAQ and monitoring. IoT enables the creation of extensive WSNs that facilitate proper data transfer and remote monitoring capabilities. By integrating IoT with SHM systems, real-time condition monitoring can be conducted more efficiently and cost-effectively. These networks eliminate the need for extensive cabling, reducing installation complexity, and enabling monitoring in previously inaccessible or remote locations. In addition, IoT allows for centralized data processing, where information from distributed sensors is acquired and analyzed in central stations such as PCs, providing comprehensive insights into structural health [74, 97].

The application of IoT in industrial SHM contexts is particularly noteworthy. SHM systems enabled with IoT ensure the continuous monitoring of machinery and structural components.

This integration not only improves operational efficiency by minimizing downtime, but also reduces maintenance costs by enabling predictive maintenance strategies. Similarly, in civil engineering, IoT facilitates the remote monitoring of large-scale structures such as bridges, dams, and pipelines, where traditional SHM approaches may be impractical. By deploying IoT, SHM systems can deliver improved scalability and accessibility, marking a significant advancement in condition monitoring practices [74,97]. These developments underline the transformative impact of IoT on SHM, highlighting its potential to enhance safety, reliability, and cost-effectiveness in the monitoring of critical structures.

Recent advances in the literature indicate that many of the limitations associated with SHM systems relying on wired DAQ systems can be effectively addressed through the implementation of WSNs [15, 68]. Traditional wired systems often face challenges such as high installation costs, complex cable management, and limited scalability, especially for large-scale or remote structures. In contrast, WSNs eliminate the need for extensive wiring, significantly reducing the complexity of installation and maintenance while enhancing the flexibility and adaptability of SHM systems. In these wireless practices, sensor nodes are strategically deployed throughout the structure to monitor critical parameters such as vibration, strain, and temperature. The collected data are then transmitted wirelessly to a central processing unit, where advanced algorithms analyze signals for damage detection, localization, and assessment [15, 68].

The literature reports on the successful application of WSNs in monitoring various civil engineering structures, such as buildings, bridges, and dams [1, 5, 105]. These implementations highlight the capability of WSNs to enable real-time monitoring and timely actions, thereby improving the safety and longevity of critical infrastructure. Beyond civil engineering, wireless SHM systems have also been developed for composite structures, which are widely-used in the aerospace industry. In this context, WSNs play a vital role in overcoming the challenges associated with monitoring lightweight and highly stressed composite materials, ensuring the early detection of issues such as delamination, cracks, or fiber breakage. Such systems are commonly termed Cyber-Physical System (CPS), in which the physical component involves the sensing process using PZTs or other sensors mounted to composite structures, while the cyber component focuses on the wireless transmission of sensor data for further analysis [34, 35].

Further research into the design, optimization, and application of WSNs for SHM continues to expand this field, with studies exploring advancements in sensor technologies, energy efficiency, and data processing algorithms. Comprehensive discussions and insights into these developments are provided in studies focused on wireless SHM, including those addressing civil and aerospace applications [5, 92].

Although IoT-enabled SHM systems offer promising opportunities for scalability and cost-effectiveness, their implementation also introduces several challenges related to data management, synchronization, and system miniaturization. Current SHM systems face significant limitations that obstruct their efficiency and practical application, particularly in aerospace applications. Many existing systems rely on a simple peer-to-peer wireless communication model with only two nodes, rather than an extensive network, making it difficult to scale for large structural components such as aircraft. To fully monitor such structures, multiple sensing nodes are required. Another critical challenge is the physical size of these systems, as a lack of miniaturization limits their integration into weight-sensitive and compact aerospace environments. Furthermore, wireless networks involving multiple remote sensors require a shared clock for precise time synchronization to capture accurate sensing data. Low power consumption is another essential factor to ensure sustainability and extended operational capabilities. Overcoming these limitations is crucial for the advancement of SHM technologies, enabling the development of efficient, miniaturized, and high-performing systems that can meet real-world demands.

Although existing SHM techniques have proven to be effective in controlled laboratory environments, cost-effective and easily implementable solutions are still needed for practical, real-world applications. This PhD study has proposed innovative approaches involving miniaturized and multifunctional hardware designs as a solution. RF microcontrollers are used to address these gaps by establishing wireless networks that eliminate the need for cable connections. This not only reduces system weight but also enhances portability, making these solutions more suitable for on-board aerospace applications. A critical feature of some developed systems is the implementation of a shared clock for time synchronization within the wireless network. For example, the shared clock implementation allows for the precise capture of timestamps alongside sensor data in the event of an impact, enabling accurate calculation of the TDoA for passive

sensing signals across sensor nodes.

The proposed solutions also prioritize affordability, making them suitable for widespread implementation. By optimizing power consumption, these systems achieve improved energy efficiency, extending their operational life and reliability. For wireless data transmission, one of the two most common wireless communication protocols is implemented based on projects, which are ZigBee and Bluetooth LE. The integration of Bluetooth LE technology ensures compatibility with smartphones, providing user-friendly control and monitoring capabilities. In addition, these projects offer a comprehensive methodological framework, detailing clear implementation processes that enhance the practicality of these approaches. With these advances, the proposed systems have great potential to improve the on-board monitoring of the structural health of composite structures by addressing current limitations.

2.2 Sensors Used in SHM

Sensors are critical components of SHM, enabling the assessment, detection, and evaluation of structural conditions to ensure integrity and safety. Their ability to capture real-time data on strain, temperature, vibration, and displacement is fundamental to identifying damage and guiding maintenance strategies. This section reviews various sensor technologies applied in SHM, focusing on their operating principles, applications, and advancements based on the selected literature. PZTs and fiber optic sensors are commonly used in SHM applications.

PZT transducers have proven instrumental in detecting structural damage through high-frequency techniques, including Lamb wave propagation and impedance measurements. These sensors are used in generating and receiving ultrasonic guided waves, making them ideal for monitoring defects such as cracks, delaminations, and corrosion. For example, PZT sensors embedded in distributed networks were used in an aircraft wing panel, implementing ultrasonic guided waves for defect detection and growth monitoring despite challenges caused by rivet rows and paint-induced attenuation. The efficiency of the sensors was further enhanced by employing the Reconstruction Algorithm for Probabilistic Inspection of Defects (RAPID) algorithm, which provided accurate defect localization and size estimation through correlation-based data

processing [113]. Experimental studies validated their effectiveness, demonstrating their ability to detect and map defect growth in both simulated crack and corrosion scenarios.

The operational stability of PZT transducers is heavily influenced by their bonding integrity to the structure. Bonding defects can alter the impedance spectrum and wave characteristics, potentially leading to diagnostic errors. Techniques such as self-diagnostic monitoring have been developed to ensure sensor reliability, distinguishing sensor failure from structural damage [78]. These advances underscore the importance of robust sensor diagnostics in maintaining the reliability of SHM systems.

PZTs have become a cornerstone technology in the field of SHM due to their a number of advantages, including ease of installation, lightweight design, and structural compactness. These characteristics make PZTs highly adaptable for integration into a wide variety of monitoring systems, particularly in applications where minimizing weight and preserving the structural integrity of the monitored structure are critical. Their versatility and cost-effectiveness have contributed to their widespread implementation in various industries, including civil engineering, aerospace, and mechanical systems [73].

One of the primary methods for employing PZTs in SHM is passive sensing. In this approach, PZTs serve solely as receivers, detecting and capturing external impacts or vibrational responses from the structure. This passive method is particularly useful for monitoring dynamic events, such as impacts, collisions, or sudden load changes, as it allows the PZT sensors to capture the natural response of the structure. Passive sensing requires minimal energy consumption and is well-suited for scenarios where external excitation of the structure is not feasible or desirable. For instance, in aerospace applications, passive sensing can be used to detect bird strikes or debris impacts on aircraft fuselages during flight [73].

In addition to passive sensing, active sensing is another widely employed method for damage detection using PZTs. Unlike passive sensing, active sensing involves the dual functionality of PZTs as both actuators and receivers. In this approach, PZTs actively excite the structure by generating high-frequency signals, such as guided Lamb waves, which propagate through the material. These waves interact with any defects or damage, such as cracks, delaminations, and the PZTs subsequently measure the reflected or transmitted wave responses. This method

enables the precise localization and characterization of damage within the structure [47, 93].

Active sensing is particularly advantageous for detecting internal and subsurface damage, which might be difficult to detect in traditional inspection methods or passive sensing alone. For example, in composite materials used in aerospace applications, active sensing can effectively detect delamination or matrix cracking by analysing the characteristics of wave propagation. Moreover, controlling the excitation signal enables customization of wave frequency and amplitude to improve the detection sensitivity for particular damage types. This flexibility makes active sensing a powerful tool for comprehensive structural diagnostics [47].

Both passive and active sensing methods provide complementary capabilities, making PZTs highly versatile for SHM applications. Passive sensing is good at energy efficiency and monitoring dynamic external events, while active sensing offers deeper diagnostic insights and greater precision in damage detection and localization. Integrating both methods into a single SHM system can provide a robust and comprehensive monitoring solution capable of addressing a wide range of structural health issues.

PZTs play a crucial role in SHM due to their adaptability and effectiveness in both passive and active sensing modes. These methods, supported by advances in signal processing and data analysis, continue to enhance the ability of SHM systems to provide accurate, reliable, and real-time structural integrity assessments in critical applications.

Beyond PZTs, FOS is another widely-used sensor technology in SHM applications, offering a lightweight design, high sensitivity, resistance to EMI, and durability in harsh environments such as bridges and pipelines [21, 75]. FOS can also provide spatial resolution to detect localized damage in large structures, which complements the role of PZT transducers. More details on FOS can be found in [7, 64].

In addition to PZTs and FOS, other sensors are also used in the SHM field to provide additional information about the structure and its environmental condition. These sensors are strain gauges, accelerometers, and environmental sensors that measure such as ambient temperature, pressure, and humidity [14].

Strain gauges are widely used in SHM for measuring strain in structural elements, providing essential data for assessing structural performance. Electrical resistance strain gauges are partic-

ularly valued for their high sensitivity and ability to capture dynamic strain variations. However, their low zero-stability often results in drift over time, necessitating frequent recalibration to maintain accuracy. In contrast, vibrating wire strain gauges offer superior long-term stability, making them ideal for quasi-static measurements in applications such as dams or bridges where consistent monitoring over extended periods is critical. Despite their stability, vibrating wire gauges are less effective for dynamic monitoring due to their design limitations [56].

Accelerometers play a crucial role in SHM by capturing the dynamic responses of structures, including vibrations, modal properties, and acceleration levels. These sensors are essential for assessing structural integrity, particularly in scenarios involving dynamic loads, environmental influences, or operational stresses. Accelerometers are highly valued for their ability to provide precise measurements that form the basis for vibration-based damage detection and modal analysis, which are critical for evaluating the health of large and complex structures. A notable example of their application is a bridge monitoring system, where Micro-Electro-Mechanical Systems (MEMS) accelerometers were deployed to measure a wide range of structural responses. These included high-intensity vibrations caused by extreme events, such as strong winds or earthquakes, as well as low-amplitude ambient vibrations resulting from normal operational loads. The versatility of MEMS accelerometers made them ideal for this application, as they could capture both high-frequency and low-frequency responses with a high degree of precision [54].

Temperature sensors are a critical component in SHM systems due to the significant impact that environmental conditions, particularly temperature fluctuations, can have on structural performance and the accuracy of monitoring data. Variations in temperature can cause thermal expansion or contraction in materials, which may be misinterpreted as structural damage if not adequately considered. By incorporating temperature sensors, SHM systems can compensate for these effects, ensuring more reliable and accurate measurements.

These sensors are often integrated with other monitoring technologies to provide a comprehensive understanding of structural behaviour under varying environmental conditions. For example, in the SHM system installed on the Golden Gate Bridge, temperature sensors were deployed alongside MEMS accelerometers. This integration ensured that temperature-induced variations in material properties or sensor output did not compromise the accuracy of vibration

measurements. The data from the temperature sensors allowed for environmental compensation during structural analysis, allowing the monitoring system to distinguish between changes caused by environmental effects and those indicative of potential damage [54].

The comparison of common sensor types used in SHM is demonstrated in Table 2.1 along with their advantages and disadvantages.

Table 2.1: Comparison of common sensor types Used in SHM

Sensor Type	**Advantages**	**Disadvantages**
PZT (Piezoelectric Transducers)	• Suitable for both active and passive sensing modes • Lightweight and compact • Capable of high-frequency ultrasonic wave generation and reception • Effective for internal damage (e.g., delaminations, cracks) • Cost-effective and easy to integrate	• Performance depends on proper bonding to structure • Susceptible to bonding defects, leading to false diagnostics • May require external excitation in active mode

Sensor Type	Advantages	Disadvantages
Fiber Optic Sensors (FOS)	• Resistant to electromagnetic interference (EMI) • Lightweight and flexible • High sensitivity • Suitable for long-distance or distributed sensing • Resistant to harsh environments (e.g., pipelines, bridges)	• Higher initial cost • Requires specialized interrogation equipment • Installation can be complex and fragile under certain mechanical conditions
Strain Gauges	• High sensitivity to strain changes • Widely available and cost-effective • Suitable for dynamic and static strain measurements • Vibrating wire types offer long-term stability	• Require frequent calibration • Vibrating wire types are unsuitable for dynamic loading • Limited resistance to EMI

Sensor Type	Advantages	Disadvantages
Accelerometers	• Capture dynamic structural responses (vibration, acceleration) • Suitable for modal analysis and vibration-based damage detection • Wide frequency range	• Sensitive to environmental noise • Accuracy can be influenced by temperature or drift • Limited in detecting static or slowly changing structural parameters
Environmental Sensors (e.g., Temperature)	• Critical for compensating environmental effects on structural response • Improve accuracy of other sensor outputs (e.g., strain, vibration) • Essential for long-term SHM reliability	• Do not directly measure structural damage • Must be used in conjunction with other sensors • Sensor drift or lag may affect real-time compensation

2.3 WSNs in SHM

2.3.1 IoT, Wireless Systems, and WSN Architecture in SHM

The advancements in the field of the IoT have significantly expanded the capabilities of wireless communication, enabling the formation of extensive networks of interconnected "things" that

can properly transfer data and facilitate intelligent remote actions. These IoT-enabled systems rely on data generated by sensors that monitor ambient conditions such as temperature, vibration, strain, and acoustic emissions [40]. By processing these real-time data, IoT systems enable improved decision-making processes and automated responses, creating opportunities for increased efficiency and reliability in various applications.

This transformative technology has gained considerable attention in the field of SHM, where it provides reliable, cost-effective, and continuous condition monitoring. The integration of IoT reduces the dependency on manual inspections and periodic checks by enabling the real-time assessment of structural integrity. Such systems contribute to operational efficiency by reducing maintenance effort and optimizing maintenance schedules, ensuring that resources are allocated effectively while enhancing the safety and longevity of critical infrastructure [74].

Beyond general condition monitoring, IoT has also proven highly effective in damage detection applications, where its capabilities are used to detect, localize, and evaluate structural damage at an early stage. Through the deployment of advanced sensing networks, IoT systems can capture critical data on structural responses under dynamic loads or environmental stressors, enabling the precise diagnosis of damage such as cracks, delamination, or corrosion. This early detection not only improves the service conditions of the structure by proactively addressing potential failures, but also significantly reduces maintenance costs [97].

IoT represents a critical innovation in the field of SHM, providing enhanced reliability, scalability, and cost-effectiveness for damage detection and condition monitoring applications. Its ability to detect damage at an early-stage, improve structural service conditions, and reduce maintenance costs demonstrates its significant potential in modern infrastructure management [40, 74, 97].

SHM hardware equipped with wireless systems offers significant advantages over traditional wired DAQ techniques. Wireless systems address many limitations of wired approaches, such as the complexity of installation and scalability issues. These systems are highly scalable, making them ideal for large-scale structures such as passenger aircraft and long-span bridges, where extensive cabling would be impractical. In addition, its installation is simpler and less labour-intensive compared to wired systems, offering greater flexibility and cost-efficiency [55, 67].

WSNs are a particularly promising component of SHM systems. These networks consist of distributed sensor nodes that wirelessly collect and transmit data, enabling comprehensive structural monitoring. WSNs improve system robustness and energy efficiency while reducing the dependency on centralized processing. This makes WSNs an effective solution for real-time damage detection and long-term monitoring applications. As an example in the aerospace field, lightweight wireless systems meet strict weight constraints and enable real-time monitoring of critical components by improving safety and reducing maintenance costs [1].

A detailed review of existing wireless SHM technologies and their applications can be found in Abdulkarem et al. [1], which highlights the potential of WSNs to transform SHM practices by improving efficiency, reliability, and scalability in various industries.

Recent advances in the field of SHM suggest that many of the challenges associated with traditional wired DAQ systems can be effectively addressed through the implementation of WSNs [15, 68]. Unlike wired systems, which require extensive cabling and complex installations, WSNs offer a flexible approach by deploying wireless sensor nodes throughout the structure. These nodes are designed to monitor critical structural health parameters, such as vibration, strain, and temperature, allowing for real-time assessment of structural integrity.

In this wireless-based approach, the sensor nodes gather critical data during the monitoring process, which is then transmitted wirelessly to a central station. This central hub serves as the repository for collected data, where it performs processing and evaluation to detect, localize, and quantify damage. Eliminating physical cabling not only simplifies installation, but also enhances the scalability of the system, allowing it to be implemented in large or complex structures. Furthermore, the wireless architecture supports monitoring in remote or inaccessible locations, making it an attractive option for a wide range of applications [15, 68].

Although SHM systems employing WSNs have been widely implemented in civil engineering applications, such as the monitoring of bridges, buildings, and dams, there has also been growing interest in their use for aerospace structures. In the aerospace industry, composite materials are increasingly used due to their lightweight and high-strength properties, but these materials also have unique damage mechanisms, such as delamination and matrix cracking. Wireless SHM systems are particularly suited to monitor such composite structures, providing real-time

information on their condition and enabling early detection of damage [34, 35].

These wireless SHM systems are often categorized as CPSs, which integrate physical sensing capabilities with wireless communication technologies. The "physical" component of CPS in this context involves the sensing process, typically carried out by a DAQ unit equipped with PZTs or other sensors mounted directly onto the composite structure. These sensors are responsible for capturing structural responses under dynamic loads or external impacts. In contrast, the "cyber" component refers to the wireless transmission of collected sensor data to a central processing unit for analysis and decision-making. This integration of physical and cyber elements enables efficient and accurate monitoring of critical structures, reducing the reliance on manual inspections and periodic maintenance.

WSNs are playing a critical role in the advancement of SHM techniques, addressing many of the limitations associated with traditional wired systems [1, 55, 67]. These wireless systems offer significant advantages, including scalability for large-scale structures and simplified installation processes. Eliminating extensive cable reduces both the complexity and cost of implementation, making WSNs an attractive option to monitor various structures such as buildings, bridges, and aircraft [55, 67]. This flexibility has allowed WSNs to emerge as a critical technology in the field of SHM.

One of the primary benefits of WSNs is their scalability, which enables the monitoring of large or complex structures by deploying several sensor nodes in critical areas. These nodes communicate wirelessly, allowing data to be collected from distributed points and transmitted to a central station for processing and analysis. This architecture ensures that WSNs can provide comprehensive coverage of structural health, even in challenging environments or remote locations where wired systems would be impractical. Furthermore, the decentralized nature of WSNs improves the robustness of the system, since failures in individual nodes can be compensated for by re-routing data through alternative paths within the network [67].

Despite the numerous advantages offered by IoT, WSN architectures, their integration into engineering applications, particularly in SHM, presents several technical challenges. A primary limitation is the energy constraint inherent to battery-powered nodes, which necessitates trade-offs between performance and power consumption, especially for real-time or high-resolution

sensing. Wireless communication further introduces reliability concerns, as signal attenuation, interference, and latency variability can compromise data transmission integrity. Maintaining accurate time synchronization across distributed sensor nodes is also technically demanding but essential for time-based localization techniques such as TDoA. In addition, these systems increased network complexity as the number of nodes increases. Despite long-term benefits, the cost of custom wireless modules, synchronization solutions, and power-efficient designs can be significant, causing a higher initial setup cost. Finally, wireless and electronic performance may degrade under extreme environmental conditions due to the effects of temperature and humidity.

Researchers are increasingly focusing on algorithms and signal processing methods to optimize the performance of WSN-based SHM systems. These efforts aim to enable real-time data analysis, facilitating early detection of impacts or structural damage, and supporting proactive maintenance strategies. For example, advanced algorithms are designed to analyze wave propagation characteristics, strain signals, and vibration patterns to detect anomalies with high precision. Signal processing techniques such as time-frequency decomposition, machine learning models, and damage index calculations are being integrated to enhance the diagnostic capabilities of WSNs [58, 114].

In addition to real-time detection, researchers are also exploring solutions to optimize the deployment and operation of WSNs. Sensor placement strategies are being developed to maximize coverage while minimizing the number of sensors required, ensuring cost-effectiveness. Data fusion techniques are used to combine information from multiple sensor nodes, improving the reliability and accuracy of damage assessments. In addition, energy-efficient communication protocols are being prioritized to extend the operational life of sensor nodes, particularly in scenarios where battery replacement or frequent maintenance is not feasible. Low-power hardware designs and energy harvesting technologies are also being investigated to enhance sustainability and reduce the environmental footprint of WSNs [1].

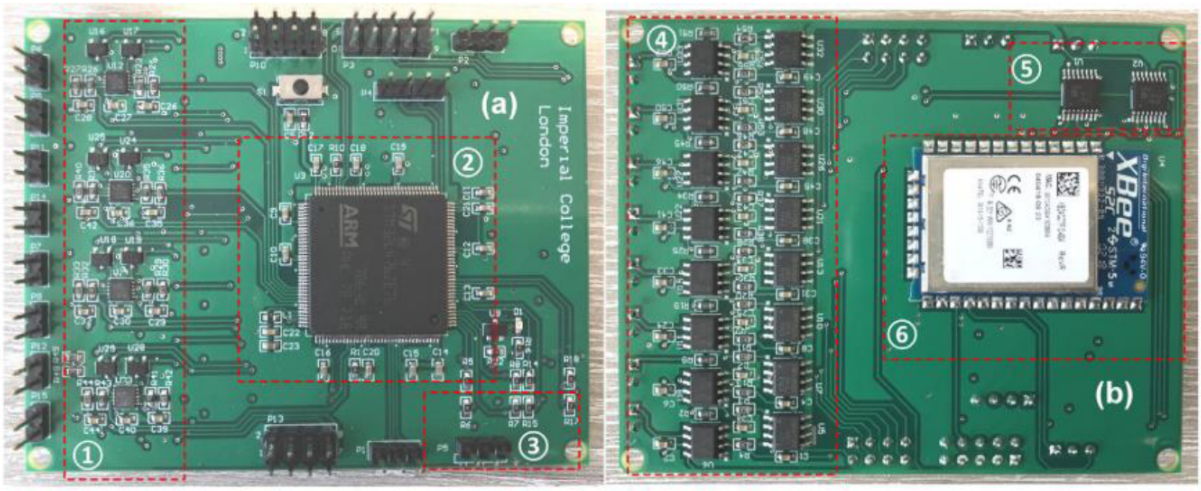


Figure 2.3: Wi-Act, top and bottom sides respectively [34]. Image reproduced with permission of the rights holder, Elsevier Science & Technology Journals [A.1].

2.3.2 Applications, Case Studies, and Challenges in SHM

Several studies have contributed to the enhancement of WSN-based SHM prototypes, demonstrating the potential of these systems for real-world applications. Fu et al. [34] proposed an energy-efficient CPS designed specifically to monitor the structural health of aircraft on-board. This system utilizes a WSN with strategically distributed PZTs to detect damage in aircraft. The approach ensures a comprehensive coverage of critical structural components while maintaining energy efficiency to suit aerospace applications. The hardware prototype developed in their study is shown in Fig. 2.3.

Building on this work, the same research group developed another system known as the Wireless Structural Health Monitoring System (WSHMS). This system was specifically designed to identify impacts on composite airframes, emphasizing low-power consumption and high responsiveness to enable continuous monitoring without compromising battery life or performance. By addressing the unique challenges associated with composite materials, such as delamination and micro-cracks, the WSHMS provides a robust solution for the aerospace sector [35]. The hardware prototype developed in their study is shown in Fig. 2.4.

In these two studies [34, 35], the ZigBee wireless communication protocol was implemented to enable efficient data exchange during sensing operations. The low power requirements

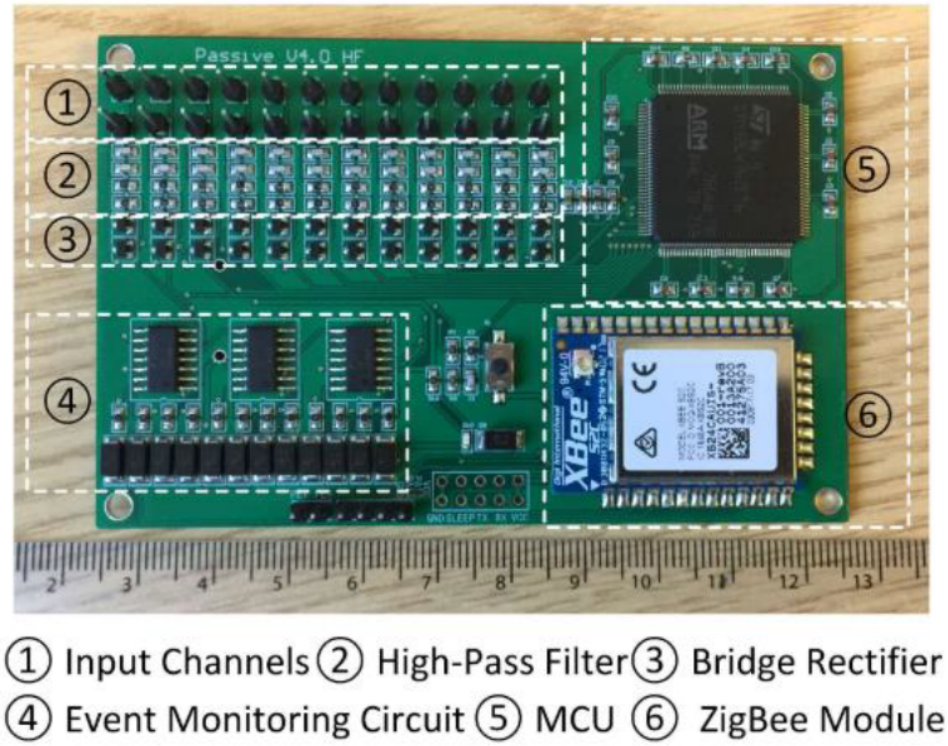


Figure 2.4: Wi-Pass [35]. © 2019 IEEE

and reliable short-range communication of ZigBee make it well-suited for SHM applications, particularly in scenarios where energy efficiency is critical.

Swartz et al. [95] advanced the functionality of an existing wireless sensing unit by improving its measurement accuracy and optimizing it for in-network data processing. To enable efficient wireless communication, they integrated Chipcon CC2420, a single-chip IEEE 802.15.4-compliant radio, making the system suitable for use in civil infrastructure applications such as bridges and buildings. This integration ensured reliable data transmission and contributed to the development of energy-efficient and scalable SHM systems.

Harms et al. [41] introduced a WSN-based on the SmartBrick device, a low-power solution developed for SHM applications. SmartBrick serves as the base station, coordinating with sensor nodes to measure key structural parameters such as vibration and strain. The system uses ZigBee for short-range communication between sensor nodes, while Global System for Mobile Communications (GSM) facilitates long-range communication and remote control capabilities. This dual-communication architecture enables autonomous operation and supports the monitoring of larger structures, including multi-span bridges, by deploying multiple interconnected

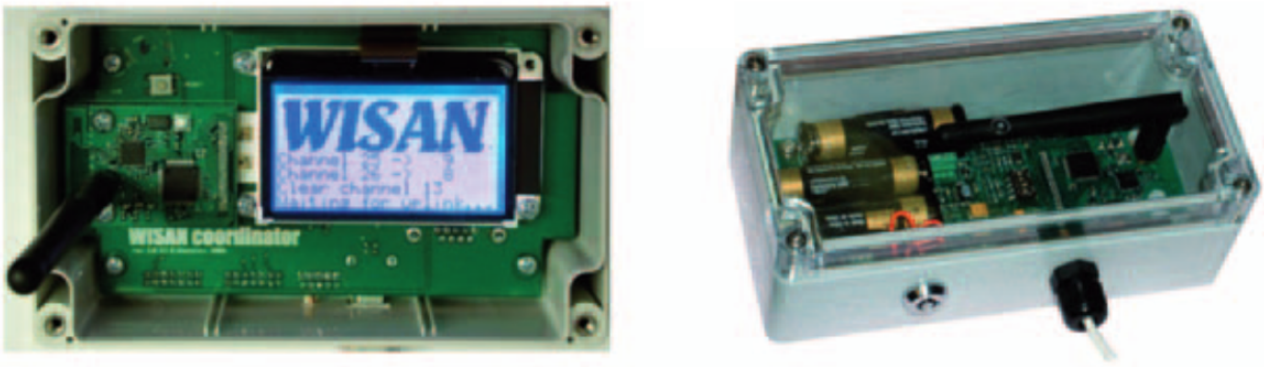


Figure 2.5: WISAN Coordinator and sensor node [84]. Image reproduced with permission of the rights holder, Sage Publications [A.2]

devices. The primary focus of this system is to minimize power consumption, ensure long-term sustainability, and reduce the need for frequent maintenance.

Sazonov et al. [84] proposed a Wireless Intelligent Sensor and Actuator Network (WISAN) specifically designed for scalable SHM applications. The system addresses a critical challenge in structural monitoring by achieving synchronous DAQ across multiple distributed sensors. This capability is particularly important for vibration-based SHM, where accurate time synchronization is essential for effective analysis. By enabling synchronous operations, WISAN provides a robust solution for applications requiring precise structural health diagnostics, further advancing the state of wireless SHM technologies. The hardware prototype developed in their study is shown in Fig. 2.5.

In addition to these notable developments, other research efforts have further explored the potential of WSN-based SHM systems. These include investigations into energy-efficient designs, advanced sensing technologies, and robust DAQ frameworks to enhance the performance and reliability of SHM systems in diverse applications. Notable contributions can be found in studies that focus on areas such as environmental adaptability, algorithmic optimization, and cost-effective sensor deployment strategies [5, 45, 61, 70, 92, 104, 107, 115].

Despite its significant advantages, such as ultra-low power consumption and compatibility with smartphones, the utilization of Bluetooth LE in SHM remains relatively unexplored. Bluetooth LE offers a promising solution for wireless data transmission. However, existing studies reveal limitations in their current implementations for SHM.

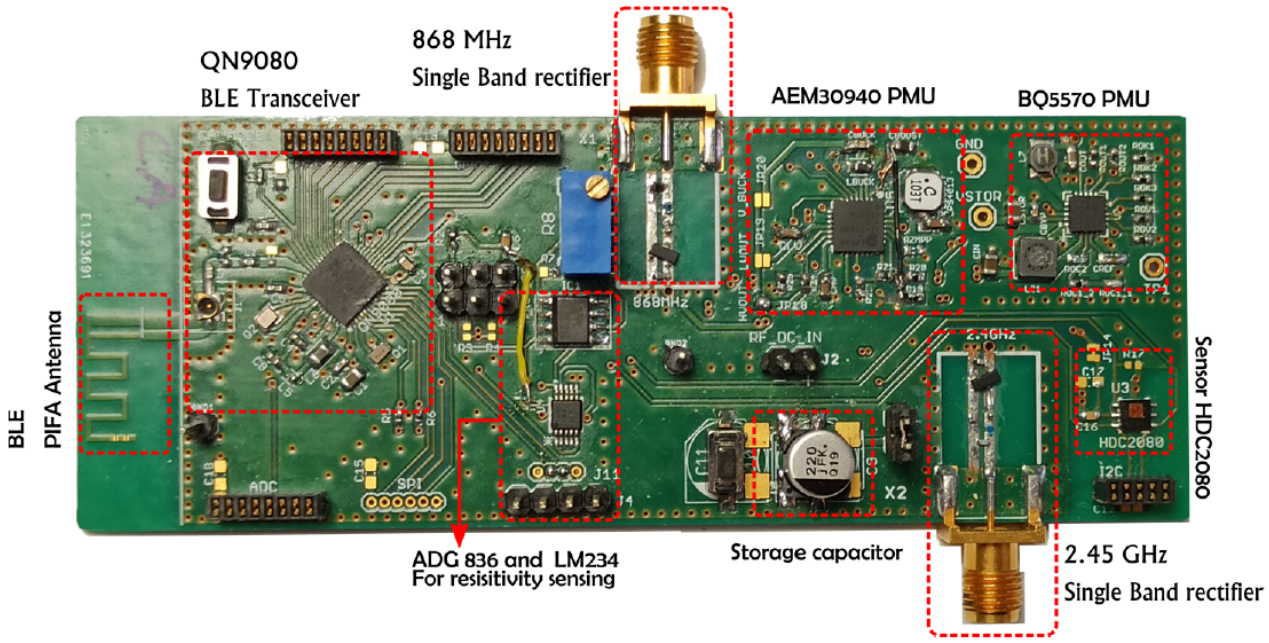


Figure 2.6: Fabricated hardware by Sidibe et al. [89]. Creative Commons CC BY 4.0 licence.

Sidibe et al. [89] introduced a battery-free wireless sensing node designed to monitor critical parameters in reinforced concrete, such as temperature, humidity, and resistivity. The hardware prototype developed in their study is shown in Fig. 2.6. The system used Bluetooth LE for wireless data transmission but operated solely in broadcasting mode. In this mode, data are transmitted without encryption or authentication, limiting its security and suitability for sensitive applications. Furthermore, the broadcasting mode allows for only minimal data payloads, restricting the ability of the system to handle larger datasets effectively. Similarly, Loubet et al. [65] developed a battery-free wireless sensing node utilizing Bluetooth LE for monitoring reinforced concrete, highlighting its energy efficiency but also operating in broadcasting mode, which shares the same constraints.

Expanding on these concepts, Sinha et al. [90] proposed an innovative framework combining WSNs with fog computing, utilizing Bluetooth LE for data transmission. The framework also integrated 5G network features to reduce power consumption and enhance data processing capabilities. A sensor algorithm was introduced to maximize the service life of the WSN. However, while the framework demonstrated improved power efficiency, integration of a complete DAQ system for SHM was not addressed.

Le et al. [59] presented another notable application of Bluetooth LE by integrating it into a

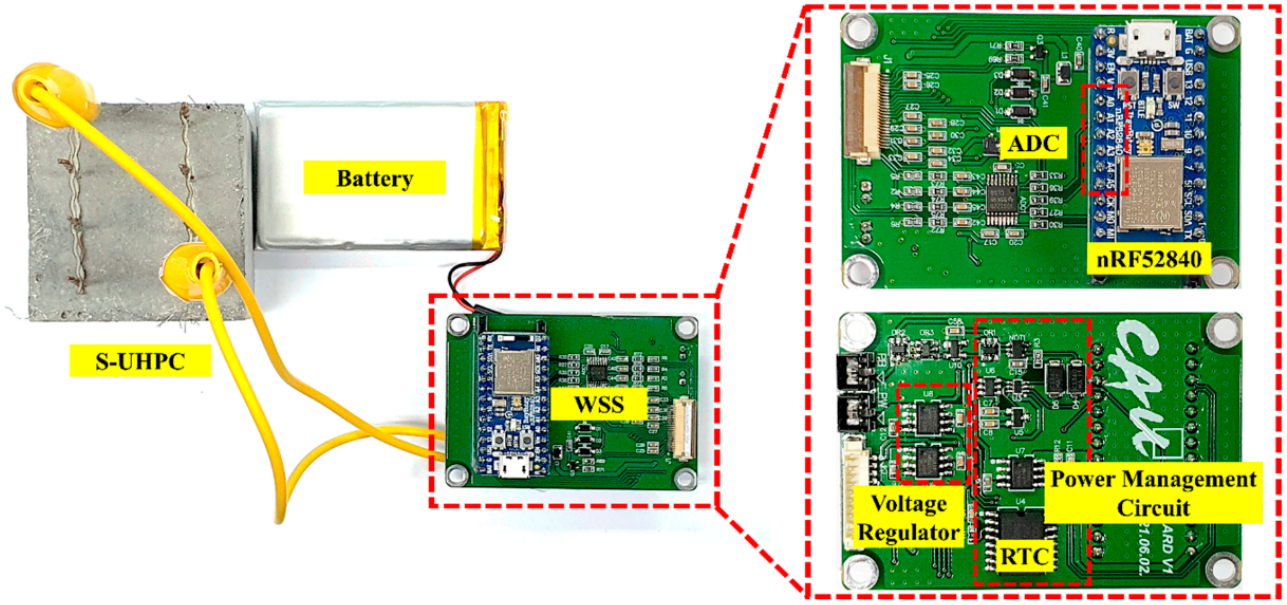


Figure 2.7: Fabricated hardware by Le et al. [59]. Creative Commons CC BY 4.0 licence.

wireless sensor system embedded within smart ultra-high performance concrete. This system was able to detect and wirelessly transmit real-time stress and impact data. Bluetooth LE beacons were used for data transmission, but the system, like others, relied on broadcasting mode, which limited its security and capacity for handling substantial data volumes. The hardware prototype developed in their study is shown in Fig. 2.7. Similarly, Fort et al. [33] developed an IoT sensor node utilizing Bluetooth LE for monitoring artworks and large wooden structures, particularly in museums and church environments. While the system was customized for specific applications, it also utilized broadcasting mode for data transmission, making it less suitable for large-scale SHM applications that require robust and secure data handling. The hardware prototype developed in their study is shown in Fig. 2.8.

Other existing wireless sensor node prototypes are presented in Fig. 2.9.

A key limitation of these studies is their broadcasting mode for data transmission. Although broadcasting is energy efficient and suitable for simple applications, it lacks encryption, authentication, and sufficient payload capacity, making it unsuitable for large-scale and secure SHM systems. Furthermore, the proposed systems predominantly support peer-to-peer communication, limiting their ability to collect sensing data simultaneously from multiple nodes. This lack of a practical WSN approach for SHM inhibits the efficient acquisition and analysis of

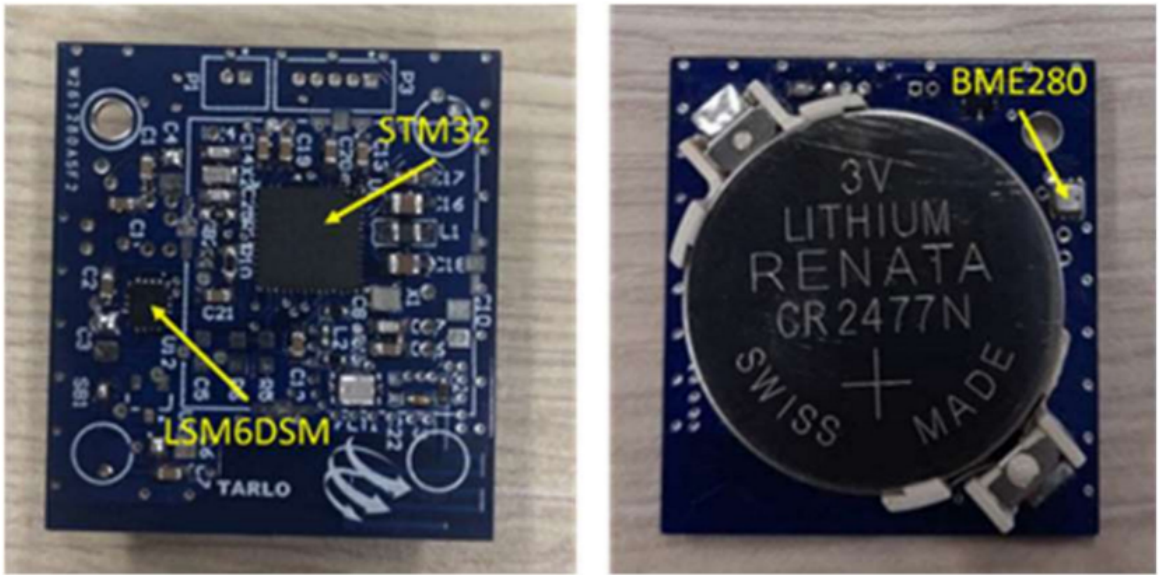


Figure 2.8: Fabricated hardware by Fort et al. [33]. Creative Commons CC BY 4.0 licence.

data in real-time, which is critical for monitoring large or complex structures. Future research must focus on addressing these gaps by developing secure, scalable, and multi-node compatible Bluetooth LE systems developed specifically for SHM applications.

Further studies in the field of WSNs for SHM emphasize key attributes such as system responsiveness, robustness, and energy efficiency, which are critical for ensuring reliable and sustainable monitoring solutions [74]. These advances have significantly contributed to the evolution of WSN-based SHM methodologies, allowing them to be adapted to a wide range of structural applications, including bridges, buildings, aircraft, and industrial facilities.

Despite the extensive exploration of ZigBee as a communication protocol in SHM systems, the potential of Bluetooth LE technology has not been fully realized in this domain. Bluetooth LE offers several notable advantages over traditional protocols, particularly its ultra-low power consumption and inherent compatibility with widely available consumer devices, such as smartphones and tablets. These features make Bluetooth LE an attractive option for enabling real-time data access and user-friendly interfaces in SHM applications. However, studies exploring the practical application of Bluetooth LE for SHM remain relatively limited, and most efforts focus on small-scale prototypes or specific use cases rather than comprehensive and scalable implementations [33, 59, 89, 90].

One of the key advantages of Bluetooth LE lies in its ability to operate with minimal

energy requirements, enabling the development of wireless sensing systems capable of extended operational lifespans. This is particularly beneficial for SHM applications in remote or hard-to-access locations, where frequent battery replacements are impractical. Moreover, its compatibility with smartphones allows for easy integration of monitoring systems into existing practices, enhancing accessibility for users, and reducing the need for specialized equipment. However, despite these advantages, the application of Bluetooth LE in SHM faces challenges related to its limited data transmission capacity and security features, particularly when using the broadcast mode [59, 89].

In addition, Bluetooth LE-based SHM systems currently lack the scalability and robustness required for large-scale structural monitoring. While ZigBee has been extensively used to create multi-node networks capable of aggregating data from numerous sensors, Bluetooth LE systems predominantly support peer-to-peer communication or simple broadcasting, limiting their ability to manage complex sensing operations effectively. This constraint has inhibited the widespread implementation of Bluetooth LE in SHM applications where synchronized data collection and centralized processing from multiple sensor nodes are essential [90].

Despite these limitations, recent studies have demonstrated the potential of Bluetooth LE for SHM when coupled with innovative approaches. For example, researchers have proposed combining Bluetooth LE with advanced algorithms and complementary technologies such as fog computing and 5G networks to address its shortcomings in scalability and data management. Such integrations aim to further reduce power consumption while improving the capacity for real-time data processing and secure communication [90].

Although several studies have been recently conducted on monitoring structures using the WSN-based SHM technologies discussed above, the majority of these systems have been developed for civil engineering applications, including the monitoring of bridges, railways, and buildings. In contrast, aircraft components are particularly constructed from advanced composite materials.

The challenges associated with composite materials are particularly significant in the context of WSN-based SHM systems. Unlike traditional materials, composites exhibit anisotropic behaviour, which means that their mechanical properties vary depending on the direction of

applied stress. This anisotropy, combined with the layered structure of the composites, makes damage detection and localization more challenging. For example, delamination, a common damage mode in composites, occurs between layers and is often invisible to surface inspections.

In addition, aircraft applications have strict constraints on weight, size, and energy consumption, which must also be addressed in system design. Unlike civil engineering structures, where power sources and space are often more readily available, aircraft SHM systems must operate with minimal weight and within limited physical allowances to maintain fuel efficiency and aerodynamic performance. Wireless communication protocols, such as ZigBee or Bluetooth LE, must be optimized for energy efficiency and low latency to ensure reliable data transmission without adding significant weight or complexity to the system.

In summary, while WSN-based SHM technologies have made significant advances in civil engineering, their application to aerospace structures, particularly those involving composite materials, presents distinct challenges. Addressing the requirements of aircraft systems is essential for developing effective and reliable SHM solutions for the aerospace industry. This requires a multidisciplinary approach that combines hardware design, advanced sensing technologies, and energy-efficient wireless communication to meet the specific needs of this critical application domain. This study introduces innovative miniaturized systems that incorporate wireless communication, eliminating the need for physical wiring, and significantly improving practicality for aerospace applications compared to similar existing prototypes [3, 33, 35, 45, 53, 59, 61, 84, 89, 91, 115] in the literature. For example, the PSN introduced in this study is the same size as £2 and weighs 3.7 grams. Another system called MSS is built on a very thin flexible PCB (thickness of 0.1 mm), and the weight of an MSS is only 0.5 grams. These proposed systems are smaller and lighter than their counterparts. Another key difference in this study is the custom GUI developed for data processing such as collection, visualization, decision-making, and saving.

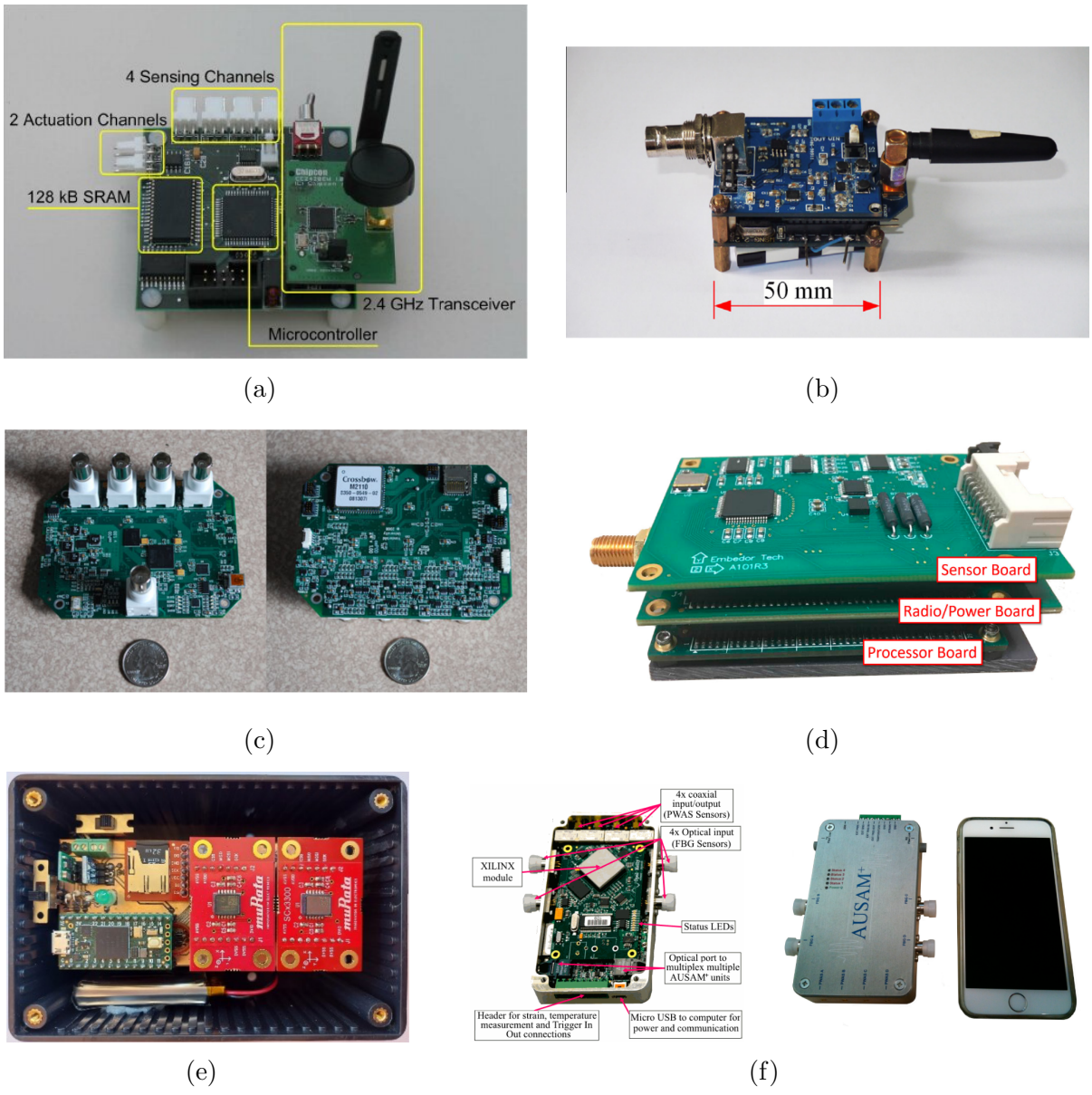


Figure 2.9: Wireless sensor node prototypes: (a) Narada wireless sensing platform [53]. Image reproduced with permission of the rights holder, American Society of Civil Engineers [A.3], (b) WSNG2 Prototype [45]. Image reproduced with permission of the rights holder, Elsevier Science & Technology Journals [A.4], (c) AEPod Prototype [61]. Image reproduced with permission of the rights holder, Springer Nature BV [A.5], (d) Xnode smart sensor [115]. Creative Commons CC BY 4.0 licence., (e) Fabricated hardware by Ando et al. [3]. © 2023 IEEE, (f) AUSAM+ system [91]. Creative Commons CC BY 4.0 licence.

Chapter 3

SHM System Design Principles and Development Strategies

This chapter outlines the design principles and development strategies that are considered for all SHM developments in this PhD study. To address the miniaturized and energy-efficient requirements of in-service SHM, several CPS solutions are developed for specific SHM functionality. Tailoring the functionality of the system to dedicated tasks (e.g. passive only) will allow flexibility in the design to reach the minimum weight and power targets.

The proposed SHM systems represent a convergence of advanced engineering and practical innovation, with the aim of delivering a solution for in-service health monitoring. By addressing critical challenges such as scalability, energy efficiency, and real-time monitoring, these systems pave the way for the broader adoption of SHM technologies in aerospace and other industries. The integration of machine learning further underscores the potential of systems to evolve into intelligent monitoring platforms, ensuring long-term structural integrity and safety.

The following section outlines the specific CPS design objectives as well as design principles.

3.1 System Goals and Design Philosophy

The main goal of the proposed SHM systems is to develop compact, wireless, and energy-efficient solutions specifically designed for composite structures. The proposed systems aim to address

the current limitations in SHM by integrating advanced sensing, DAQ, wireless communication, and machine learning technologies. Through this approach, the proposed systems ensure early detection and localization of structural impacts while remaining lightweight, cost-effective, and easy to implement in real-world settings.

The SHM systems proposed in this PhD study aim to accomplish the objectives listed below, addressing the essential requirements associated with aerospace applications:

- **Impact Detection and Localization:**
  - Enabling the precise detection and localization of structural damage, including impact events, by implementing passive sensing methods with PZTs and advanced signal processing techniques.
  - Integrating a shared clock into the wireless network to capture the timestamp of the impact event on composite panels.
- **Miniaturization and Integration:**
  - Developing compact PCBs with integrated functionalities such as sensing, amplification, DAQ, and wireless communication. Miniaturized systems ensure compatibility with weight-sensitive aerospace environments.
- **Energy Efficiency:**
  - Optimizing power consumption by implementing low-power components, event-triggered sensing mechanisms, and sleep modes. The systems are designed to operate for extended periods using batteries.
- **Wireless Communication:**
  - Replacing traditional wired connections with WSNs using protocols such as Bluetooth LE and ZigBee to improve scalability, portability, and simplicity of installation.
- **Real-Time Monitoring and User Interaction:**

  - Enabling real-time DAQ, transmission, and visualization through GUIs. The systems ensure a proper integration with user-friendly platforms for data analysis and decision-making.

- **Machine Learning Integration:**

  - Using machine learning techniques, such as k-Nearest Neighbors (kNN), to improve the accuracy and reliability of impact localization by training models on high-resolution timestamp and signal data.

To achieve the above-mentioned objectives successfully, the design philosophy of the proposed SHM systems is based on the principles of modularity, scalability, and interdisciplinary integration, which are expanded below:

- **Multi-Functional Hardware Design:**

  - Hardware components are developed to maximize functionality while minimizing size and weight. For example, a Passive Sensing Node (PSN) integrates a microcontroller with wireless communication capability, ADCs, and comparators into a compact architecture.

- **Event-Triggered Sensing:**

  - The systems adopt event-triggered architectures, activating DAQ only when critical thresholds are exceeded. This minimizes false alarms and conserves power by focusing on significant impact events.

- **Software-Driven Flexibility:**

  - The development of GUIs in Python provides flexibility for data visualization, processing, and storage. This software-centric approach eliminates dependencies on proprietary tools such as LabView, promoting extensibility and accessibility.

- **Scalability and Modularity:**

  - The systems are designed to scale across multiple sensor nodes, allowing modular deployment in large composite structures. Each node functions independently, but integrates seamlessly within a centralized wireless network.

- **Compliance with Aerospace Standards:**

  - The design complies with aerospace-specific requirements, including lightweight construction, robust operation, and minimal interference with existing aircraft systems.

Given the emphasis on wireless communication for eliminating cabling and enabling modular sensor deployment, regulatory compliance becomes a crucial factor in integrating the proposed systems into aerospace environments. Wireless data transmission in aircraft structures must comply with strict aviation regulations to ensure safe operation without interference with critical avionics. In addition, power management strategies, particularly the use of lithium batteries, require careful consideration to comply with aviation safety guidelines.

The systems proposed in this PhD study are powered by coin-cell or rechargeable lithium-ion/polymer batteries, designed for long-term operation with minimal energy consumption. While lithium batteries are widely used in wireless sensing applications, their use in aviation environments is subject to regulatory approval. The Federal Aviation Administration (FAA) provides guidance on electronic systems in aircraft through regulations such as the Advisory Circular (AC) 20-184. FAA AC 20-184 provides specific guidelines for the safe use of lithium batteries in aircraft systems, ensuring that they do not pose a risk of fire or explosion during operation [29].

Wireless transmission in aircraft structures must comply with strict aviation regulations to ensure that EMI does not affect critical avionics. The FAA enforces strict regulations on the use of electronic devices, ensuring that wireless transmissions do not interfere with avionics or critical aircraft systems. Furthermore, AC 91.21-1D provided by FAA outlines the conditions under which wireless systems, including ZigBee and Bluetooth, can be used in aircraft environments [30].

3.2 Overview of the Proposed SHM Systems

The following four SHM systems have been designed, developed and tested, which form the proposed CPSs within this PhD study.

1. Design and Development of a ZigBee-based SHM System for Composite Structures: This system consists of a compact DAQ unit with multi-channel, a WSN, and a dedicated software interface, all combined into a single platform (60 x 70 mm 4-layer PCB) that does not depend on external tools such as LabView or Matlab. Its multi-stage approach covers signal capture, wireless transmission through ZigBee, and integrated data processing for composite structures.

2. Passive Sensing Node: It is specifically designed to detect impact events through a miniature battery-driven architecture that transmits sensor data over Bluetooth LE. Rather than capturing continuous signals, this system enters a low-power state until an impact energy higher than a predefined threshold occurs, after which it is activated to sample the impact-induced response within 0.1 μs. Due to its event-triggered operation and coin-cell power source, the hardware achieves both small size (diameter of 28.4 mm and 3.7 grams) and extended operational lifetime, making it ideal for applications requiring minimal maintenance. The design provides a practical and affordable solution for distributed impact detection in composite structures.

3. Multi-Sensor SHM System: Unlike previous systems that focus on specific sensing approaches, the Multi-Sensor SHM System integrates multiple sensing techniques into a single flexible PCB measuring only 3 cm by 3 cm. It not only captures PZT-based signals, but also records strain, vibration, and ambient parameters such as temperature, pressure, and humidity. This capability provides a more comprehensive view of structural behaviour by correlating mechanical responses with potential environmental influences. Its Bluetooth LE connection enables wireless operation without external wiring. Hence, the proposed MSS is sufficiently lightweight (around 0.5 grams) and compact for large-scale deployment.

4. Integrated Active-Passive Sensing System: This system unites guided wave actuation and passive impact monitoring into a single four-channel platform (100 x 65 mm), thus addressing the need for continuous monitoring in SHM applications. A dedicated DAC

supplies controlled actuation waveforms, enabling effective excitation of composite panels and subsequent acquisition of structural responses. The IAPS system allows to toggle smoothly between active and passive methods.

This chapter presents the development and application of the first CPS: ZigBee-based SHM system, while the remaining three proposed systems are presented in the following chapters.

3.3 Design and Development of a ZigBee-based SHM System for Composite Structures

3.3.1 Introduction

The proposed system consists of a miniaturized on-board DAQ, WSN, and a user-friendly GUI. The end-to-end functionality consists of DAQ, the transmission of sensing results wirelessly, data visualization, and processing using the developed software with GUI. This approach does not require other software tools, such as LabView and Matlab, to visualize and process sensor data. All systems are integrated into one platform with this concept.

In the field of SHM, there are various detection methods consisting of different types of sensors, such as fiber optic, ultrasonic, strain gauges, and PZTs [8,82,108]. PZTs especially have a wide range of applications in the field of SHM because of their advantages such as their small size and weight, low power, and ease of installation. When PZTs are only used as receivers to sense and capture external events such as foreign object impacts, this implementation method is called passive sensing [73]. Active sensing is also another widely-used method for damage detection. In active sensing, PZTs act as both actuators and receivers in turn, to excite the structure and measure the response [47, 93].

WSN-based SHM has emerged as an effective approach for structural monitoring with the objective of improving damage detection [14, 77, 97]. Comprehensive details on the existing wireless technologies utilized in SHM can be found in the referenced review paper [1]. Table 3.1 presents a comparison of various WSN-based SHM prototypes, including the system developed in this PhD study, based on critical attributes such as damage detection methodology, number

Table 3.1: Comparison of the wireless sensor prototypes for WSN-based SHM

Prototypes	**Active**	**Passive**	**Channel Number**	**ADC Resolution**	**MCU**	**Wireless Module**
WI-Act [34]	Yes	No	8	12-bit	STM32L476ZET6	DIGI XBee
WI-Pass [35]	No	Yes	12	12-bit	STM32L476ZET6	DIGI XBee
Narada [95]	No	Yes	4	16-bit	Atmel Atmega128	Chipcon CC2420
Wireless sensor [104]	No	Yes	4	16-bit	Atmel Atmega128	MaxStream 9XCite
Thinner wireless node [70]	No	Yes	8	10-bit	Atmega128 L	DIGI XBee
SmartBrick V2.0 [41]	No	Yes	2	12-bit	TI CC2480	CC2420
WISAN coordinator [84]	No	Yes	12	12-bit	TI MSP430F1611	Chipcon CC2420
WSNG2 [45]	No	Yes	-	16-bit	2 processors-Arm	CC2430
PWSMS [107]	No	Yes	-	-	TI MSP430F149	CC2530
AEPod Prototype V1.0 [61]	No	Yes	8	12-bit	Atmel Atmega1281	Atmel AT86RF23
Xnode smart sensor [115]	No	Yes	8	24-bit	NXP LPC4357	Atmel AT86RF23
This study [19]	Yes	No	8	12-bit	STM32L476ZET6	DIGI XBee 3

of acquisition channels and type of deployed RF module. Although several studies have explored damage detection applications using WSN-based SHM systems, the majority of these systems have been primarily designed for civil engineering applications, including bridges and buildings which are not weight sensitive.

In this PhD, a ZigBee-based SHM system was designed for wireless guided wave acquisition and sensing. To enable wireless transmission of sensing data, a wireless network is established using Radio Frequency (RF) modules compatible with various communication protocols, including IEEE 802.15.4, ZigBee, and DigiMesh. Additionally, a GUI has been developed to manage the entire system, addressing the complexity in this multi-stage SHM approach. In the initial phase, a conceptual framework is presented to illustrate the integration and coordinated operation of the the modules of the system; namely DAQ, WSN, and GUI.

The DAQ system and the RF module are integrated into a single electronic circuit board, which includes a microcontroller and additional essential components such as signal amplifiers and power supply circuits. The proposed unit has been designed to demonstrate key features such as lightweight, energy efficiency, compact size, multi-channel sensing, and actuation capabilities. Another critical goal is to provide a user-friendly GUI for efficient system management and facilitate wireless data transmission through the WSN implemented with RF modules.

3.3.2 ZigBee-based SHM System Design

Challenges

Establishing a wireless network comprising multiple sensors requires careful consideration of various network topologies and wireless communication protocols to handle the transmission of large volumes of sensing data effectively. In addition, a GUI must be developed to manage the entire system, including monitoring, wireless network management, data visualization, and damage detection and localization. Furthermore, considerations such as sampling rate, power efficiency, and fault tolerance present additional constraints [1]. The critical factors that were addressed in the design of WSN-based SHM include:

- Smart and miniaturized DAQ system with the capabilities of wireless data transmission, battery operated, lightweight, high sensing accuracy, low power, reliability, and robustness.
- Wireless communication modules to establish a WSN with the capabilities of scalability and flexibility.
- Interactive GUI with computational software to remotely and autonomously manage the entire system.

The Proposed System Design

The developed system was constructed on a PCB that incorporates all necessary circuits, including amplification and switching circuits, along with an RF module. The electronic circuit board designed in this study is a 4-layer PCB. Additionally, a notable characteristic of the PCB is its compactness, with outline dimensions of 60 mm by 70 mm in the printed prototype.

The PCB designed in this study incorporates five primary functional circuits, each serving a critical role in the overall system. These include a Microcontroller Unit (MCU), an RF module for wireless communication, op-amp circuits for actuation and sensing processes, and Integrated Circuits (ICs) for switching purposes.

1. **MCU:** For the MCU, STM32L476ZE, an ARM-based microcontroller from STMicroelectronics, was chosen. This high-performance microcontroller features a Cortex-M4 core

with a 32-bit architecture and 144 pinouts, making it well-suited for the computational and control demands of the system [94].

The MCU serves as the central control unit, coordinating all processes within the system by executing predefined instructions. For instance, actuation signals are generated using the DAC peripheral of the MCU based on predefined data sets, enabling precise actuation control. Similarly, the sensing signals collected by the PZTs are initially in analog form. These signals are digitized through the ADC peripheral available in the MCU, allowing the data to be processed effectively. This combination of functional circuits and the high-performance MCU ensures its proper operation by managing both the actuation and sensing processes, as well as facilitating wireless communication through the RF module.

2. **RF module:** The RF module is a crucial component in achieving wireless communication within the design. For this purpose, a XBee 3 RF module, developed by Digi International, was selected. This module is highly versatile, supporting multiple wireless communication protocols, including ZigBee, DigiMesh, and others, making it suitable for a wide range of applications [25].

   In addition to the transmitter and receiver pins that facilitate serial data communication with microcontrollers, The XBee 3 is equipped with additional functional pins to enhance design flexibility. For example, the XBee 3 features digital and analog input/output pins that enable the direct integration of various external components, such as temperature sensors, without requiring additional interfacing circuitry. Another particularly advantageous feature is the inclusion of a sleep request pin, which allows the XBee 3 module to enter a low-power sleep mode. This functionality is especially beneficial for reducing power consumption in systems where data transmission is occasional or infrequent. These essential pins have been integrated into the RF module to support various applications, including those covered in this study.

3. **Op-amp circuits for actuating:** The amplification circuit for the actuating signal in this design utilizes an operational amplifier configuration. This approach was selected due to the nature of the MCU output, which generates a positive voltage ranging from 0 to

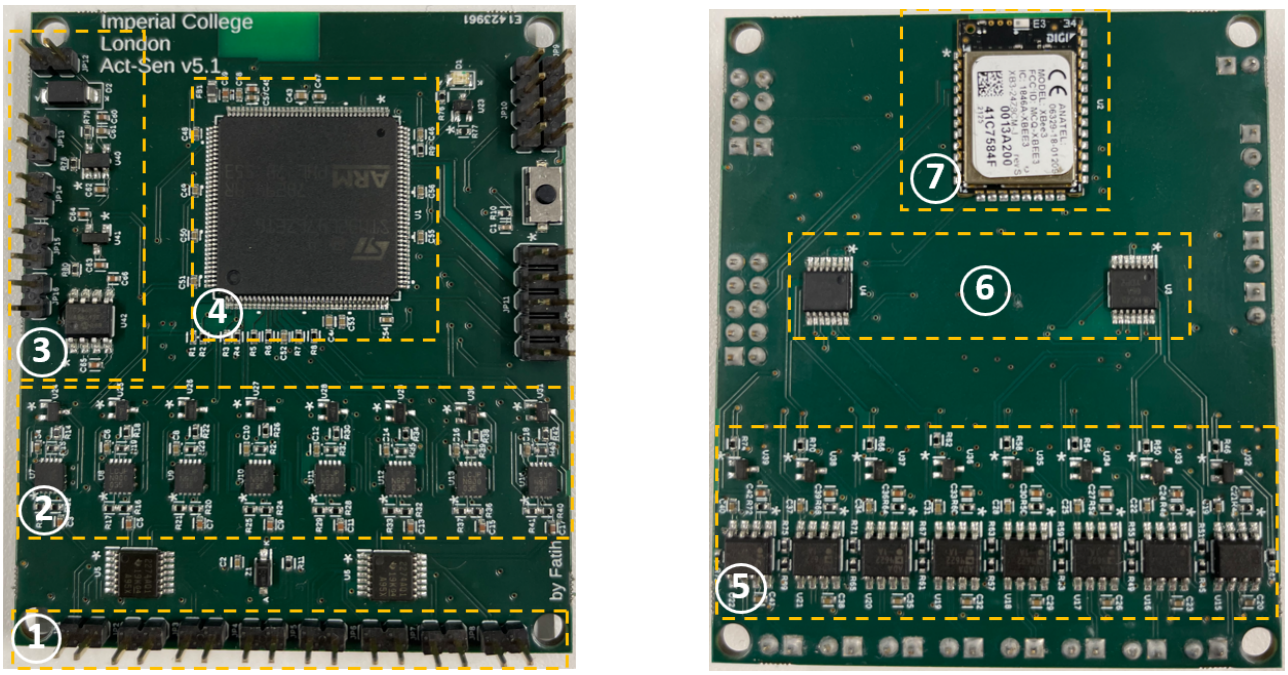
3.3V. To meet the requirements of the actuating signal, it was necessary to amplify and shift this output to achieve the desired voltage range of -3.3 V to +3.3 V. The inverting op-amp configuration effectively converts the positive-only signal from the MCU into a bipolar voltage range.

The IC component selected for this amplification circuit was a single op-amp configuration. This indicates that each actuating channel requires an individual IC component to perform the necessary amplification. While this design choice may increase the number of components on the PCB, it provides flexibility and precision for each actuating channel. This flexibility allows for customized amplification to meet the requirements of individual channels by ensuring consistent and reliable performance across all actuating processes within the system.

4. **Op-amp circuits for sensing:** To amplify the sensing signal and apply the necessary offset, an IC component with a dual op-amp circuit configuration was selected. This design choice allows each IC to handle two sensing channels simultaneously, reducing the number of required components and optimizing the PCB layout. The use of a dual op-amp IC enhances the efficiency of the system and minimizes the physical space occupied by the sensing amplification circuit. This approach is particularly beneficial for applications that require multiple sensing channels because it ensures scalability and maintains the precision needed for accurate signal acquisition.

5. **Switching mechanism:** In the developed system, the actuating channels have been sequentially selected by utilizing a switching module. This approach ensures the systematic activation of channels for signal transmission. the MCU is tasked with transmitting both the actuation signal and the corresponding channel selection command to the switching module. This coordinated operation enables the switching module to route the generated signal to the designated channel. While one channel actively transmits the actuating signal, the remaining channels are configured to simultaneously collect the sensing signals, which facilitates efficient DAQ and signal processing within the system.

   In addition, the transistors utilized in both the actuating and sensing op-amp circuits



(a) Top side (b) Bottom side

① Channels ② 2-stage ADC amplification ③ Power supply circuit ④ Microcontroller
⑤ DAC amplification ⑥ Switching module ⑦ XBee 3 RF module

Figure 3.1: The design of the ZigBee-based SHM system, 4-layer PCB with the dimensions of 60x70 cm, (a) top side and (b) bottom side

serve an identical function. Specifically, they are incorporated to control the enable and disable states of the amplification process by interfacing with the shutdown pins of the IC components. This functionality is critical for implementing the switching mechanism, which allows a single channel to perform dual functions, serving both the actuating and sensing processes.

This design aspect significantly reduces power consumption by deactivating unused amplification circuits during operation. This feature is particularly advantageous for energy-sensitive systems, such as those implemented in WSNs for SHM applications, where power efficiency is a critical design consideration. In general, the use of switching transistors allows one to enable dynamic switching between actuation and sensing functions by preventing signal interference and considerably reduces power consumption.

PCB layout and Considerations

In reference to the PCB layout illustrated in Fig. 3.1, the surface layers, specifically the top and bottom layers, are utilized to mount electronic components and routing signal traces essential for circuit operation. The majority of the components used in this layout are Surface-Mount Devices (SMDs), which are soldered directly onto the PCB surface, which reflects a compact and efficient assembly method. However, some components, such as pin headers, employ through-hole mounting, which involves inserting their leads through the PCB for enhanced mechanical strength.

The allocation of components between the layers is systematic to optimize the functionality of the board by considering the available space. Components such as pin headers, MCU, and sensing op-amp circuits are placed on the top layer. This layer is prioritized for elements that require direct user interaction or frequent access during operation and testing. In contrast, the bottom layer is designated for other critical components, including the actuating op-amp circuits, the XBee 3 RF module, and the switching modules. This arrangement minimizes interference between signal paths and ensures an efficient and organized layout by contributing to the overall reliability and performance of the PCB design.

Some electronic components, such as RF modules, require precise considerations during their placement on the PCB to ensure optimal functionality. For RF modules such as the XBee 3, their positions must be carefully evaluated to maximize performance and reliability. A critical requirement for wireless communication modules involves maintaining a designated keep-out area around the RF antenna. This area must be left non-conductive and free from any metallic objects to prevent interference or attenuation of RF signals, which could significantly degrade communication efficiency.

Furthermore, the keep-out zone should adhere to the recommendations provided in the datasheets or design notes accompanying the RF module. For example, the guidelines in the user manual of the XBee 3 RF module specify that no ground planes, copper traces, or other metallic components should be present within the area near the antenna. This ensures that the radiation pattern remains unobstructed to enhance the transmitting and receiving signal. When placed within enclosures, non-metallic materials are preferable to avoid blocking or reflecting RF

signals; in cases where a metallic enclosure is unavoidable, external antennas are recommended. These considerations are essential to ensure compliance with regulatory standards and achieving the best possible RF performance for the designed system [25].

Signal interference is crucial in PCB design to ensure the development of a robust and reliable electronic system. Interference between different signals, particularly in systems where both high- and low-voltage signals operate simultaneously, can lead to degraded performance or even system malfunction. In this specific design, careful attention has been paid to mitigate potential cross-talk between sensing and actuating signals. To achieve this, the sensing and actuating op-amp circuits have been placed adequately on separate PCB layers.

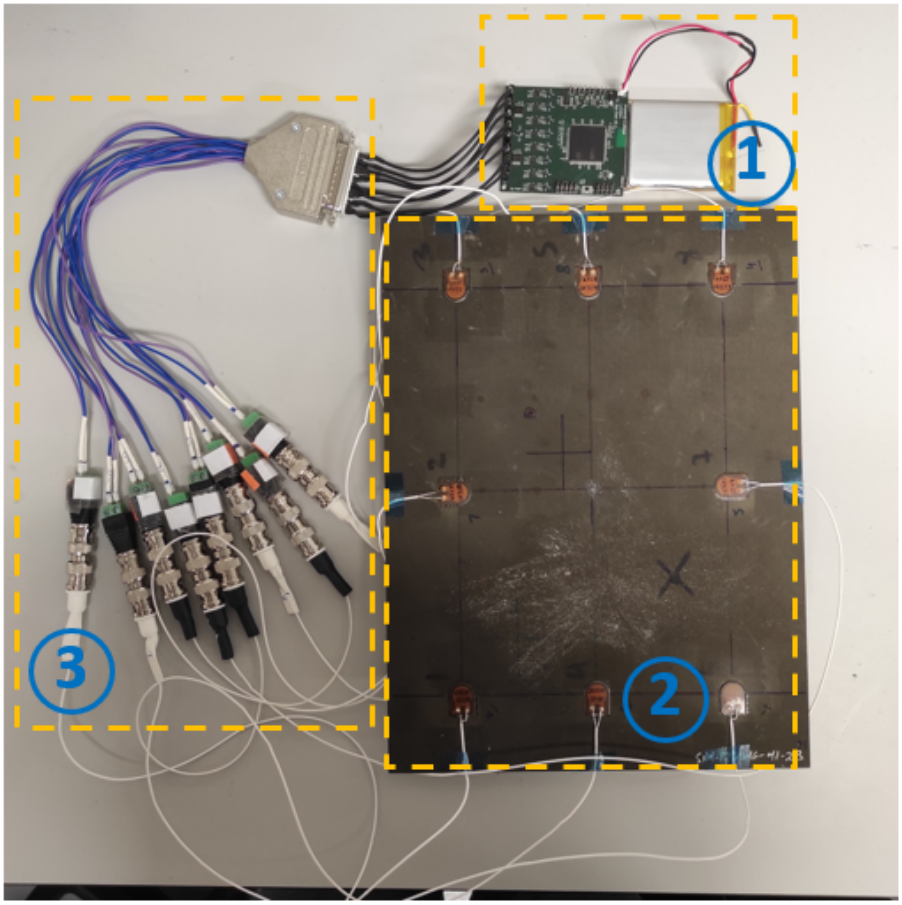
This strategic separation is particularly important given the difference in voltage levels between signals. Actuating signals, which can reach higher voltage levels such as ±3.3 V, have the potential to interfere with low-voltage sensing signals, often measured in millivolts. Such interference could corrupt the integrity of the sensing signals, leading to inaccurate DAQ or degraded functionality of the overall system. By isolating these circuits on different layers, the design effectively minimizes electromagnetic coupling and ensures that the signals operate independently without mutual disruption. This approach highlights the importance of PCB layout optimization in achieving high-performance electronic designs.

System Implementation

To validate the functionality and multi-channel acquisition capability of the designed system, a flat composite panel with eight PZT sensors was tested, as shown in Fig. 3.2.

The ZigBee-based SHM system was achieved with a miniaturized DAQ system integrated with a wireless communication module. This compact unit was powered by a rechargeable Lithium-Polymer (Li-Po) battery. The wireless connectivity of the unit is implemented through the RF module, which facilitates proper data exchange in real time. Furthermore, the physical connections between the DAQ unit and the composite panel were established using robust and reliable connectors, specifically BNC and D-sub types, to ensure high-fidelity signal transmission and ease of assembly during the experimental procedure.

One of the critical steps in active sensing applications is the generation of a actuating signal



① Battery-powered miniaturized DAQ system with RF module ② Flat composite panel with 8 PZTs ③ Sensor connections using BNC and D-sub connectors

Figure 3.2: Experimental setup to monitor the structural health of the composite panel

to excite structures with guided waves for SHM. The excitation of the structure is typically achieved using specific signal types, such as a sine wave modulated with a Hanning window (commonly referred to as a tone-burst) or chirp signals. These signal types are selected because of their suitability for propagating guided waves within the monitored structure.

To generate these signals, a predefined array of digital signal data is utilized within the DAC peripheral of an MCU. Once the signal is generated, it is used to excite the composite structure via the PZT sensor connected to the specified channel. Meanwhile, the remaining PZT sensors, seven sensors in this configuration, detect and record the structural response caused by the excitation.

The sensing signals captured by the piezoelectric sensors are at low voltage levels, typically within the range of ± 5 to ± 10 mV. Due to this low amplitude, these signals are subjected to an

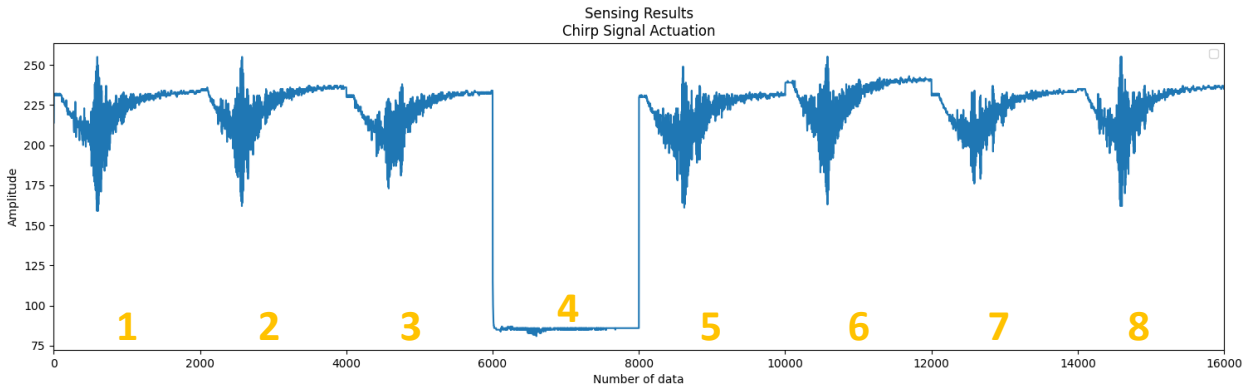


Figure 3.3: Example record of the captured sensing signals from the composite structure

amplification process to ensure that they are suitable for further processing by the MCU.

The next critical step in signal processing is to convert these amplified signals from their original analog form to digital format. This conversion is accomplished using the ADC peripheral available in the MCU. This two-step process, signal amplification and analog-to-digital conversion, ensures that the raw sensor data are appropriately conditioned and formatted for efficient processing within the digital domain.

Once the composite panel was excited with the generated actuation signal, the structural response was recorded by a set of PZTs. As an illustrative example, a single dataset of the recorded signals is presented in Fig. 3.3. This dataset contains the recorded response from eight individual PZT sensors, in a continuous string. Each channel is labelled in the figure for clarity. The fourth PZT was acting as an actuator. Consequently, no sensing signal is present in the channel.

The actuating-sensing cycle is performed sequentially for each PZT within the system, following the predefined order specified in the application code. During each cycle, the designated PZT transducer is tasked with actuation, while the remaining sensors capture the resulting structural response. This process ensures that comprehensive data are collected for monitoring the composite structure.

Afterwards, the sensing data acquired during each cycle are subsequently transmitted wirelessly to a central processing unit (e.g., PC). This wireless communication enables efficient data collection without the need for physical connections, making the system well-suited for real-time monitoring applications. Once received by the central unit, the data are plotted and

saved to be used for other processes.

To enable further analysis and evaluation of the acquired data, the developed GUI processes and visualizes the transmitted signals. Fig. 3.4 presents the processed sensing data obtained from the experimental procedure, in which each PZT sensor sequentially acted as an actuator while the remaining sensors recorded the structural response. To improve the signal-to-noise ratio and measurement reliability, the DAQ was repeated ten times for each actuation event. The collected data were then wirelessly transmitted to the central processing unit, where they were processed in the GUI. The results from these ten repetitions were averaged before plotting. The GUI displays the processed signals in eight subplots, each corresponding to a different actuation event. The numbering format (e.g., (8,1)) represents the actuation-response relationship, where the first number indicates the actuating PZT sensor, and the second represents the sensor capturing the response. This structured visualization provides a clear representation of the structural response distribution and wave propagation characteristics across different sensing locations.

Actuation Signal Generation

In the field of SHM, certain types of alternating signals are commonly utilized as actuating signals due to their effectiveness in exciting the structure with certain frequency and mode, and facilitating accurate response analysis. Among these, tone-burst and chirp signals are frequently used, each offering distinct advantages for various SHM applications, such as frequency control, mode selectivity, and signal clarity while reducing interference and spectral leakage. To generate these actuating signals, a numerical array of signal data is first constructed, taking into account a range of characteristic parameters. These parameters include the specific type of signal to be generated, its amplitude, the number of cycles, and the frequency, all of which are carefully defined to meet the requirements of the application.

The generation of these signals is carried out using the DAC peripheral integrated within the STM32 MCU. This DAC operates with a 12-bit resolution, which allows the representation of digital signal values within a range spanning from 0 to 4096 discrete levels. The high resolution of the DAC ensures a precise translation of the digital numerical array into a corresponding

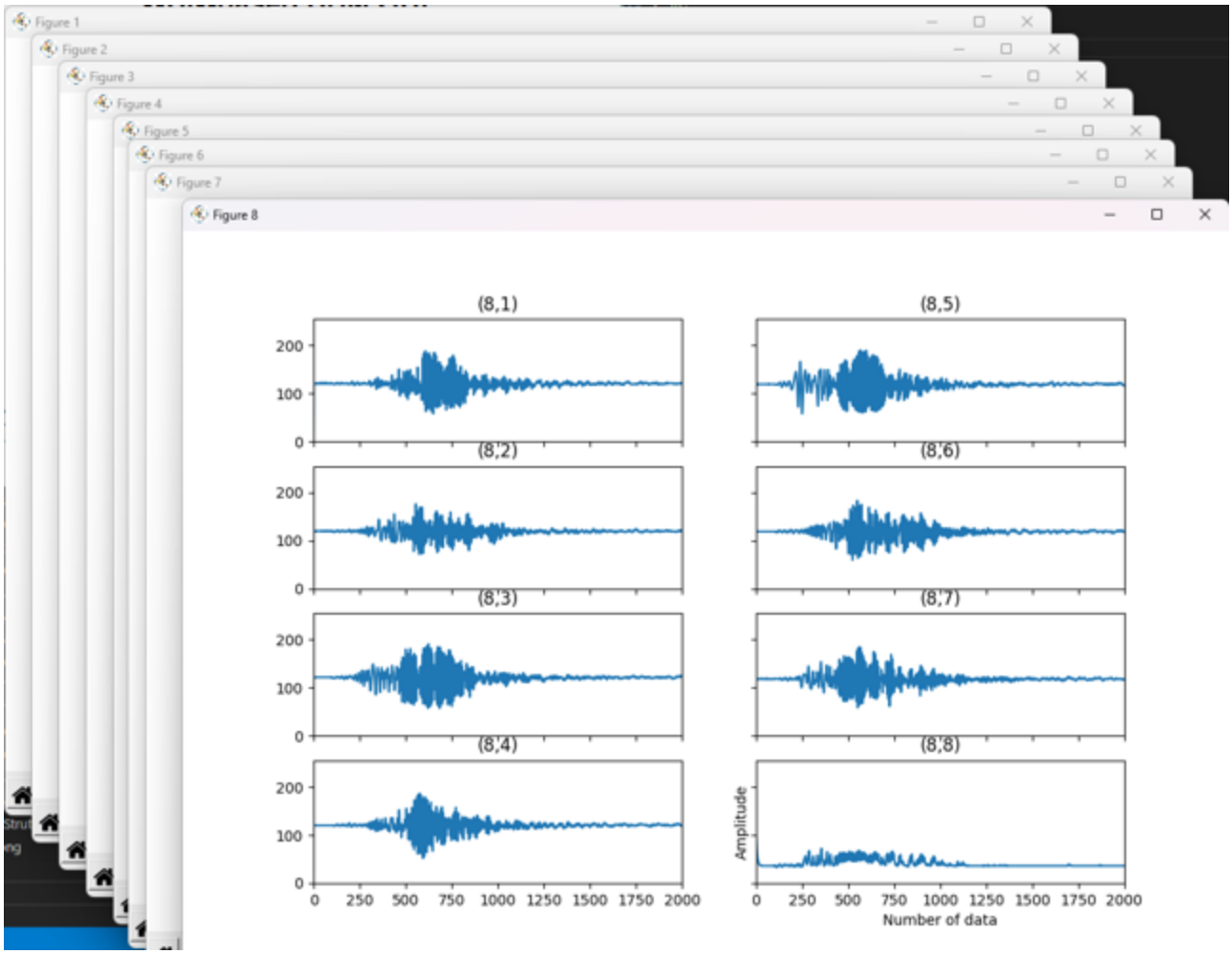


Figure 3.4: Active sensing results processed and visualized by the developed GUI

analog waveform. This capability is crucial for accurately exciting the structure and obtaining reliable data for subsequent analysis in SHM processes.

The formulation of the actuation tone-burst signal, denoted as S_{tb}, is given by

$$S_{tb} = A \cdot \sin\left(2\pi \cdot N \cdot \frac{i}{n_s}\right) \cdot \frac{1}{2}\left[1 - \cos\left(\frac{2\pi i}{n_s - 1}\right)\right] + A_0, \quad (i = 1, 2, 3, \ldots, n_s) \tag{3.1}$$

where A represents the amplitude of the signal. The parameter N specifies the number of cycles contained within a single actuation signal, while n_s indicates the total number of samples used to generate the waveform. In addition, A_0 denotes the offset value, which shifts the amplitude of the entire signal to centre it within a specific range by ensuring that the waveform oscillates around a desired baseline.

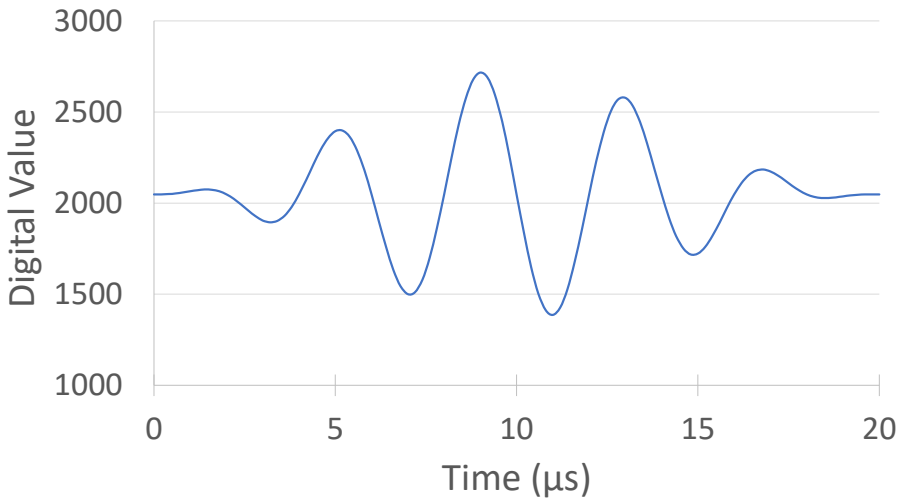


Figure 3.5: 250 kHz tone-burst signal with 5-cycle

According to the Nyquist theorem, the sampling frequency must be at least twice the highest frequency present in the signal being sampled to ensure accurate reconstruction [18]. For the case of a tone-burst actuation signal, commonly employed to excite guided waves in composite structures, the actuation signal is synthesized digitally and output through a DAC. The actuation frequency (f_{tb}), which defines the central frequency of the tone burst, is governed by both the sampling frequency f_s of the DAC and the number of discrete samples n_s used to represent a single period of the actuation signal.

The actuation frequency (f_{tb}) can be expressed as

$$f_{tb} = \frac{N \cdot f_s}{n_s} \tag{3.2}$$

where N denotes the number of cycles within the tone-burst waveform, and n_s represents the total number of samples over the complete waveform duration.

As an example, a 250 kHz tone-burst signal with 5-cycle is shown in Fig. 3.5 for a DAC with a sampling frequency of 5 MHz. Considering a 12-bit resolution, the amplitude and offset values of a desired tone-burst signal were determined.

The chirp signal is another widely-used actuation waveform. Unlike tone-burst signals, chirp signals are formed by a frequency that varies over time. This variation allows chirp signals to cover a range of frequencies within a single actuation, making them particularly effective for applications requiring wide-spectrum excitation.

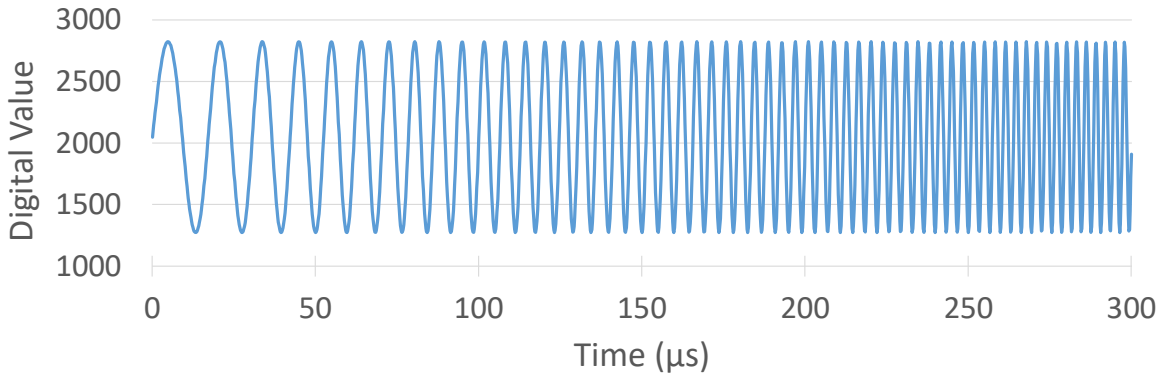


Figure 3.6: Chirp signal varying from 50 to 350 kHz

To generate the chirp actuation signal, denoted as S_{ch}, the mathematical expression is defined as

$$S_{ch} = A \cdot \sin\left[2\pi \cdot \left(f_0 \cdot t + \frac{(f_1 - f_0)}{2T} \cdot t^2\right)\right] + A_0 \tag{3.3}$$

where f_0 represents the initial frequency, while f_1 denotes the final frequency of the chirp signal. The parameter T defines the total duration of the chirp window, while t corresponds to the elapsed time at each specific time step within this window. Both T and t are measured in seconds to maintain consistency in temporal units. This formulation ensures precise control over the frequency modulation characteristics of the chirp signal.

For the same DAC features (12-bit resolution and 5 MHz sampling frequency), an example chirp signal is also plotted in Fig. 3.6. The range of the chirp signal is 50 to 350 kHz along with a chirp window of 300 μs. The amplitude and offset values can be adjusted based on the desired chirp signals.

ZigBee Wireless Communication

Each unit is equipped with a dedicated wireless communication module, which serves as a vital component for data transmission in the SHM system. These sensing units can be strategically distributed across critical regions of the aircraft, such as the wing and fuselage, where structural integrity is vital. Furthermore, distributed sensing units are designed to establish a robust wireless communication network among themselves. This network facilitates the proper transmission of sensing data from local units to a central processing station. This arrangement not only

improves the efficiency of DAQ and processing, but also minimizes the need for widespread wiring. Therefore, weight and complexity are reduced in the SHM system of an aircraft.

The primary objective of implementing the RF module is to facilitate the wireless transmission of the sensing data. Once the sensing data are transmitted wirelessly to a central station, they are processed, visualized, and saved to be used in the analysis of the integrity of the structure.

The RF device utilized in this study was an XBee module from DIGI. This module offers versatile functionality by supporting multiple wireless communication protocols, including IEEE 802.15.4, ZigBee, and DigiMesh. Among these, ZigBee is an industry-standard protocol widely adopted and supported by numerous vendors beyond DIGI, ensuring compatibility across various devices. In contrast, the DigiMesh protocol is company-specific to the XBee module, offering unique features specific to the ecosystem of DIGI. In this study, the ZigBee protocol was selected and implemented with the XBee 3 module, the most advanced iteration of the XBee series. This combination was used to enable efficient and reliable over-the-air data transmission. The adoption of the ZigBee protocol ensures robust communication with standardized reliability.

ZigBee Protocol:

The ZigBee protocol defines three distinct device types within its network architecture: **coordinator**, **router**, and **end device** as shown in Fig. 3.7. Each type of device plays a unique role in the network, enabling efficient communication and data management. In any ZigBee network, there is a singular **coordinator** device which is responsible for initiating and establishing the network, managing its overall configuration, and enabling other devices, such as routers and end devices, to join the network. In addition, the coordinator ensures network security by implementing appropriate encryption and authentication protocols. Due to its central role in maintaining the integrity and functionality of the network, the coordinator must remain continuously active and cannot enter a low-power or sleep mode [24].

Routers, in contrast, perform a dual function within the network. In addition to transmitting and receiving data packets, they also facilitate the routing of these packets between other devices. Although routers possess features similar to the coordinator, such as allowing other routers and end devices to connect to the network, they lack the same degree of administrative control. Importantly, such as the coordinator, routers cannot enter sleep mode and must remain active

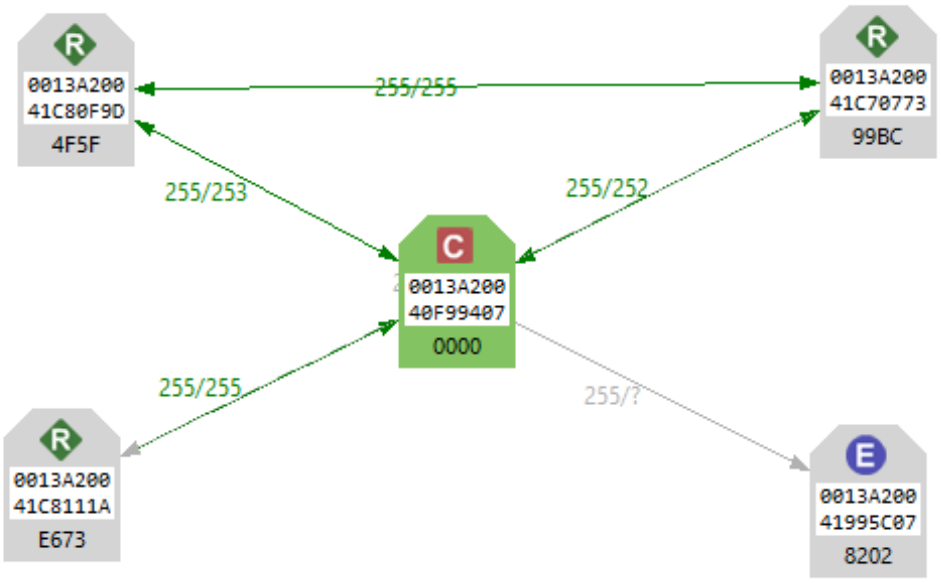


Figure 3.7: ZigBee star-topology network including central (C), router (R) and end device (E)

to maintain proper data flow within the network. However, unlike the coordinator, multiple routers can coexist within a ZigBee network, contributing to its scalability and robustness [24].

End devices represent a simplified version of the router in terms of functionality. Unlike coordinators and routers, end devices are not involved in routing or network management tasks. A key distinction of end devices is their ability to enter low-power or sleep mode when not in active use. This feature makes end devices particularly suitable for battery-powered applications where energy efficiency is a critical consideration. In general, these three types of devices enable the ZigBee protocol to provide a flexible, scalable, and energy-efficient solution for wireless communication [24].

Network security is a critical component of the ZigBee protocol, given its widespread application in wireless communication systems where data integrity, confidentiality, and protection against unauthorized access are critical. To address varying levels of security requirements, ZigBee supports three distinct security models, which are residential, standard, and high-security. Each model is used to meet specific use-case scenarios, ranging from simple home automation systems to more demanding industrial or enterprise environments requiring enhanced protection [24].

The XBee module incorporates robust encryption mechanisms to protect data. For example,

a key element of its security architecture is the network key, which is utilized to encrypt both the Application Support sub-layer and the data being transmitted over the network. This encryption ensures that sensitive information remains protected from potential interception during communication [24].

Wireless Concept for Entire SHM process with GUI

The proposed SHM system integrates various hardware components, including a microcontroller, an RF module, and a central processing unit, each of which plays a critical role in achieving the comprehensive goal of effective SHM. These devices are programmed using different programming languages. However, they are required to operate in a synchronized manner to ensure proper execution of the intended tasks.

The implementation of this approach requires a detailed examination of each stage, which includes DAQ, wireless data transmission, and subsequent data processing. Each phase of the system must be carefully coordinated to maintain precision and reliability throughout the monitoring process. To achieve this, the proposed methodology introduces a structured framework that clearly outlines the functionality of each device and the interactions between them, ensuring that all components work in coordination.

To facilitate understanding of the operation of the system, a model has been developed. This model provides an explanation of the individual stages and highlights the interrelationships among the devices. The proposed model and its operational framework are visually represented in Fig. 3.8, which offers a clear illustration of how the various elements are integrated to form a cohesive and efficient SHM system.

The MCU is programmed using the C programming language, which offers the low-level control and efficiency required for precise operations. Within this system, the MCU plays a crucial role in handling critical functions such as DAQ, actuation, and sensing. Specifically, the MCU is responsible for exciting the actuator, collecting multiple sensor data, and ensuring that the sensing process operates with accuracy and reliability.

Once the sensing data are collected from the PZTs mounted on the composite panel, the MCU interfaces with the RF module to execute the wireless transmission of these data. This

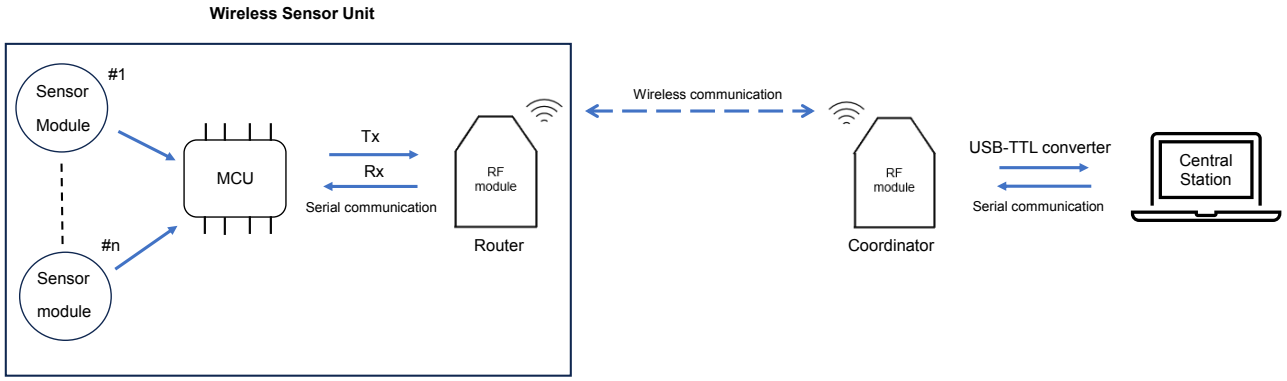


Figure 3.8: ZigBee-based SHM data flow

communication is achieved through the use of the Universal Asynchronous Receiver Transmitter (UART) protocol, a widely adopted serial communication standard. The UART protocol establishes a direct, point-to-point communication link between the MCU and the RF module using two dedicated pins. These pins are configured as a transmitter (Tx) and a receiver (Rx), enabling bi-directional data exchange between the two components.

In the RF module interfaced with the MCU, data is prepared for wireless transmission to the central device within the network. XBee devices provide support for the Application Programming Interface (API) operating mode, which defines the structure and methodology for data exchange. In this mode, information is transmitted in the form of packets, commonly referred to as API frames. These frames contain not only the core data that are being transmitted, but also additional metadata essential for communication. This metadata includes addressing details to identify target and source nodes, transmission-specific information, and indicators of success or failure during the transmission process [24]. All of this information ensures accurate routing, reliable delivery, and comprehensive feedback on the status of each transmission.

To facilitate wireless transmission through the ZigBee protocol, all relevant information must be organized into a structured packet format that adheres to the API frame standard. This structuring process is achieved by programming the XBee module using the MicroPython language, an efficient programming language specifically developed for embedded systems. This approach ensures proper integration between the MCU and the RF module for effective and reliable wireless communication.

Afterwards, the data packet containing the sensing information is transmitted wirelessly

to another XBee module interfaced with a central station, such as a PC. The exchange of information between the coordinator module and the central station is also performed through UART. This particular XBee module serves as the coordinator within the ZigBee-based network architecture. As the central node, the coordinator is responsible for managing the network and receiving data packets from distributed sensing units.

Once the data packet reaches the central station, the necessary information is extracted. This includes not only the sensing data collected from the monitored structure, but also metadata such as the address of the sending device. These details are crucial for ensuring the traceability and organization of data within the monitoring system.

The central station has many functions and capabilities. Its primary functions include visualizing and processing the collected data and providing a user-friendly GUI as shown in Fig. 3.9. These functionalities are essential for the successful implementation and operation of the proposed system, as they enable efficient data handling and proper user engagement.

To achieve these objectives, software development is essential for properly managing the system. During the software development phase, the Python programming language was chosen as the primary tool due to its numerous advantages. Python offers an extensive library and framework ecosystem that significantly accelerates development tasks such as data processing, visualization, and network communication. Additionally, the portability of Python ensures that the software can be easily adapted to different platforms and environments, enhancing the flexibility and scalability of the system.

In addition, the integration of components programmed in different programming languages poses its own set of challenges. Each component must be designed to work in harmony with the others, regardless of the language used in its development. This interoperability is crucial for the proposed system to perform its intended functions. Therefore, a comprehensive approach to system design, which includes both software and hardware considerations, is necessary to overcome these challenges to achieve a reliable and effective SHM system.

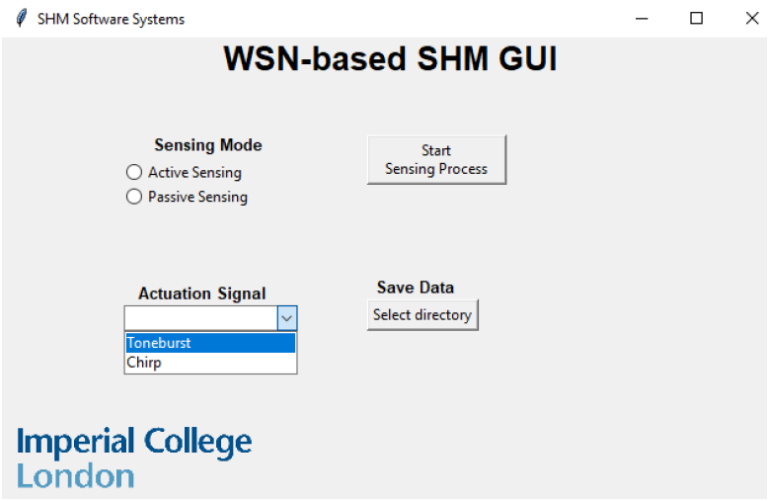


Figure 3.9: The GUI developed for the ZigBee-based SHM system

3.3.3 Conclusions

This study presents a design framework for a ZigBee-based DAQ and processing system tailored for SHM applications. The research examines the challenges associated with developing and implementing such a system, focusing on compact on-board DAQ and reliable wireless communication. The proposed design addresses these challenges by integrating key functionalities into a unified platform.

The developed system consists of a compact PCB integrating a DAQ unit and an RF module, powered by a microcontroller. Its technical specifications, design considerations, and integration within the complete SHM system was discussed comprehensively. In addition, the study details the methods used to generate essential actuation signals, such as tone-burst and chirp waveforms, which are critical for structural excitation in SHM applications.

A key feature of the proposed system is the integration of RF modules and wireless communication protocols. The DIGI XBee 3 wireless module and the ZigBee protocol were selected to establish a WSN. The entire framework was implemented through embedded programming in C and MicroPython for the MCU and RF modules, respectively, while the GUI was developed in Python. The GUI incorporates advanced data visualization, real-time processing, and WSN management for seamless user interaction.

Beyond its core functionalities, the proposed system offers significant advantages by streamlining the entire SHM process. Unlike conventional approaches that require multiple software

tools such as LabView or MATLAB for different tasks, this system centralizes DAQ, wireless transmission, and GUI-based processing within a single integrated platform. While traditional tools provide versatility, switching between them can be time-consuming and inefficient. The proposed system eliminates this complexity, enhancing efficiency with a unified and user-friendly interface. Furthermore, it is designed with flexibility, allowing future enhancements through software modifications, making it scalable and adaptable to evolving SHM requirements.

Chapter 4

Passive Sensing Node

This chapter is focused on the development of a modular, compact, and energy efficient Passive Sensing Node (PSN) for impact detection and localization for the purpose of in-service SHM. The system combines passive impact sensing using PZT sensors with a low-power WSN that employs Bluetooth LE for data transmission and incorporates a shared-clock mechanism for precise time synchronization and TDoA analysis. Key developments include a coin-cell battery-powered, compact hardware design, a GUI for real-time data visualization and control, and the integration of a kNN machine learning model that fuses TDoA and ADC amplitude features to accurately localize impact events. The system performance is validated through a series of experiments to detect and localize impact events on a composite plate.

4.1 Introduction

Passive SHM is essential for identifying external incidents such as impacts on structures, particularly in lightweight composite plates that are commonly used in aerospace structures. PZTs are essential components in SHM, as they generate electrical charges in response to mechanical stress and vibrations. The signals recorded by PZTs enable impact localization [1]. Advanced algorithms for real-time data processing, such as those proposed by Zhong et al. [114], have significantly improved the SHM capability to detect and localize impacts. Real-time monitoring ensures the continuous acquisition and processing of data, providing timely detection of structural changes. Advances in SHM, such as improved sensors, wireless communication

protocols, and data analysis methods, enhance the accuracy and efficiency of these systems [58, 105].

Passive sensing for aircraft structures focuses on detecting, localizing, and analysing external impact events by capturing and processing waves propagated through the structure. These waves are generated by impact events and recorded by embedded PZT sensors within the structure [36, 86, 88]. This approach enables the identification and characterization of impacts that could potentially compromise the structural integrity of the aircraft.

However, not all detected impacts pose a significant risk to structural integrity. Impacts must be carefully assessed to determine their criticality, as non-critical impacts can lead to unnecessary false alarms, reducing the efficiency and reliability of the system. Differentiating between critical and non-critical impacts is, therefore, a key component of a robust SHM system [52, 85].

To address this challenge, a threshold-based mechanism is employed to enhance system effectiveness. This threshold acts as a sensitivity filter, ensuring that only signals corresponding to impacts considered relevant to structural integrity are recorded and processed. By suppressing signals below the defined threshold value, the system minimizes unnecessary data collection and processing, maintaining a focus on events of interest from the perspective of SHM. This approach ensures that the monitoring system remains efficient and reduces the likelihood of false alarms, thereby improving the overall reliability and operational utility of the SHM system [35].

WSNs consist of small low-power sensor nodes that wirelessly transmit data from their environments, making them highly scalable and adaptable for monitoring large or inaccessible structures [5]. Compared to traditional wired systems, WSNs simplify installation and reduce maintenance costs, while enabling real-time detection of impacts in critical infrastructures such as aircraft and bridges [92]. WSNs allow simultaneous detection and localization of impacts through comprehensive sensing coverage and centralized data analysis, offering cost-effective and energy-efficient solutions. By supporting remote monitoring and flexible system design, WSN-based SHM systems enable efficient decision-making and proactive maintenance methods in aerospace, civil engineering, and transportation sectors [77, 97].

Research efforts focus on improving SHM including WSNs and PZT sensors. Fu et al. [34] developed an energy-efficient cyber-physical system for SHM in aircraft, employing PZT

transducers and strategically distributed sensor nodes throughout the structure . Their work also introduced a low-power wireless structural health monitoring system (WSHMS) designed to detect impacts in composite airframes [35]. Other contributions, such as those by Swartz et al. [95] and Harms et al. [41], focused on optimizing wireless sensing units and integrating IEEE 802.15.4-compliant radios for improved accuracy and network performance in civil infrastructures. Additional notable works on WSN-based SHM include those by Sazonov et al. [84] on synchronous data acquisition and vibration analysis , and studies such as [45, 61, 70, 104, 107, 115], which further advance WSN capabilities for SHM.

Bluetooth LE has seen limited application in SHM despite its notable benefits, including low-power consumption and compatibility with smartphones. For example, Sidibe et al. [89] developed a battery-free wireless sensing node designed to monitor physical parameters such as temperature, humidity, and resistivity in reinforced concrete structures. This system employed Bluetooth LE for wireless data transmission but operated exclusively in broadcasting mode. In this mode, data are transmitted without encryption or authentication, and its low payload capacity restricts the amount of data that can be sent.

Sinha et al. [90] proposed an advanced framework combining WSNs and fog computing, utilizing Bluetooth LE for data transmission and integrating 5G network capabilities to minimize power consumption. The framework included a head sensor algorithm designed to enhance the service life of the WSN, although it did not incorporate a data acquisition system for SHM. Another study by Le et al. [59] introduced a wireless sensor system integrated with ultra-high-performance concrete, capable of sensing and transmitting real-time stress and impact data. This system used Bluetooth LE beacons for data transmission. However, these beacons also relied on broadcasting mode, which limits security and payload capacity.

Similarly, Fort et al. [33] developed an IoT sensor node utilizing Bluetooth LE for monitoring large wooden structures and artworks, particularly in museums and churches . Like previous studies, this system used broadcasting mode for data transmission. Although broadcasting mode offers simplicity, it lacks the security required for robust wireless communication and is not suitable for transmitting large volumes of sensing data. Furthermore, the systems proposed in these studies rely primarily on peer-to-peer communication, including only two nodes (central

and peripheral). None of them offers a practical WSN design capable of collecting data from multiple nodes simultaneously during an SHM application, which remains a significant limitation in using Bluetooth LE for SHM.

Although advances in hardware and wireless data transmission significantly enhance sensor data collection, processing these data into actionable insights remains a critical challenge. To address this, Machine Learning (ML) methods, particularly k-Nearest Neighbors (kNN), are gaining attraction in SHM applications for their simplicity and efficacy in impact localization tasks. This approach, as described by Farrar et al. [28] and Worden et al. [106], uses supervised learning to compare new data with existing patterns and determine the location of structural damage. kNN operates by identifying the nearest neighbours within a feature space to classify or predict damage locations. Combined with signal features extracted through advanced decomposition methods [114], kNN provides a robust framework for precise and real-time impact localization in SHM systems.

The current state of SHM systems is marked by several significant limitations that obstruct their efficiency and practical deployment. Most existing systems rely on basic peer-to-peer wireless communication without a network consisting of multiple nodes, which is insufficient for monitoring large structural components such as those found in aircraft. These structures require multiple sensing nodes to ensure comprehensive on-board monitoring, a need that current systems struggle to meet. Another critical issue is the use of low-computational-power processors, which restrict the performance of SHM systems in applications that demand higher processing capabilities.

The physical size of many SHM systems poses a further challenge, as their lack of miniaturization limits their integration into compact and weight-sensitive aerospace environments. For effective implementation in such settings, the systems must be considerably smaller and lighter. Furthermore, wireless networks used in SHM systems require a shared clock to achieve precise time synchronization among multiple remote sensors. This synchronization is essential for acquiring accurate time-stamped sensing data, which is critical for effective damage detection and localization.

Power consumption also remains a significant concern. SHM systems must operate with

minimal energy requirements to ensure sustainability and enable continuous long-term monitoring. Overcoming these limitations is essential for the advancement of SHM technologies, enabling the development of more efficient, compact, and high-performance systems suitable for real-world applications. Addressing these challenges will open new possibilities to improve the safety, reliability, and operational capabilities of SHM in demanding environments. This chapter introduces an innovative miniaturized system that incorporates wireless communication, eliminating the need for physical wiring and significantly improving practicality for aerospace applications. The system employs a WSN that uses the Bluetooth LE protocol.

4.2 The Proposed System

In the proposed system, PSNs are deployed as both peripheral and central nodes, each fulfilling distinct roles within the WSN. The peripheral PSNs are distributed across the composite panel as remote sensor nodes as shown in Fig. 4.1, responsible for detecting impact-induced signals and wirelessly transmitting the acquired data. In contrast, a single central PSN, physically connected to a PC via UART serial communication, functions as the network coordinator, managing data collection and maintaining time synchronization across the system. Although the same hardware platform is utilized for both central and peripheral PSNs, their operational differences are defined by software variations tailored to their specific functions.

The central PSN firmware is designed to handle multiple simultaneous Bluetooth LE connections, ensuring time synchronization with all peripheral nodes while forwarding collected data to the PC for further processing. In contrast, peripheral PSNs operate in low-power mode, remaining in the sleep state until an impact is detected. Upon activation, they acquire impact signals using an ADC, timestamp the event with a shared clock, and wirelessly transmit the processed data to the central PSN. This software-based differentiation enables efficient impact monitoring, with synchronized timestamping and reliable data acquisition across the WSN.

Passive sensing with the proposed system is detailed in Fig. 4.2. When an external impact occurs on the composite panel, the impact-induced signal is first attenuated and rectified. The resulting signal is then analyzed by a comparator to assess its amplitude, which serves as an

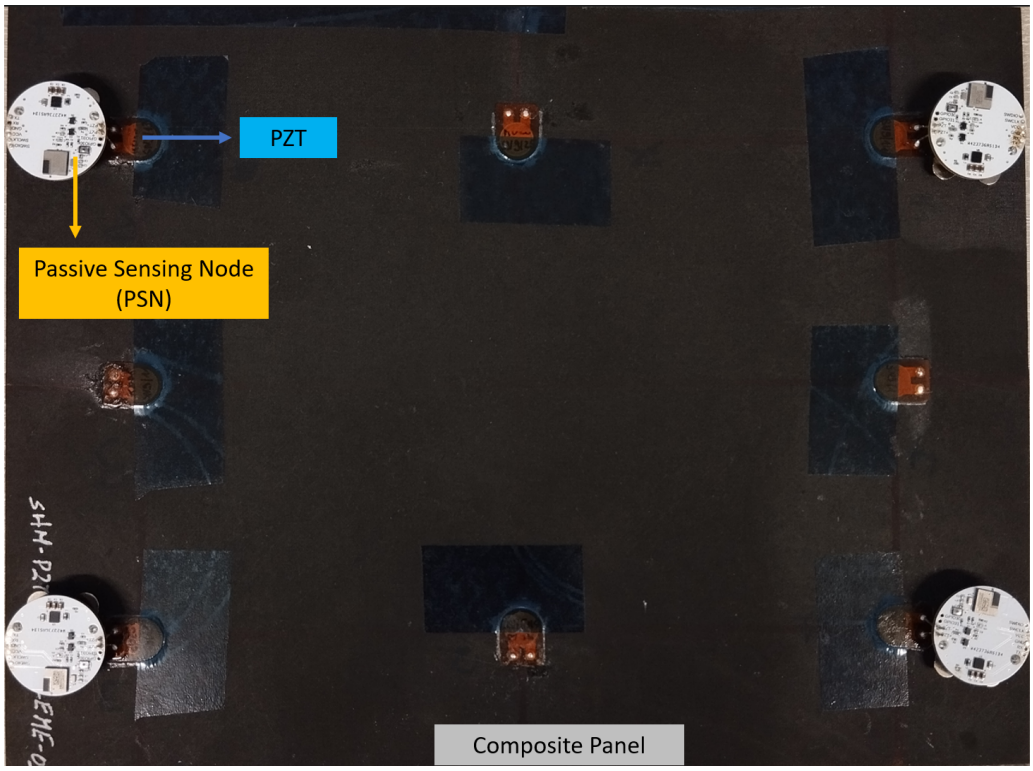


Figure 4.1: Composite panel with PZTs and Passive Sensing Nodes (PSNs)

indicator of the intensity of the event.

There are studies to estimate the impact force on composite plates to determine critical impacts [36, 52, 85]. This study is based on the relevant impact energies that are probable in an aircraft, considering the maximum amplitude of the generated signals and the sensing range of the MCU.

There is a built-in comparator within the MCU, the comparator continuously monitors the voltage signal and determines whether it exceeds a predefined threshold value. The threshold value can be selected between 0 to 3.3 V, covering the entire range. Therefore, the proposed system offers great flexibility because the threshold value varies on the basis of structural properties such as thickness of the plate and material properties (e.g. damping).

The value of 1.2 V was determined for the composite panel used in the experiment with a hammer to make impacts, to ensure accurate recording of the impact-induced signals and to avoid noise. The threshold is adjustable based on probable impact energies, and for each structure needs to be tuned. Another threshold value can be easily selected. This value is an example to show the event-triggered mechanism.

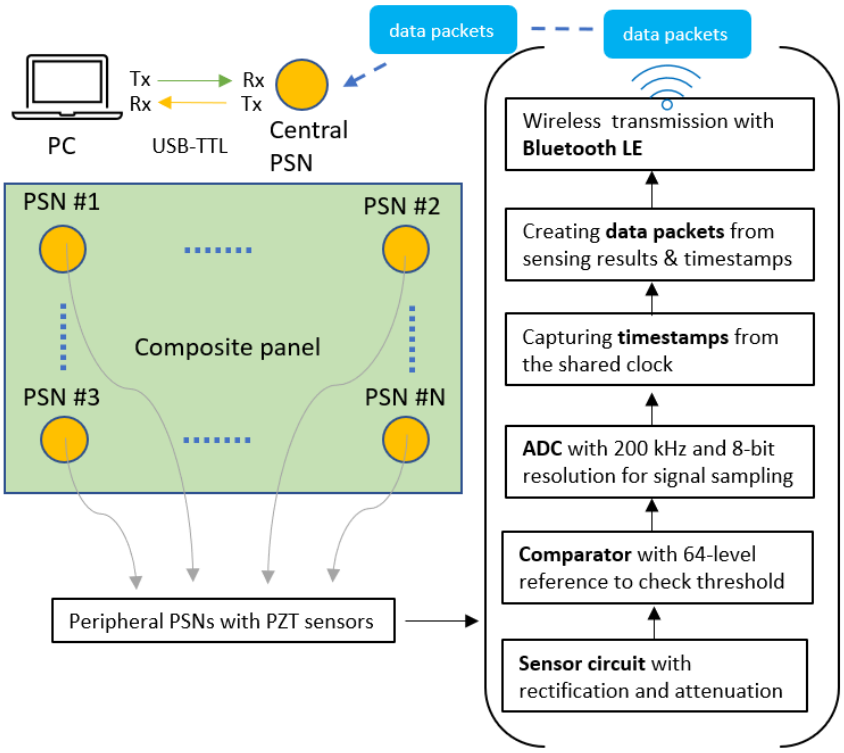


Figure 4.2: Passive sensing system with PSNs

If the threshold is surpassed, the system transitions from sleep mode to active state, triggering the ADC peripheral. At this stage, a timestamp is captured from a shared clock, and the ADC initiates the sampling process to convert the analog signals acquired from the PZTs into digital data.

Since Bluetooth LE communication has a strict limitation on the number of bytes per packet, the sampled signal is segmented into smaller data packets before transmission. These packets contain both the sensing results and the corresponding timestamps.

Once the data packets are successfully collected in the central PSN, they are sent to a PC through the UART serial interface. This enables a detailed assessment of the structural integrity of the composite panel, facilitating real-time impact detection and monitoring.

In the following sections, several key aspects of the proposed system will be explored in detail. First, the importance of time synchronization among multiple PSNs will be discussed, highlighting the methods used to achieve precise timing coordination across the network. Second, low-power operation will be examined in the system, focusing on sleep mode and event-triggered wake-up mechanisms that ensure energy efficiency. The wireless data transmission approach

will then be outlined, emphasizing its modularity and scalability for network expansion. In addition, the lightweight and miniaturized design of the system will be presented, highlighting its suitability for aerospace applications. The processing capabilities, including real-time impact detection and localization will also be detailed. Finally, a dedicated GUI for data processing and visualization will be introduced, illustrating its role in facilitating efficient data acquisition and analysis. These sections collectively provide a comprehensive overview of the system architecture and its suitability for SHM applications.

4.2.1 Time Synchronization among Multiple PSNs

When multiple PSNs are deployed on a large structure, it becomes essential to record timestamp information alongside the sensing data collected from these nodes. Accurate timing is critical for understanding the sequence and correlation of events detected by the network. The proposed system in this study has been specifically designed to address the challenges of timing accuracy and synchronization within a WSN. Its primary objective is to ensure that events and tasks across multiple devices are synchronized with both high precision and minimal power consumption, which is particularly important for energy-constrained systems.

The inclusion of precise timestamp data is crucial in calculating the TDoA of impact signals between the PSNs mounted on the composite panel. Using high-resolution timing information, the system can accurately determine the relative time at which signals reach different nodes. This capability not only enhances the precision of impact localization but also ensures efficient operation without compromising energy efficiency.

In the presented system, the central PSN plays a dual role in managing the WSN. It not only establishes the network for wireless data communication with multiple peripheral PSNs but also serves as the primary timing reference for the entire system. The central device maintains a master clock and periodically transmits synchronization packets to peripheral devices within the network. These peripherals then adjust their local timers based on the information received in the synchronization packets, ensuring that all devices within the network operate according to a unified time reference and ensures precise timestamping of impact events.

Wireless communication protocols, such as Bluetooth LE, abstract the complexities of

managing radio hardware, simplifying the process of developing applications. However, when precise synchronization is necessary, the operational characteristics of these protocols play a critical role, especially if they do not inherently support timekeeping functionalities. For example, in the case of Bluetooth LE, the protocol ensures reliable data packet delivery through mechanisms such as retransmissions. These retransmissions occur transparently in the application layer, which can introduce challenges in achieving precise synchronization, as the timing behaviour of such processes is not directly accessible to the application.

The configuration of RF parameters is a crucial step in enabling effective communication between devices, particularly for achieving time synchronization within a wireless network. Key parameters such as the RF channel and the device address are set to establish a dedicated communication pathway. In this study, a single RF channel is utilized specifically for transmitting time synchronization packets. The channel selected for this purpose is channel 80, which corresponds to a frequency of 2480 MHz. This channel is one of the designated frequencies used by Bluetooth LE during the advertising phase of its communication protocol, as outlined in [26]. By using a dedicated channel for synchronization packets, the potential interference with other BLE operations is minimized, ensuring more reliable timing communication between devices.

In the wireless network, one node is designated as the timing master, responsible for transmitting synchronization packets at predefined intervals. The remaining nodes, known as timing slaves, adjust their timers based on the synchronization information received from the master. Each timing slave operates an independent 16 MHz free-running timer to manage local timing. This process ensures a synchronized timing reference across all nodes in the network.

To enable accurate timing operations and provide a mechanism for visualizing timer states, hardware features such as GPIO Tasks and Events (GPIOTE) and Programmable Peripheral Interconnect (PPI) are utilized. GPIOTE allows for precise control of General-Purpose Input/Output (GPIO) events triggered by the timer, while PPI enables efficient communication between peripherals without involving the CPU.

Unlike timing slaves, the timing master uses two distinct timers to maintain the primary clock for network synchronization. The first timer, known as the synchronization timer, runs continuously without interruption and remains unmodified by the timing master, ensuring a

stable reference for the network.

The second timer in the timing master operates in counter mode and is tasked with tracking the number of times the synchronization timer overflows or resets. This functionality is essential for maintaining an accurate measure of time beyond the range of the synchronization timer. To calculate precise timestamp information, the timing master combines the count of overflows or resets recorded by the second timer with the current value of the synchronization timer. This method ensures that the timestamp remains accurate even over extended periods.

This approach provides an effective solution for achieving wireless timer synchronization. The system is capable of reaching high levels of synchronization accuracy. However, various practical challenges, such as packet loss, propagation delays, and signal reflections, may introduce errors and affect the overall precision of the synchronization process. Addressing these factors is critical to maintaining reliability and performance in real-world applications.

4.2.2 Low-Power Operation (Sleep Mode & Triggered Wake-Up, Battery-Powered)

The proposed system is designed to operate with minimal energy consumption, ensuring long-term functionality without the need for frequent maintenance. To achieve this, a combination of event-triggered wake-up functionality and optimized power management techniques has been implemented.

One of the key strategies employed is the use of a sleep mode, where the system remains in a low-power state when no significant structural events are detected. This significantly reduces energy consumption during idle periods, conserving battery life. The system transitions from sleep mode to active operation when an impact event is detected. This transition is managed through a programmable comparator that monitors the incoming signal from the PZT sensors. When the amplitude of the detected signal exceeds a predefined threshold value, the comparator triggers the activation of the system, allowing data acquisition and processing to begin.

In this implementation, the activation time of the ADC and the threshold value are critical parameters to ensure that the ADC is activated on time and the severity of the impact is

examined correctly. Based on these considerations, the comparator is configured before operation. In the configuration, the threshold value can be selected in a 64-level reference ladder. For faster activation of the ADC, the interrupt event of the comparator is generated in high-speed mode. The time required to generate an interrupt event is demonstrated when the comparator is in different modes in Table 4.1 [100].

Table 4.1: Time to generate interrupt event in the different modes of the comparator

Mode	Required time
t_powersave	0.6 μs
t_balanced	0.2 μs
t_speed	0.1 μs

The fast activation of the ADC in the proposed system ensures that no data is lost once the threshold value is exceeded. Given that the sampling frequency is set to 200 kHz, each sample is acquired every 5 μs. The comparator, configured in high-speed mode, generates an interrupt event in just 0.1 μs, which is significantly faster than the sampling period. This rapid response guarantees that the ADC is triggered almost instantaneously an impact event occurs, allowing it to start sampling without delay. As a result, the system effectively captures critical signal variations immediately after the threshold is crossed, preserving the integrity and accuracy of the acquired data.

This event-triggered mechanism ensures that the system prioritizes critical impact events while ignoring minor disturbances that do not pose a threat to the structural integrity of the monitored structure.

To further optimize the power efficiency of the system, the management of clock sources plays a crucial role. The ANNA-B402 module is equipped with two types of clocks: a high-frequency clock and a low-frequency clock. The high-frequency clock is provided internally by a high-precision 32 MHz crystal integrated into the module. In contrast, the low-frequency clock can be provided by the Resistor–Capacitor (RC) oscillator, synthesized from the fast clock, or externally by a 32.768 kHz crystal. For applications requiring minimal current consumption, particularly in power-saving modes, it is essential to use an external high-precision 32.768 kHz crystal [100].

When an external crystal is not used, the module relies on periodic calibration of its internal

clocks to maintain accuracy. However, this calibration process results in increased power consumption, which can be a significant drawback for battery-operated systems. To address this issue and optimize the energy efficiency of the system, an external 32.768 kHz crystal has been integrated into the system design, along with the necessary capacitors. This addition ensures that the low-frequency clock operates with high precision, eliminating the need for frequent calibration, and thereby significantly reducing overall power consumption.

For power supply, each PSN operates on a compact coin-cell battery (CR-2032), which provides a stable voltage of 3 V and an energy storage capacity of 240 mAh. The components of the system have been carefully selected to ensure compatibility with low-power operation, including the RP604 buck-boost DC/DC converter, which maintains a regulated 3.3 V power supply while consuming minimal quiescent current (0.3 µA). This voltage regulation circuit ensures efficient power delivery while preventing fluctuations that could compromise system stability.

The combination of event-triggered sensing, optimized power management, and a compact battery-operated design makes the system energy-efficient, cost-effective, and suitable for deployment in remote or inaccessible locations where regular battery replacement is impractical.

4.2.3 Wireless Data Transmission

The proposed system utilizes wireless data transmission to eliminate the need for wired connections, ensuring flexibility, modularity, and ease of deployment in SHM applications. The system is designed to support multiple PSNs in a distributed sensing architecture, allowing scalability and network expansion.

Wireless communication within the system is facilitated by a star-topology network established using Bluetooth LE. A central device acts as the primary hub, managing connections with multiple peripheral sensor nodes. This setup allows data from spatially distributed PSNs to be collected and processed efficiently, enabling real-time impact detection and localization.

Each PSN is equipped with an RF microcontroller, which integrates both processing and wireless communication functionalities, eliminating the need for external RF modules. This compact and modular design enhances system adaptability, making it possible to deploy

additional sensing nodes without significant reconfiguration. The Bluetooth LE protocol enables low-power, energy-efficient communication while ensuring reliable data exchange across the wireless network.

Data transmission is performed in structured packets, where each PSN sends digitized impact response signals and precise timestamp information wirelessly to the central device. These packets contain unique sensor identifiers, ensuring that incoming data can be correctly attributed to its originating node. Given the nature of wireless communication, packets may arrive in a non-sequential order; however, the inclusion of sensor identifiers allows for accurate data management.

The modularity of the proposed system is further enhanced through network expansion capabilities. The Multi-Nordic UART Service (Multi-NUS) framework has been employed, allowing the central device to manage multiple simultaneous connections with PSNs. By modifying and extending the standard NUS Central Role, the system can support communication with up to 20 peripheral devices. Additionally, the network architecture can be designed to be expanded further by introducing additional hubs or configuring certain nodes to function as sub-network hubs.

Antenna design is a critical aspect of wireless communication systems as it has a direct impact on the reliability and range of the communication link. Recognizing its importance, an antenna pattern has been specifically designed to optimize the performance of the integrated internal antenna within the ANNA-B402 module, as shown in Fig. 4.3. The design approach strictly followed the protocols specified in the system integration manual [99], ensuring compatibility with the module specifications and achieving effective signal transmission.

A key consideration in the design is a specified keep-out area around the antenna pattern. This keep-out area, which must remain non-conductive, is required on both the top and bottom layers of the PCB. The absence of conductive materials in this region is essential to prevent radio signals from being reflected by nearby conductive components. Such reflections can interfere with the propagation of the signal, potentially causing data loss or communication failures. By ensuring the proper implementation of this design requirement, the risk of missing data is minimized, allowing reliable and uninterrupted wireless transmission of PSN data.

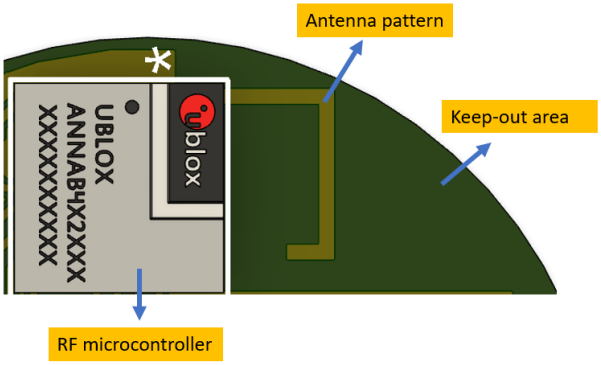


Figure 4.3: Antenna pattern design

To enhance the security of wireless communication within the WSN, the Filter Accept List method has been employed. This method introduces a security layer by restricting access to only specific devices identified in the predefined list during the advertising and scanning phases of the Bluetooth LE connection process. By allowing communication only with authorized and pre-approved devices, the Filter Accept List ensures that only bonded and authenticated devices can establish connections within the network. This approach effectively mitigates the risk of unauthorized access, thereby safeguarding the integrity and confidentiality of the data that are exchanged in the WSN.

By eliminating wired connections, the proposed system achieves greater flexibility in deployment, reduced installation complexity, and lower overall system weight, critical factors in aerospace applications. The distributed sensing capability enabled by wireless transmission ensures that impact events can be accurately detected and localized across composite structures. Furthermore, the ability to easily add new sensing nodes without modifying the core infrastructure makes the system highly adaptable for various monitoring scenarios.

4.2.4 Lightweight and Miniaturized Design

The proposed system is designed with a strong emphasis on miniaturization and lightweight construction, making it particularly well-suited for aerospace applications where weight constraints are critical. The weight of SHM systems directly impacts the overall efficiency and performance of aircraft, making it essential to develop a compact and lightweight sensing solution. The integration of PSN on a compact PCB ensures ease of deployment while maintaining the required

sensing and processing functionalities.

To achieve these objectives, the ANNA-B402 [101] RF microcontroller module was selected as the core processing unit, as it integrates both microcontroller and Bluetooth LE communication functionalities within a single ultra-compact package. This advanced module is built on the Nordic Semiconductor nRF52833 chip, which combines a high-performance RF core with an Arm Cortex-M4 processor. With a footprint of only $6.5 \times 6.5 \times 1.2$ mm, this module significantly reduces the space required for processing and wireless communication, eliminating the need for additional external RF modules, which would otherwise increase the overall PCB size and complexity. This integration enables a high level of miniaturization while preserving processing power and communication capabilities.

The PCB layout has been optimized for low-profile, lightweight implementation, following strict design constraints to minimize the overall form factor. The use of surface-mount components further enhances compactness and ensures a low-weight, highly efficient circuit board. The thin and lightweight PCB structure makes the system suitable for direct installation on composite aircraft structures without adding significant mass or bulk, which is crucial in applications where additional weight must be minimized.

By integrating sensing, processing, and wireless transmission within a single compact PCB, the system eliminates the need for bulky wiring or additional external hardware, significantly reducing both installation complexity and overall weight. This lightweight and self-contained design ensures that the system remains scalable and adaptable, making it highly effective for real-world aerospace applications where weight constraints and space efficiency are paramount.

4.2.5 Processing Capability (Decision-Making, Detection, Localization)

The proposed system integrates an advanced processing framework that enables real-time decision-making, impact detection, and localization of structural events. This capability is essential for assessing the health and integrity of composite structures under operational conditions.

The processing unit within each PSN is responsible for handling data acquisition, pre-processing, and wireless transmission. The system is designed to operate with minimal latency, ensuring that impact events are detected and processed efficiently. To achieve this, the microcontroller embedded within the PSN manages real-time data collection from the PZT sensors and converts the signals into digital format through a built-in ADC, and transmits the structured data packets to a central node.

At the central node, data packets are sent to a base station such as a PC to implement an ML-based impact localization algorithm. The system utilizes TDoA features in combination with ADC-based impact response data to estimate the impact location. A kNN model has been trained using controlled impact experiments, allowing the system to predict impact locations with high accuracy. This approach utilizes spatial information from multiple PSNs, improving the reliability of impact localization.

The decision-making process within the system follows a hierarchical structure:

1. **Local Event Detection:** Each PSN evaluates the incoming PZT sensor data using a programmable comparator to determine if the signal exceeds a predefined value.

2. **Wireless Data Transmission:** If an event is detected, the digitized sensor response and timestamp data are transmitted to the central node.

3. **Impact Localization:** The central node sends data to a PC through serial communication (UART). The developed GUI applies time-synchronized analysis in conjunction with PZT sensor data across multiple PSNs to estimate the impact location.

The ability to perform real-time impact detection and localization enhances the effectiveness of the system in SHM applications. With ML-based localization, the proposed system enables efficient monitoring of composite structures.

4.2.6 GUI for Data Processing

To facilitate efficient data acquisition, post-processing, and visualization, a dedicated GUI has been developed using Python. This GUI provides a flexible and user-friendly platform

for monitoring and analysing the data collected from the wireless sensing network. Unlike proprietary software solutions such as LabVIEW, the custom-developed GUI offers a cost-effective and adaptable alternative, specifically tailored to meet the requirements of passive sensing applications in SHM.

The GUI is designed to support real-time visualization of impact events and structural responses. With the wireless data transmission system, it ensures the efficient handling of sensor data packets received from multiple PSNs. The interface provides a direct means for users to assess the structural response without requiring additional post-processing tools such as MATLAB, thereby streamlining the workflow.

By implementing the robust data processing capabilities of Python, the GUI efficiently manages and processes large volumes of sensor data while maintaining a lightweight and responsive interface. Its customizable nature allows for modifications and expansions based on specific application needs, ensuring adaptability across different SHM scenarios. This development significantly improves the practicality of the proposed system by providing a streamlined and efficient approach to real-time data acquisition, processing, and impact analysis.

4.3 System Implementation

The proposed system was implemented on a two-layer PCB, with the design objective of achieving a compact form. To achieve this goal, components of minimal dimensions were selected, provided that they met the necessary performance criteria. In terms of physical dimensions, the circular PCB measures 28.4 mm in diameter, which corresponds to the size of a 2-pound coin, as illustrated in Fig. 4.4.

In addition to its compact size, the system is also remarkably lightweight. The developed PSN weighs only 3.7 grams in its basic configuration without a battery. When equipped with a coin-cell battery, the total weight increases to just 6.6 grams, making it highly suitable for applications requiring minimal weight.

Another notable aspect of this system is its affordability. The cost of producing a single PSN unit amounts to approximately £25, highlighting its potential for cost-effective deployment.

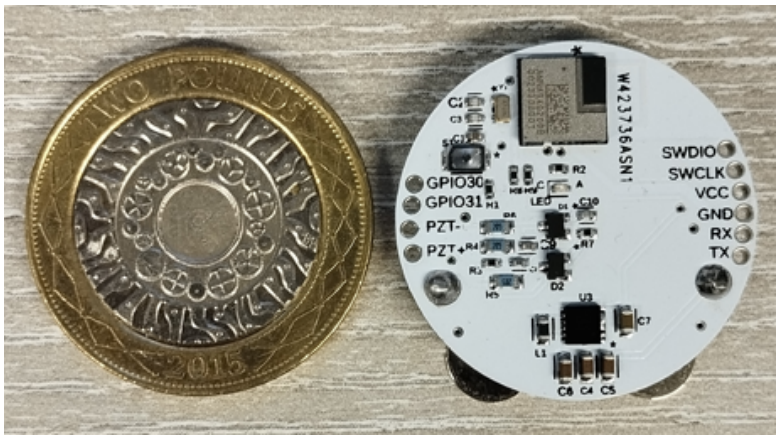


Figure 4.4: Comparison of PSN and £2 coin

A summary of these key specifications, including size, weight, and cost, is provided in Table 4.2.

All components of the system were carefully arranged on the top layer of the PCB, with the only exception being the battery holder, which was mounted on the bottom layer to optimize the overall layout and functionality. This arrangement was chosen to ensure effective use of the available space while maintaining the desired compact design.

To provide a comprehensive overview of the system structure, the block diagram of the PSN is illustrated in Fig. 4.5. Each functional block within the diagram is labelled with its specific role, enabling a clear understanding of how the various components contribute to the operation of the system.

The designed PSN consists of three primary functional modules, each developed to effectively execute the passive sensing process. These modules are illustrated in Fig. 4.6 and include the sensor circuit, which incorporates rectification and attenuation features; the power supply unit, which includes a buck-boost DC/DC converter; and the RF microcontroller, which integrates an ADC, a comparator and wireless communication capabilities.

In the sensor circuit, the sensing signal captured by a PZT sensor is initially in analog form and contains both positive and negative voltage components. However, MCUs cannot process

Table 4.2: The specifications of PSN

	Specifications
Diameter	28.4 mm
Weight	3.7 g
Cost	25 £

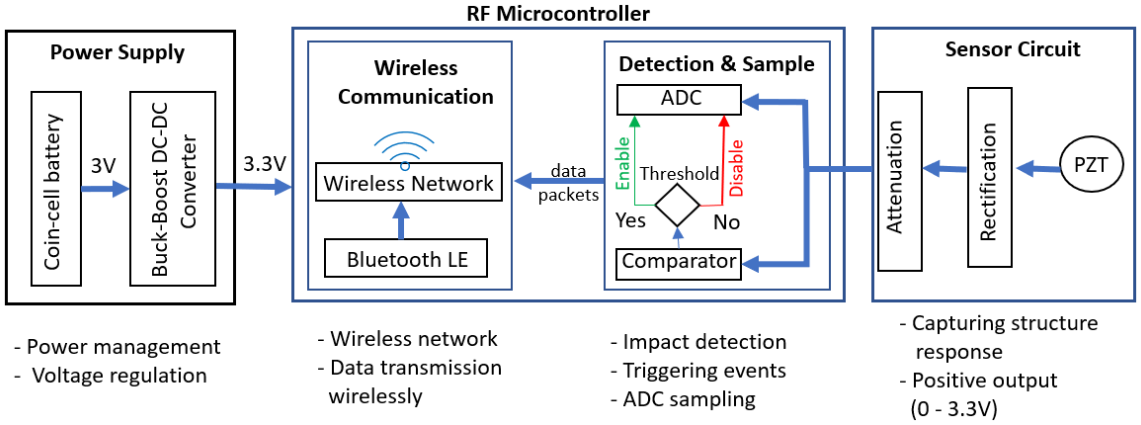


Figure 4.5: The system block diagram of the PSN with their functions

signals with negative voltages, requiring signal transformation before digital processing. To achieve this, a dedicated rectifying circuit is implemented to eliminate negative components. In addition, the signal is subjected to attenuation to limit its voltage within the operational range of the MCU. This step is crucial, as excessive voltage levels could potentially damage the MCU. By combining rectification and attenuation, the processed signal becomes suitable for safe and accurate digital processing by the microcontroller.

The system is powered by a CR-2032 coin-cell battery, which can be conveniently inserted into the battery holder located on the underside of the PCB. This compact design successfully accommodates all necessary functions while eliminating the need for external cable connections. The overall configuration ensures that the PSN is not only efficient, but also practical for applications that require minimal size and wireless operation.

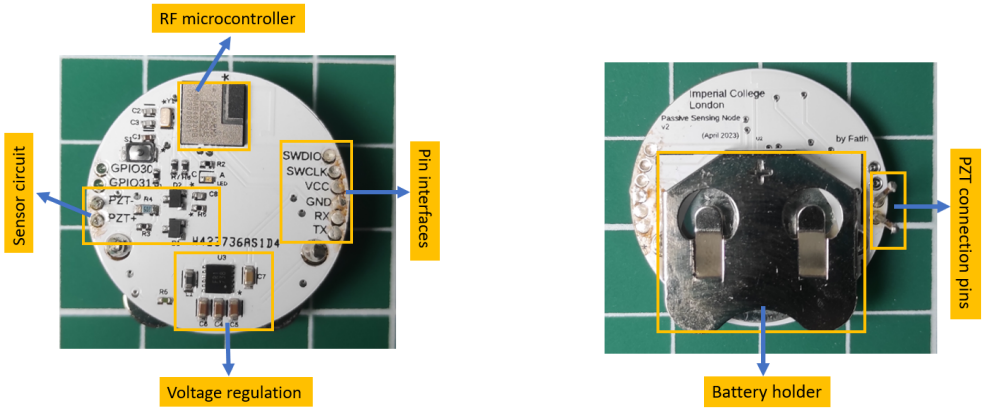


Figure 4.6: The modules of PSN, (a) Top view (b) Bottom view

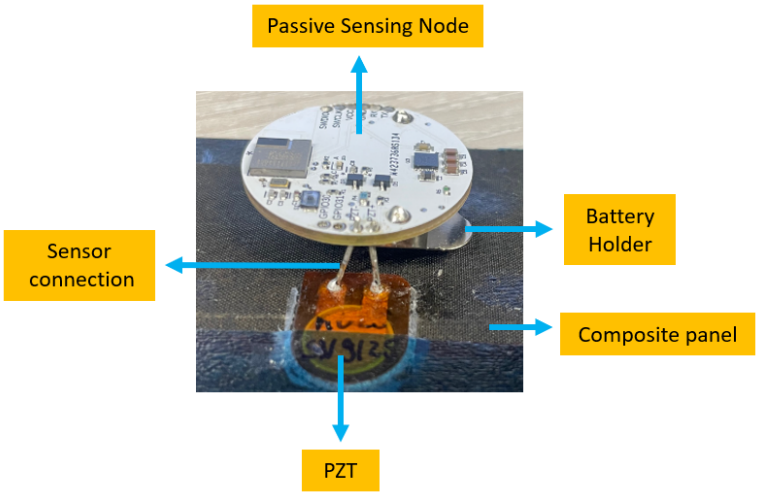


Figure 4.7: The installation of a peripheral PSN to the PZT sensor mounted on the composite panel

The passive sensing process and wireless communication using Bluetooth LE were experimentally evaluated to determine the overall performance of the system. During the experiments, a total of five PSNs were utilized. Four of these PSNs were installed on a composite panel, which functions as peripheral devices within the Bluetooth LE wireless network. The installation of one of the peripheral PSNs on the composite panel is illustrated in Fig. 4.7.

To establish the sensor connection between the PSNs and the PZTs, the two pads (+/-) on each PZT were soldered directly to their corresponding pins on the PSN. This method ensures that only two pins need to be soldered for the successful installation of each PSN onto the composite panel. This straightforward process significantly simplifies the installation and replacement of PSNs by avoiding the complexity of installing the wired system. This ease of implementation makes the system highly practical for real-world applications.

The proposed system has been developed with low power consumption as a fundamental design consideration. As a result, it can operate efficiently using a compact coin-cell battery, which provides sufficient energy to perform all essential tasks, including data acquisition and wireless communication. In the experimental setup, a CR2032 coin-cell battery was selected and used, as shown in Fig. 4.8.

The central PSN is connected to a computer via UART serial communication. This central device plays a key role in managing the wireless network, which it achieves by scanning for

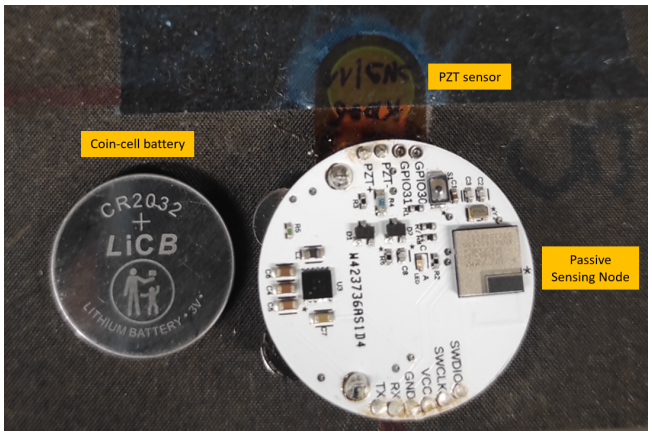


Figure 4.8: CR2032 coin-cell battery (3V, 240 mAh) used to supply power to each PSN

available peripheral devices and transmitting connection requests to establish communication.

In addition to initiating and maintaining the network, the central device has another crucial function: it serves as the primary clock of the system. By generating and distributing synchronization packets, it ensures that all peripheral devices in the network operate with synchronized timing, which is essential for coordinated data acquisition and communication.

To interface with a PC, the central PSN is linked through a USB-to-TTL converter, enabling proper communication between the PSN and the computer. The connection setup is illustrated in Fig. 4.9.

The process of verifying time synchronization within the wireless network was conducted by monitoring the behaviour of a GPIO pin available on both the peripheral and the central devices. This specific pin was assigned as a debug pin. The debug pin toggles its state under the control of the timer, which functions as a shared clock across the network.

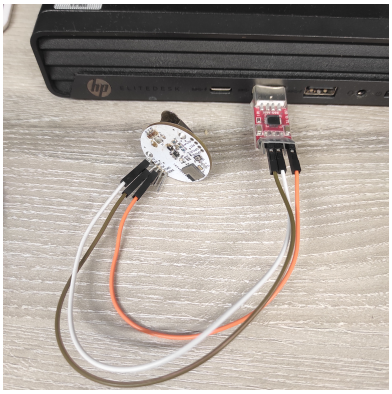


Figure 4.9: The central PSN connected to the PC with USB-TTL converter

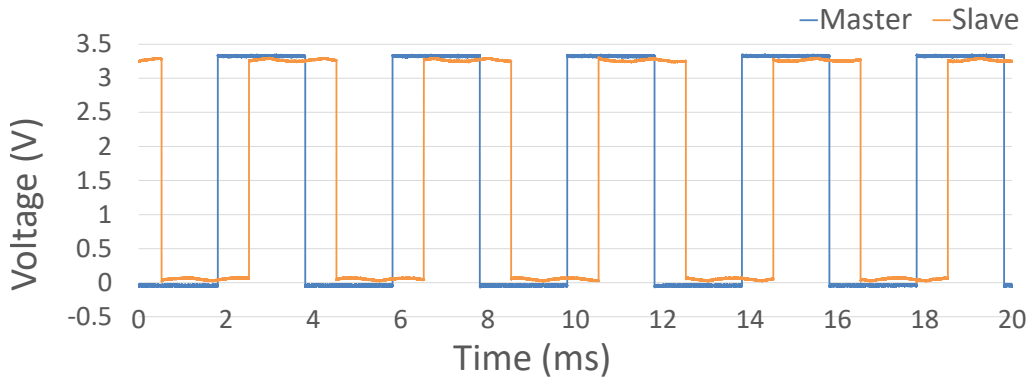


Figure 4.10: Non-synchronous timers of master (central) and slave (peripheral) devices

To assess synchronization accuracy, the outputs of the toggling debug pins on the central PSN and the peripheral PSN devices were compared. This comparison allowed for the detection of any timing differences between the devices. The verification procedure was carried out using a digital oscilloscope, specifically the TiePie Handyscope HS5, which enabled precise observation and analysis of the timing signals. This approach ensured that the synchronization mechanism within the network was functioning as intended.

When time synchronization is not enabled within the wireless network, the synchronization timers of the central and peripheral devices operate independently, resulting in a lack of coordination between them. This asynchronous behaviour is clearly demonstrated in Fig. 4.10, which highlights the disparity. In this scenario, the debug pins of the central and peripheral devices fail to toggle simultaneously, indicating the absence of synchronization across the network.

When the central device transmits synchronization packets, the peripheral devices use the information contained in these packets to update their local timers accordingly. This synchronization process is performed periodically at a defined interval, ensuring that the devices maintain coordinated timing within the network. The frequency at which these synchronization packets are transmitted can be configured within the application code, providing flexibility for different operational requirements.

Once synchronization is established, a shared clock is successfully implemented across the wireless network. The effectiveness of this synchronization can be observed by monitoring the debug pins of the devices. When synchronized, the debug pins toggle simultaneously, as

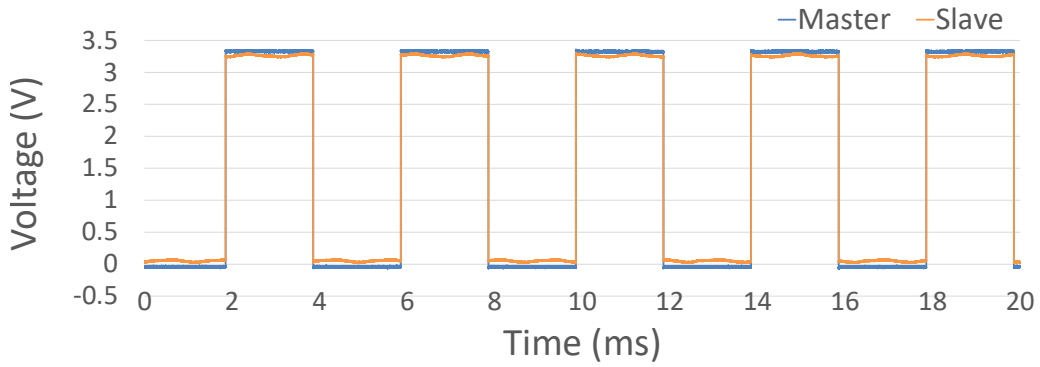


Figure 4.11: Synchronous timers of master (central) and slave (peripheral) devices

illustrated in Fig. 4.11. The comparison is made by examining the overlap of the vertical signals, where the toggling times indicate successful synchronization.

It is important to note that slight variations in the minimum and maximum voltage levels between the devices may occur. These differences are attributed to the use of different voltage sources, which can influence precise output levels but do not affect the overall synchronization accuracy.

The difference in timing between the signals of the central device and the peripheral devices within the wireless network, under conditions of time synchronization, is illustrated in Fig. 4.12. This figure provides a clear representation of the slight temporal offset that exists between the devices.

According to measurements taken using the oscilloscope, this difference is approximately 100 nanoseconds. This minor variation indicates the level of precision achieved by the synchronization mechanism. Although devices are highly synchronized, the observed time offset may result from factors such as signal propagation delays, hardware processing times, or inherent limitations in clock accuracy. However, the small scale of this time difference demonstrates the effectiveness of the synchronization process in maintaining closely coordinated timing across the network.

To improve the wireless communication process using Bluetooth LE, several protocol specifications were adjusted, including changes to Physical Layer (PHY) radio modes, data length parameters, and Maximum Transfer Unit (MTU). Moreover, the memory buffers on both the peripheral and central devices must be updated appropriately to achieve data exchange properly. Failure to update these buffers can result in loss of data during wireless transmission between peripheral and central devices. These buffers play a critical role in ensuring that all data

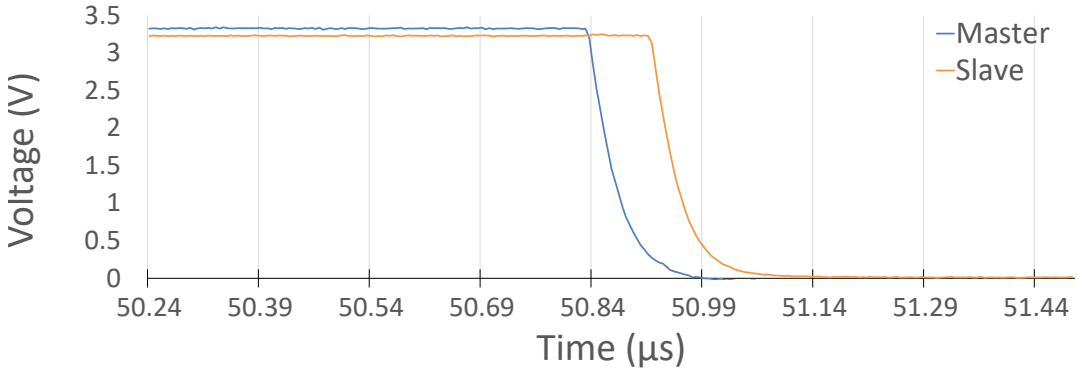


Figure 4.12: Time difference between master (central) and slave (peripheral) devices

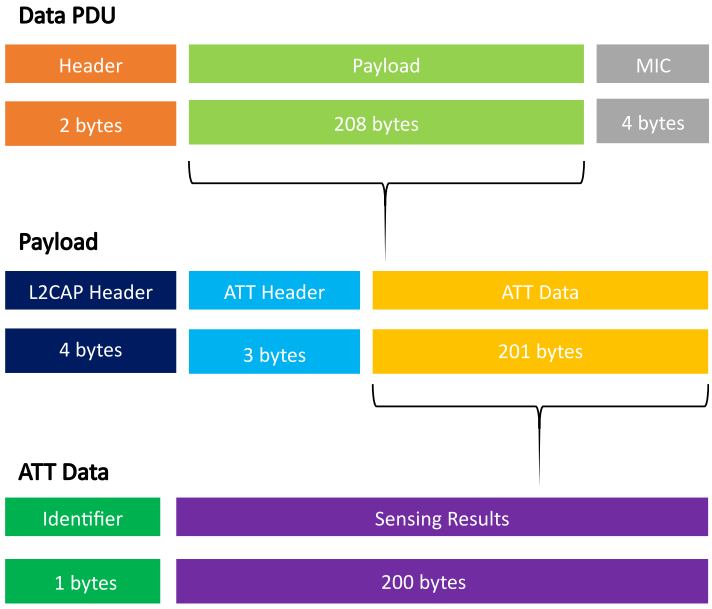


Figure 4.13: Bluetooth LE packet created to wirelessly transmit sensing results

transmitted over the air are properly stored, preventing any loss of information during the communication process.

The various components of the Bluetooth LE data packet, created to transmit the sensing results, are illustrated in detail in Fig. 4.13. Each data packet contains specific headers, as specified by the requirements of wireless communication protocols. For this application, sensing results up to 200 bytes in size can be included within each data packet. Additionally, a 1-byte unique identifier is appended to each packet to distinguish the source PSN transmitting the data packets. Alongside these headers and the sensing data, a complete Protocol Data Unit is formed, preparing the packet for transmission over the Bluetooth LE network.

In this experiment, one of the protocol specifications that was modified is the PHY radio mode. The default PHY mode, referred to as 1M PHY, operates at a data rate of 1 megabit per second (1 Mbps) and is universally supported by all Bluetooth LE devices. Beyond this standard mode, Bluetooth version 5.0 introduced two additional radio modes: 2M PHY and Coded PHY. Each of these modes addresses different purposes depending on the requirements of the application. For example, the 2M PHY mode is advantageous when faster data transmission is required, as it doubles the data rate to 2 Mbps. However, this mode comes with trade-offs, including increased power consumption and a reduced communication range. In contrast, the Coded PHY mode is optimized for extending the communication range, but it achieves this at the expense of a lower data rate compared to the other modes. In the context of this study, the 2M PHY mode was selected because the application involves the wireless transmission of a significant volume of sensing data.

The MTU and the data length are two distinct parameters in Bluetooth LE communication, although they are often closely related in practice. The MTU specifies the maximum number of bytes that can be transmitted in a single Generic Attribute Profile (GATT) operation, while the data length defines the maximum number of bytes that can be included in a single Bluetooth LE packet. If the MTU exceeds the data length, the data are fragmented into smaller segments for transmission. In contrast, transmitting all data in a single packet improves efficiency by reducing the number of bytes sent over the air. This is because each Bluetooth LE packet contains a 3-byte header, and minimizing the number of packets reduces the overhead, ultimately saving time and energy. These improvements result in higher throughput for the Bluetooth LE connection.

In this study, to improve the efficiency of wireless data transmission, the MTU and data length were updated to their respective maximum allowable values of 247 and 251 bytes. Following these adjustments, the data packet size and the corresponding buffer sizes were configured to accommodate 201 bytes, which includes a 1-byte unique identifier for each packet. This setup enables efficient wireless transmission of passive sensing results with the updated system specifications.

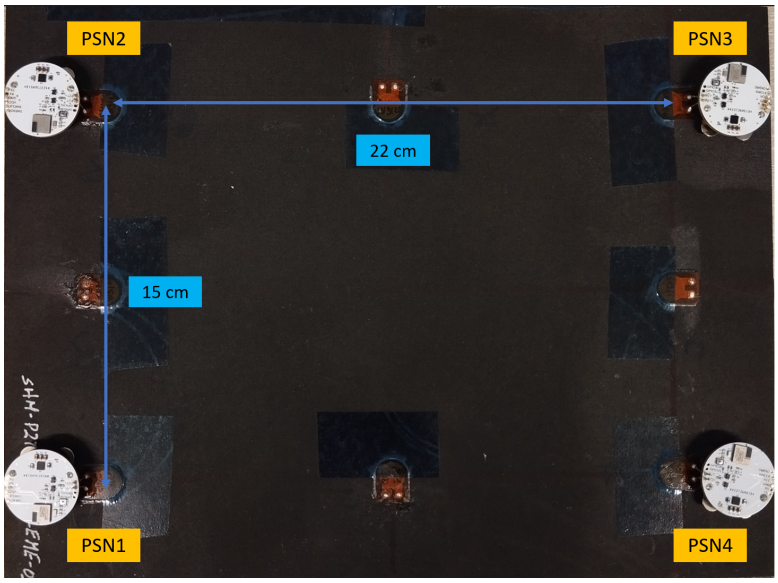


Figure 4.14: PSNs and the distance between the sensors

4.4 PSN Performance Evaluation

The performance of the PSN was systematically evaluated at every stage of the process, covering data acquisition, wireless transmission, time synchronization, and data visualization. When an event, such as an impact, is detected by the PZT sensor, signal processing begins by removing the negative portion of the sensing signal. The positive portion is then attenuated to ensure that it remains within a range that the MCU can handle. If the voltage of the processed signal exceeds a predefined threshold value, the system is awakened by the built-in comparator.

Once the comparator activates the system, a timestamp is immediately captured from the shared clock, and the ADC peripheral is triggered to sample the sensing signal simultaneously. After the sampling process is complete, the digitized sensing signal along with the timestamp is packaged into data packets and transmitted wirelessly to the central device using Bluetooth LE.

In this experimental setup, the central device receives these data packets from four separate PSNs on composite plate as shown in Fig. 4.14. Subsequently, the central device forwards the received packets, which include both the sampled sensing signals and their corresponding timestamps, to a PC. On the PC, the transmitted data are processed and displayed in real-time as plotted signals. In addition, all data received are saved to a specified directory on the PC. This is achieved through a custom-developed GUI. This comprehensive process ensures effective collection, transmission, and analysis of the sensing data at all stages of the experiment.

4.4.1 Integrated GUI for PSN

An image of the GUI panel is presented in Fig. 4.15, which illustrates the user interface developed for managing communication and data processing tasks. The panel includes two drop-down menus that allow users to select the appropriate port and baud rate to establish serial communication between the central device and the PC. This setup enables efficient data exchange between the two devices. The timestamps from the four wireless sensor nodes are displayed in microseconds, providing precise temporal information for each event.

The GUI includes several interactive buttons to control various functions. The "Start Serial" and "Stop Serial" buttons are used to initiate or terminate the serial communication channel, ensuring proper operation during data transfer. Another important feature is the "Select Save Directory" button, which allows users to choose a specific directory on the PC to store the received timestamp and ADC data.

The interface also integrates machine learning functions. The "Start Training" button initiates the system training process using the kNN machine learning method. Once the model is trained, the "Load Model" button enables users to upload both the trained model and the associated training data for subsequent tasks. After loading the model, the "Estimate Impact Location" button becomes active, allowing users to begin the process of estimating the impact locations based on the available data.

In cases where the necessary data are not fully collected, for example, if an impact fails to trigger all sensor nodes, the "Reset Buffers" button is provided. This feature allows the user to clear and refresh the data buffers, enabling another attempt at data collection for both system training and impact location estimation. This design ensures flexibility and reliability in handling incomplete data scenarios.

4.4.2 Acquisition and Digital Conversion of Passive Sensing Signals with GUI-Based Visualization

In this experiment, passive sensing signals are captured and digitized using an ADC configured with a sampling rate of 200 kHz and a resolution of 8 bits. As a result, the ADC outputs digital

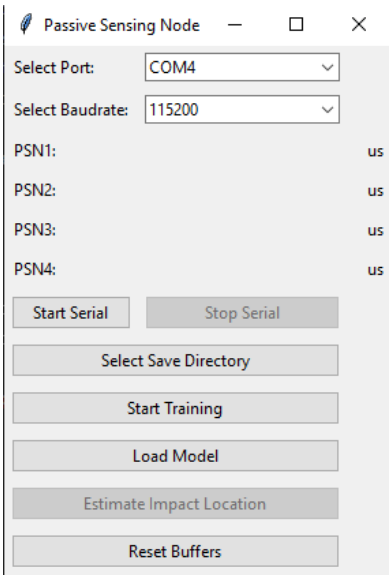


Figure 4.15: The developed GUI for PSN

values represented as unsigned 8-bit integers, which can range from 0 to 255. These digital values correspond to the sampled amplitude of the input signal and are used to quantify the voltage levels.

To interpret the ADC output in terms of voltage, a mathematical conversion is applied. This conversion maps the digital values back to their corresponding voltage levels, using the following formula given by

$$V_{conv} = \frac{D \cdot V_{ref}}{2^n \cdot G} \tag{4.1}$$

where V_{conv} is results of the voltage after conversion, D is the digital output of ADC, V_{ref} is the internal reference voltage of ADC, n is the resolution, and G is the gain of ADC. n is 8 due to 8-bit resolution as specified before. V_{ref} and G are, respectively, set to 0.6 V and 1/6 in the ADC configuration settings of the microcontroller.

The ratio V_{ref}/G also determines the input range of the ADC. Therefore, the input range, $[(0.6V)/(1/6)]$, is 3.6 V for the ADC of the microcontroller. Using information, the input range for the passive sensing signal can also be calculated in the PSN system. To achieve this, the attenuation level should be considered. The attenuation level is set to 2 in the sensor circuit, which results in the passive sensing signal being captured up to approximately 8 V using PSN.

Impacts are applied to the composite panel equipped with PSNs using a hammer to simulate

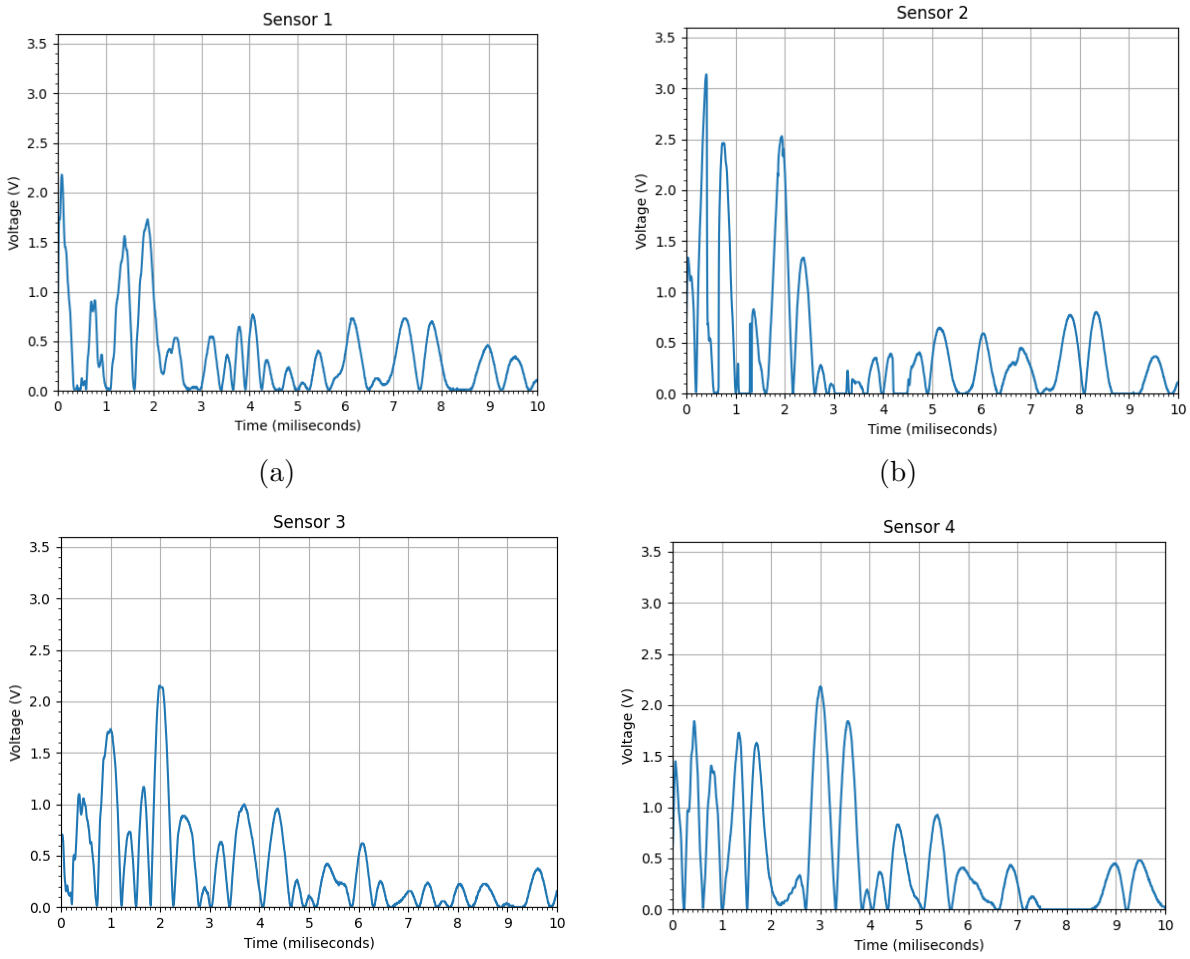


Figure 4.16: Wirelessly-Transmitted Passive Sensing Results, (a) PSN 1 (b) PSN 2 (c) PSN 3 (d) PSN 4

events for testing and evaluation purposes. Following these impacts, the passive sensing signals and corresponding timestamps are successfully transmitted from the four PSNs to the central device. The transmitted data, which include the sensing results and time information, is then processed and visualized using the GUI. The GUI effectively displays the results, as demonstrated in Fig. 4.16, providing a clear and comprehensive representation of the signals and timestamps collected during the experiment.

The developed GUI provides the functionality to plot the sensor data transmitted by each PSN individually. This feature is particularly important because not all PSNs may be triggered during an impact event, especially if the impact occurs at a location far from a specific sensor. In such scenarios, the signal amplitude may fall below the predefined threshold value, preventing the PSN from activating and initiating signal sampling.

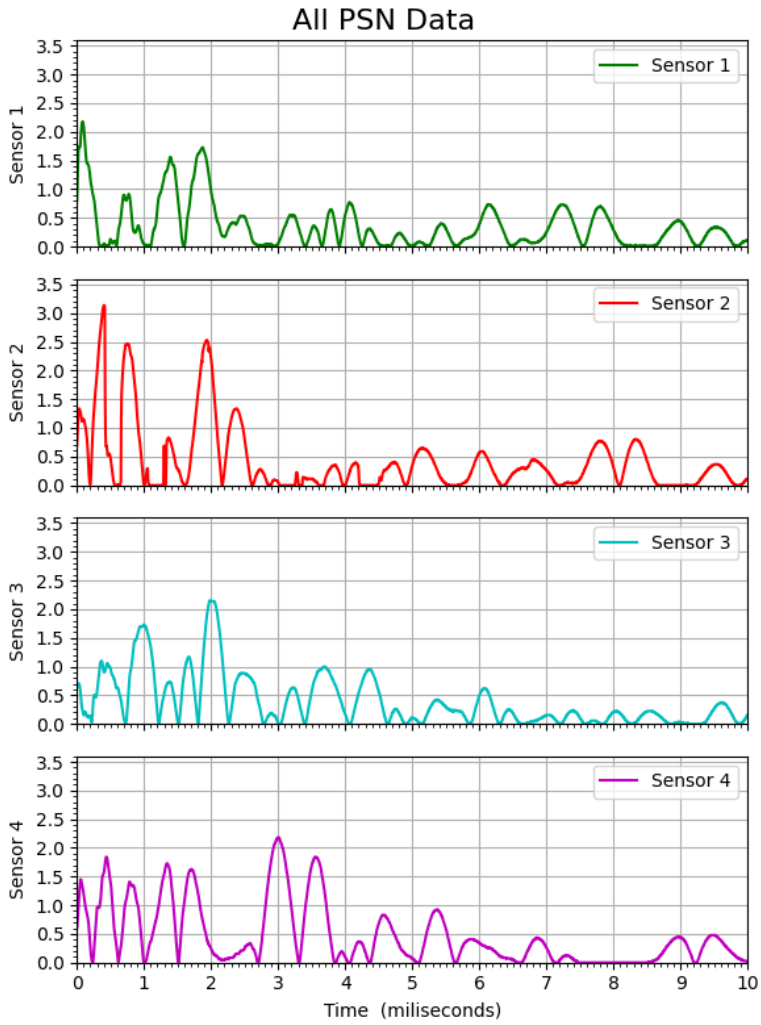


Figure 4.17: All PSN Data

On the other hand, when all PSNs successfully capture and transmit their respective sensor data, the GUI is capable of plotting all the data together on a single graph. This combined visualization allows for a more straightforward comparison of the signals from different PSNs. An example of such a graph combining data from all PSNs into one display, is shown in Fig. 4.17. This dual functionality ensures that the GUI provides flexibility in data representation, accommodating both individual and collective analyses of the sensing results.

4.4.3 Comparative Validation of PSN Measurements Against Digital Oscilloscope Data

The accuracy and effectiveness of the proposed system were validated by performing a comparative analysis with the performance of a digital oscilloscope (TiePie Handyscope HS5). To ensure consistency and compatibility between the measurements, several settings of the oscilloscope were configured to match those used in the PSN. Specifically, the oscilloscope was set to operate with an 8-bit resolution and a sampling rate of 200 kHz, identical to the parameters employed in the PSN system.

In addition, the trigger level of the oscilloscope, used as the threshold for signal detection, was adjusted to correspond to the threshold voltage of the PSN system. Given the attenuation level of 2 in the sensor circuit, the threshold value on the oscilloscope was set to 1.2 V, which is equivalent to the PSN threshold voltage of 0.6 V multiplied by the attenuation level. This alignment of settings ensured a meaningful comparison between the proposed system and the oscilloscope, providing a reliable basis for evaluating the system performance.

To conduct a comparison between the results, the PZT sensor was simultaneously connected to both the oscilloscope and the PSN. This setup ensured that both systems recorded the same impact event under identical conditions. The impact was generated with a hammer and the resulting signal was captured by both devices.

The captured signal from the oscilloscope was saved using its dedicated software tool. Meanwhile, the signal captured by the PSN was wirelessly transmitted to the central device. From there, it was processed and stored using the GUI developed for this system.

The data collected from the oscilloscope are presented in Fig. 4.18, while the corresponding data obtained from the PSN is illustrated in Fig. 4.19. These visualizations provide a clear basis for comparing the performance of the two systems in capturing and processing the same sensing signals.

To compare the results, only the positive portion of the signal recorded by the oscilloscope is considered, as the PSN system processes signals with the negative portion removed. To ensure consistency in the comparison, the signal obtained from the PSN is scaled by multiplying it with

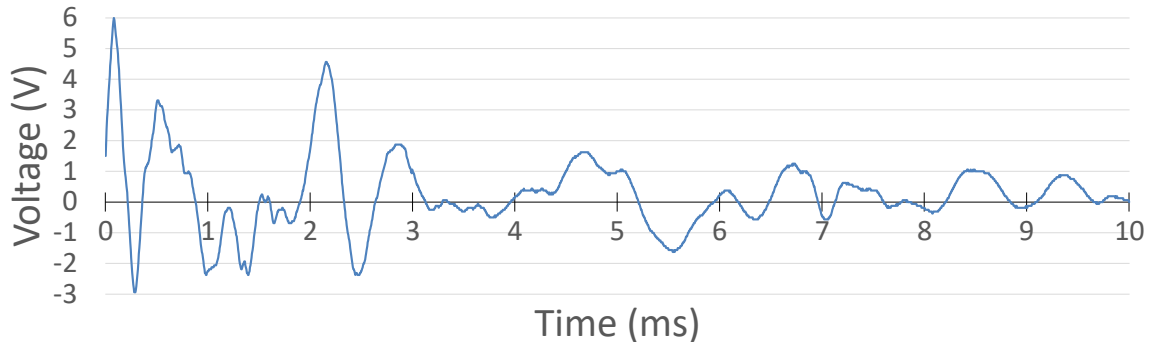


Figure 4.18: Digital oscilloscope result

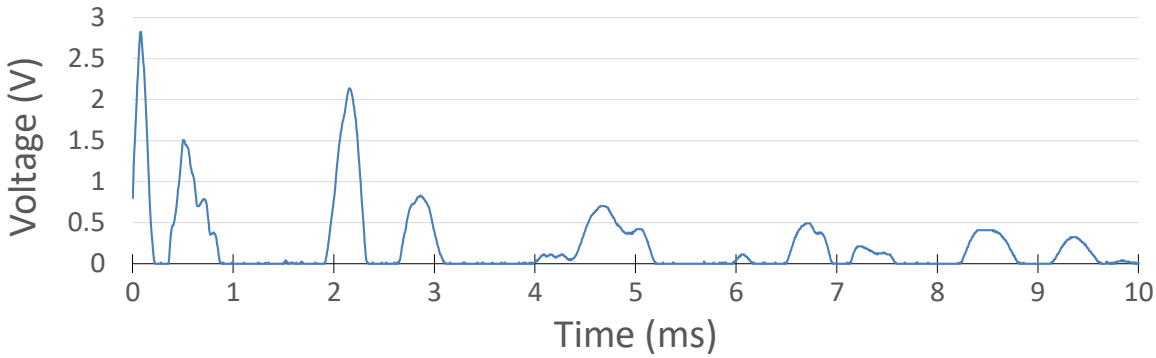


Figure 4.19: PSN result

the attenuation factor, which is set to 2. The resulting comparison is illustrated in Fig. 4.20.

As shown in the figure, the signal patterns from both systems are identical, demonstrating a high degree of agreement in their respective waveforms. The signals are closely matched in the time domain, validating their temporal precision. Although there is a slight variation in amplitude between the two, this difference is minimal and does not significantly affect the overall comparison. These results validate the capability of the PSN system to accurately capture and transmit sensing data comparable to that of the oscilloscope.

The comparison test was also conducted for other PSNs positioned at different locations on

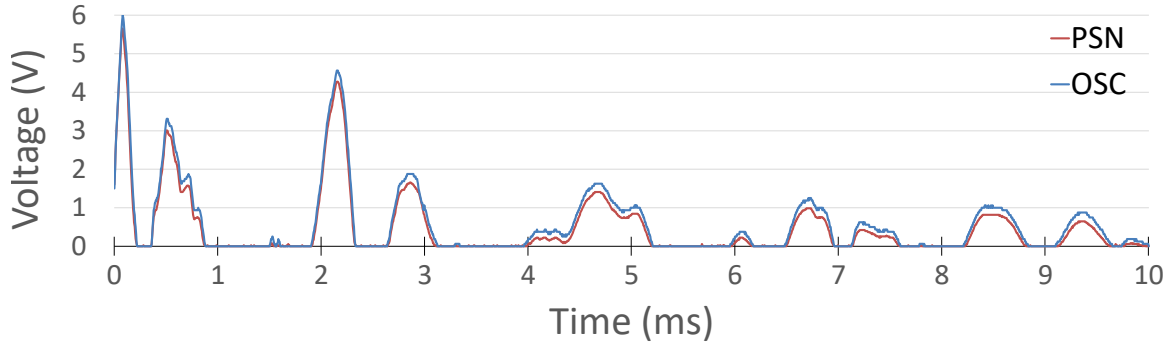


Figure 4.20: The comparison of the oscilloscope and PSN data

Table 4.3: Timestamps and TDoA in the event of impact around each sensor

	Impact 1		Impact 2		Impact 3		Impact 4	
	Timestamp	TDoA	Timestamp	TDoA	Timestamp	TDoA	Timestamp	TDoA
PSN 1 (μs)	55683878	0	156390678	257	236497760	922	274343172	295
PSN 2 (μs)	55684205	327	156390421	0	236497265	427	274343530	653
PSN 3 (μs)	55684386	508	156390873	452	236496838	0	274343150	273
PSN 4 (μs)	55684224	346	156391073	652	236497295	457	274342877	0

the composite plate, producing highly consistent results. These findings further validate the robustness and reliability of the PSN system in accurately capturing and processing impact signals.

4.4.4 Timestamp Acquisition and TDoA Analysis in Impact Testing

When an impact occurs on the composite panel, a timestamp is captured from the shared clock within the wireless network, alongside the passive sensing signal. This timestamp is recorded in microseconds to enable a more precise observation of the TDoA for each PZT sensor. The timestamp in microseconds is stored as a 64-bit integer to prevent overflow and ensure accurate timekeeping.

To evaluate the performance of the shared clock and the time synchronization mechanism within the wireless network, deliberate impacts were applied near each sensor using a hammer. Following each impact event, the corresponding timestamps were transmitted wirelessly to the central device for analysis. The recorded timestamps for sensors 1 through 4, as received by the central device, are demonstrated in Table 4.3.

The results in the table confirm the expected behavior of the system: the timestamp consistently exhibits the smallest value for the sensor located closest to the point of impact. These results demonstrate the accuracy and reliability of the shared clock and synchronization within the wireless network.

4.4.5 Power Consumption

The energy efficiency of the PSN is critical to ensure an extended operational lifetime. To quantify the power consumption of the system, current measurements were performed using the

Table 4.4: Measured current consumption under different operating conditions

Operating Condition	**Current Consumption**
Standby (No wireless connection)	45 μA
Time synchronization	1.3 mA
Impact Detection (Wireless transmission active)	6.7 mA

Digital Multimeter 34465A from Keysight. These measurements were performed under three distinct operating conditions that represent the typical states of the PSN:

1. **Standby Mode:** In this state, the sensor node is maintained in a low-power sleep mode with no active wireless connection or data transmission. This condition reflects the baseline energy consumption when the system is idle.

2. **Time synchronization:** In this mode, the PSN has successfully established a wireless link, and time synchronization is maintained across the network. The increased activity associated with maintaining connectivity results in higher power usage compared to the standby state.

3. **Impact Detection:** During this condition, the sensor node is fully active, processing the impact event, triggering the ADC for signal sampling and transmitting data wirelessly. Power consumption remains constrained until all data packets are transmitted in milliseconds, which includes the total energy required for acquisition, processing, and communication.

Table 4.4 summarizes the measured current consumption for each operating condition. These measurements are fundamental for assessing the overall energy requirements of the PSN.

To calculate power consumption, the fundamental electrical formula can be expressed as

$$P = I \cdot V \tag{4.2}$$

where P is power in watts (W), I is current in amperes (A), V is voltage in volts (V). PSN operates at a supply voltage of 3.3 V. Using this voltage, the power consumptions are calculated and presented for each mode in Table 4.5.

Table 4.5: Power consumption under different operating conditions

Operating Condition	**Power Consumption**
Standby (No wireless connection)	148.5 μW
Time synchronization	4.29 mW
Impact Detection (Wireless transmission active)	22.11 mW

4.4.6 Range Testing

The appropriate range in wireless communication is critical to successfully transmit data between peripheral and central devices in the network. The wireless communication range is influenced by factors including the modulation scheme (e.g., standard 1M PHY versus long-range coded PHY), transmit power, and the propagation environment, where real-world conditions such as absorption and reflection can significantly degrade signal strength. Furthermore, antenna orientation and type further affect the effective range achieved [38, 98].

To evaluate the communication range in the proposed system, all experiments were conducted outdoors under line-of-sight conditions to minimize multipath fading and signal absorption effects that are typically encountered indoors.

To determine the maximum reliable distance, the devices initially established a communication link. The peripheral and central nodes were then gradually separated while maintaining the connection. The test concluded when the connection can no longer be re-established, using the LED on the PSN as a visual tool indicating the connection status.

In this evaluation, the effective communication range was examined using different levels of radio transmission power and modulation schemes. Two TX power levels (0 dBm and +8 dBm) were tested alongside three modulation schemes: Coded PHY, 1M PHY, and 2M PHY. The lower TX power setting serves as a baseline measurement for the radio sensitivity, while the higher TX power setting is used to examine potential range extension. Furthermore, comparing the modulation schemes provides insight into the range improvements achieved with advanced long-range coding techniques. Table 4.6 summarizes the measured range performance for each combination.

Table 4.6: Effective Communication Range for Different TX Powers and Modulation Schemes

TX Power	**Coded PHY**	**1M PHY**	**2M PHY**
0 dBm	65 m	35 m	20 m
+8 dBm	170 m	95 m	50 m

4.5 Impact Localization

The proposed system consists of wireless sensor nodes that are responsible for recording data generated by impact events. Each sensor node, called the PSN, is designed to capture the timestamp of an impact event along with the corresponding ADC signals. Once these data are collected, they are wirelessly transmitted to the central device within the network.

The central device serves as the hub for collecting all data received from the individual sensor nodes. After gathering the information, it promptly forwards the collected timestamps and ADC signals to a central station via a serial port interface. This ensures that the acquired data are available for further processing, analysis, or visualization at the central station.

This application incorporates a total of four PSNs and one central device to maintain and manage the wireless network. The PSNs are strategically positioned at the four corners of the panel to ensure adequate coverage for data collection. Impact data is collected from 17 distinct points evenly distributed across the surface of the panel.

These 17 points represent the locations where impact data are recorded for training purposes, enabling the system to effectively learn and predict the relationships between impact positions and the corresponding sensor data. This process, including training and impact location estimation, was achieved with the ML-based kNN algorithm. The kNN algorithm is a supervised learning method used for classification and regression. In the context of impact localization, the kNN regression estimates the coordinates of an unknown impact by finding the k nearest training samples in the feature space and averaging their positions.

For a given test sample, the predicted impact location y_{pred} is computed with the following equation given by

$$\mathbf{y}_{\text{pred}} = \frac{1}{k} \sum_{i=1}^{k} \mathbf{y}_{(i)} \tag{4.3}$$

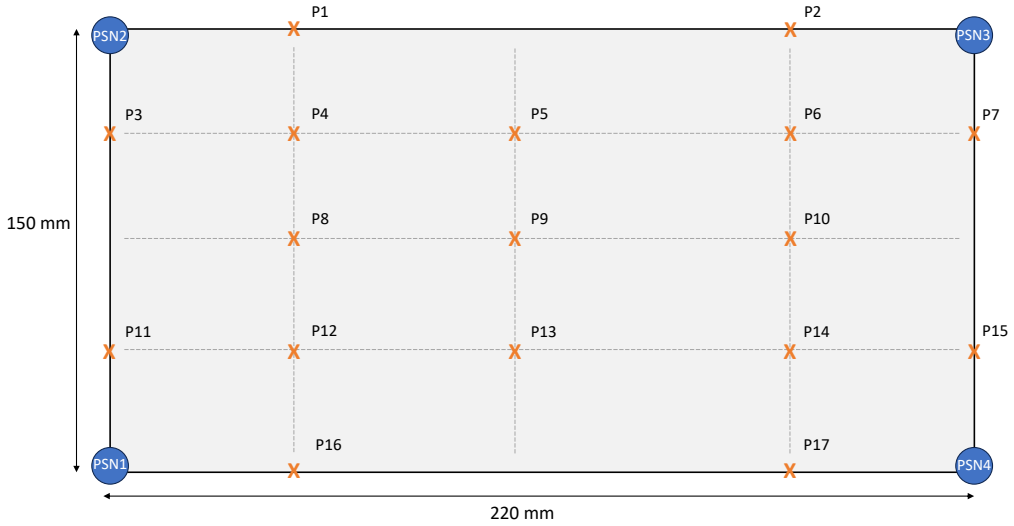


Figure 4.21: Impact estimation training setup

where k is the number of nearest neighbours, $y_{(i)}$ represents the known coordinates of the n-th nearest neighbour.

The neighbours are determined on the basis of the smallest Euclidean distance between the feature vectors. The Euclidean distance d between two feature vectors x_1 and x_2 is calculated with the following equation defined as

$$d(\mathbf{x}_1, \mathbf{x}_2) = \sqrt{\sum_{j=1}^{n} (x_{1,j} - x_{2,j})^2} \tag{4.4}$$

where n is the number of features in the feature vector.

The placement of the PSNs at the corners of the panel, along with the distribution of the 17 training points, is illustrated in Fig. 4.21. This arrangement highlights the experimental setup, which is designed to ensure reliable data collection for the ML model while maximizing the accuracy of the system performance.

Fig. 4.22 shows the kNN-based impact localization for different k ($k = 1, 2, 3$) values, demonstrating how the kNN model is used to estimate an unknown impact location based on learned training data. A smaller k can make the estimation more sensitive to noise, while a larger k can cause overly smoothed estimations, potentially reducing precision.

In the context of feature extraction for this application, two distinct types of feature are utilized to determine the localization of impacts: TDoA and ADC signal values. These features

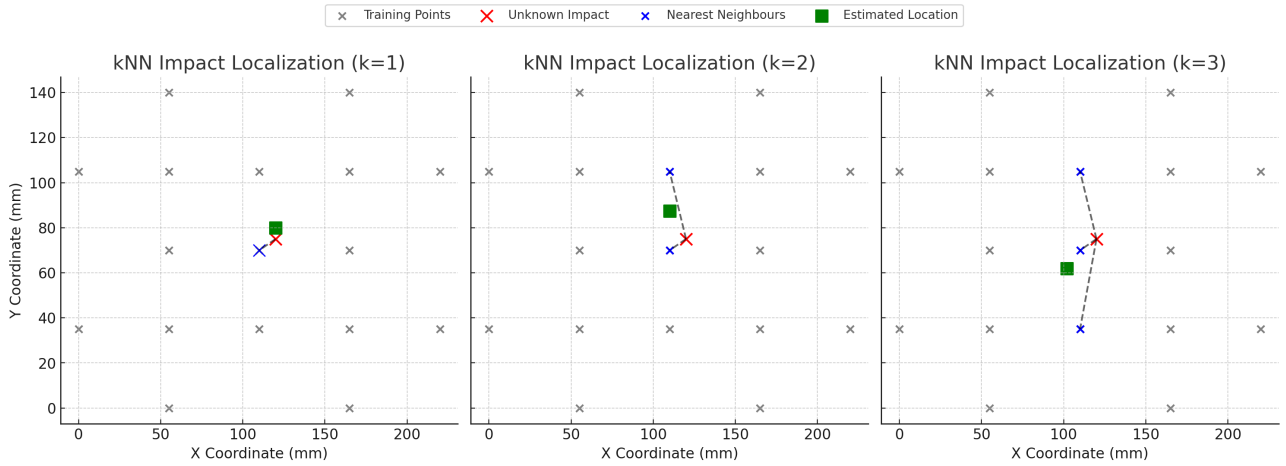


Figure 4.22: Visualization of kNN-based impact localization for different k values

are combined into a well-organized format to serve as input for training the impact localization model. Specifically, the extracted features are structured into a unified vector representation that integrates both the TDoA and the ADC signal values associated with each impact event.

This standardized feature vector provides a consistent framework for describing impact events, enabling the system to effectively process the data for machine learning purposes. Once the feature vectors are prepared, they are used to train the kNN model, which is designed to estimate the location of future impacts based on the learned relationships between the input features and their corresponding spatial positions.

For every impact event, the timestamp corresponding to the arrival of the impact signal is recorded at each sensor in the network. To extract meaningful spatial information about the impact location, the TDoA values are calculated for unique pairs of sensors. These TDoA values capture the relative differences in signal arrival times between sensors, providing critical data about the spatial distribution of the impact signal across the sensor array.

In this setup, TDoA values are calculated for six unique pairs of PSNs. The computed TDoA values are organized into a six-dimensional vector, represented as $TDoA = [PSN1 - PSN2, PSN1 - PSN3, PSN1 - PSN4, PSN2 - PSN3, PSN2 - PSN4, PSN3 - PSN4]$. Each element of this vector corresponds to the time difference between signal arrivals at two specific sensors in the array.

The ADC signal values provide essential information about the amplitude of the detected impact signal at each sensor. These values are characterized by two key metrics: the peak and

the average of the ADC results for each sensor. For every sensor in the network, the peak and average ADC values are calculated based on the sampled signal generated by the impact event.

In the case of four PSNs, this process results in eight distinct ADC values, two for each sensor. These values are organized into an eight-dimensional vector, expressed as ADC =[$Peak_1$, Avg_1, $Peak_2$, Avg_2, $Peak_3$, Avg_3, $Peak_4$, Avg_4]. Each entry in the vector represents either the peak or average ADC result from a specific sensor, with $Peak_n$ and Avg_n corresponding to n-th the sensor.

A combined feature format is used for the purpose of training the machine learning model. In this format, the training data for each impact point is constructed by integrating the TDoA and ADC feature vectors, which incorporate both temporal and amplitude-related information about the impact event.

This integration results in the creation of a 14-dimensional feature vector for each recorded impact event. The combined feature vector is represented as $FeatureVector = [TDoA, ADC]$, where the six-dimensional TDoA vector provides information about the relative arrival times of the impact signal at the sensors, and the eight-dimensional ADC vector represents the amplitude characteristics of the detected signal, including the peak and average values for each sensor.

During the training phase, each feature vector is associated with the corresponding coordinates (x, y) of the known impact location. This pairing ensures that the spatial position of each impact is accurately mapped to its respective feature vector. The kNN algorithm utilizes these feature vectors to analyze and learn the spatial relationships present in the timing and amplitude data. Identifying patterns within the training dataset, the model develops the ability to estimate the location of new impact events by comparing their feature vectors to those stored in the training dataset. The robustness of the KNN model can be enhanced by increasing the size of the training data set, which can involve repeating measurements or introducing additional impact points.

The trained kNN model is subsequently employed for the real-time localization of impact events. When a new impact is detected, the system immediately captures the TDoA and ADC values from each sensor, processing these data in real-time to estimate the location of the impact. The estimated location is then displayed, providing a continuous and dynamic visualization of

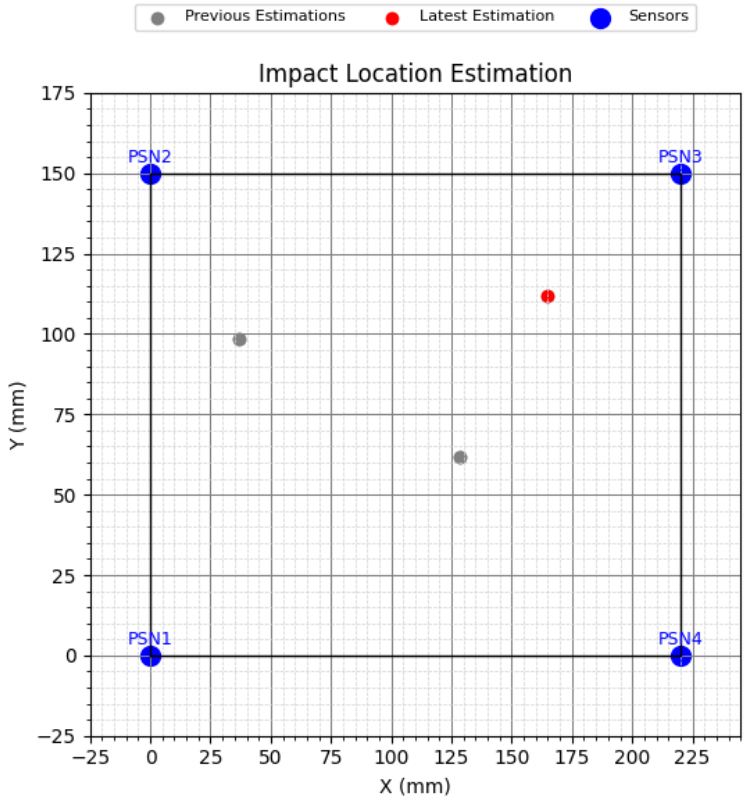


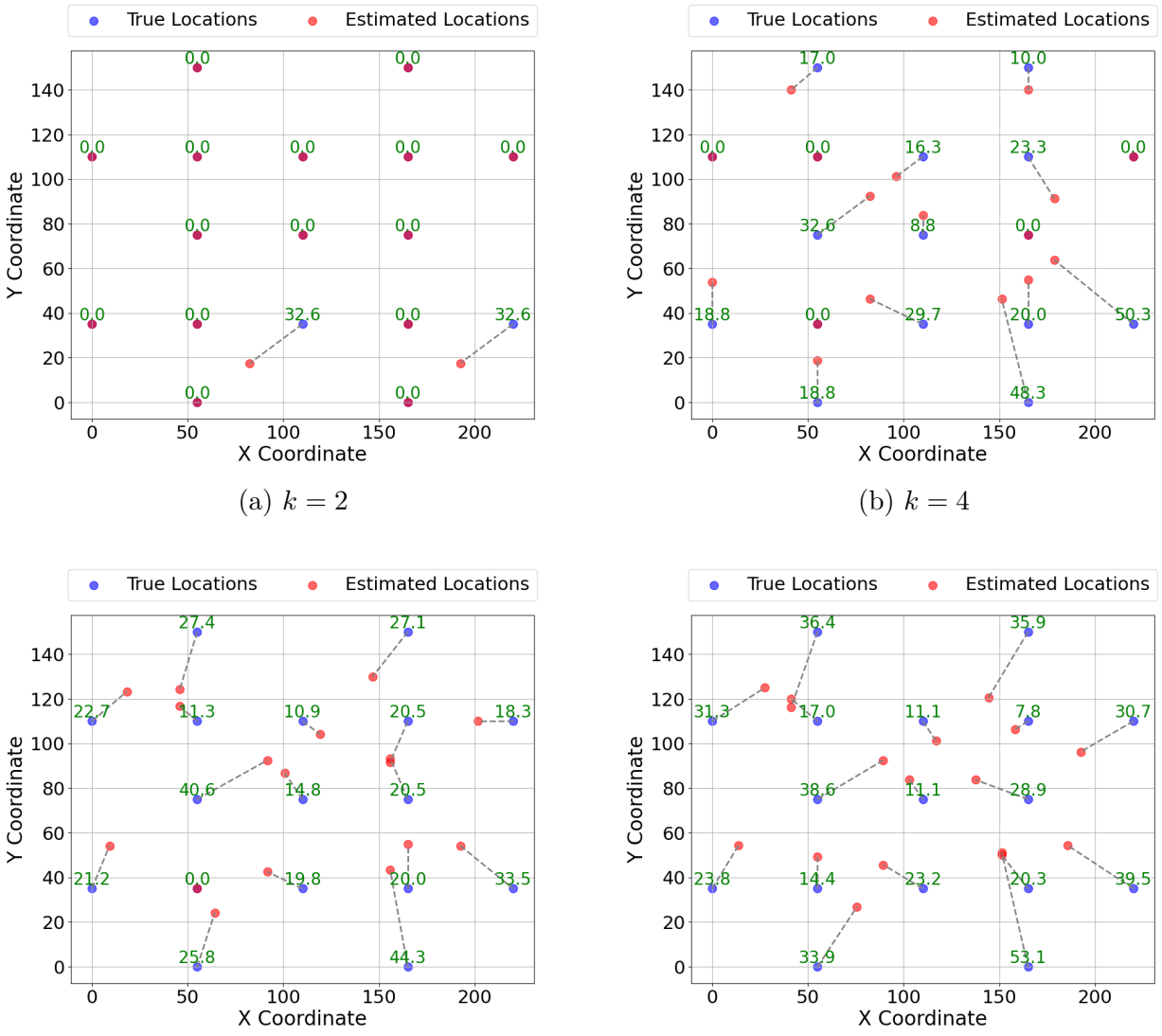
Figure 4.23: Real-time impact location estimation with the GUI

all recorded impacts.

This visualization is updated with each new estimation, plotting the most recent impact location while preserving the previous estimations for easy reference. An example of this visualization can be observed in Fig. 4.23, which illustrates the functionality of the system for impact localization. In the figure, gray points represent the estimated locations of previous impacts, while the most recent impact is highlighted in red. This colour distinction ensures that the latest impact is easily identifiable, enabling straightforward tracking and analysis of impact locations over time.

To quantify the performance of the impact localization system, the dataset was partitioned into distinct training and testing subsets using an 80/20 split. The target variables, which represent the known impact positions, were separated from the remaining feature set.

Afterwards, a kNN regression model was trained on the training dataset. The model, having learned the mapping between the combined feature vectors and the corresponding spatial coordinates, was subsequently used to estimate the impact locations for the test data.



(a) $k = 2$ (b) $k = 4$

(c) $k = 6$ (d) $k = 8$

Figure 4.24: Visualization of true vs estimated impact locations for different number of neighbours (k) values

Fig. 4.24 shows the true and estimated impact locations on the composite panel for different k values in the proposed kNN-based impact localization model. True impact points are marked in blue, while estimated locations are shown in red, with dashed lines indicating the localization error. The green numerical values represent the Euclidean error at each point. As k increases, predictions become more stable due to averaging, reducing sensitivity to noise but sometimes shifting further from the actual impact locations. Smaller k values allow more precise estimations, but can be more affected by local variations. The optimal k balances accuracy and robustness, minimizing localization errors while maintaining reliability.

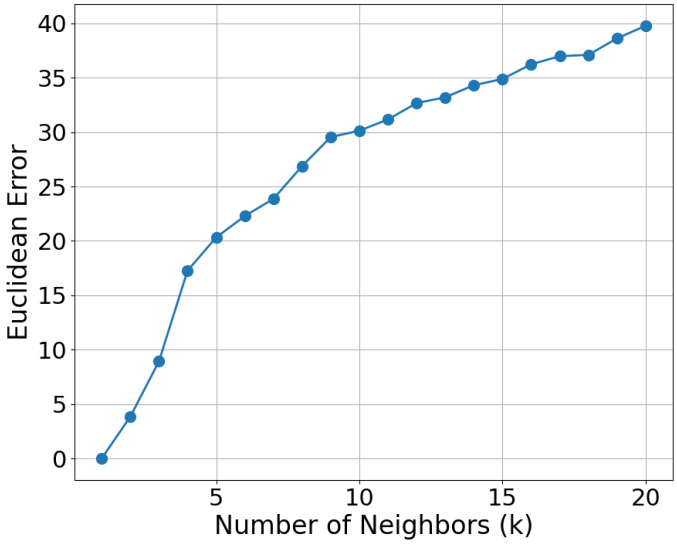


Figure 4.25: Effect of number of neighbours (k) on impact localization error

Fig. 4.25 illustrates the effect of the number of neighbours (k) on the Euclidean localization error in the proposed kNN-based impact localization. As k increases, the localization error follows an upward trend, indicating that using a larger number of neighbours leads to a reduced precision in impact localization. For smaller k values, the error remains relatively low, suggesting that the model effectively captures local variations in the sensor data.

To evaluate the localization accuracy, the Euclidean error between the predicted and true impact coordinates was calculated for each impact event using the following equation that can be expressed as

$$e_i = \sqrt{(x_{\text{pred},i} - x_{\text{true},i})^2 + (y_{\text{pred},i} - y_{\text{true},i})^2} \tag{4.5}$$

where $(x_{\text{true},i}, y_{\text{true},i})$ denotes the true impact location and $(x_{\text{pred},i}, y_{\text{pred},i})$ the estimated location for the i-th sample.

Based on the Euclidean error, the metrics were calculated as follows:

- Mean Euclidean Error (MEE):

$$\text{MEE} = \frac{1}{N} \sum_{i=1}^{N} e_i \tag{4.6}$$

which provides the average distance between the estimated and the true locations.

- Root Mean Squared Error (RMSE):

$$\text{RMSE} = \sqrt{\frac{1}{N}\sum_{i=1}^{N} e_i^2} \tag{4.7}$$

emphasizing larger errors by squaring the deviations before averaging.

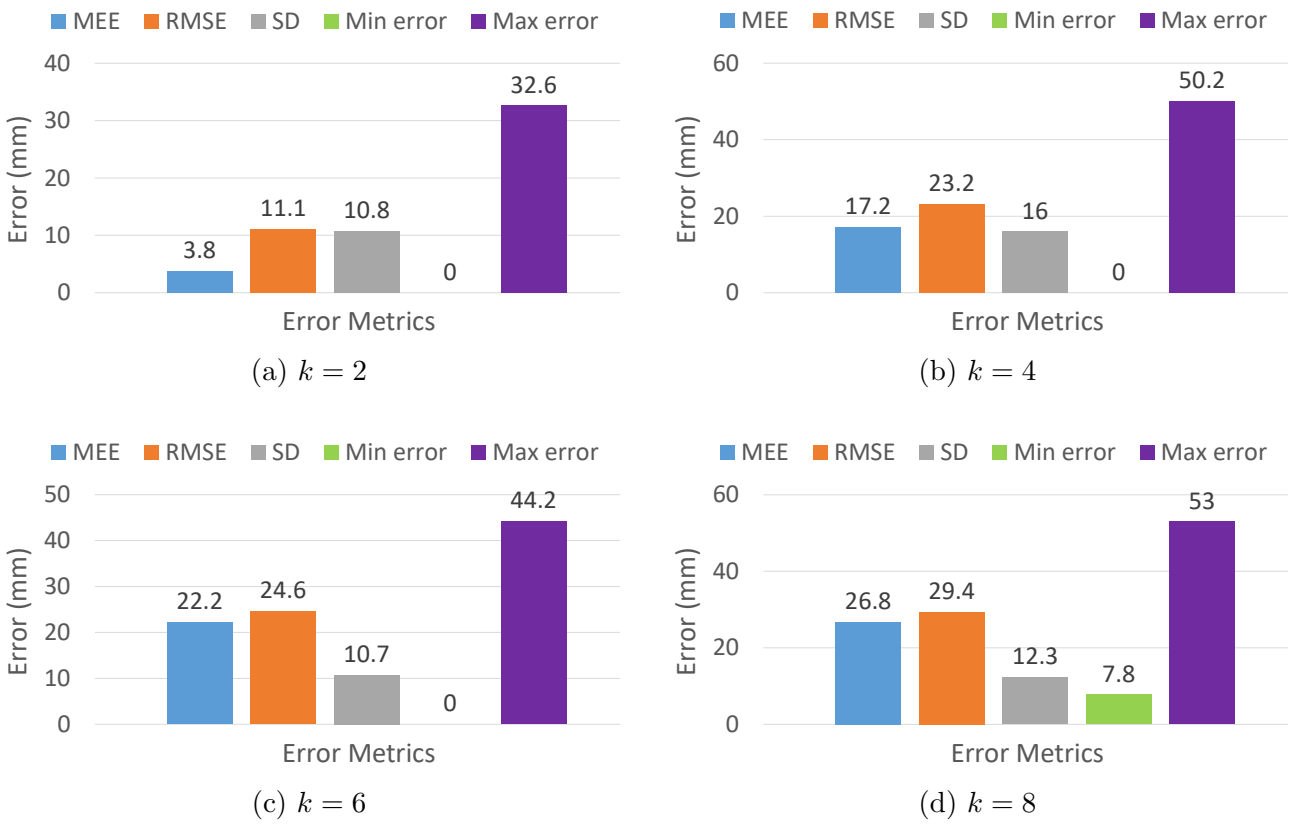
- Standard Deviation (SD) of error:

$$\text{SD} = \sqrt{\frac{1}{N}\sum_{i=1}^{N}\big(e_i - \text{MEE}\big)^2} \tag{4.8}$$

reflecting the variability or consistency of the error distribution across samples.

In Equation 4.6, 4.7 and 4.8, N represents the total number of samples (i.e., impact events) in the dataset for which both the true and estimated locations are available. Essentially, it is the number of individual predictions over which the error metrics are averaged or analysed. Each of these equations plays an important role in quantifying different aspects of the model performance in impact location estimation.

Fig. 4.26 shows the error metrics calculated for the proposed kNN-based impact localization, showing different number of neighbours (k) values. The MEE provides an overall measure of accuracy by indicating the typical distance between the estimated and the true impact locations, while the RMSE emphasizes larger deviations by squaring individual errors before averaging. As shown in Fig. 4.26, both MEE and RMSE remain relatively low at $k = 2$ but increase significantly for larger k values, indicating that using more neighbours can degrade localization accuracy. The maximum error highlights the worst-case scenario, rising from 32.6 at $k = 2$ to 53 at $k = 8$, which is especially critical for safety-sensitive applications. The minimum error is zero at $k = 2, 4, 6$, reflecting the potential for perfect localization in some cases, but it increases to 7.8 at $k = 8$. Finally, the SD captures the consistency of the model performance, showing how much the errors fluctuate around the mean. Collectively, these metrics underscore the trade-off between accuracy and robustness: smaller k values can result in lower average errors but may



(a) $k = 2$ (b) $k = 4$

(c) $k = 6$ (d) $k = 8$

Figure 4.26: Error metrics for different number of neighbours (k) values

be more susceptible to local variations, while larger k values tend to produce more stable but less precise estimates.

The proposed system achieves impact localization by employing a combination of TDoA calculations, signal amplitude analysis, and kNN regression. The integration of these features into the kNN regression model allows the system to effectively analyze patterns within the data and estimate the position of impacts with high accuracy. Designed for real-time operation, the system is well-suited for applications requiring rapid and reliable localization of impacts within a predefined area.

4.6 Conclusions

In conclusion, this study presents the PSN as an innovative and practical SHM system for detecting and capturing impact signals in composite structures. Designed as a cost-efficient and scalable solution, the PSN integrates compact data acquisition capabilities with an IoT-based

framework. The compact PCB with a diameter of 28.4 mm and a lightweight construction of 3.7 grams without a battery (6.6 grams with a battery) ensure seamless integration into weight-sensitive environments, making it particularly well-suited for aerospace and other structural monitoring applications.

The proposed system introduces wireless communication, eliminating the need for physical cabling and being especially advantageous for aerospace applications. The Bluetooth LE protocol has been implemented for wireless data transmission. The system operates with minimal power consumption, supported by a coin-cell battery.

Time synchronization within the wireless network was achieved by implementing a shared clock. The central device transmits synchronization packets and the sensor nodes adjust their local clocks using the data contained within these packets. This shared clock system allows for the precise capture of timestamps when an impact occurs on the composite structure. Timestamp data are essential for calculating the TDoA between sensors, providing critical temporal information for impact localization.

The functionality of the shared clock was experimentally evaluated by generating impacts near the sensors. The results demonstrated a clear variation in the arrival times of the signal at different sensors, confirming the effectiveness of the synchronization mechanism. The shared clock exhibits sensitivity at the microsecond level, enabling highly accurate measurements. This precision supports more detailed and reliable assessments of impacts on the composite structure.

A set of experiments was conducted to assess the performance of the proposed system. Following the visualization and analysis of the collected PZT signals, the findings confirmed the ability of the system to accurately detect and capture passive sensing signals resulting from impacts on composite structures. The accuracy of the system was validated by comparing its results with those obtained from a digital oscilloscope, demonstrating the reliability of the proposed approach.

The proposed impact localization system utilized four PSNs strategically positioned at the corners of the panel, and specific impact points were defined to enable data collection and model training. Two key features were extracted for impact localization: TDoA between unique pairs of PSNs and the amplitude of the ADC signals. These features were structured into

a standardized 14-dimensional vector, which was used to train a kNN model for accurately estimating the locations of impact events. The impact localization system demonstrated high precision, which makes it effective in detecting structural impacts in aerospace applications.

During real-time operation, the trained model continuously processed incoming data, allowing the system to provide accurate and dynamic impact localization. The results were visually represented by the GUI, showing the estimated locations of the impacts and enabling real-time tracking of events over time. This approach integrated temporal and amplitude-based feature analysis with the kNN algorithm, ensuring reliable performance for SHM applications that require real-time localization of impacts.

Energy efficiency was evaluated through current measurements in different operating states, including standby mode, time synchronization, and active impact detection. The results demonstrated that the system operates with minimal power consumption, particularly in standby mode. In addition, wireless communication range tests were also conducted under line-of-sight conditions, evaluating the performance at different transmit power levels (0 and +8 dBm) and modulation schemes (CODED, 1M and 2M PHY). These evaluations confirm that the system is both energy-efficient and is capable of maintaining robust wireless communication, which makes it suitable for SHM applications in large-scale composite structures.

In summary, the developed SHM system establishes a framework for further research and industrial adoption, particularly in applications involving impact detection in composite structures.

Chapter 5

Multi-Sensor SHM System

This chapter presents a compact IoT-based Multi-Sensor System (MSS) for SHM. The system integrates a PZT for impact detection, a strain gauge for measuring mechanical deformations, an accelerometer for capturing dynamic responses, and an environmental sensor that monitors temperature, pressure, and humidity, all mounted on a flexible 3 × 3 cm PCB. Dedicated analog conditioning circuits ensure that PZT and strain signals are accurately processed, while wireless communication through Bluetooth LE enables real-time DAQ and precise time synchronization across sensor nodes. Experimental evaluations on composite panels and aluminium specimens confirm that the system reliably records high-fidelity PZT signals, strain variations, and acceleration responses, with performance comparable to commercial instruments. In general, the proposed solution offers a low-power, miniaturized, and robust platform for the different applications in SHM.

5.1 Introduction

SHM refers to the continuous observation and evaluation of the condition of a structure using integrated sensor systems during operation. Initially developed as an extension of Non-Destructive Testing methods, SHM addresses the growing need for efficient maintenance strategies in modern engineering fields such as aerospace, civil infrastructure, and transportation. The primary goals of SHM are to improve the safety of structures, minimize the maintenance-related inoperative period, and reduce the unnecessary mass associated with over-designed components [5, 80].

These objectives are increasingly critical given the economic and environmental pressures faced by industries to optimize resource use while maintaining high-reliability standards. Lightweight structures, particularly in aerospace and transportation, require precise monitoring due to uncertainties in loading conditions, environmental influences, and material properties, which can lead to design redundancy and costly inspections [13]. SHM provides a pathway to predictive maintenance strategies, reducing safety-related inspections and allowing condition-based repairs that ensure structural reliability and regulatory standards [37].

Although SHM has significant potential to improve structural reliability and maintenance strategies, there is no unique SHM solution that can detect all types of damage in metals and composites, they often have to be tailored to the type and severity of potential damage in a structure (e.g., delamination in composites or cracks in metals). [20, 57]. For example, dynamic methods such as guided ultrasonic waves are sensitive to changes in stiffness, but can be heavily influenced by environmental factors such as temperature and humidity, which introduce noise and reduce accuracy [50]. Static methods, such as strain-based monitoring using fiber optic sensors, are less susceptible to environmental variations but lack the ability to detect global structural changes [42].

Among these challenges, the environmental sensitivity of many SHM techniques remains a critical limitation to their effectiveness. For example, guided waves and electromechanical impedance methods are strongly affected by temperature changes, which change material properties and signal propagation, leading to false alarms or reduced detection capabilities [20, 50, 81]. Noise from operational environments, such as mechanical vibrations or electromagnetic interference, further complicates signal interpretation and often requires extensive signal processing to extract meaningful data [6].

To overcome these limitations, multi-sensor systems have emerged as a transformative approach in the field of SHM. Unlike conventional single-method systems, multi-sensor systems combine multiple SHM techniques, implementing various physical principles to provide complementary data that improve the accuracy and reliability of damage detection and evaluation [42,92]. By integrating these techniques, multi-sensor systems enable the simultaneous evaluation of global and localized structural changes, leading to more detailed damage assessments [1, 76].

The integration of multiple sensor types not only enhances impact detection but also enables usage monitoring through load reconstruction and shape sensing, while accounting for environmental influences. By combining data from PZT, strain gauge, and accelerometer sensors, it is possible to estimate applied loads and track structural deformations, facilitating a more comprehensive evaluation of composite structures [76]. Furthermore, the use of additional environmental sensors for the monitoring of temperature and humidity allows the system to compensate for external influences, improving the robustness of the analysis [39, 50].

More information on multi-sensor SHM systems can be found in [57]. This review paper highlights the potential of multi-sensor SHM systems for comprehensive damage assessment in metal and composite structures. By integrating static methods such as strain sensing with dynamic methods such as guided waves, these systems effectively detect, localize, and quantify damage under varying environmental conditions. Data fusion at raw, feature, and decision levels ensures robust evaluation of diverse sensor inputs, overcoming the limitations of single-method SHM. The importance and need for data fusion for multi-sensor systems are covered in these studies [4, 12, 49].

In recent years, various multi-sensor systems for SHM have been proposed, each offering unique features suited for different structural and environmental conditions. Some systems prioritize inertial measurements and tilt detection to monitor large civil structures, incorporating MEMS-based accelerometers and inclinometers with embedded controllers for real-time data processing and management [3]. Others combine multiple sensing modalities, such as guided wave-based inspections, optical fiber sensing, and piezoelectric transducers, to achieve broader diagnostic capabilities in a single platform [91]. Advanced methodologies have emerged that minimize requirement on baseline references by integrating symbolic data analysis and clustering algorithms, improving the adaptability and real-time detection capabilities of SHM frameworks [83]. Energy efficiency and scalability are also key considerations, with some systems employing modular architectures, low-power components, and frequency-hopping spread spectrum communication to ensure reliable, long-term DAQ even in complex environments [71]. Multi-parameter sensory inputs, such as fiber optic strain sensors, chloride sensors, and resistivity probes, have expanded the scope of SHM to include material degradation and corrosive

processes [60], and the use of compressed sensing techniques has enabled the reconstruction of high-fidelity signals from undersampled measurements [22]. Furthermore, emerging approaches have integrated semi-passive RFID-based sensors to reduce energy consumption while providing dynamic strain and acceleration measurements [48].

Despite these advances, current multi-sensor SHM systems generally face several limitations. Many solutions adopt a single sensor modality or exclude important environmental parameters that are crucial for comprehensive diagnostics. For example, while a given system may be good at detecting inertial vibrations [3], it may lack environmental sensors needed to account for temperature or humidity effects, potentially reducing the accuracy of damage detection. Similarly, integrated solutions employing multiple sensing types often do not achieve a sufficiently compact form factor or may rely on the combination of multiple rigid PCBs, limiting their applicability in weight-sensitive platforms such as aircraft [3, 48, 71, 91].

Power consumption and communication constraints further complicate large-scale deployments. Wireless communication capabilities may consume significant energy due to the old 5 V powered Bluetooth modules [3] and may not be suitable to establish extensive sensor networks that cover large structures due to their wireless communication topology [48, 71]. These shortcomings in wireless communication result in limited scalability and continuous long-term monitoring.

Moreover, while some systems integrate multiple sensors, they may still fail to achieve true multi-sensor capability due to the deployment of the same type of sensor rather than offering different sensor types that provide more information about the structure and its operational environment [83].

The implementation of multi-sensor SHM systems involves several challenges, primarily due to the complexity of integrating diverse sensors, managing vast amounts of data, and ensuring system reliability. WSNs for SHM must address issues such as sensor deployment, and decentralized data processing to maintain connectivity and accuracy under resource constraints [9]. Moreover, the synchronization of sensing data across distributed networks poses significant difficulties due to clock drift and hardware-induced delays, which requires advanced synchronization algorithms [62]. Energy limitations also constrain the deployment of wireless

sensors, which makes multi-source energy harvesting techniques vital for extending operational lifespan [27, 69].

These collective shortcomings, such as large dimensions, heavier configurations, the lack of environmental sensors for compensation, elevated power consumption, and limited sensing diversity, underscore the need for a more integrated and refined solution. This work addresses these challenges by introducing a fully integrated, miniaturized, and IoT-based multi-sensor platform specifically designed for on-board SHM applications in the aerospace industry. The system features a flexible (3 cm × 3 cm) PCB that incorporates PZT, strain gauge, accelerometer, and environmental sensors, offering comprehensive structural assessments while minimizing both size and weight. The incorporation of low-power Bluetooth LE communication further enables scalable wireless deployment, avoiding additional cabling, and enhancing suitability for aircraft applications where weight and wiring complexity are critical concerns.

In addition to hardware developments, this work also presents a GUI for managing the entire DAQ and communication process. The GUI facilitates data collection from a central node within the WSN, providing capabilities for data visualization, analysis, and storage. This ensures a streamlined and user-friendly environment for monitoring and analysing SHM data.

5.2 Principle of Multi-Sensor System for SHM

The proposed system is based on the idea of integrating several different sensing elements into a single compact platform. Constructed on a flexible PCB dimensioned only 3 cm by 3 cm, the system combines a PZT, a strain gauge, an accelerometer, and an environmental sensor that is capable of measuring air temperature, humidity, and pressure. By integrating these sensors, it enables the observation of both mechanical and ambient factors that influence structural integrity and long-term performance.

Based on the proposed design, each sensing element plays a distinct role in monitoring critical structural and environmental parameters for SHM applications. The PZT element records the structural vibration that arises under loads and dynamic events. The strain gauge monitors variations in strain distribution, which can indicate potential fatigue or accumulation

of damage over time. The accelerometer quantifies structural responses to external forces, such as aerodynamic effects or turbulence, thereby supporting the identification of shifts in dynamic characteristics. Complementing these measurements are the environmental parameters recorded by the combined sensor for temperature, humidity, and pressure, all of which influence material properties and the behaviour of the structure under various operating conditions.

To enable effective DAQ and analysis, the data from each sensor is collected by a compact on-board electronic unit, which processes the signals for subsequent wireless transmission. Inclusion of Bluetooth LE communication removes the need for extensive wiring, allowing direct placement of the sensor node on key structural areas. Such a configuration can be reproduced across multiple locations to form a wireless sensing network, providing spatially distributed data critical for understanding and predicting the health of the aircraft over time.

This wireless capability is complemented by a design that prioritizes low power consumption and durability. Hence, this miniaturized system is designed to operate with low power requirements and withstand the demanding environment of flight operations. By achieving a balance between functionality, mass, and form factor, the platform supports continuous or periodic monitoring tasks.

In practice, these design principles allow multi-sensor systems to be strategically deployed on critical regions of composite structures, enabling comprehensive monitoring. All data acquired from the sensors available in the MSSs are transmitted through Bluetooth LE to the central device in the wireless network. This central device is connected to a base station, such as a PC. The base station is equipped with a GUI that can display these incoming sensor data in real time and save them for long-term study. The central device performs data processing steps to extract meaningful parameters from the raw signals. For example, it converts voltage measurements from the strain gauge circuit into strain values and extracts the peak voltage value from the PZT signal. The graphical interface then transforms these processed results into graphs and charts that allow one to examine variations in structural behaviour over time. The design and operational principles of the proposed miniaturized MSS for SHM are represented in Fig. 5.1.

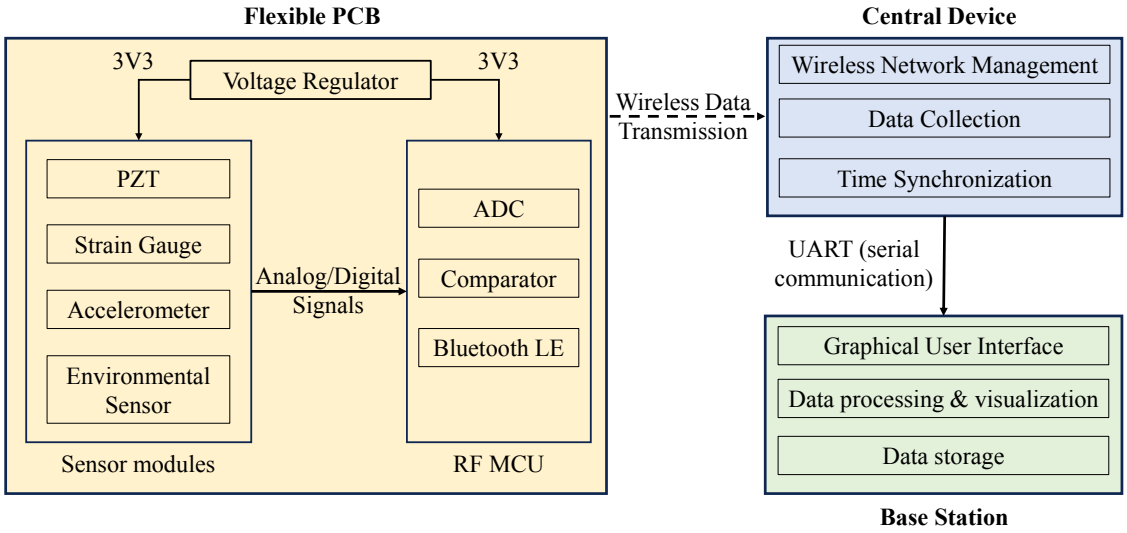


Figure 5.1: Conceptual block diagram of the miniaturized MSS for SHM

5.3 Multi-Sensor SHM System

This section presents the architecture and key features of the Multi-Sensor SHM System, which is designed for wireless, low-power, and miniaturized structural health monitoring. It covers the RF MCU, which integrates Bluetooth LE for efficient data transmission, ensuring seamless communication across sensor nodes. The power management strategy is discussed, highlighting low-power operation, energy-efficient design, and battery selection for long-term functionality. The Sensors and DAQ subsection describes the integrated sensing elements, including PZT sensors, strain gauges, an accelerometer, and an environmental sensor, along with their roles in structural monitoring. Additionally, the Wireless Communication subsection outlines the antenna design and network topology, ensuring reliable data transmission for SHM applications.

5.3.1 RF MCU

The MSS incorporates Bluetooth LE communication, eliminating the need for external wireless modules. This integrated Bluetooth LE functionality allows wireless data transmission between sensor nodes and a central data collection unit, enabling real-time monitoring without physical connections. Bluetooth LE communication supports a low-power, energy-efficient protocol, making it suitable for long-term operation in SHM applications.

The core of the system is the ANNA-B402 module from uBlox, which is built on the Nordic

Semiconductor nRF52833 chip. This module integrates a high-performance Arm Cortex-M4 processor, providing efficient processing for signal acquisition, filtering, and real-time data analysis [101].

The ANNA-B402 module is a stand-alone Bluetooth 5.1 Low Energy solution, offering several key features:

- Ultra-compact form factor (6.5 × 6.5 × 1.2 mm), making it ideal for miniaturized systems.
- Low power consumption with multiple power-saving modes (sleep mode, standby mode, and power-off mode).
- Comprehensive range of interfaces, including SPI, I2C , UART, and GPIOs, allowing seamless communication with various sensors and external components.
- Integrated RF core, reducing the need for external RF modules and simplifying hardware design.

By incorporating both processing and wireless communication within a single compact module, the MSS achieves an optimized balance between performance, power efficiency, and miniaturization.

5.3.2 Power Management

To ensure reliable and efficient operation, the MSS employs a DC-DC buck-boost voltage regulator, which provides a stable power supply when powered by either a coin-cell battery or a lithium-ion/polymer battery. This regulator ensures a consistent voltage level, allowing the system to function efficiently under varying power conditions.

The system is designed with low-power operation strategies to extend battery life. These strategies include:

- **Sleep Mode Implementation**: The MSS remains in a low-power state when no impact is detected, significantly reducing power consumption.

- **Threshold-Based System Activation:** When an impact-induced signal exceeds a predefined threshold value, the entire system is activated by the built-in comparator within the RF MCU. The ADC begins sampling PZT and strain gauge sensor signals, while the accelerometer measures acceleration, and the environmental sensor records air temperature, pressure, and humidity.

To further enhance power efficiency, the MSS includes an external 32.768 kHz crystal oscillator. The ANNA-B402 module is equipped with a high-frequency 32 MHz clock for standard operations and a low-frequency clock, which can be sourced internally using an RC oscillator or externally from a 32.768 kHz crystal [100].

When an external crystal is not used, the module must calibrate its internal clock periodically to maintain accuracy. This calibration process increases power consumption, which is undesirable for battery-operated systems. To avoid unnecessary power drain and ensure precise timing, an external 32.768 kHz crystal has been incorporated into the system. This provides a stable low-frequency clock, eliminating the need for frequent calibration and significantly reducing overall power consumption.

The choice of a CR-2032 coin-cell battery is particularly beneficial for miniaturized SHM applications. This battery offers a capacity of 240 mAh at 3 V, which is sufficient to support the DAQ and wireless communication tasks in the proposed system. In addition, its small size (20 $\times$ 3.2 mm) makes it an ideal power source for compact embedded systems. While the CR-2032 is non-rechargeable, it presents a cost-effective alternative to lithium-ion batteries, which are typically larger, heavier, and more expensive.

By integrating power-efficient hardware components and software-driven energy optimization techniques, the MSS achieves long-term operation without frequent maintenance, making it well-suited for SHM applications.

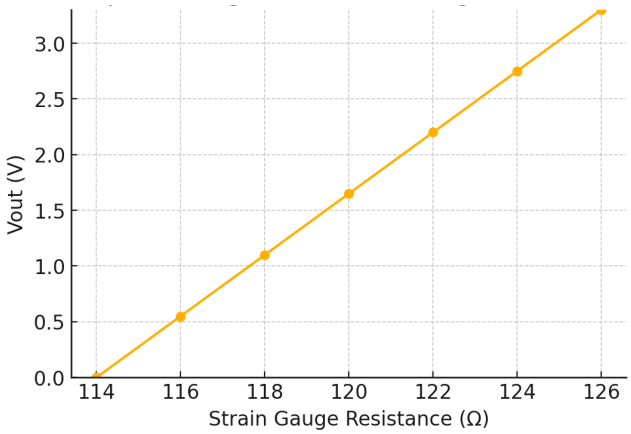


Figure 5.2: Output voltage vs strain gauge resistance

5.3.3 Sensors and DAQ

Strain Gauge Sensor

The MSS incorporates a strain measurement module based on a quarter-Wheatstone bridge configuration, designed to detect small mechanical deformations in composite structures. The strain gauge sensor (120 ohm) is connected as one of the four resistive elements in the bridge, while the remaining three are fixed precision resistors (120 ohm).

To accurately measure the differential voltage produced by strain-induced resistance changes, the system employs an instrumentation amplifier (INA333 from Texas Instruments).

A precision voltage reference (REF35160 from Texas Instruments) supplies a stable low-noise reference voltage to both the Wheatstone bridge and the instrumentation amplifier, ensuring that any variations in the output are primarily due to mechanical strain rather than fluctuations in power supply.

Once amplified, the strain signal is digitized using the ADC of the MCU, allowing for real-time monitoring and further processing. By combining a precision reference source, a stable bridge configuration, and a low-noise amplifier, the MSS achieves high-accuracy strain measurement, making it well-suited for SHM applications. Based on the circuit configuration, the expected output voltage is presented corresponding to the resistor value of the strain gauge sensor as shown in Fig. 5.2.

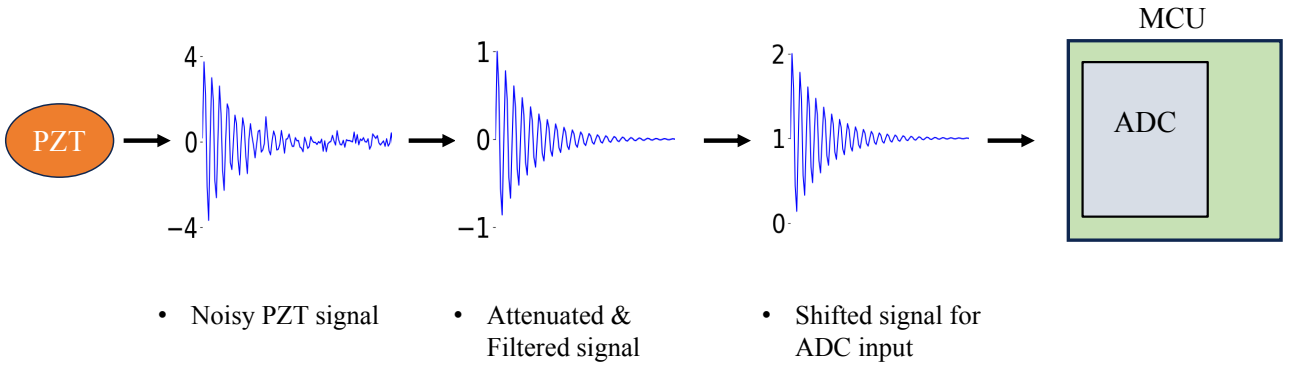


Figure 5.3: PZT signal acquisition stages

PZT sensor

The PZT sensor module is designed to detect impact-induced signals and convert them into measurable voltage. To achieve this, the system employs a charge amplifier circuit based on an operational amplifier (LTC6087 from Analog Devices).

The raw PZT signal undergoes several conditioning stages:

- **Attenuation:** The signal is first attenuated by a factor of 2 to prevent saturation and maintain linearity.
- **Filtering:** A low-pass filter is applied with a resistor (51 ohm) and a capacitor (4.7 nF), resulting in a cut-off frequency of 664 kHz to remove high-frequency noise and improve signal clarity. If PZT signals are mostly less than 100 kHz, a cut-off around 500–700 kHz is acceptable. For filter circuit design and capacitor-resistor values, the reference design provided by Analog Devices was considered [2].
- **Reference Voltage Adjustment:** A reference voltage, generated using an operational amplifier (AD8691 from Analog Devices), shifts the signal to ensure it remains within the input range of the ADC.

After these adjustments, the processed analog signal is converted to digital form via the ADC of the MCU, allowing real-time impact detection and further analysis. This ensures reliable impact sensing and improves SHM accuracy. The acquisition stages of the PZT signal are visualized in Fig. 5.3.

Accelerometer

The MSS integrates a BMA400 accelerometer from Bosch Sensortec, designed for low-power motion sensing applications. The accelerometer provides digital output via Serial Peripheral Interface (SPI) protocol, ensuring efficient communication with the MCU. By using the SPI interface, the system benefits from fast and reliable data transfer, reducing latency in impact detection and motion analysis.

The BMA400 accelerometer supports [11]:

- Three-axis acceleration measurement, enabling comprehensive motion sensing and structural vibration analysis.
- Configurable measurement ranges of ±2g, ±4g, ±8g, and ±16g, allowing adaptability for different SHM applications.
- 12-bit digital resolution, ensuring precise acceleration measurements essential for impact and vibration analysis.
- Adjustable output data rates of up to 800 Hz, optimizing the balance between power consumption and response time.

By integrating acceleration data with PZT and strain gauge measurements, the MSS provides a comprehensive evaluation of structural integrity, enabling real-time SHM applications. The accelerometer communicates with the MCU via the SPI interface, ensuring fast and efficient data transfer. The accelerometer provides real-time acceleration data, which is used for impact analysis, vibration monitoring, and structural response assessment.

Environmental Sensors

The MSS incorporates a BME280 environmental sensor from Bosch Sensortec, which enables measurement of air temperature, atmospheric pressure, and humidity. Unlike the PZT and strain gauge sensors, which provide analog outputs, the BME280 sensor features a fully digital output, eliminating the need for additional signal conditioning.

This sensor also communicates with the MCU via the SPI interface, ensuring fast and efficient data transfer. It supports the following features [10]:

- **Three environmental parameters:** Temperature, pressure, and humidity.
- **High-resolution digital output:** 20-bit resolution for temperature and pressure, and 16-bit resolution for humidity.
- **Power consumption:** Low-power operation, making it ideal for long-term monitoring applications.

By integrating the BME280 sensor, the MSS enhances its capability to correlate structural responses with environmental conditions, providing valuable insights for SHM applications. The collected environmental data ensures that variations in temperature, pressure, and humidity can be accounted for in structural assessments, improving the accuracy and reliability of impact detection and damage evaluation.

The MCU configures these sensors and reads these measurements through the SPI which is a serial communication protocol. This protocol establishes a specific set of signals, including clock, input, output, and chip select lines, to enable efficient data transfer between the MCU and individual sensors as shown in Fig. 5.4. This approach eliminates the need for additional analog conditioning for these inputs.

5.3.4 Wireless Communication in MSS

The MSS utilizes an integrated antenna within the ANNA-B402 module, providing Bluetooth LE wireless communication for real-time SHM. The wireless network follows a star topology, where multiple sensor nodes communicate with a central unit. This structure enables efficient data collection, minimizes interference, and optimizes energy usage while ensuring reliable performance for SHM applications.

To achieve stable and interference-free wireless transmission, a custom antenna pattern is designed based on the integration guidelines of the uBlox system [99]. One of the critical design considerations is the implementation of a non-conductive keep-out area around the antenna.

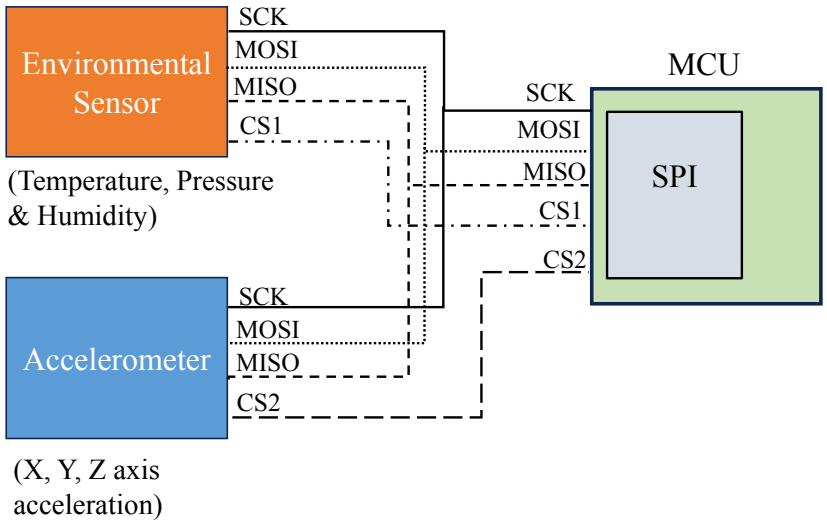


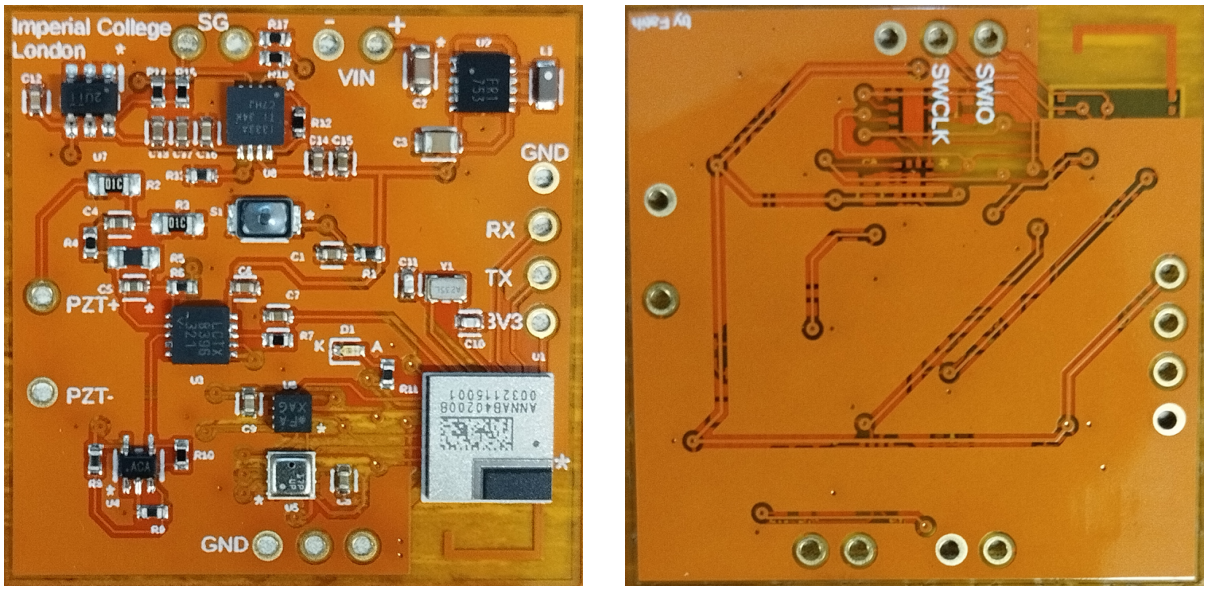
Figure 5.4: Serial communication (SPI) between MCU and sensors with digital output (BMA400 and BME280)

This area is maintained on both the top and bottom layers of the PCB, preventing signal reflections from nearby conductive components. Without this isolation, metallic traces or ground planes could interfere with the radiation pattern, significantly degrading signal strength, and increasing data loss.

The key design considerations for antenna performance optimization include:

- **Unobstructed transmission path:** Ensuring that the antenna is not covered by metallic components, which could cause unwanted signal attenuation.
- **PCB layout optimization:** Properly routing traces to minimize interference and electromagnetic coupling between the antenna and other circuit components.
- **Ground plane design:** Implementing an appropriate ground clearance region to enhance the antenna efficiency and signal propagation characteristics.

By implementing these antenna design principles, the MSS ensures robust wireless data transmission, enhancing its applicability for SHM applications where reliable and efficient communication is crucial.



(a) (b)

Figure 5.5: Multi-Sensor SHM system in two-layer flexible PCB, (a) Top view (b) Bottom view

5.4 MSS System Implementation

The proposed system was implemented on a flexible two-layer PCB to meet the miniaturization requirement, a key design objective. Small-sized components were carefully selected to ensure they provided the necessary performance while minimizing the overall footprint. The dimension of the prototyped PCB is only 3 cm by 3 cm. The developed system is lightweight, weighing just around 0.5 grams. Furthermore, the total cost of producing each MSS is approximately £80, making it a cost-effective solution. The prototype of the developed system is presented in Fig. 5.5. As shown in the figure, all components are placed on the top layer of the flexible PCB.

5.4.1 Function Modules in MSS

In the proposed MSS, There are six function modules to perform the sensing process for SHM. The first module in the system is the strain gauge module that converts mechanical strain into electrical signals. A quarter-Wheatstone bridge circuit is implemented with an instrumental amplifier to acquire the strain data from the structure. The second is the PZT module that includes the charge amplifier circuit that provides voltage outputs correlated with the vibrational energy. The PZT signal is completely shifted to the positive side using a reference voltage to be

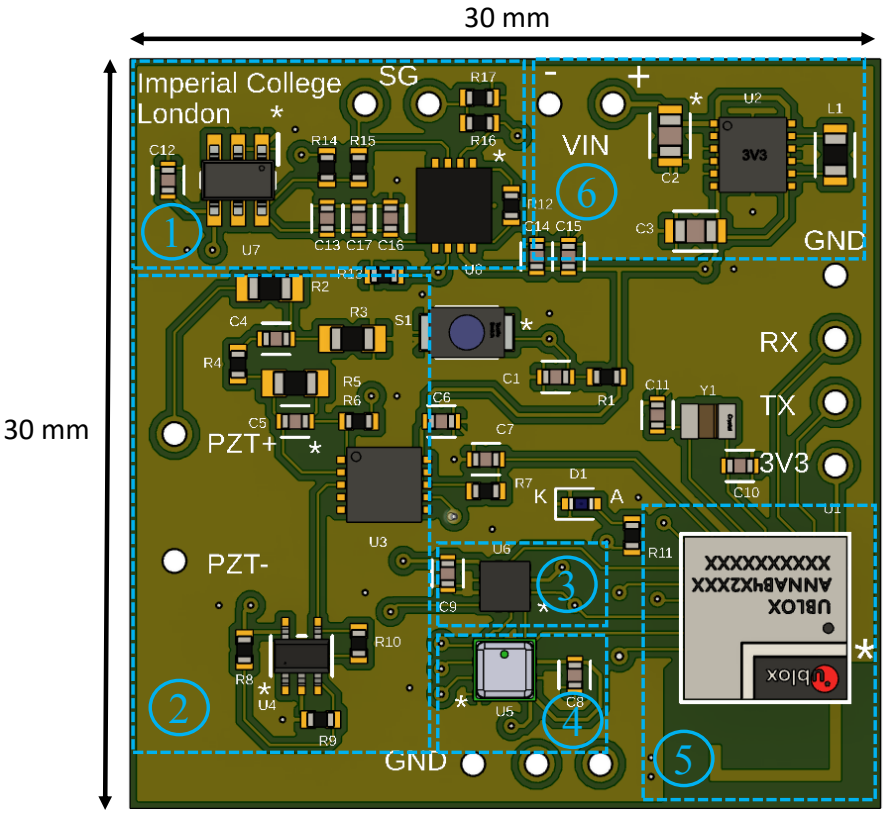
processed later by a microcontroller. The voltage output range of both the strain gauge and the PZT modules is adjusted, from 0 to 3.3 V, allowing ADC to properly sample and convert their electrical signals to digital values. Otherwise, a high-voltage input may permanently damage the ADC.

Unlike the strain gauge and PZT modules, both the accelerometer and environmental sensor modules have digital output for the sensors measurements. These sensor devices can be configured, and their measurements are read through the SPI serial interface. Using a single SPI interface, the MCU communicates with only one device at a time. To manage successful data reading from different devices, the chip selection pins are used to select the sensor required to communicate. While the environmental sensor measures air temperature, pressure, and humidity to support continuous monitoring of environmental parameters that may influence structural performance, the accelerometer is responsible for measuring acceleration in three axes.

Another critical module is the RF microcontroller, including the necessary peripherals in this study such as the ADC and the comparator. The ADC is responsible for sampling the signals coming from the strain gauge and PZT modules, while the comparator is used to enable an event-triggered mechanism in the proposed system. This module also manages serial and wireless communication protocols. The module supports Bluetooth LE to transmit data wirelessly to a central device that establishes the wireless network. While the SPI interface is used to communicate with the accelerometer and environmental sensor devices, UART is also implemented for data exchange between the module and any device supporting this serial interface.

The power management module consists of the buck-boost DC/DC converter for voltage regulation to maintain stable electrical conditions across all components. A fixed voltage input (3.3 V) is provided to the system.

All function modules mentioned above in the Multi-Sensor SHM system are represented in Fig. 5.6.



① Strain Gauge module ② PZT module ③ Accelerometer module ④ Environmental sensor module ⑤ RF MCU module ⑥ Power management module

Figure 5.6: The function modules of Multi-Sensor SHM system

5.4.2 Wireless Network Implementation in MSS

Bluetooth LE has been used to establish a star-topology network characterized by its simplicity, compactness, and adaptability. This configuration is based on two primary device roles: central and peripheral. A central device functions as a hub, enabling connections to multiple peripheral devices, supporting data transfers up to the 2 Mbps limit, suitable for applications with high data demands [17]. To implement this topology, the Nordic UART Service (NUS) was used, which extends the central role of NUS to accommodate up to 20 peripherals. Further scalability was achieved through additional peripherals, termed the Multi-NUS solution. This extension was facilitated by software libraries such as the Connection Context Library, which simplified the configuration and evaluation processes.

Building on this framework, a WSN was developed using the star-topology network and the Multi-NUS solution. To ensure secure wireless communication, the Filter Accept List method

was used, restricting network access to devices explicitly included in the list. This approach ensures that only authorized and bonded devices can establish connections, enhancing the security and reliability of the network.

Time Synchronization in MSS

In this study, time synchronization is also implemented in a wireless network. The proposed system ensures precise timing and synchronization in WSNs for SHM. A central node, acting as the timing master, transmits synchronization packets to peripheral nodes (timing slaves), which update their local timers to achieve a shared clock. Accurate timestamp information enables TDoA calculations for impact signals. Synchronization is implemented using Bluetooth LE on a single RF channel (2480 MHz), with each node running a 16 MHz free-running timer. The timing master operates two timers: a continuously running synchronization timer and a counter to track overflows, while timing slaves adjust their timers upon receiving synchronization packets. Detailed information on time synchronization in the wireless network can be found in Section 4.2.1.

Packet Structures for Sensor Data Handling

In the WSN developed for this study, an MSS serves as a fundamental node. Each MSS integrates multiple sensors to monitor various parameters, such as the PZT signal, strain, acceleration, environmental conditions, and timestamps. The network may contain several MSS nodes, all of which transmit data wirelessly to a central device. Effective communication within this network requires the ability to identify which MSS has transmitted a particular data packet and the type of data it contains. This identification is essential for ensuring accurate data categorization, processing, and interpretation, particularly in a system where multiple sensor nodes operate simultaneously.

To address this requirement, a structured data packet format was designed. Each packet begins with a byte identifying the MSS from which it originates. For example, a byte value of 1 in string format indicates that the data are from MSS 1. The second byte in string format specifies the type of data included in the packet. A value of 1 corresponds to ADC data,



Figure 5.7: Format of ADC data packet

which can include PZT or strain gauge sensor readings; a value of 2 indicates timestamp data; 3 represents environmental sensor data such as temperature, pressure, and humidity; and 4 corresponds to accelerometer data. Each packet ends with a newline character (`\n`) to signify the conclusion of the data packet and enable proper processing by the central device.

The inclusion of a newline character is critical for ensuring that the central device can efficiently identify the end of each packet and separate incoming data streams. This differentiation enables the central device to verify that all data in the packet have been received before preparing the packet for transmission to a base station. While only the ADC data packet has a fixed length, others may have a different amount of data in the packet each time.

By combining a well-defined packet structure and unique identifiers for each data type, this system ensures that both the source and content of each packet are clearly identified within the WSN. This approach minimizes the risk of misinterpretation and improves the overall reliability and performance of the system.

Building upon the structured packet format described above, the specific format and content of each type of data packet are outlined below. Each packet type is customized to the specific sensor data it contains, ensuring efficient transmission and accurate interpretation by the central device.

- **ADC packet:** It begins with a byte identifying the MSS, followed by a byte specifying the packet type (value 1 for ADC data). The subsequent data block contains digital values that represent the readings of the PZT or strain gauge sensor. Each ADC packet contains sensor data of 200 bytes in integer format. The packet format is represented in Fig. 5.7.

- **Timestamp packet:** It begins similarly, with a byte identifying the MSS and another byte indicating the data type (value 2 for timestamp data). The rest of the packet contains the timestamp of impact in microseconds and string format. The packet format is represented

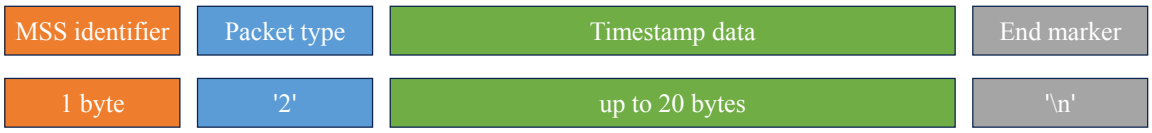


Figure 5.8: Format of timestamp data packet

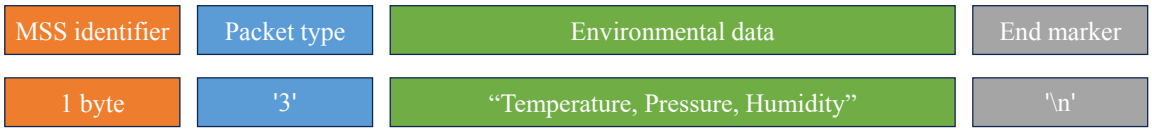


Figure 5.9: Format of environmental data packet

in Fig. 5.8.

- **Environmental data packet:** After the MSS identifier byte followed by the byte indicating the packet type (value 3 for environmental data), the packet consists of temperature (°C), pressure (Pa) and humidity ($\%RH$) respectively. The comma (,) is used as a delimiter to separate the different types of measurement in the packet. This allows the base station to easily distinguish and extract sensor data from the packet to properly process them. The packet format is represented in Fig. 5.9.

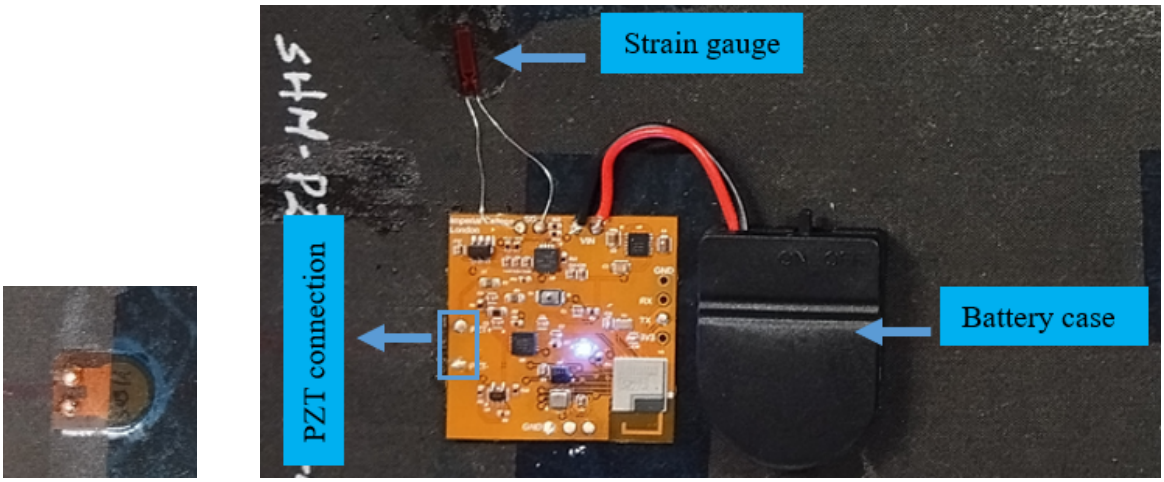
- **Accelerometer packet:** In the same way, the packet begins with the identifier byte for the MSS and then the second byte specifies the packet type (value 4 for accelerometer data). Following that, X, Y and Z axis data are respectively represented in integer format with 12-bit resolution and separated with commas similarly to the environmental data packet. The packet format is represented in Fig. 5.10.

5.4.3 Experimental Setups for Different SHM applications

To integrate the Multi-Sensor SHM system to a structure, the PZT terminals available on the flexible PCB can be soldered directly to a PZT sensor shown in Fig. 5.11a, and the PZT sensor



Figure 5.10: Format of accelerometer data packet



(a) (b)

Figure 5.11: Multi-Sensor SHM system on a composite panel, (a) PZT sensor (b) MSS integration

is placed under the flexible PCB to reduce the amount of wiring, as shown in Fig. 5.11b. In addition to the PZT sensor, a strain gauge mounted on the structure can also be soldered using the assigned terminals on the PCB. In contrast to other sensors, the accelerometer and environmental sensors are available directly on the PCB, eliminating the need for additional connections. Lastly, to power up the system, the power rails are soldered from the battery case which houses the CR-2032 coin-cell battery. The MSS is completely functional for monitoring the health of the structure as displayed in Fig. 5.11.

First Experimental Setup

The first experimental setup consists of a composite panel of dimensions 22 cm by 15 cm equipped with four Multi-Sensor SHM systems as shown in Fig. 5.12. In this example, the MSSs include strategically placed PZT sensors, accelerometer, and environmental sensors to capture comprehensive data for SHM applications. The MSSs act as wireless sensor nodes in the WSN formed with Bluetooth LE. They are responsible for collecting and transmitting structural response data along with environmental information.

The setup aims to evaluate the performance of the Multi-Sensor SHM system in detecting changes in the structural properties of the composite material under various conditions. Wireless communication allows remote monitoring and DAQ without physical connections, thereby reducing wiring complexity.

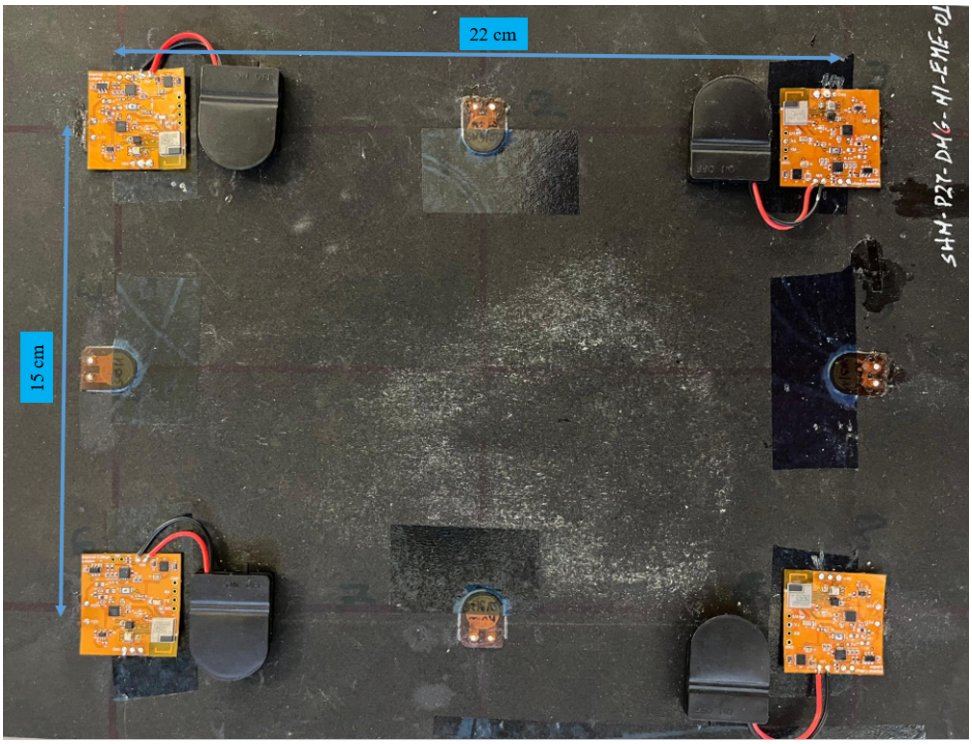


Figure 5.12: Multiple MSSs setup on a composite panel

In the event of critical impact crossing predefined threshold values, each MSS is triggered and wakes up from the sleep mode immediately. The response of the structure is then recorded by the PZT sensor. Meanwhile, the timestamp of the impact is also captured from the shared clock in the wireless network. In addition, the acceleration in three axes is collected along with environmental condition measurements which are temperature, pressure, and humidity.

There is a critical point where the comparator in the MCU is used to detect voltage transitions in the PZT sensor output. Its configuration includes a 64-level reference ladder to set the threshold voltage, and it generates interrupts in a high-speed mode to activate the system immediately. Because the PZT signal is shifted to the positive side, the system uses 1.65V as the reference level around which the signal oscillates.

Based on the example plots shown in Fig. 5.13, the comparator can be configured to generate either an Event Up or an Event Down, each triggered when the input signal crosses a single threshold level in the upward or downward direction, respectively. However, relying on only one threshold does not capture both possible directions of the PZT signal when it first crosses the reference. This may cause the system to be triggered with delay and miss some part of the initial signal. Instead, an Event Cross with two predefined threshold levels is needed. In this

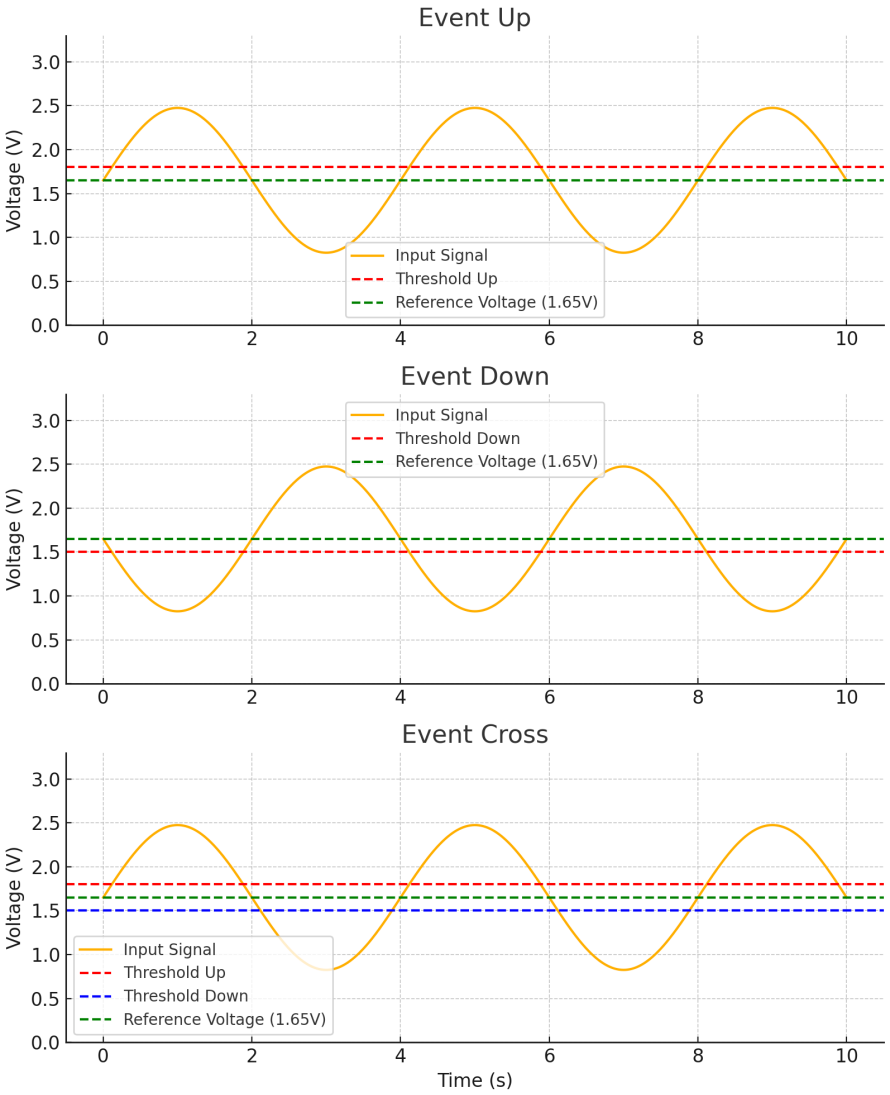


Figure 5.13: Comparator events with threshold aspect

approach, both upward and downward trends of the PZT signal are monitored. As a result, the comparator output accurately reflects the initial crossing event, regardless of whether the PZT signal moves above or below the reference at the beginning.

All data acquired after the impact are wirelessly transmitted to the central device in the wireless network by each MSS. The central device sends all collected data packets to a base station such as a PC through serial communication.

These data packets are processed based on their packet types by the GUI running on the base station as shown in Fig. 5.14. When the GUI is running, a save directory is first selected, and then the port and baud rate can be set for the serial communication with the central device. The Start and Stop buttons are used to open and close the serial port. When the Start button

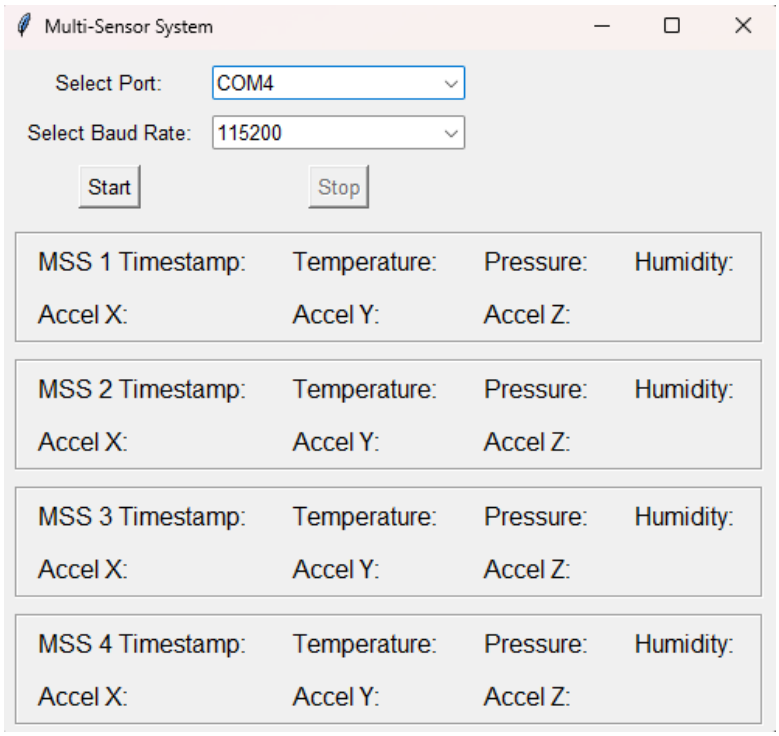


Figure 5.14: Multi-Sensor System GUI

is activated, the GUI is ready to read the serial data coming from the central device.

For each MSS, some information such as timestamp, temperature, pressure, humidity, and acceleration in three axes is directly displayed on the GUI while the PZT sensor data are plotted in a different window after all impact-induced data arrive at the base station.

Second Experimental Setup

The Multi-Sensor SHM system can be configured and programmed based on the requirements of an application, offering flexibility. In the second experiment, only the strain gauge and accelerometer sensors are used, and the strain and acceleration measurements are continuously recorded in the structure simultaneously. An aluminium specimen is used as shown in Fig. 5.15 to be subjected to large deformation and observe a wider range of strain value as composite panels are much stiffer. Therefore, the aluminium specimen is more suitable to assess the performance of the strain gauge and accelerometer modules in the MSS.

In this experiment, the strain gauge is placed in the middle of the aluminium specimen. While one side of the specimen is clamped on the desk, the force is applied to another side upward and downward to observe changes in the strain. The accelerometer is integrated on the

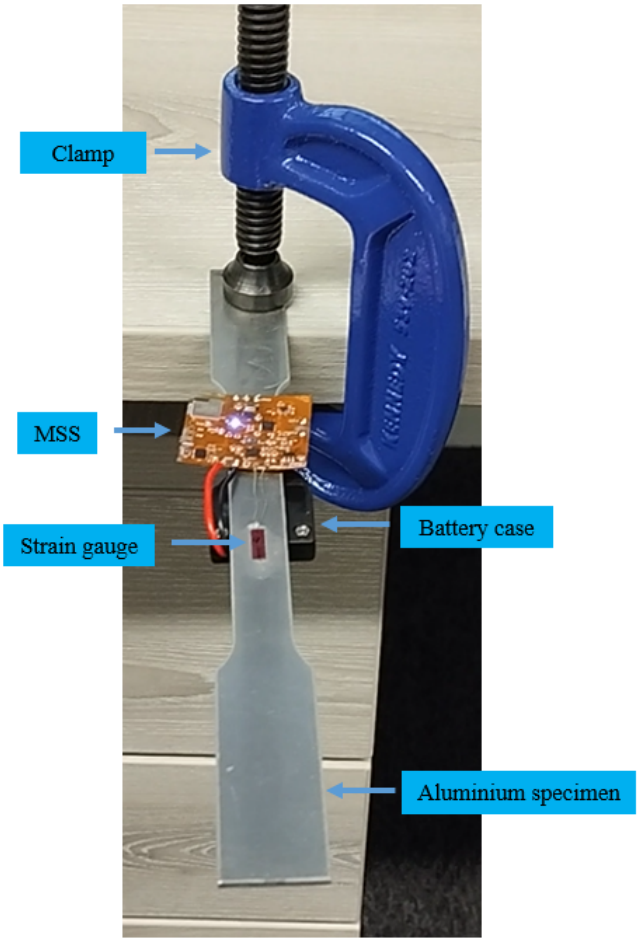


Figure 5.15: Experimental setup for strain measurement with aluminium specimen

flexible PCB and is ready to record as well.

Before starting the experiment, there is a challenge that should be considered. That is, the offset in the strain gauge measurements is a common issue that requires calibration to ensure accurate and reliable data. This offset can result from various factors, including initial imbalances in the Wheatstone bridge due to resistor tolerances or inconsistencies in the bonding of the strain gauges to the structure. Temperature changes can also affect the resistance of the strain gauges and bridge components, leading to offset in the absence of any applied force. In addition, the signal conditioning circuit, particularly the amplifiers, may introduce inherent offset voltages. Residual stresses within the structure or fluctuations in the power supply to the Wheatstone bridge can further contribute to deviations in the baseline measurement. Environmental noise, such as electromagnetic interference, may also influence the observed offset.

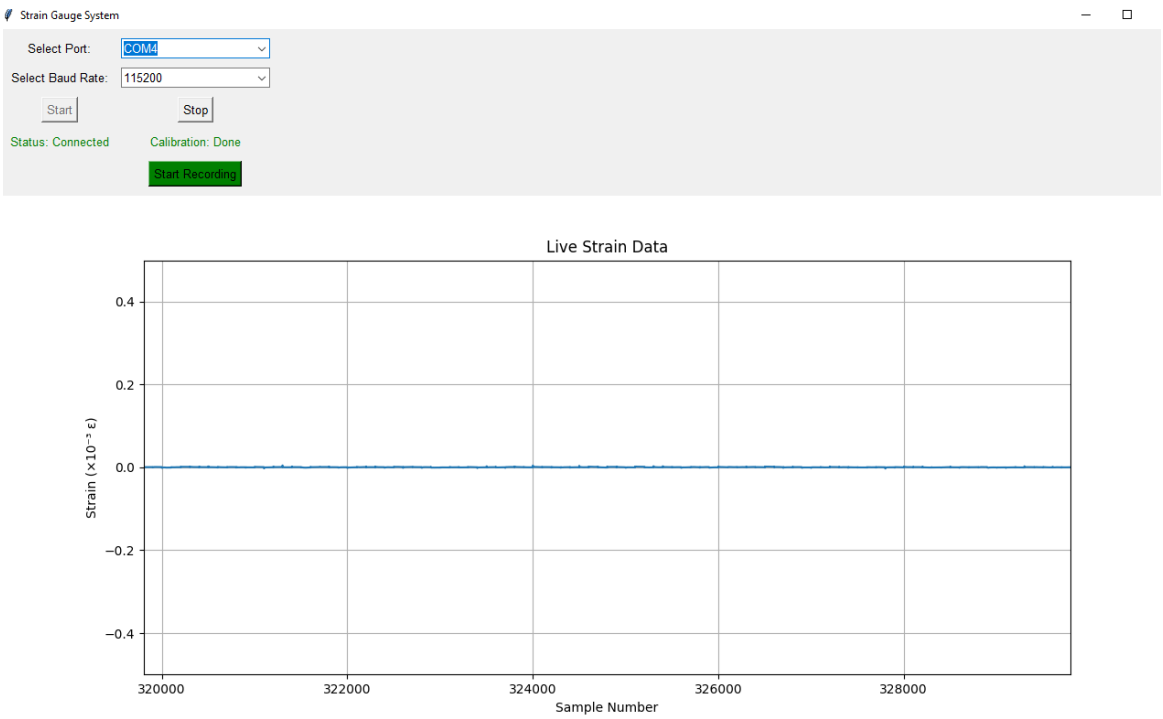


Figure 5.16: GUI modified for strain measurement

To address these challenges, the calibration procedure in the system involves determining the offset when the structure is in steady condition without any applied force. During this phase, 1000 initial samples are collected and averaged. The calculated average value represents the offset. This offset is then subtracted from subsequent measurements to correct for any baseline error. This approach ensures that the strain gauge outputs are calibrated accurately, improving the overall precision of the measurements.

The GUI is modified for this experiment with new functionalities to calibrate the system and display real-time data streams coming from the serial port. As shown in Fig. 5.16, the GUI provides a continuous visualization of the data, allowing users to monitor the state of the system in real-time. The GUI also includes indicator messages to display the status of the serial port (connected / disconnected) and the calibration (not started, in progress, and done), providing users with critical information during operation. In addition, the real-time data stream can be saved by clicking the Start Recording button for further data processing subsequently.

5.5 Results and System Performance of MSS

The proposed Multi-Sensor SHM system is designed for versatile deployment. For example, it supports both event-triggered DAQ where composite panels are impacted to acquire multi-modal sensor data as well as continuous monitoring of real-time strain and acceleration. Its precise time synchronization further enables an accurate correlation of sensor outputs. The system verification and validation is carried out for different scenarios.

5.5.1 Application 1: Event-triggered experiment to acquire all types of sensor data

In the first experiment, impacts, which exceed predefined threshold values, are made using a hammer on the composite panel as shown in Fig. 5.12. Afterwards, each MSS wirelessly transmits timestamp, PZT signal, accelerometer, and environmental sensor data to the central device. The GUI process all packets coming from the central device, and each module is labelled (e.g. 'MSS 1', 'MSS 2', etc.). The concurrent outputs from multiple sensor modules are displayed, such as timestamp in microseconds and a set of measurements: temperature (°C), pressure (Pa), humidity ($\%RH$), and acceleration in the X, Y and Z axes (12-bit digital format) as shown in Fig. 5.17.

In addition, the PZT signals generated by the impact are plotted and displayed in a different window as shown in Fig. 5.18. These PZT signals are plotted after a set of signal conditioning on the hardware side, such as filtering, attenuation, and shifting. Therefore, the signal voltage range is from 0 to 3.3 V and oscillating around 1.65 V as configured in the circuit. For a data-acquisition window of 10 ms in each MSS, 1000 samples are taken due to the sampling frequency of 100 kHz in the ADC.

5.5.2 Application 2: Real-time continuous strain and acceleration DAQ

In the second experiment, only the real-time strain and acceleration measurements of the aluminium specimen are displayed and recorded. An example of the real-time data stream is

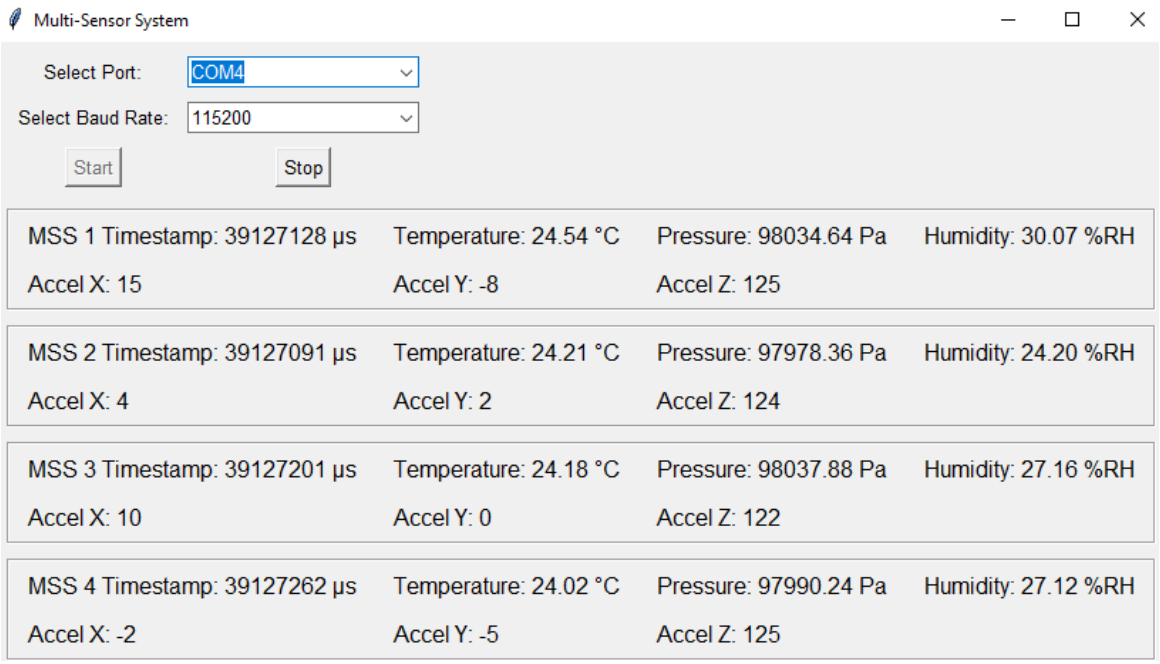


Figure 5.17: Timestamps and sensor data from four MSSs in the wireless network

shown in Fig. 5.19 from the strain measurement.

When a force is applied to a specimen, the resulting strain depends on the direction of the force relative to the structure. The strain is a dimensionless measure of deformation, representing the relative change in length of a material under stress. It can be categorized into tensile strain (positive strain) and compressive strain (negative strain).

In addition, the accelerometer sensor measurement is also shown in Fig. 5.20 for three axes separately. The results are expressed in meters per square second (m/s^2).

5.5.3 Application 3: Timestamp experiment for impacts

Time synchronization is also achieved in the wireless network, and its results are evaluated. When an impact occurs on the composite panel, the system acquires the timestamp from the shared clock in the wireless network together with the sensing signal. Storing the timestamp in microseconds offers a more precise measurement of the TDoA for each PZT sensor. An unsigned 64-bit integer variable is used to represent the timestamp in microseconds, avoiding the overflow issue encountered with lower-bit variables.

To evaluate the performance of the shared clock and time synchronization, a hammer was used to strike near each sensor, and the resulting timestamps were transmitted wirelessly to the

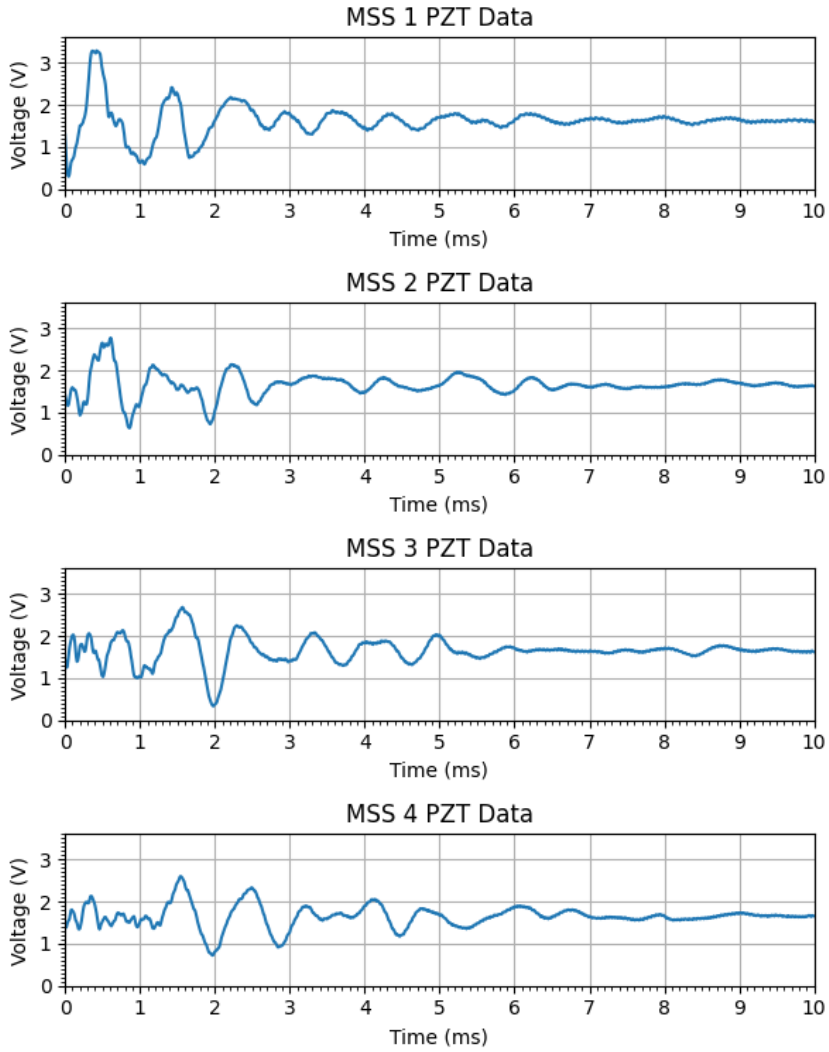


Figure 5.18: PZT signals from four MSSs in the wireless network

central device. Table 5.1 presents the TDoA collected from the MSSs 1 through 4. As expected, the sensor nearest the impact point consistently exhibited the earliest timestamp.

In addition to the applications, the performance of the system is evaluated by comparing its measurement outputs with those obtained from commercial instruments. For example, the acquisition of PZT signals is directly compared with that recorded by a digital oscilloscope configured with equivalent resolution and sampling frequency, while real-time strain and acceleration data are similarly verified against established devices. The close correspondence between sensor outputs and those from commercial equipment confirms the ability of the system to capture and transmit accurately.

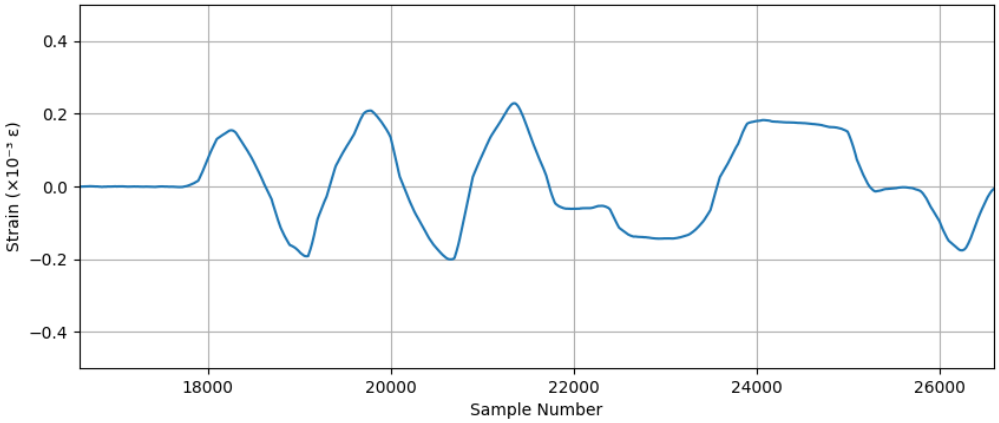


Figure 5.19: Real-time strain data display

Table 5.1: TDoA in the event of impact around each MSS

	Impact 1 TDoA	Impact 2 TDoA	Impact 3 TDoA	Impact 4 TDoA
MSS 1 (μs)	0	82	233	165
MSS 2 (μs)	88	0	253	265
MSS 3 (μs)	254	218	0	54
MSS 4 (μs)	267	255	100	0

5.5.4 PZT signal acquisition performance

The accuracy of the proposed system for measuring PZT signals was verified through a comparative assessment against a digital oscilloscope (TiePie Handyscope HS5). To maintain consistency and compatibility among the measurements, the configuration of oscilloscope was aligned with that of the MSS. In particular, the oscilloscope was set to operate at a 12-bit resolution and a sampling rate of 100 kHz, mirroring the parameters employed in the MSS system.

In addition, the trigger level of the oscilloscope, used as a detection threshold, was adjusted to align with the threshold voltages of the MSS system. Since the sensor circuit applies an attenuation factor of 2 and offset of 1.65 V, the oscilloscope thresholds were set to -0.3 V and 0.3 V and, corresponding to the MSS thresholds of 1.8 V and 1.5 V. This alignment of parameters ensured a valid comparison between the proposed system and the oscilloscope, providing a robust basis to assess the performance of the proposed system.

To achieve a comparison of the results, the PZT sensor was connected in parallel to both the oscilloscope and the MSS, ensuring that each system captured the identical impact event under uniform conditions. The impact was produced with a hammer and both devices simultaneously

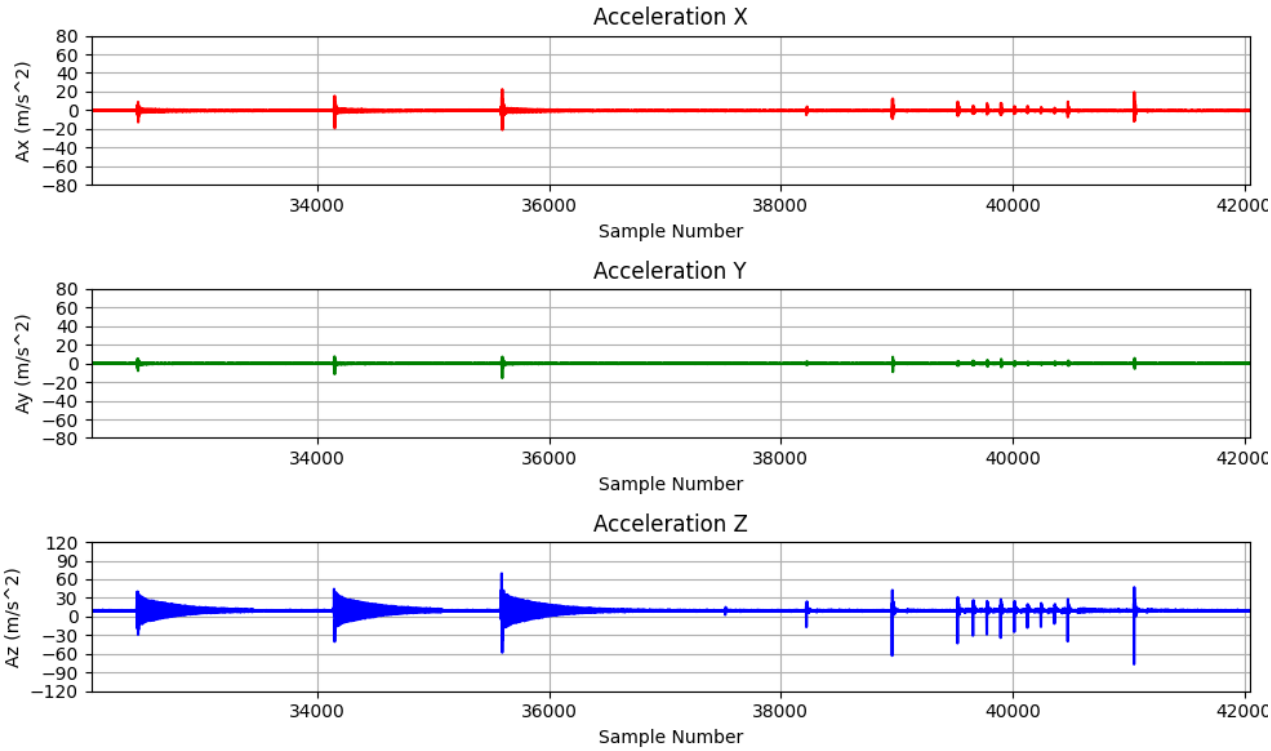


Figure 5.20: Real-time acceleration data display for three axes

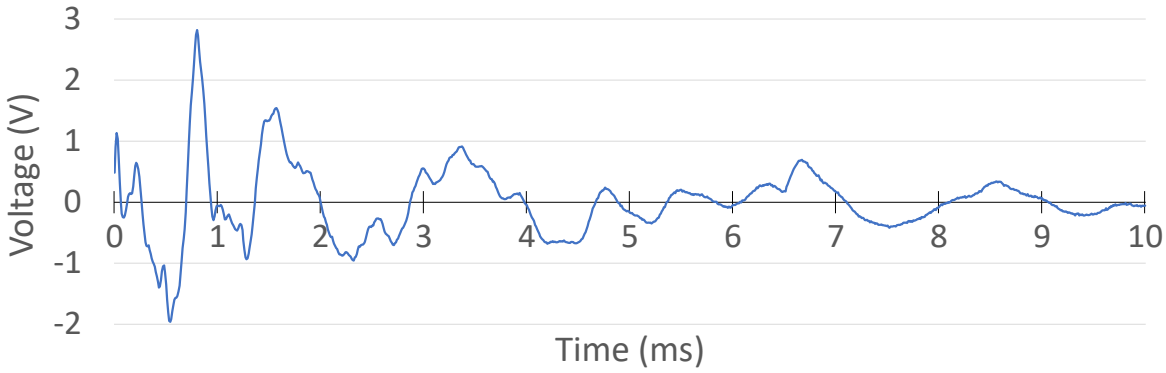


Figure 5.21: Digital oscilloscope measurement of the PZT signal

recorded the resulting signal.

The signal acquired by the oscilloscope was saved through its dedicated software tool. In parallel, the MSS-acquired signal was transmitted wirelessly to the central device, where it was subsequently processed and recorded using the custom GUI developed for the system.

The data acquired from the oscilloscope are presented in Fig. 5.21, while the corresponding data obtained from the MSS are shown in Fig. 5.22. These visualizations offer a clear basis for comparing the performance of both systems in capturing and processing the same sensing signals.

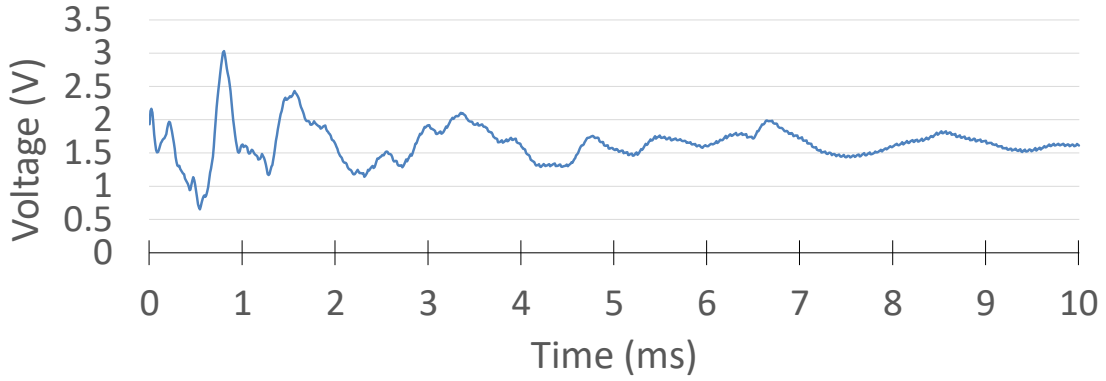


Figure 5.22: MSS PZT result

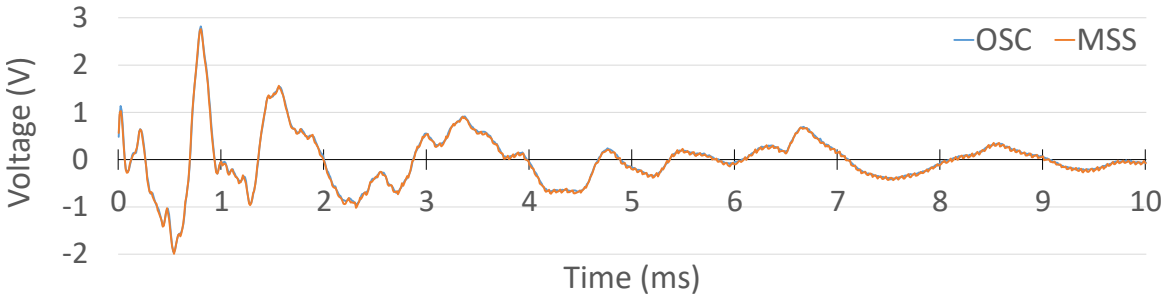


Figure 5.23: The comparison of the oscilloscope and MSS results

For comparison purposes, the MSS output must first be shifted by its offset (1.65 V) and then scaled by the attenuation factor of 2. The resulting comparison is shown in Fig.5.23. The signal patterns from both systems overlap each other and match exactly, validating the MSS PZT acquisition. The signals closely align in the time domain, confirming their temporal precision. These findings confirm that the MSS system can accurately capture and transmit sensing data comparable to that of the oscilloscope.

5.5.5 Continuous strain and acceleration data acquisition performance

The capability of the proposed MSS for real-time strain and acceleration measurement was evaluated against a commercial DAQ system (Genesis HighSpeed DAQ hardware and Perception software from HBK, formerly HBM). The objective of this evaluation was to assess the ability of the system to continuously monitor and record strain and acceleration responses in a structure under mechanical loads. Unlike event-triggered impact detection, this experiment focused on

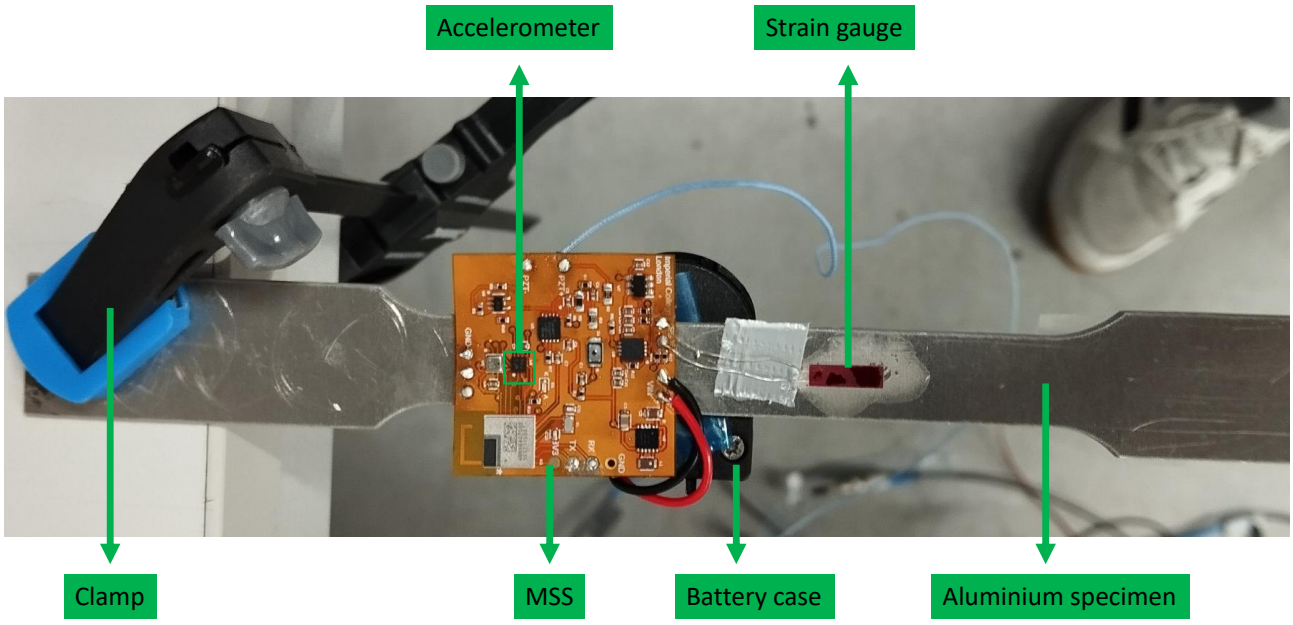


Figure 5.24: Experimental setup to compare acceleration and strain gauge measurements between the proposed MSS and a DAQ system, top view

continuous acquisition of strain gauge and accelerometer data, enabling real-time observation of structural deformations and dynamic responses.

To validate the system performance, an MSS was integrated with an aluminium specimen for strain and acceleration measurements. Aluminium was selected because of its relatively lower stiffness compared to composite materials, allowing for larger deformations and a wider strain range. The specimen was clamped on one side as shown in Fig. 5.24, and an external force was applied at the other end to induce strain and acceleration variations.

As shown in Fig. 5.24, a strain gauge sensor was attached to the specimen and connected to the MSS. In addition, the MSS has an on-board accelerometer (BMA400 from Bosch Sensortec) as introduced earlier. To compare the results, another strain gauge sensor and accelerometer (Model 352A24 from PCB Piezotronics) were attached to the bottom as shown in Fig. 5.25 and connected to the commercial DAQ system.

Subsequently, external alternating forces were applied to the specimen, and measurements were recorded from the strain gauge and accelerometer sensors using both the MSS and the commercial DAQ system simultaneously.

The next sections present the experimental results, discussing the accuracy and reliability of strain and acceleration measurements captured by the MSS.

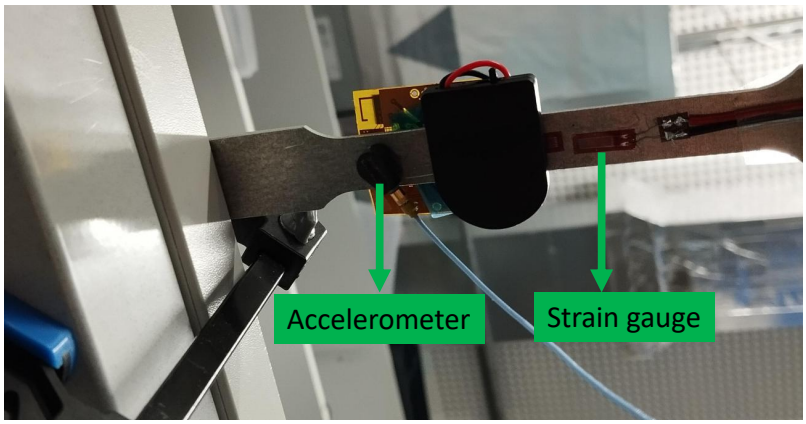


Figure 5.25: Experimental setup to compare acceleration and strain gauge measurements between the proposed MSS and a DAQ system, bottom view

Comparison of strain gauge measurements

For strain gauge measurements, the sampling frequency was set to 1 kHz for both the MSS and the commercial DAQ system. The result of the commercial DAQ system is presented in Fig. 5.26.

For the same applied forces, the strain measurement with the MSS is given in Fig. 5.27. Due to the positions of the strain gauge sensors, one of them was attached on the top side while another on the bottom side of the specimen, the strain measurement obtained using the MSS is inverse relative to those recorded by the commercial DAQ, as expected. This is because one strain gauge sensor measured tensile strain while another measured compressive strain under the same load, and vice versa. Therefore, when the strain measurement of the MSS was

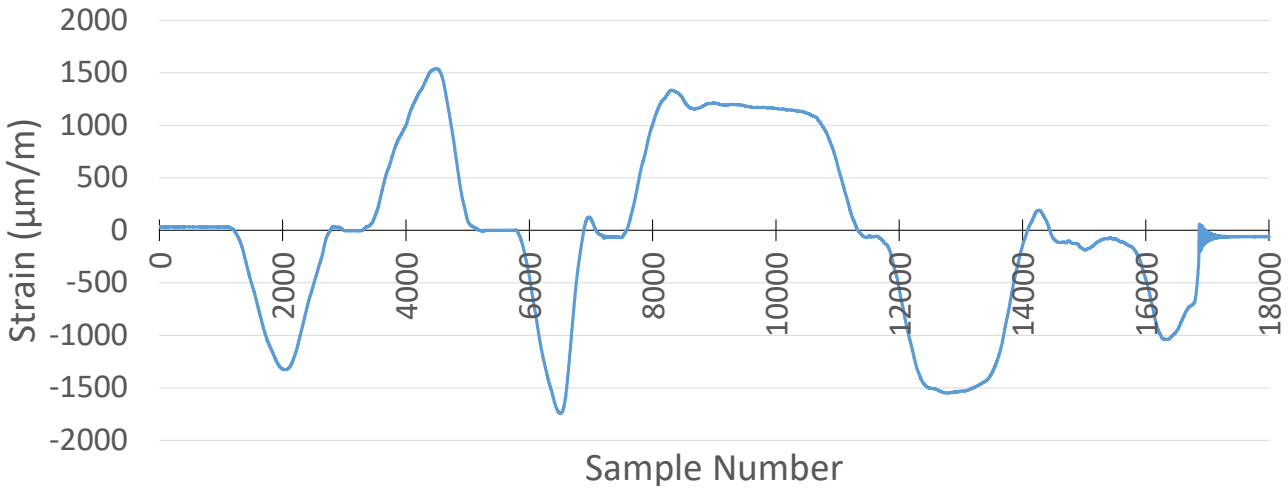


Figure 5.26: Strain gauge measurement with HBK DAQ system

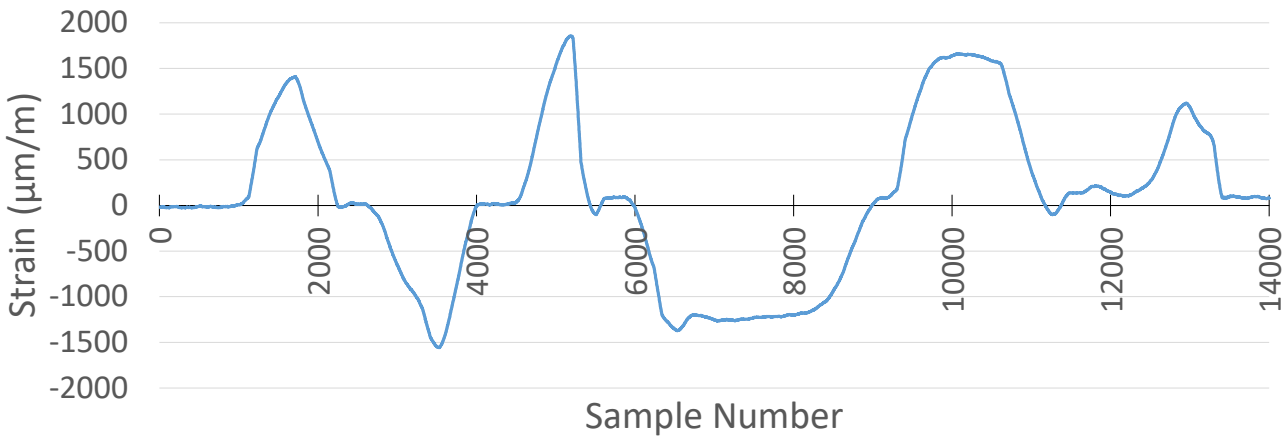


Figure 5.27: Strain gauge measurement with the proposed MSS system

reversed, the pattern and peak values of the measurement were almost the same as those of the commercial DAQ.

When comparing the results from the MSS and the commercial DAQ system, another critical point observed was that the sample numbers taken were different for the same measurement period, although both systems had the same sampling frequency of 1 kHz. while the commercial DAQ system recorded 18000 samples, the MSS captured 14000 samples in the experiment performed.

The reason is that the MSS records strain values until its predefined buffer becomes full, and then data are transmitted wirelessly to be processed. In this period of wireless data transmission, there is a very short delay in processing the strain values. Therefore, the MSS had a lower sample number for the same measurement period than the commercial DAQ system. However, as observed from the measurements in Fig. 5.26 and Fig. 5.27, the overall strain patterns and peak values are nearly identical. These short delays caused by each data packet transmission wirelessly result in a reduction in the sampling frequency for the MSS.

To compare the results, the measurement obtained by the MSS was reversed and stretched in the same time domain with the commercial DAQ system. The comparison is shown in Fig. 5.28. The two signals exhibit closely matching waveforms with similar amplitudes and peak strain values.

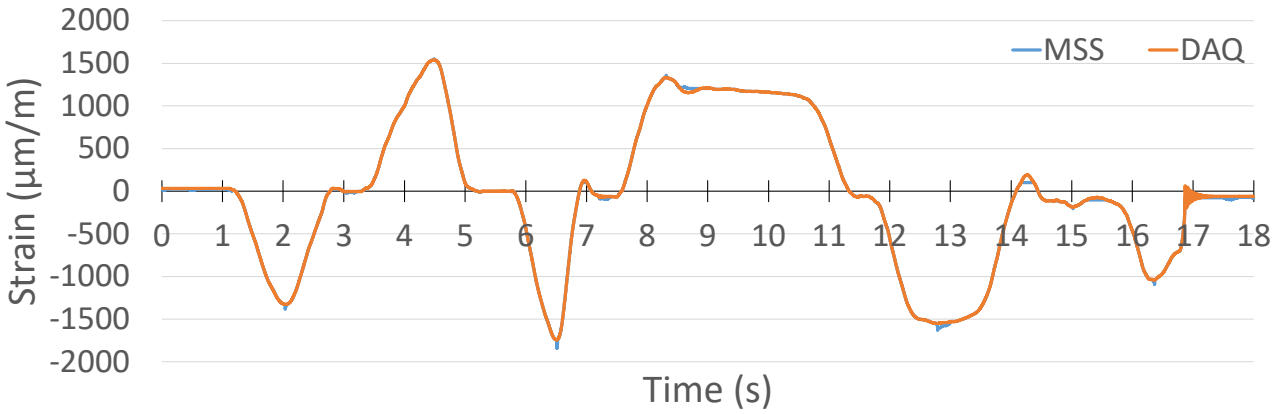


Figure 5.28: Comparison of strain gauge measurement between the proposed MSS and HBK DAQ system

Comparison of acceleration measurements

For comparison of the acceleration results between the MSS and the commercial DAQ systems, external forces were applied to vibrate the specimen to observe their decay patterns. The comparison was achieved in Z-axis because model 352A24 from PCB Piezotronics measures only the acceleration in Z-axis while the on-board accelerometer in the MSS can measure the acceleration on 3 axes (X, Y, and Z).

Furthermore, the sampling frequency of the commercial DAQ system to measure the acceleration was 1 kHz while the output data rate of the on-board accelerometer was set to 800 Hz, the allowable maximum rate.

The acceleration measurement collected from the commercial DAQ system is shown in Fig. 5.29.

Meanwhile, the acceleration recorded by the MSS in the Z-axis is plotted in Fig. 5.30.

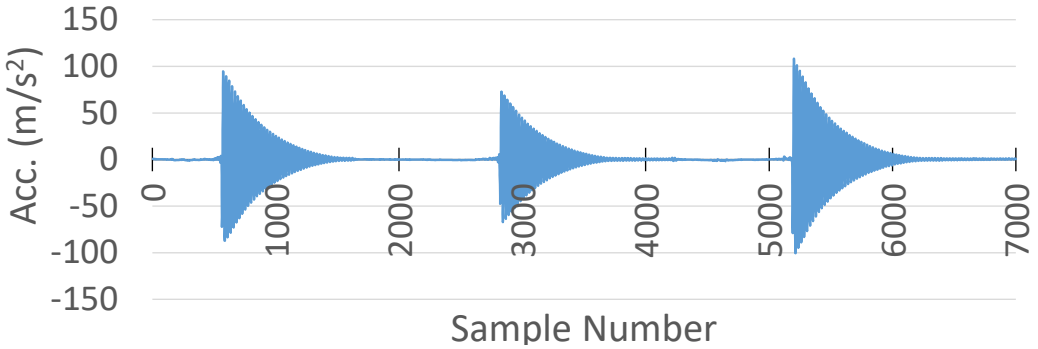


Figure 5.29: Acceleration measurement with HBK DAQ system

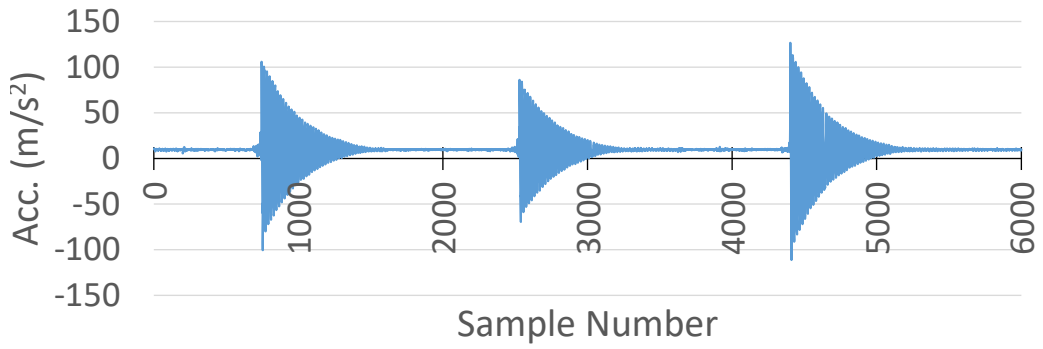


Figure 5.30: Acceleration measurement with the proposed MSS system

Similarly to the comparison of the strain measurements, the MSS had a lower sample number than the commercial DAQ system. The first reason was the short delay caused by the wireless communication as discussed earlier in the strain measurement comparison. Secondly, the output data rate of the on-bard accelerometer in the MSS was already slower than that of the commercial DAQ system.

Another critical point is that there is an offset in the acceleration measurement with the MSS as shown in Fig. 5.30. This offset is +1g on the Z-axis because the sensor is experiencing Earth's gravitational acceleration [11].

Therefore, to compare the results, the offset in the MSS acceleration measurement was removed and stretched in the same time domain with the commercial DAQ system. Their comparison in the same time domain is shown in Fig. 5.31. In addition, a close-up comparison is also provided in Fig. 5.32.

Although the MSS exhibited higher amplitudes in the initial peaks in the negative direction, both the MSS and commercial DAQ signals shared a similar oscillatory profile and decay pattern, validating the MSS acceleration output. This difference in peak amplitudes could be attributed to variations in accelerometer mounting locations and substrate properties, which may influence the signal response.

In summary, the proposed MSS showed reliable and accurate performance in capturing both strain and acceleration measurements compared to the commercial DAQ system. Minor variations in sampling frequency were observed because of short wireless transmission delays. The MSS consistently reproduced the essential waveforms, decay patterns, and peak values measured by the commercial DAQ system. In general, the MSS demonstrates reliable real-time

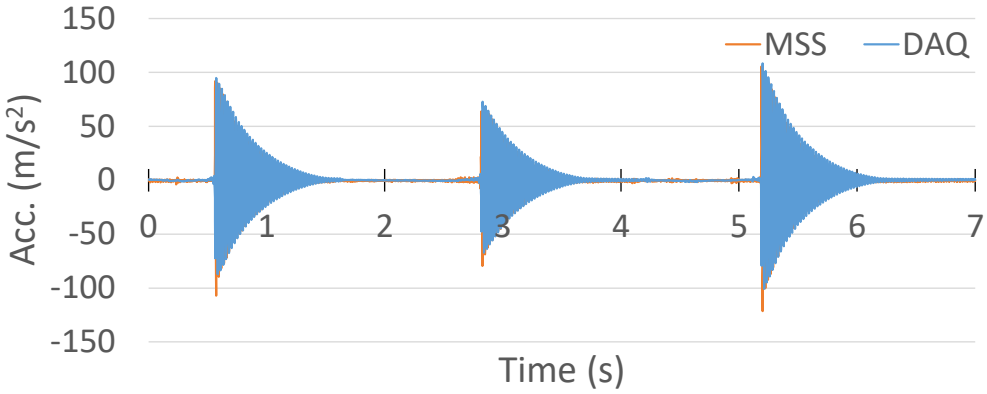


Figure 5.31: Comparison of acceleration measurement between the proposed MSS and HBK DAQ system

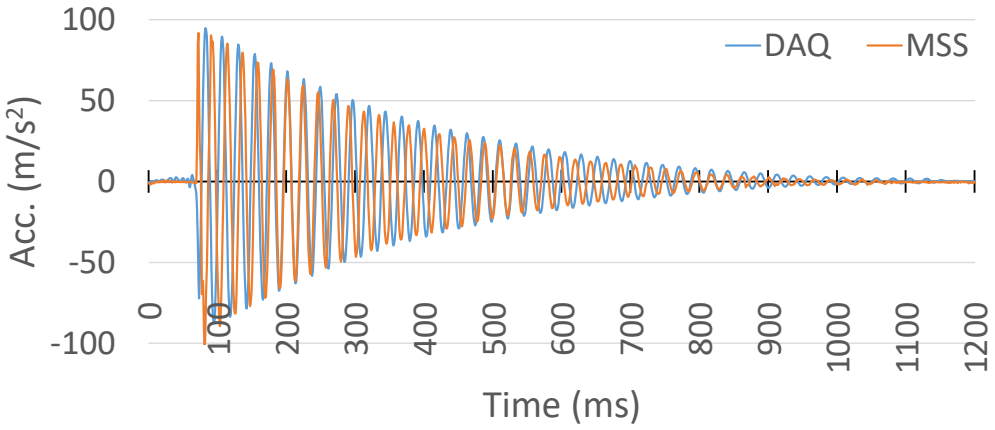


Figure 5.32: A close-up comparison of acceleration measurement between the proposed MSS and HBK DAQ system

DAQ and serves as a suitable and cost-effective option for continuous SHM.

5.5.6 Power Consumption

Ensuring high energy efficiency in the proposed system is essential for maximizing its operational lifespan. To evaluate the power usage of the MSS, current measurements were recorded using the Keysight 34465A Digital Multimeter under three representative operating conditions.

1. **Standby Mode:** In this condition, the sensor node remains in a low-power sleep state, with no active wireless communications or data transmissions. This scenario represents the baseline power consumption when the system is idle.

2. **Time synchronization:** the MSS has successfully established a wireless connection and

Table 5.2: Characterized current draw across multiple operating states

Operating State	**Current Consumption**
Standby (No wireless connection)	55 μA
Time synchronization	1.3 mA
Impact detection (Wireless transmission active)	7.5 mA

Table 5.3: Power consumption across multiple operating states

Operating State	**Power Consumption**
Standby (No wireless connection)	181.5 μW
Time synchronization	4.29 mW
Impact detection (Wireless transmission active)	24.75 mW

maintains network-wide time synchronization. These additional activities results in higher power consumption compared to the standby state.

3. **Impact detection:** During this mode, the sensor node is fully active, processing the impact event, capturing timestamp, measuring acceleration and environmental data, and transmitting data packets wirelessly. This power consumption is limited until all data packets are transmitted in milliseconds, reflecting the combined energy demands of acquisition, processing, and communication.

Table 5.2 summarizes the measured current consumption for each operating state, providing key insights into the overall energy requirements of the MSS.

To calculate power consumption, the formula can be used in Equation 4.2. MSS operates at a supply voltage of 3.3 V. Using this voltage, the power consumptions are calculated and demonstrated for each state in Table 5.3.

5.5.7 Range Testing

Ensuring an adequate wireless communication range is essential for reliable data transfer between peripheral and central devices within the network. This range is determined by several factors, including the modulation scheme (e.g. standard 1M PHY versus long-range coded PHY), transmit power, and the propagation environment, where effects such as absorption and reflection can substantially weaken the signal. Moreover, the orientation and type of antenna further influence the effective range achieved [38, 98].

Table 5.4: Achieved Communication Range under Various TX Power Levels and Modulation Strategies

TX Power	**Coded PHY**	**1M PHY**	**2M PHY**
0 dBm	60 m	28 m	15 m
+8 dBm	160 m	75 m	40 m

Based on these considerations, the communication range of the proposed system was evaluated. All experiments were conducted outdoors under line-of-sight conditions to minimize multipath fading and signal absorption effects that are typically encountered indoors.

To determine the maximum reliable distance, the devices initially formed a communication link. The peripheral and central nodes were then gradually separated while maintaining the connection. The test concluded once the connection could no longer be re-established, with an LED on the MSS serving as a visual indicator of the connection status.

In this evaluation, the effective communication range was examined using various levels of radio transmission power and modulation schemes. Two TX power levels (0 dBm and +8 dBm) were tested along with three modulation schemes: Coded PHY, 1M PHY, and 2M PHY. The lower TX power setting provided a baseline measure of radio sensitivity, while the higher TX power setting was used to assess potential range extension. Furthermore, comparing the modulation schemes offered insight into the achievable range enhancements. Table 5.4 summarizes the range performance measured for each configuration.

5.6 Conclusions

This work presented a miniaturized, IoT-based multi-sensor system intended for on-board SHM of aerospace structures. The primary goal was to produce a sensing platform that includes various sensor types, low power consumption, and wireless connectivity. The developed system features a compact and flexible PCB measuring 3 cm $\times$ 3 cm and weighing approximately 0.5 grams. It integrates PZT, strain gauge, accelerometer, and environmental sensors for comprehensive structural monitoring. This arrangement allows the system to capture both mechanical and environmental data that influence structural integrity. The hardware design ensures minimal weight and compact dimensions, thus addressing aerospace requirements where

additional mass or size might degrade performance or limit the number of feasible sensing nodes.

The use of a single RF microcontroller featuring Bluetooth LE enables the creation of a low-power, spatially distributed sensor network that reduces wiring needs and simplifies sensor placement. Through a star-topology design, several sensor modules communicate with a central node, which then relays data to a base station for recording and analysis. This approach is adaptable to different types of structures or testing conditions and can accommodate a variety of monitoring tasks, from impact detection to long-term strain measurements.

A key element of the proposed setup is the customized GUI designed for data processing and visualization. This interface simplifies interaction with the system, promoting user-friendliness and enabling efficient data analysis. In addition, different GUI configurations were customized to accommodate various experiments, thus offering versatility in DAQ and processing.

Time synchronization was also performed by incorporating a shared clock into the wireless network, which comprises five nodes. While the central device sends synchronization packets, each sensor node updates its local clock using the data contained in these transmissions. By applying the shared clock, the system records timestamps whenever an impact occurs on the composite structure, enabling the calculation of TDoA among the sensors. The performance of the shared clock was examined by impact tests near sensor nodes, which revealed a clear variation in signal arrival times.

Experimental evaluations demonstrated the reliability of the developed platform. First, multiple miniaturized systems were placed at various positions on a composite panel to measure PZT, acceleration, temperature, pressure, and humidity data. The system responded promptly to impact events and transmitted high-frequency signals in real time, matching results from a calibrated digital oscilloscope. Subsequently, these signals can be used to localize impacts following the algorithm presented in Section 4.5.

Second, the MSS demonstrated its versatility in measuring real-time strain and acceleration by applying it to a strain gauge mounted on an aluminium specimen. Calibration procedures effectively eliminated offsets from the Wheatstone bridge, ensuring accurate strain measurements. Comparative tests with a commercial DAQ system showed that the MSS captured structural responses with closely matching signal patterns and peak values. Minor discrepancies in sample

count, due to wireless transmission delays, had no significant impact on measurement accuracy. These results confirm that the MSS is capable of reliable continuous monitoring.

Power consumption was evaluated by measuring current draw across various operational states, including idle standby, time synchronization, and active impact detection. The results confirm that the system is well-suited for long-term SHM applications with minimal power requirements. In addition, range testing was performed to examine Bluetooth LE communication under various transmission power (0 and +8 dBm) and modulation schemes (CODED, 1M and 2M PHY). The findings confirm that the MSS provides reliable wireless coverage suitable for aircraft and structural applications.

These results confirm that the integrated multi-sensor platform is a promising alternative to larger, more complex SHM solutions. The system performance in capturing both localized and global structural changes supports applications where comprehensive diagnostics are required. In addition, the fully integrated wireless approach points to future scalability for sensor arrays distributed over large structures.

The miniaturized flexible PCB described in this work is particularly promising for 'smart-skin' implementations. Using a flexible substrate and compact sensor integration, the platform is designed to accommodate complex or curved surfaces on aerostructures. This feature supports distributed sensing across large areas, providing detailed measurements of vibration, strain, and environmental variables. In addition, the integration of low-power wireless communication simplifies the installation by eliminating extensive wiring and reducing total mass, both critical considerations in flight.

Another beneficial extension is to incorporate energy harvesting modules into the platform, such as vibration-based or solar-based solutions. These modules could supplement or even replace conventional batteries, improving system longevity and reducing maintenance demands for large-scale sensor deployments. In combination with the flexible sensor board, such energy-harvesting approaches make it possible to create self-sustaining 'smart skin' systems capable of continuous structural monitoring under real-world operating conditions.

Chapter 6

Integrated Active-Passive Sensing System

This chapter introduces the Integrated Active-Passive Sensing (IAPS) System, a miniaturized, multi-channel platform designed for SHM applications. The system combines active sensing, which employs guided wave excitation for damage detection, with passive sensing, which captures impact-induced signals for real-time monitoring. The hardware implementation, including external ADC/DAC, charge amplifiers, and Bluetooth LE communication, is detailed alongside its 4-layer PCB design.

The experimental results confirm the effectiveness of the passive sensing mode, including selectable attenuation levels and multi-channel signal acquisition. The active sensing mode successfully generates actuation signals, but practical constraints on sampling rate and SPI communication bandwidth are identified and discussed.

The chapter concludes with an evaluation of the system performance, limitations, and potential improvements, emphasizing the significance of this miniaturized, integrated approach for SHM in aerospace applications.

6.1 Introduction

SHM integrates active and passive sensing strategies to ensure the integrity of critical structures through continuous assessment of their condition. Active sensing involves the application of controlled excitations, such as wave propagation or electromechanical impedance methods, allowing piezoelectric sensors to detect anomalies by generating and analyzing diagnostic signals, as in the case of detecting delamination in composite structures via PZT sensors. In contrast, passive sensing relies on naturally occurring signals, including acoustic emissions from crack growth or impacts, to detect structural changes in real time. By integrating these complementary approaches, SHM enables the timely identification of potential damages and supports informed maintenance decisions, ensuring the long-term reliability and performance of critical infrastructures [31, 46, 73, 79].

Active sensing is a vital approach in SHM, utilizing actuators and sensors to generate diagnostic signals and record structural responses, allowing the identification, localization, and quantification of damage. This method typically employs PZTs, which can both emit and receive guided waves such as Lamb waves. These waves are highly effective for large-area monitoring, as they propagate efficiently across structures with minimal energy loss. The wave propagation technique focuses on analysing Lamb waves, where specific wave modes, such as symmetric (S0) and antisymmetric (A0), exhibit varying sensitivity to different types of damage, including cracks and delaminations [110]. Changes in wave attenuation, time delay, and scattering patterns reveal damage characteristics. Ihn and Chang [47] demonstrated the potential of pitch-catch methods, where an actuator-sensor pair provides a localized damage index. This approach was validated on airframe structures, highlighting its applicability for real-time monitoring and diagnostics.

Active sensing has been successfully applied in various SHM applications, including damage detection and impact localization [32, 109, 112]. Recent advances by Wang et al. [103] utilized energy dissipation caused by tangential damping to quantitatively monitor bolt looseness, demonstrating the sensitivity of PZTs to changes in preload. Diagnostic imaging techniques, such as time-reversal and delay-and-sum algorithms, further enhance damage visualization by

using multiple sensor responses to reconstruct damage maps [66, 102, 111]. In harsh operational conditions, such as high-temperature or radiation environments, piezoelectric wafer active sensors have proven effective in enduring such stresses, enabling their use in the aerospace and nuclear industries [73]. These advances underscore the importance of active sensing as a reliable, scalable, and efficient SHM strategy.

In addition, passive sensing in SHM acquires naturally occurring signals such as vibrations from composite and concrete structures, which helps identify impact at an early stage. By analyzing data from PZTs, these methodologies can determine impact locations and measure its severity without applying external excitation [31, 46, 86, 96]. Techniques based on wave propagation, triangulation and data-driven algorithms, including Artificial Neural Networks and Bayesian neural networks, have shown promising accuracy under varying conditions [86, 96, 109]. Wireless sensor networks improve these methods by supporting extensive coverage and reduced power demands, making them suitable for long-term monitoring [96].

Mounted sensors in structures allow the real-time collection of information on changes in material state, such as delamination, cracking in composites and concrete [46, 47, 79]. Passive methods simplify installation and maintenance because they do not require active stimulation and usually consume little power [47, 73, 79, 109]. Advanced signal processing techniques, combined with low-power electronics, detect slight variations in wave propagation or strain levels, making these systems effective in aerospace, civil, and other critical sectors [31, 46, 96]. The development of new sensor materials has improved sensitivity and durability, increasing reliability in passive sensing for extended performance assessments [73, 79].

The integration of active and passive sensing into a single platform offers flexibility by utilizing the strengths of both approaches. Active sensing provides precise control over diagnostic processes and can target specific regions, while passive sensing captures real-time, spontaneous events. This dual approach improves the reliability and accuracy of damage detection, particularly in complex structures such as composite materials, where different types of damage may require distinct detection strategies. Therefore, the synergy between active and passive sensing methods represents a significant advancement in SHM, enabling robust, adaptive, and efficient monitoring solutions for diverse structural applications.

Several wireless sensor prototypes have been proposed in the literature to facilitate SHM data acquisition and transmission in various applications. For example, Fu et al. [34] introduced a CPS that integrates WSN with PZTs to detect damage. The same research group later proposed a wireless structural health monitoring system (WSHMS) focused on detecting impacts in composite airframes [35]. In a parallel effort, Swartz et al. [95] upgraded an existing wireless sensing unit to improve measurement accuracy and optimize data processing for civil infrastructure applications. Harms et al. [41] described a WSN based on SmartBrick, a low-power device serving as a base station that coordinates sensor nodes, which is particularly suited for multi-span bridge monitoring. Sazonov et al. [84] proposed a wireless intelligent sensor and actuator network (WISAN), which addresses the critical need for synchronous data acquisition in vibration-based SHM. Additional WSN-based SHM initiatives are detailed in [45, 61, 70, 104, 107, 115]. However, all of these developed systems are dedicated to active or mostly passive sensing applications only.

Existing prototypes often feature either active or passive methods, lack modularity, or rely on relatively bulky designs that limit their suitability for in-service applications. Furthermore, while low-power wireless communication has gained attention, many currently available solutions do not incorporate all sensing functions into a single, compact platform. This shortfall emphasizes the need for an integrated approach that unites miniaturized hardware, active–passive sensing methods, and reliable wireless data transmission. Furthermore, a fully integrated active-passive sensing platform requires sophisticated PCB design and careful component selection to ensure miniaturization, accurate signal capture, minimal noise interference, and reliable wireless data transmission. Such a compact multi-functional SHM system is crucial in aircraft applications where space and weight allowances are strictly limited.

Hence, this study has introduced the development of a miniaturized, integrated active–passive system equipped with wireless communication (Bluetooth LE), thus improving the health assessment of composite aerostructures by enabling both passive (early warning) and active (damage detection and characterization) sensing solutions. In addition, the proposed system is multi-channel (4 channels) and equipped with a GUI to handle the sensing data such as receiving, processing, plotting, and saving.

6.2 Development of Integrated Active-Passive Sensing System

Based on the limitations and requirements highlighted in the previous section (Section 6.1), the proposed system aims to address the absence of a compact, multi-channel platform capable of both active and passive sensing with wireless data transmission. This section details the hardware and software design considerations that support the miniaturized architecture, demonstrating how the system overcomes key barriers such as space constraints, integration complexity, and the need for robust wireless communication.

The primary objective was to integrate active and passive sensing modalities within a single PCB, ensuring minimal signal interference and reliable data acquisition in real-time. Critical design choices, such as PCB layout, component selection, and electromagnetic shielding, were made to accommodate high-frequency signals generated during guided wave-based inspections along with lower-frequency impact signal. Particular emphasis was placed on balancing the power requirements of both sensing methods to maintain a lightweight and efficient form factor suited for aircraft applications.

The design of the active and passive sensing circuits reflects their fundamentally distinct operational requirements. In passive sensing, high-energy events, such as impacts, can produce signals with relatively large amplitudes, requiring signal attenuation before being processed by the MCU. In contrast, in active sensing, guided wave–based approaches often measure signals of the order of millivolts, thus requiring amplification to bring these signals within a suitable range for processing by the MCU. These different signal scales drive unique hardware requirements, including specialized amplifier or attenuator networks to ensure accurate data acquisition in both active and passive sensing modes.

Furthermore, a four-channel input configuration was implemented to support multiple sensor nodes, thus expanding the capacity of the system for a comprehensive structural assessment. This multi-channel design is essential for accurately localizing damage and monitoring various regions of a composite structure simultaneously.

In addition, external ADC and DAC modules are integrated to support both active and

passive sensing modes. Although the sampling rate of 200 kHz in the chosen MCU is sufficient to capture passive signals of lower frequency across four channels, it does not meet the higher-frequency requirements of active sensing (e.g. guided wave propagation). Therefore, an external ADC with a higher sampling rate is used to accurately capture and analyze these high-frequency signals. Moreover, because the MCU used in this study does not include a built-in DAC, an external DAC is used to generate the actuation signal necessary to excite the structure. This setup ensures that both active and passive sensing processes are fully supported.

A fundamental aspect of the proposed system is its versatile switching mechanisms, which enable both active and passive sensing configurations based on the application. Each channel includes a dedicated slide switch to toggle between active and passive sensing modes. There are additional slide switches to allow for the selection of one of two attenuation levels in the passive sensing mode. Furthermore, the MOSFET transistors act as electronic switches to enable or disable the operational amplifiers in the active sensing; this arrangement ensures that when a PZT channel is used for actuation, its corresponding sampling circuit is powered down. When the active sensing configuration is selected, another MOSFET transistor is used to switch off the entire passive sensing circuit to reduce unnecessary power consumption. All of these MOSFET transistors are controlled by the microcontroller. This approach not only ensures efficient use of hardware resources, but also reduces unnecessary power draw by deactivating non-essential components when switching between active and passive sensing operations. In addition to slide switches and MOSFET transistors, there is also a multiplexer switch (4:1) for analog signals to route the DAC-generated actuation signal to the desired channel. In addition, while a tactile switch is implemented to reset the MCU, a toggle switch is used to switch on/off the supply voltage to the entire system.

An essential design consideration in the proposed system is the PCB layout, which is intentionally divided into four primary sections as shown in Fig. 6.1. The sections are analog, digital, power management, and isolation sections to minimize electromagnetic interference and signal cross-talk. The analog section contains the operational amplifiers and related circuitry, including switches that enable or disable op-amps and route the actuation signal to the desired channels. These switches are driven by the control signals from the MCU, which is positioned in

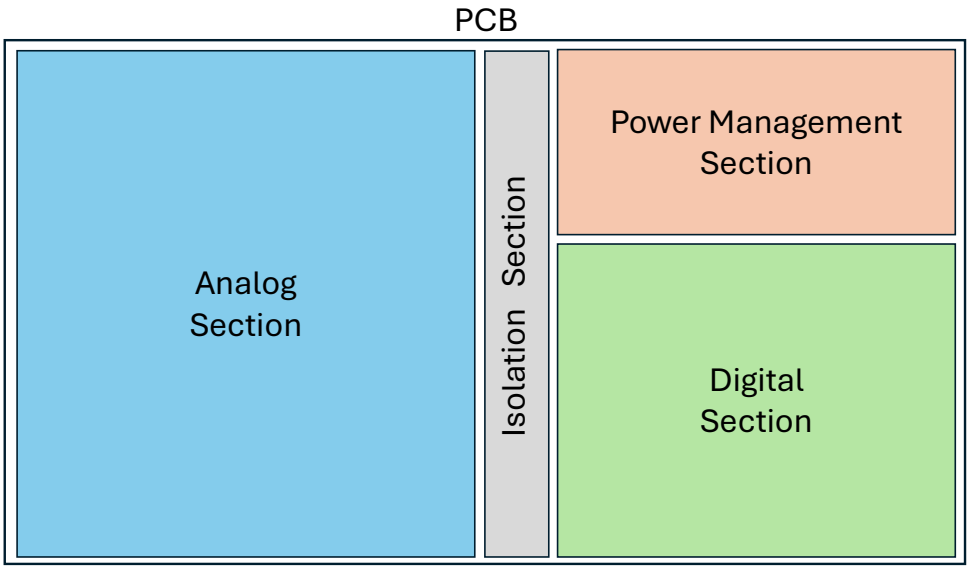


Figure 6.1: PCB layout of IAPS System

the digital domain. To prevent noise coupling when transmitting these control signals, low-pass filters are employed at the boundary between the digital and analog sections. In addition, the external ADC and DAC are strategically placed along this boundary, incorporating shielding and filtering circuits to preserve the precision of both the sensing measurement and actuation signals. Meanwhile, the power management section provides carefully regulated voltage levels for the digital and analog circuits.

To ensure stable and efficient operation of both digital and analog subsystems, the proposed system incorporates a comprehensive power management strategy. A dedicated 5V DC power connector feeds into a DC–DC regulator that supplies a stable voltage source for the microcontroller and other digital components. In parallel, two additional regulators provide positive and negative rails for analog circuitry, including the analog multiplexer switch and operational amplifiers. Furthermore, an integrated battery charging circuit supports rechargeable batteries, enabling continuous operation in situations where an external power source may be unavailable. The power management block diagram of the IAPS system is shown in Fig. 6.2.

Besides, the integration of Bluetooth LE enables wireless data transmission from the sensing platform to a central device. This choice reflects the need for low-power operation in remote or hard-to-access components of the aircraft. The communication protocol has been configured to ensure the smooth transfer of both active and passive sensing data, setting features such as

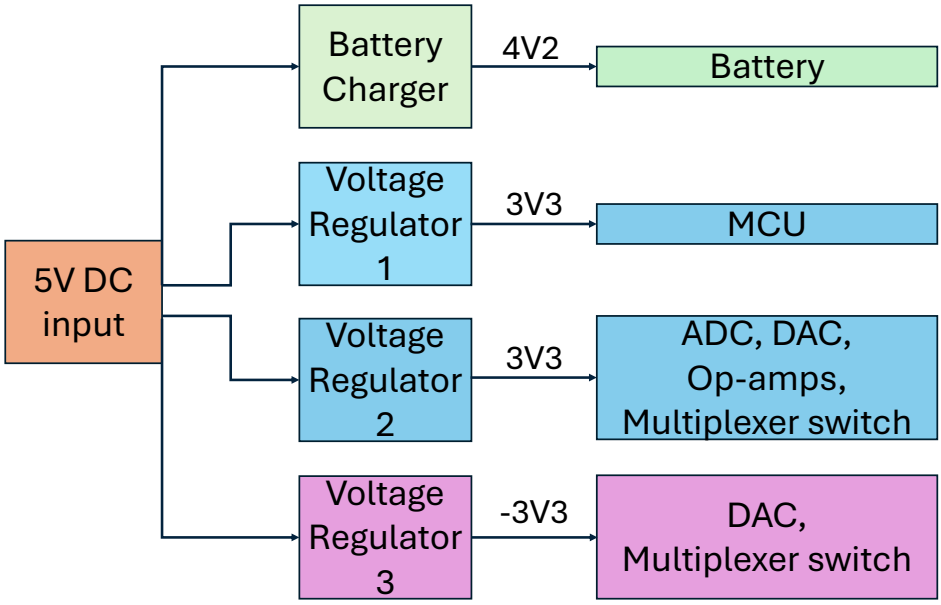


Figure 6.2: Power management block diagram of IAPS System

radio mode and connection type for security. All sensor data acquired from the PZT channels, whether operating in active or passive modes, are transmitted to the central device within the wireless network. This central device is connected to a base station such as a PC through UART serial communication.

Finally, a dedicated GUI was developed to enhance the system management and processing of data from the central device in the WSN. This GUI offers functionalities for receiving raw sensor signals, processing them through embedded algorithms, and displaying plots such as signal waveforms. In addition, the software environment allows the user to log, visualize, and save data for further analysis.

In summary, this integrated active–passive sensing system provides a unified solution to the challenges identified in the introduction by combining a miniaturized, multi-channel hardware architecture with robust Bluetooth LE communication and user-friendly data management tools. The subsequent sections will discuss each design element in detail, illustrating how the synergy of active and passive sensing works together with wireless data transmission capability.

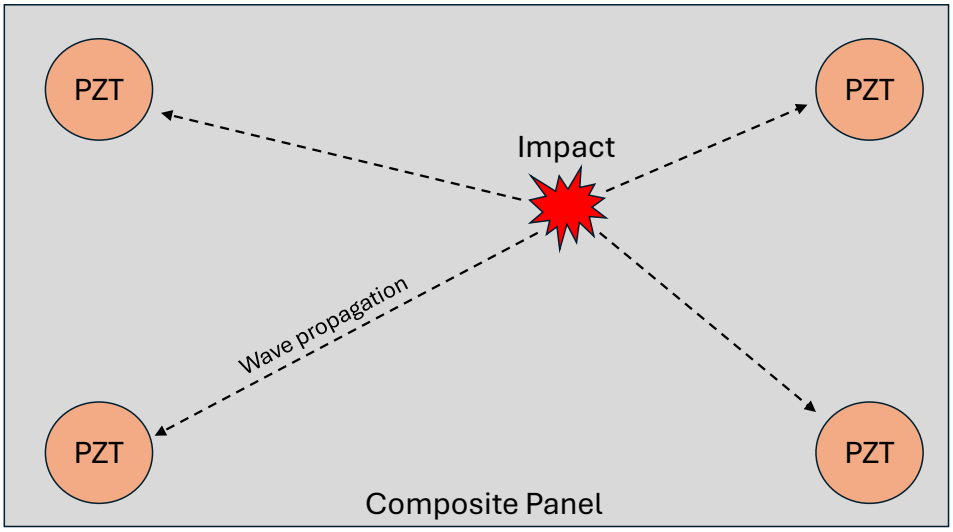


Figure 6.3: Passive Sensing illustration in the composite panel area covered by PZTs

6.2.1 Modes of IAPS System

The proposed system supports active and passive sensing methods in the field of SHM. There are four channels, and each channel is connected to a PZT sensor. PZT sensors can act as both actuators and sensors. Active or passive sensing mode can be selected by slide switches in the IAPS system.

Passive Sensing Mode

Passive sensing in the event of an impact is illustrated in Fig. 6.3. The impact-induced waves travel through the composite panel and are recorded by PZTs.

Once the passive sensing mode is selected, the active sensing circuitry is first turned off to not consume unnecessary power by sending the control signal from the MCU to the switches. Using the four PZT channels, impact-induced signals can be captured when the predefined threshold voltage is exceeded on the comparator peripheral of the MCU. These signals usually have high energy, resulting in high voltage amplitude, so they need to be attenuated for further processing. In the proposed system, there are two attenuation levels available, and the attenuation level (2 or 3 times) can be selected with the slide switches for each channel. This feature enables adaptability to different impact scenarios

Subsequently, the attenuated signals are passed through charge-amplifier circuits that

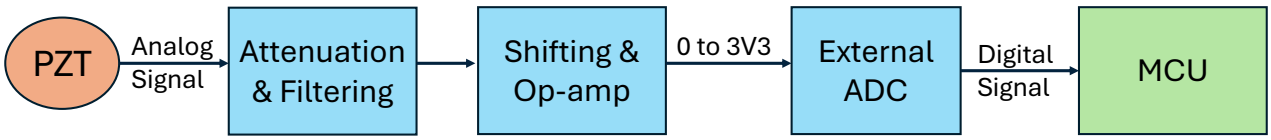


Figure 6.4: Passive sensing signal data flow

incorporate operational amplifiers to convert the PZT-generated charge to a measurable voltage. Meanwhile, the sensing signals are shifted to the positive voltage range to be sampled. Then, the passive signals from 4 PZTs are sampled with the external ADC implemented in the proposed system. Finally, the MCU reads the sampling results from the ADC through the SPI serial interface. The data flow of Passive Sensing signal is shown in Fig. 6.4 from the PZT to the MCU.

Active Sensing Mode

Similarly to the passive sensing mode, when the active sensing mode is selected, the passive sensing circuitry can be switched off by the MCU to reduce power usage. In the active sensing mode, there are two stages, namely the generation of the actuation signal to excite the structure and the capture of the response signals from the excited structure. There are a total of four PZT channels.

While one PZT is responsible for exciting the structure with the generated actuation signal, the rest of the PZTs capture the sensing signal from the structure as shown in Fig. 6.5. In the next stage, these sensing signals are also sampled by the external ADC and then read by the MCU. This active sensing cycle is repeated for four channels, which means that each PZT channel will be assigned to excite the structure in order as defined in the MCU while the remaining PZTs are responsible for the sensing signals.

There are two different types of the actuation signal widely-used in the field of SHM. They are tone-burst and chirp signals. These signals can be generated with the external DAC used in the proposed system. The digital form of the actuation signal is created by considering critical properties such as the frequency and amplitude of the signal and the DAC resolution. This predefined actuation signal is represented with an array including numbers in the digital domain.

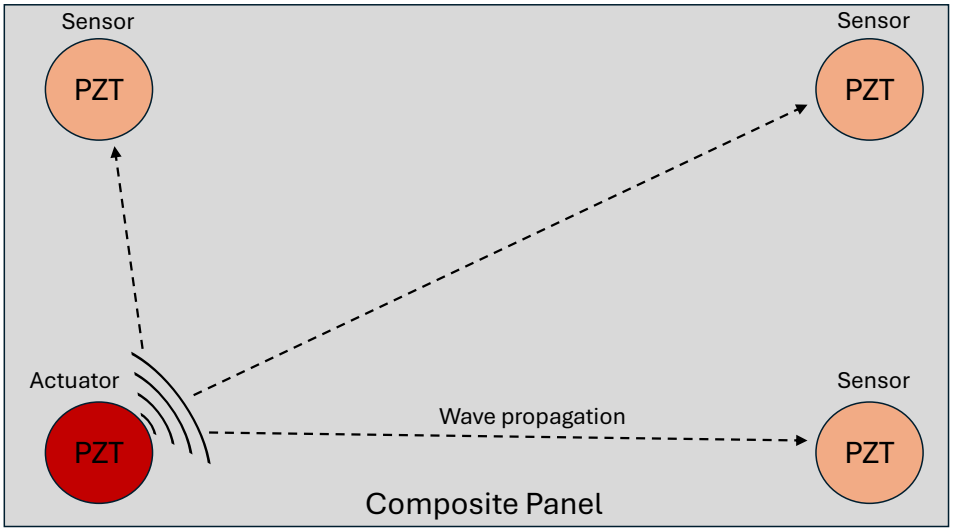


Figure 6.5: Active Sensing illustration in the composite panel area covered by PZTs

The numerical array representing the digital form of the actuation signal is sent to the external DAC by the MCU via the SPI serial interface. Based on the numerical values in the array, the DAC is responsible for converting the signal from the digital form to the analog form. The analog signal converted by the DAC is between 0 and 3.3V. Afterwards, the DAC output is amplified by using a two-channel op-amp to achieve the bipolar mode operation, which results in an actuation signal varying from -3.3 V to 3.3V .

The generated actuation signal is directed to the desired PZT channel using the multiplexer switch (4:1). This multiplexer switch is controlled by the MCU to select any channel. Therefore, the sequence of the PZT sensors can be programmed to excite the structure. The stages of actuation signal generation are shown in Fig. 6.6 from the MCU to the PZT.

After the structure is excited with the actuation signal, the remaining three PZTs record the response of the structure. The captured sensing signals are on the order of millivolts. Hence, they are amplified with the op-amps after being completely shifted to the positive side. Afterwards, the amplified sensing signals are within the appropriate range to be sampled by the

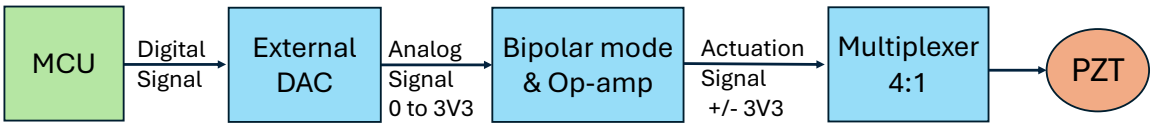


Figure 6.6: The stages of the actuation signal generation

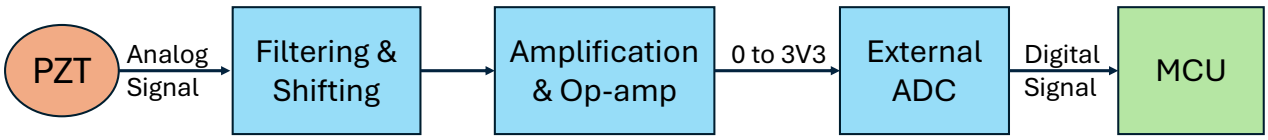


Figure 6.7: Active Sensing signal stages

external ADC. Fig. 6.7 shows the data flow of Active Sensing signal from the PZT to the MCU.

6.2.2 Hardware Design of IAPS System

The hardware design of the IAPS system brings together the requirements of both active and passive sensing in a compact, multi-channel configuration that supports real-time data acquisition and wireless communication. To achieve the goals of minimizing size, weight and signal interference, conserving power, and providing efficient control of actuation and sensing functions, the component selection and hardware design play a critical role.

The miniaturized hardware design utilizes a highly integrated processing and communication module to achieve both compactness and a reduced component count. Specifically, ANNA-B402 module was employed from uBlox as an RF microcontroller.

To achieve a higher sampling frequency in capturing active and passive sensing signals, the MAX11132 from Maxim Integrated is used. This external ADC is a high-performance, low-power ADC designed for applications requiring high-speed data acquisition. It features a conversion rate of up to 3 Mega-samples per second (Msps), ensuring rapid sampling capabilities with 12-bit resolution, and supports up to 8 analog input channels. This ADC offers flexible input configurations, including single-ended, differential, and pseudo-differential modes, making it versatile for various signal types. Its compact package measures 5 mm $\times$ 5 mm, making it suitable for space-constrained designs. In this study, while the four ADC channels are used for active sensing, the remaining four channels are assigned to passive sensing applications. For all eight ADC channels, the input configuration is set to single-ended. In addition, communication between the ANNA-B402 module and the MAX11132 external ADC is performed through the SPI serial interface.

The ANNA-B402 module does not include a built-in DAC. Therefore, the AD5452 from

Analog Devices was employed, which is a high-performance, 12-bit resolution DAC. This external DAC is used to generate actuation signals in this study. The AD5452 converts the digital values coming from the ANNA-B402 to analog actuation signals. Communication with the ANNA-B402 module is achieved with the SPI serial interface.

To provide a reference voltage for the external ADC and DAC, two MAX6071 from Maxim Integrated were used. The reference voltage is critical for an external ADC and DAC, as it defines the full-scale output range and directly impacts the accuracy, linearity, and stability of their performance. Variations in the reference voltage can lead to errors in the output signal, affecting precision in high-resolution applications. MAX6071 supplies a high-precision reference voltage of 3.3 V to the external ADC (MAX11132) and DAC (AD5452).

The AD5452 DAC can be configured for bipolar mode operation (4-quadrant multiplication) to produce output signals that span both positive and negative ranges. This configuration requires the use of two additional op-amps to enable the generation of a full-range bipolar actuation signal. To meet this requirement, AD8066, a dual-channel op-amp from Analog Devices, was selected and implemented. Using AD8066, the system successfully achieves a full-range actuation signal of ± 3.3 V to excite structures.

After the actuation signal is generated, it is routed to the desired PZT sensor among four channels through ADG1604 from Analog Devices. ADG1604 is a versatile analog multiplexer designed for efficient signal routing in multi-channel applications. It features a 4:1 channel configuration, allowing one of four input signals to be routed to a common output or vice versa, making it ideal for systems requiring flexible signal selection. The channel selection is accomplished with the control signals sent by the MCU.

To handle active and passive sensing signals, the charge amplifier circuit is implemented. This is mainly achieved by employing eight dual-channel precision op-amps (LTC6087 from Analog Devices). While four of them were used for passive sensing signals, the remaining op-amps were implemented for active sensing applications. In the passive sensing mode, the signals are attenuated due to their high energy that may permanently damage the system. In contrast, in the active sensing mode, the signals are amplified before being sampled by the ADC, since the outputs of the PZT sensors are in the order of millivolts in the active sensing mode

after structures are excited with actuation signals. Eventually, the outputs of the op-amps are sampled by the external ADC (MAX11132) in both active and sensing modes.

The LTC6087 precision op-amp has a shutdown mode relevant for signal processing applications that demand high performance with minimal power. When the shutdown pin is grounded, the op-amp is disabled and consumes minimum power. To achieve this, the shutdown pin of the op-amps is connected to an N-channel MOSFET (SI2356DS from Vishay) to be switched on/off with a control signal sent by the MCU. As a result, when the active sensing mode is selected, the passive sensing circuitry can be completely disabled with a MOSFET. In addition, in the active sensing mode, when one PZT channel is used for an actuation signal to excite the composite structure, the op-amp connected to the corresponding channel is individually disabled with the MOSFET.

To fully shift the sensing signals to the positive domain for both active and passive sensing modes, a reference voltage was provided to the LTC6087 operational amplifiers. This was realized by first reducing the 3.3 V supply to 1.65 V through a voltage divider, then buffering this voltage with a voltage follower circuit implemented using an AD8691 op-amp from Analog Devices. This configuration ensures a stable reference voltage for the charge amplifier circuits, causing the sensing signals in both active and passive modes to swing around a new zero level set at 1.65 V.

Slide switches (CAS-120A1 from Nidec Components) were used for two critical purposes in this hardware design. The first purpose was to select the active or passive sensing configuration for each PZT channel. Secondly, the same type of slide switches was used to choose the attenuation level between two different options (2 or 3 times) for passive sensing signals.

For the power supply, two Low-Dropout (LDO) voltage regulators were used to provide 3.3 V to the analog and digital circuits separately. This was achieved by deploying XC6220 from Torex Semiconductor, which is with a fixed output. To regulate a negative voltage (-3.3 V), TPS63700 DC-DC inverter from Texas Instruments was used. This negative voltage was supplied to the op-amp and multiplexer switch used in the generation of the actuation signal with the DAC. All of these supply voltages were regulated from a rechargeable Li-Po battery (3.7 V).

To enable reliable charging of the rechargeable battery, a dedicated battery management circuit was implemented on the PCB. This functionality was realized using the MCP73831 device from Microchip Technology, which serves as a charge management controller for single-cell Li-ion or Li-polymer batteries. Using a 5 V DC source, such as a USB port, the battery can be charged properly.

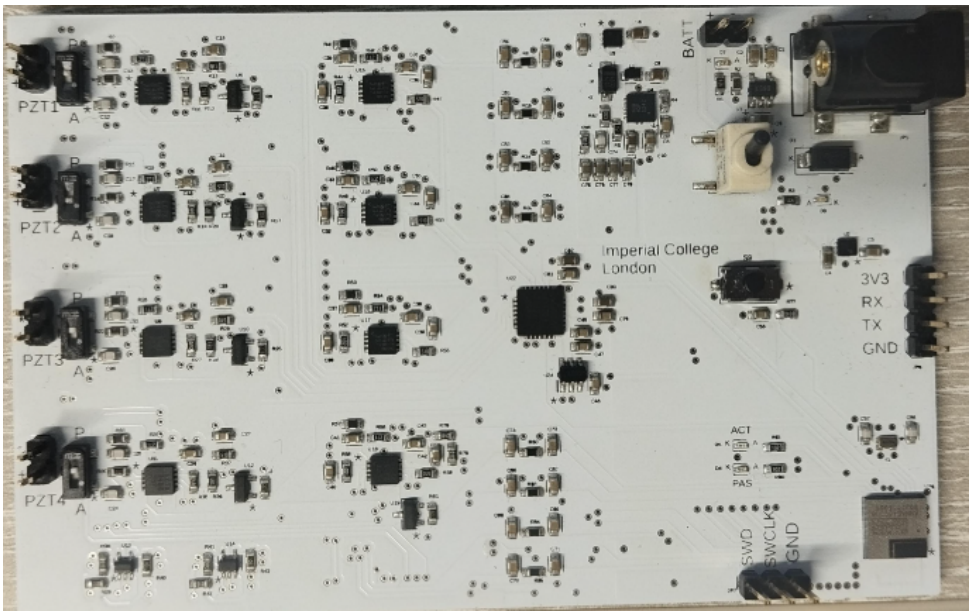
6.3 System Implementation

The developed system was implemented on a 4-layer PCB with a typical thickness of 1.6 mm to satisfy the design objectives such as the integration of active and passive sensing, and miniaturization. The layout of the PCB is carefully considered to ensure that the digital and analog sections function without any signal interference between them. Moreover, the dimension of the developed PCB is 100 mm x 65 mm. The manufactured prototype of the developed system is shown in Fig. 6.8.

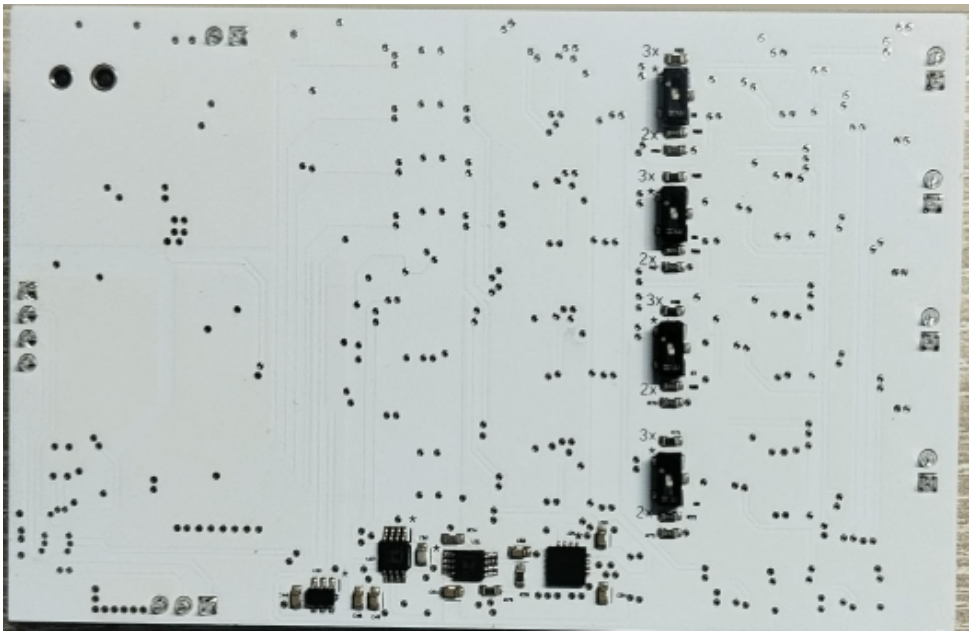
The top layer of the PCB hosts most of the components utilized in the proposed system, including the RF MCU, the PZT channel terminals, the power management circuitry, the external ADC, and the charge amplifier circuits for both active and passive sensing, as shown in Fig. 6.8a. Meanwhile, Fig. 6.8b illustrates that the bottom layer accommodates the actuation signal generation circuit, consisting of the external DAC, its amplification circuit, and the multiplexer switch, along with the slide switches used to adjust the attenuation level during passive sensing.

In the design of a 4-layer PCB that integrates both analog and digital subsystems, careful consideration of stack-up configurations and layout practices is essential to ensure optimal signal integrity and reduce electromagnetic interference. In this context, the proposed stack-up comprises power and signal (SIG+PWR) layers on the top and bottom, with the internal planes dedicated to a continuous ground reference as shown in Fig. 6.9.

This stack-up arrangement offers multiple advantages. First, placing the ground planes in the inner layers provides a robust reference for both analog and digital circuits, minimizing ground loops and improving return current paths. The continuous ground planes also help confine noise



(a)



(b)

Figure 6.8: IAPS system prototype in a 4-layer PCB, (a) Top view, and (b) Bottom view.

currents and shield sensitive analog traces from high-frequency digital switching signals. Second, by positioning the power and signal layers externally, critical signals and components can be more easily routed while maintaining proper isolation from sensitive analog nodes. This ensures that power traces can be kept short and have minimal parasitic inductance. Consequently, it is a particularly suitable approach for mixed-signal applications in which the integration of analog and digital domains demands careful grounding strategies and efficient routing.

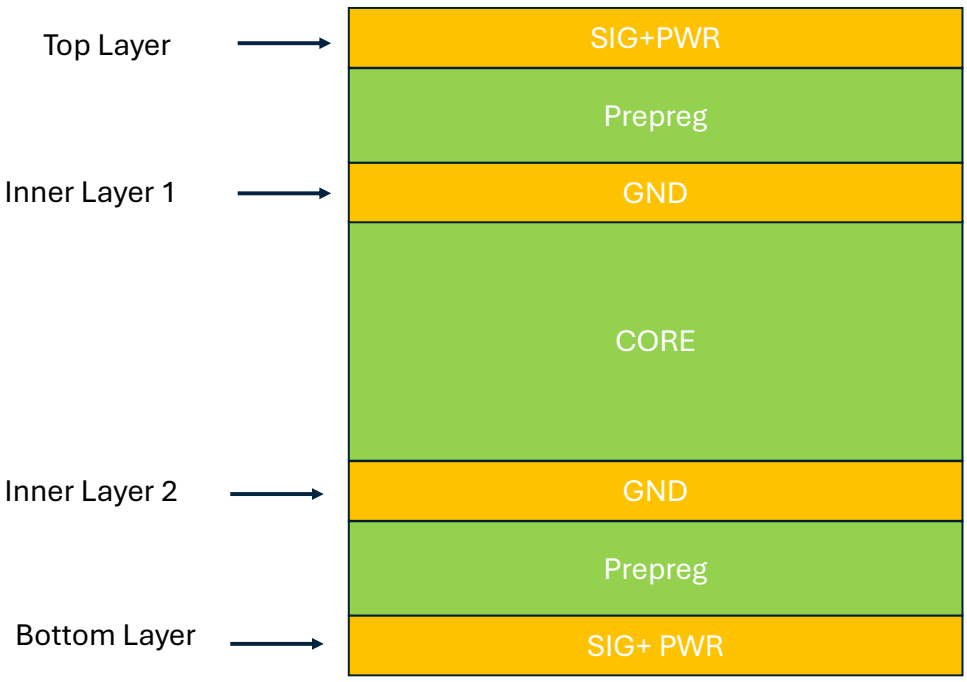
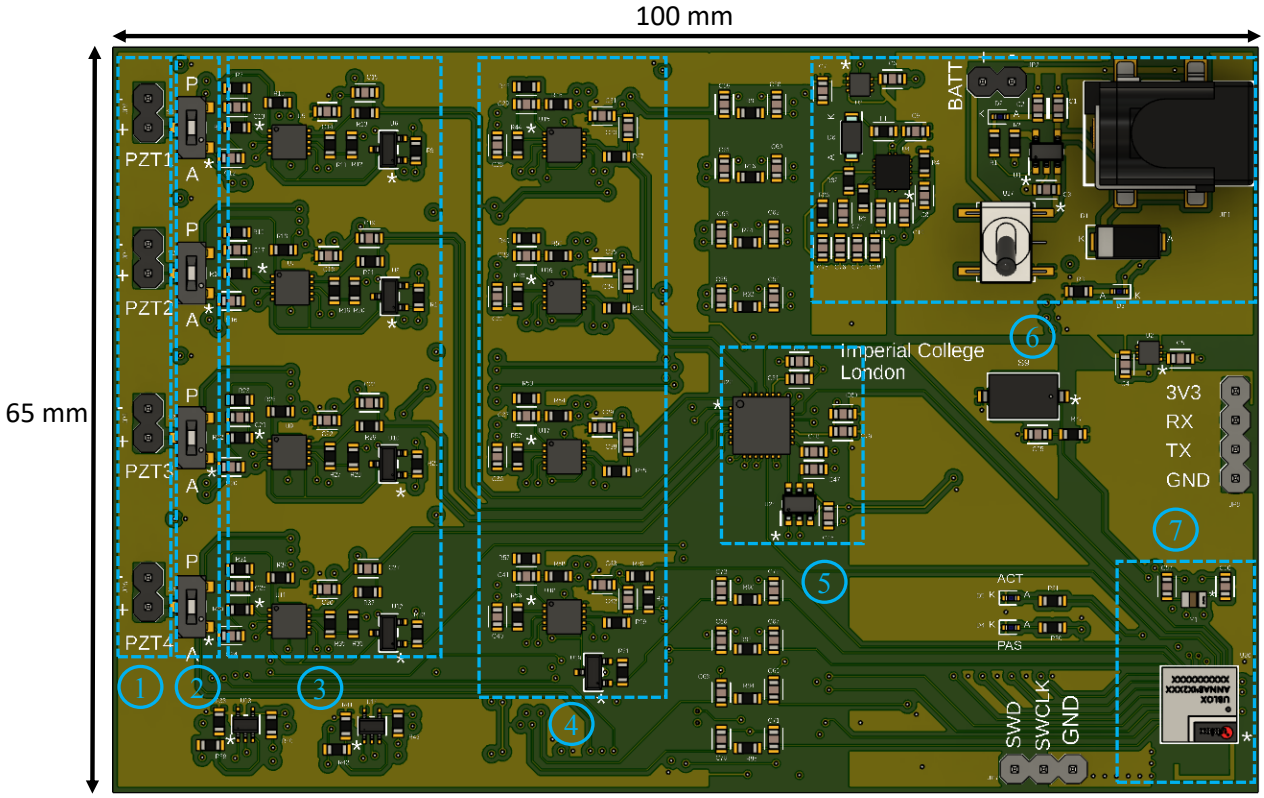


Figure 6.9: 4-layer PCB stack-up of the prototyped PCB

Fig. 6.10 shows the top-layer layout of the Integrated Active–Passive Sensing (IAPS) system. The design incorporates seven function modules, each enclosed by dashed lines, which collectively enable active and passive sensing, data acquisition, power regulation, and wireless communication. There are four PZT channels to be used in active and passive sensing applications. For each channel, the signals from PZTs can be routed to the charge amplifier module of the active or passive sensing. In the charge amplifier module, the PZT-generated charge is converted to measurable voltages to be sampled by the external ADC module for subsequent data processing and analysis. In addition, the power management module ensures reliable voltage regulation and battery charging for the entire system.

Finally, the RF MCU module integrates microcontroller functionality and wireless communication, enabling real-time data transmission and system control. In addition, the RF microcontroller incorporates essential peripherals such as the comparator to enable an event-triggered mechanism in the system. This module also manages both serial and wireless communication protocols: it supports Bluetooth LE to transmit data to a central device responsible for establishing the wireless network, while the SPI interface facilitates communication with the external ADC and DAC. Furthermore, UART is implemented for data exchange with devices that use this serial interface. Using these capabilities, the RF microcontroller ensures efficient



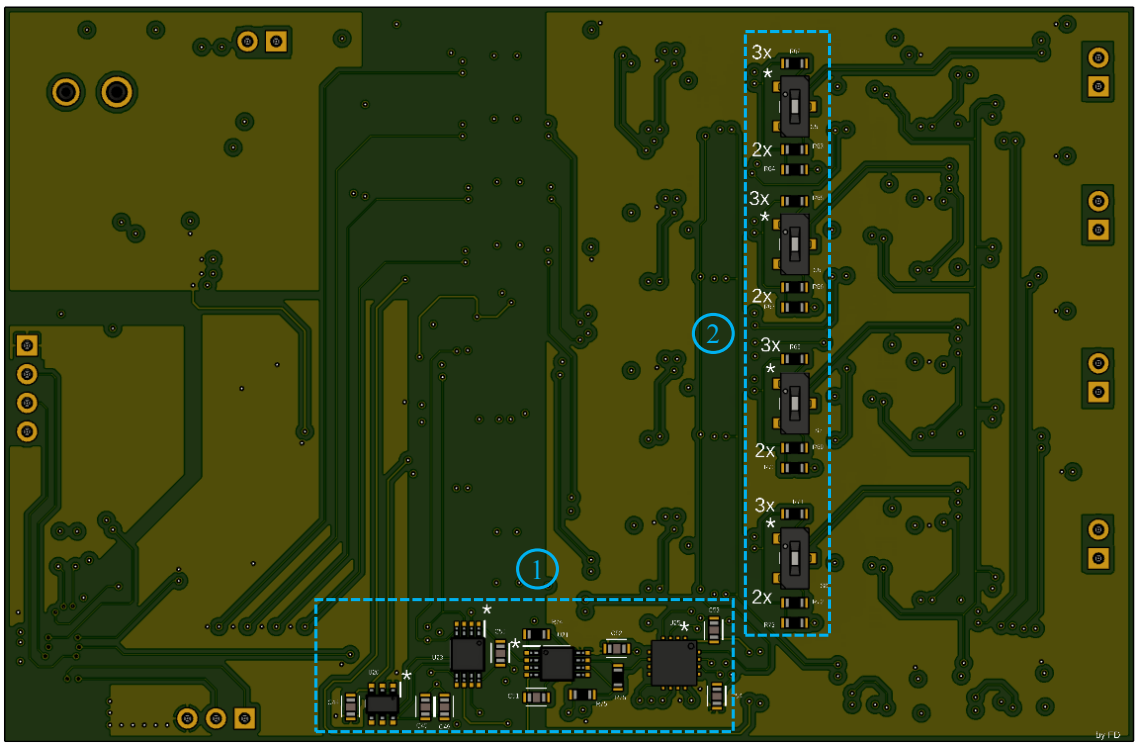
① PZT channels ② Active-Passive mode switching module ③ Active sensing charge amplifiers module ④ Passive sensing charge amplifiers module ⑤ External ADC module ⑥ Power management module ⑦ RF MCU module

Figure 6.10: The function modules of IAPS system in the top layer

coordination and control of sensing tasks.

The bottom-layer of the IAPS system, illustrated in Fig. 6.11, contains two primary functional blocks dedicated to the actuation signal generation and routing for active sensing, as well as signal attenuation for passive sensing. The actuation signal generation module converts the digital waveforms sent by the MCU into their corresponding analog forms, which drive the PZT sensors in active sensing operations. In addition, the attenuation level switching module offers two selectable attenuation settings for each PZT channel in passive sensing mode. By regulating the attenuation level, the system ensures that the energy remains within a safe range suitable for processing by the external ADC, thus preventing potential damage.

By integrating these modules on a single board, the IAPS system achieves a compact yet versatile architecture suitable for SHM scenarios that require active or passive sensing capabilities.



① Actuation signal generation module with external DAC ② Attenuation level switching module

Figure 6.11: The function modules of IAPS system in the bottom layer

6.4 Experimental Setup and Results

To evaluate the performance of the IAPS system, an experimental setup was arranged using a composite panel instrumented with PZT sensors, as illustrated in Fig. 6.12. The primary goal of this experiment was to demonstrate the feasibility of IAPS hardware (including its data acquisition and wireless communication subsystems) to capture structural signals in both active and passive sensing modes.

In Fig. 6.12, a rectangular composite panel is shown with four PZT sensors attached to the structure. These sensors are responsible for both actuation (exciting the structure in active sensing mode) and detection (wave or impact sensing in both active and passive sensing modes). A small, rechargeable Li-Po battery is included to supply power in situations where external sources may be unavailable. In addition, the developed IAPS system is available, incorporating the RF microcontroller, external ADC/DAC, and other components necessary for analog signal conditioning and wireless data transmission. The wires running between the PCB and the PZTs

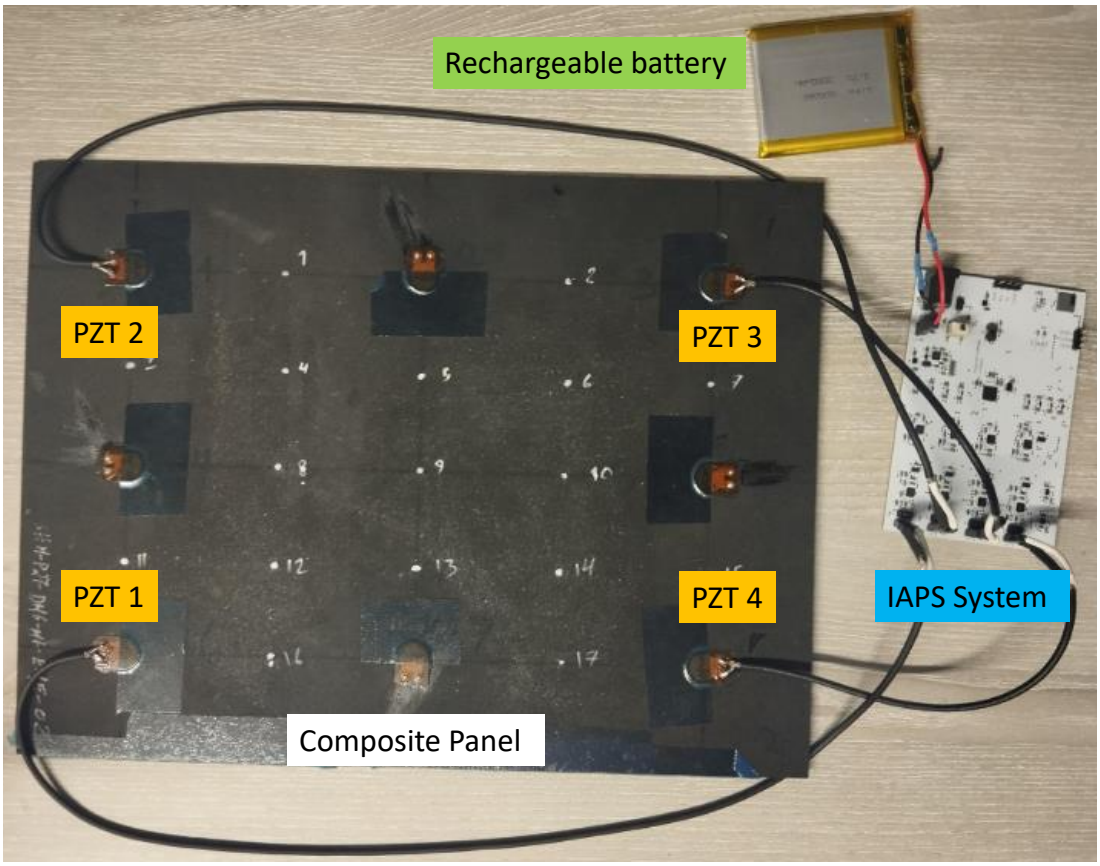


Figure 6.12: IAPS system experimental setup

are used to deliver actuation signals and transfer recoded structural responses.

By implementing this setup, each PZT sensor can be easily switched between active and passive modes through the slide switches on the IAPS system. In the active sensing mode, the system generates a predefined actuation signal (e.g., tone-burst or chirp) through one of the PZT sensors, while the other three PZTs record the resulting wave propagation. In passive mode, all PZTs remain idle (with minimal power draw) until an external impact event occurs, allowing them to capture the impact-induced signals. The entire process is managed by the RF microcontroller and then all of the acquired data are transmitted to a central device through Bluetooth LE.

After the central device sends all of the collected data to a base station such as a PC via the UART serial interface. The developed GUI performs data processing, visualization, and saving.

6.4.1 Passive Sensing Mode Verification

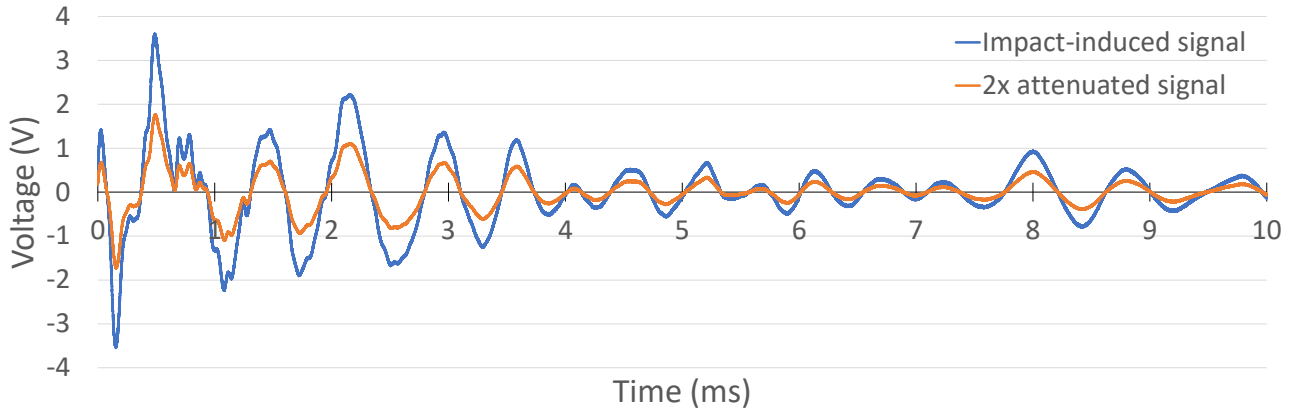
In order to assess the performance of the IAPS system in passive sensing mode, impact tests were conducted using a handheld hammer on the composite panel. First, adjustable attenuation levels were tested. One of the PZT channels was used for this purpose. Two attenuation options, namely 2× and 3×, were examined, as selectable via a dedicated slide switch on the IAPS circuit board. For comparison, a digital oscilloscope (TiePie Handyscope HS5) was used to record both the raw impact-induced signal directly from the PZT and its corresponding attenuated output from the IAPS system.

Figure 6.13 illustrates the comparison between the unattenuated impact signal and two levels of attenuation. In Fig. 6.13a, the IAPS output exhibits a voltage amplitude approximately half that of the unattenuated signal, corresponding to the 2× attenuation setting. Similarly, in Fig. 6.13b, the amplitude of the IAPS output is reduced to approximately one-third of the original signal, reflecting the 3× attenuation setting.

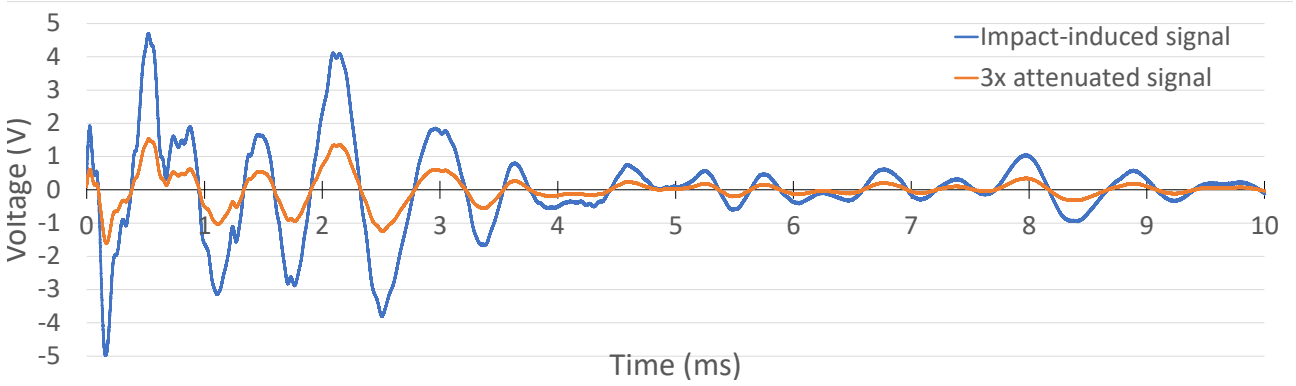
Notably, while attenuation reduces the signal amplitude, the overall waveform pattern remains consistent between unattenuated and attenuated signals, demonstrating the ability of the IAPS system to preserve essential characteristics of the impact event. This property is crucial for subsequent feature extraction in SHM, as key time- and frequency-domain attributes of the signal must remain distinguishable despite amplitude scaling. Hence, the results confirm that the IAPS system, in the passive sensing mode, can capture and condition impact-induced signals at user-selectable attenuation levels.

Secondly, the ability of the IAPS system to record impact-induced signals in passive mode was evaluated. One channel of the IAPS system was connected in parallel with a digital oscilloscope, ensuring that both devices received the same raw signal from the PZT sensor. The digital oscilloscope served as a reference, recording the unattenuated voltage response of the impact event, while the IAPS system applied a user-selectable attenuation factor (2× in this particular test) before digitizing the signal.

Fig. 6.14 illustrates the waveform recorded directly by the digital oscilloscope. This figure provides a baseline measurement of the impact-induced signal, allowing for subsequent comparisons.



(a)



(b)

Figure 6.13: Comparison of Impact-induced signals and their attenuated forms in the passive mode of the IAPS system. (a) 2 times attenuation, (b) 3 times attenuation.

Fig. 6.15 presents the corresponding signal acquired by the IAPS system operating in passive mode, where a 2× attenuation was selected in the system circuitry. Consequently, the amplitude recorded by the IAPS is lower than that shown in the raw oscilloscope measurement. However, the overall shape of the waveform, including its primary peak and pattern, remains consistent with the reference signal.

To enable a more direct, one-to-one comparison of the two measurements, the IAPS waveform was first shifted to the original zero-level. It was then multiplied by the known attenuation factor of 2 to restore the waveform to approximately the same amplitude range as the original. The result of this post-processing is shown in Fig. 6.16, where the scaled IAPS result closely overlaps with the oscilloscope measurement. This agreement confirms that the IAPS system can reliably capture the impact event while applying user-selected attenuation, without compromising the

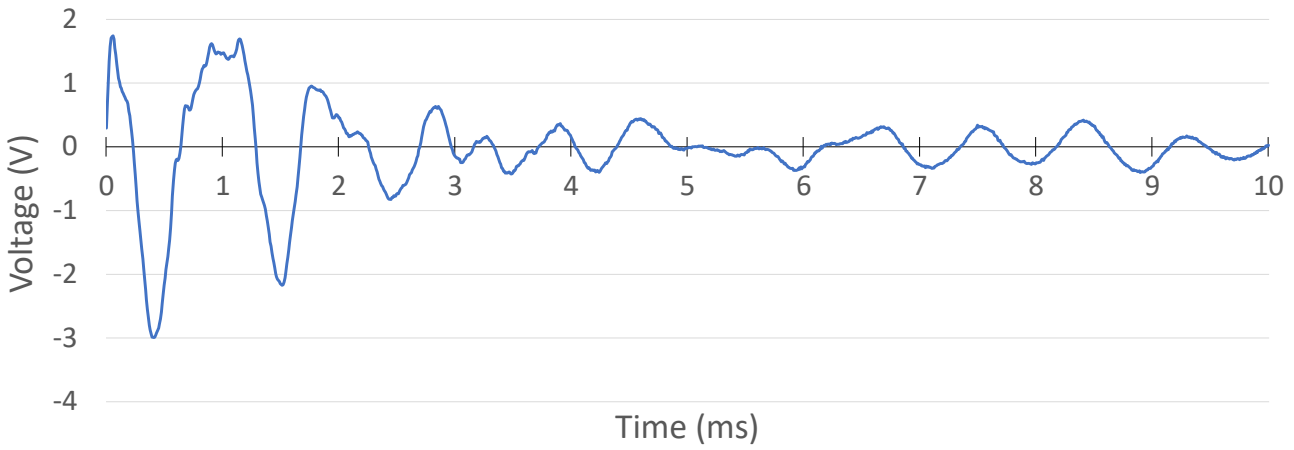


Figure 6.14: Digital oscilloscope result

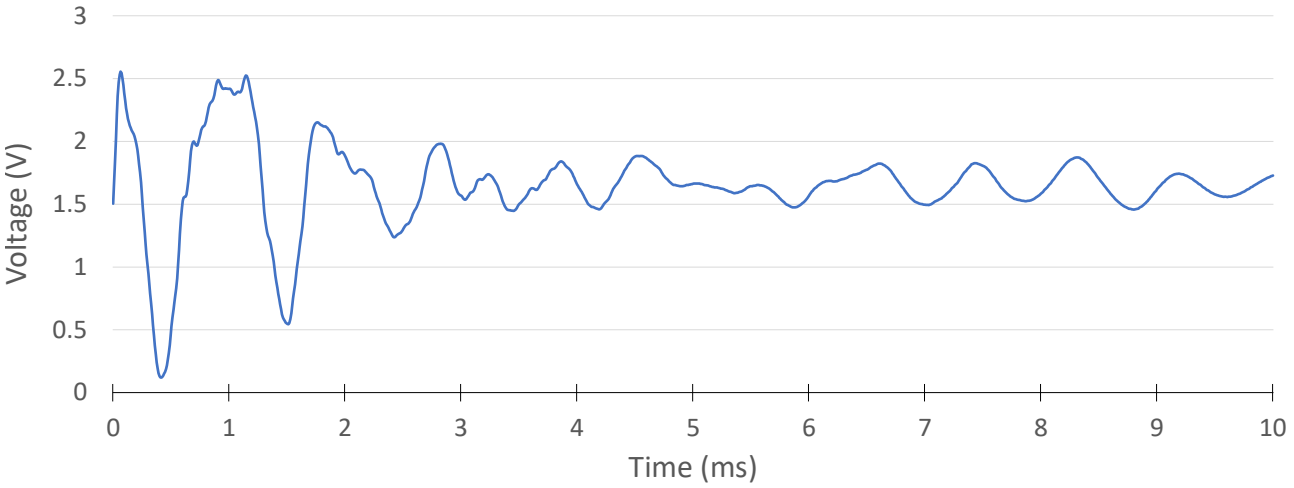


Figure 6.15: IAPS system result in the passive sensing mode

essential signal features needed for subsequent analysis.

After verifying proper functionality through the single-channel tests described above, the passive sensing capability of the IAPS system was further evaluated using all four available PZT channels. A controlled impact was applied to the composite panel using a handheld hammer, and the built-in comparator of the RF MCU monitored and detected the resulting signals. Upon detecting an impact-induced signal exceeding a predefined threshold, the comparator triggered the external ADC to begin sampling. The ADC was configured with a sampling frequency of 500 kHz, capturing 5000 continuous samples for each channel, thus providing a record of 10 milliseconds for each channel.

Once the sample buffer reached capacity, the acquired data were transmitted wirelessly to a central base station through Bluetooth LE. A custom GUI on the base station received, plotted,

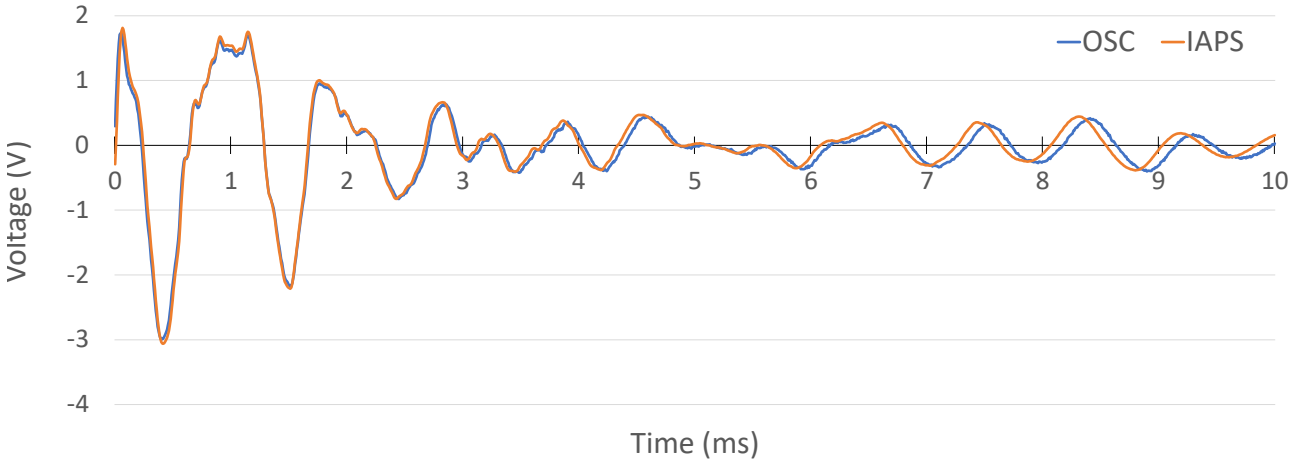


Figure 6.16: The comparison of the oscilloscope and IAPS system results

and saved the multichannel waveforms. An example of the recorded signals for each of the four PZT channels is shown in Fig. 6.17. The plots confirm that the system successfully detects and captures impact events across multiple sensors.

These results validate the multi-channel data acquisition approach of the IAPS system under passive mode operation. Specifically, the comparator-based triggering ensures that only signals exceeding the user-defined threshold are sampled, thus optimizing energy consumption and data throughput. In addition, the ability to adjust the attenuation settings and comparator value, as well as the high sampling rate and data resolution, highlights the suitability of the IAPS system for real-time SHM applications on different types of composite aerostructures.

Furthermore, passive sensing signals acquired from multiple PZT sensors, including amplitude and TDOA information, can be also effectively utilized in the ML-based detection algorithm for identifying and localizing impact events, as demonstrated in Section 4.5.

6.4.2 Active Sensing Mode

Using the slide switches, the active sensing configuration is selected to ensure that the sensing signals captured by the PZTs are routed to the amplification circuit. To achieve an active sensing application, a specific actuation signal is generated to excite a composite structure by using a PZT as an actuator. Afterwards, the response of the structure is recorded through other PZTs acting as receiver sensors.

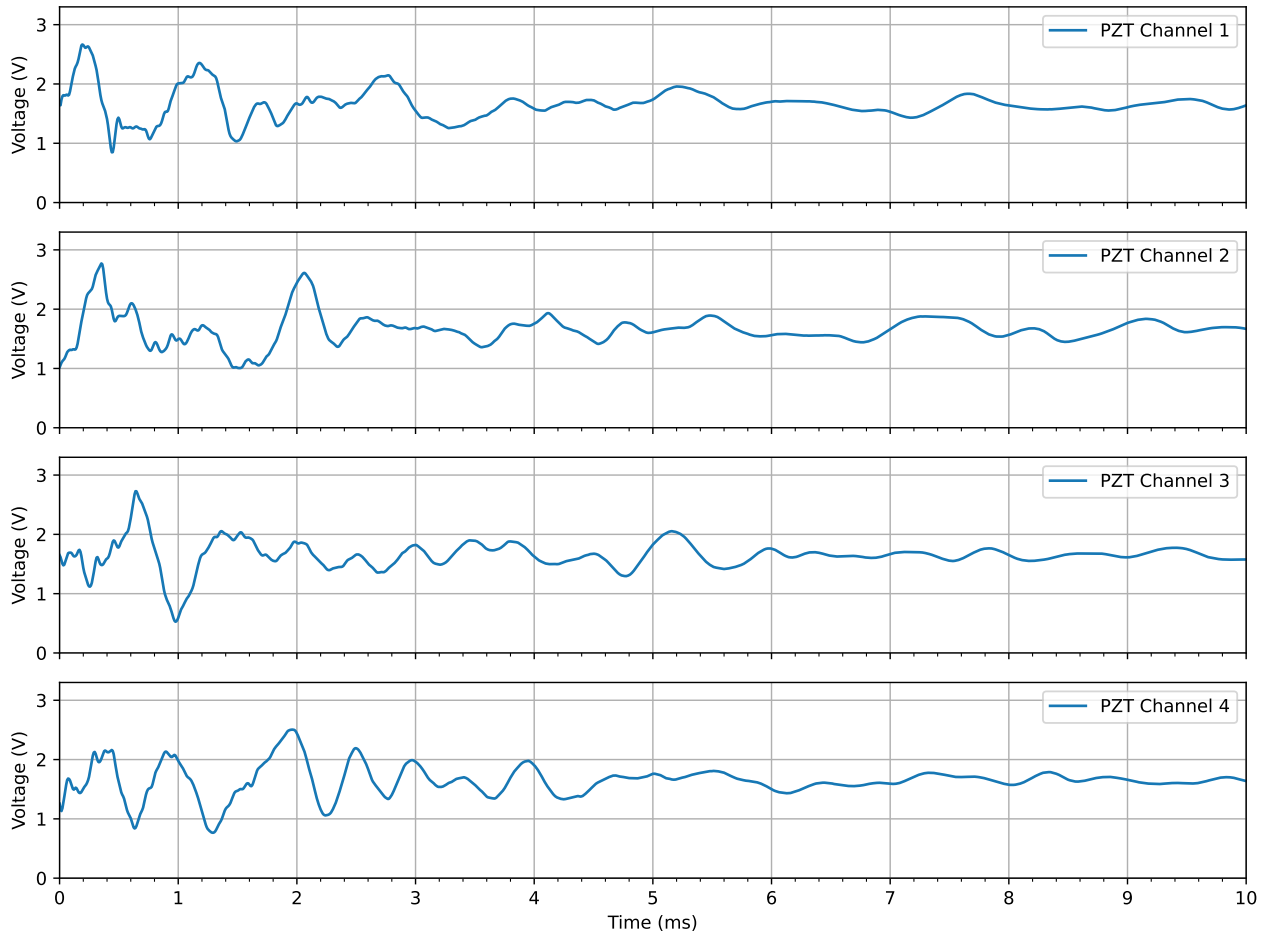


Figure 6.17: GUI plot for passive sensing results from 4 channels in the IAPS system

In the experiment performed, the tone-burst signal of 50 kHz was generated using the external DAC with 12-bit resolution. The digital values of the required signal were calculated as explained in detail in Section 3.3.2. After the calculation, the digital form of the signal is presented in Fig. 6.18.

The digital signal form represented with numerical values was sent as an array by the MCU to the external DAC through the SPI serial interface. The resulting analog form, as an output of the DAC, was amplified to the range of ± 3.3 V through the op-amp circuit. In the following stage, the amplified actuation signal was routed to a desired PZT channel with the analog multiplexer switch.

The generated tone-burst signal of 50 kHz was checked with an oscilloscope connected to the actuator PZT. The oscilloscope measurement is presented in Fig. 6.19. As shown, the expected actuation signal was generated successfully to excite the composite structure.

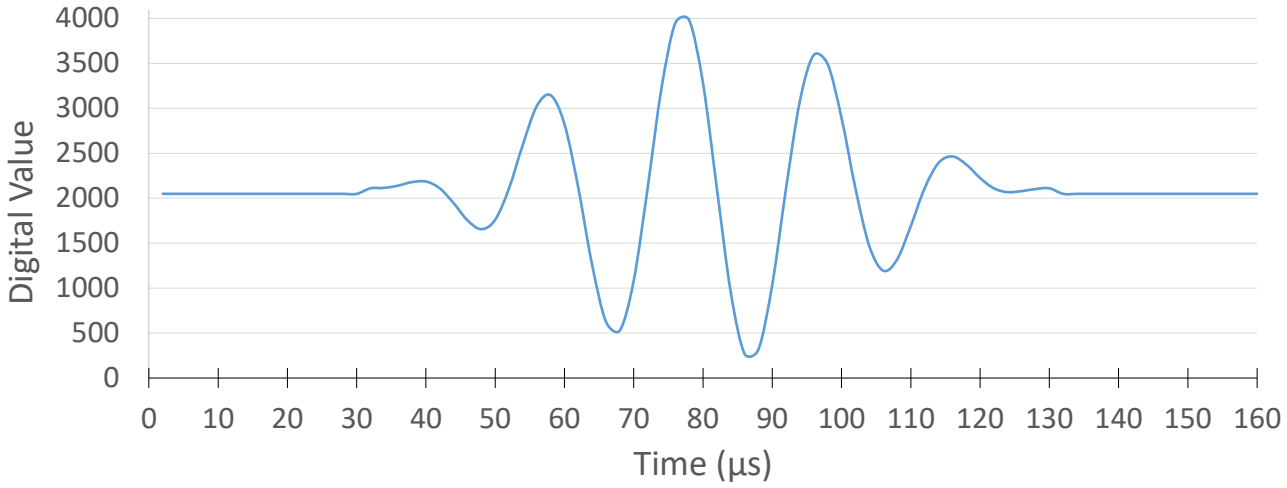


Figure 6.18: Digital form of the 50 kHz tone-burst signal for the DAC with 12-bit resolution and 500 kHz sampling rate

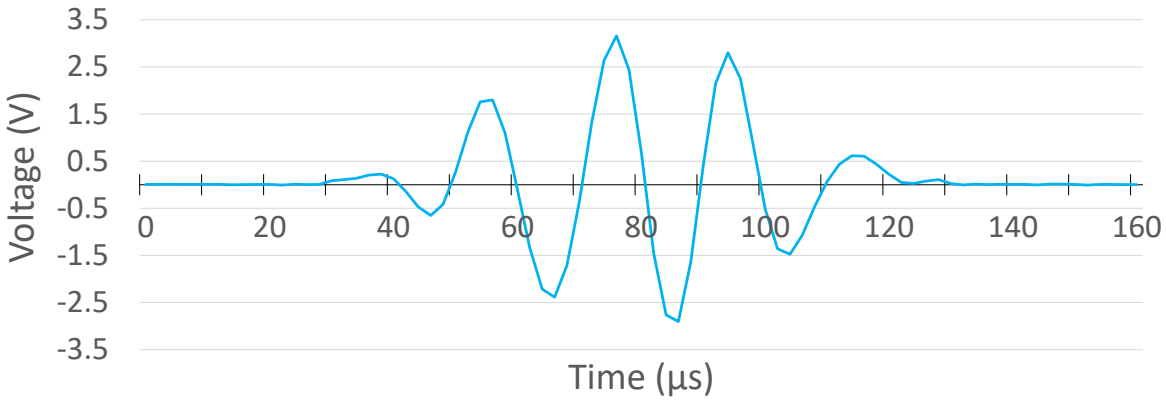


Figure 6.19: Oscilloscope measurement of the 50 kHz tone-burst signal from the actuator PZT

After the structure was stimulated with the generated tone-burst signal, the sensing results were acquired from the PZTs through the external ADC. However, certain constraints were identified during this process. For example, the resolution of the captured sensing signal was relatively low, as shown in Fig. 6.20, which is due to the low sampling frequency of each channel. Although the ADC operated at a sampling frequency of 500 kHz, each channel was sampled at a rate of 125 kHz.

Moreover, the constraints encountered in sampling the active sensing signal are further detailed and discussed in the following section.

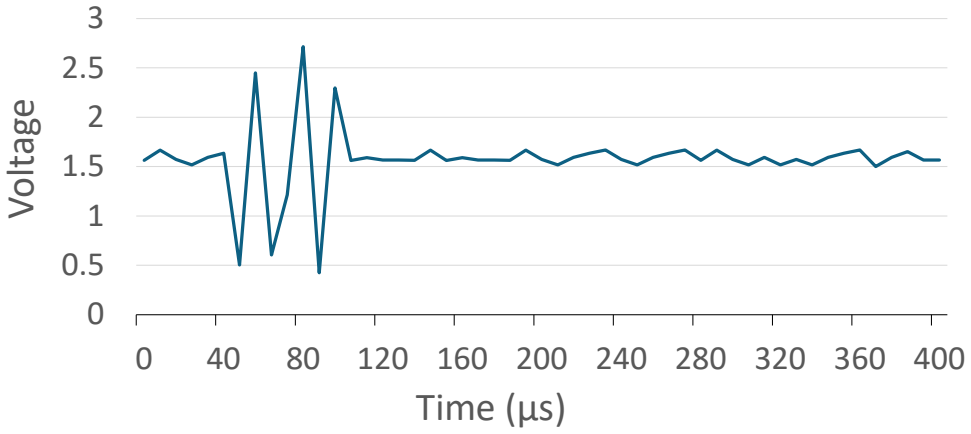


Figure 6.20: Active sensing result captured from a PZT channel

Constrains observed in sampling active sensing signals

Despite the external ADC being nominally capable of sampling at up to 3 MHz, its actual performance is tightly coupled to the serial clock frequency of the SPI interface on the MCU. The ADC supports a maximum serial clock frequency of 48 MHz, each sample requires 16 clock cycles, which leads to an effective maximum of 3 MHz sampling rate [72]. In this system, the SPI of the MCU clock is maximum 32 MHz [100], restricting the highest achievable sampling rate to 2 MHz. In practice, even this reduced rate could not be achieved. The experiments consistently reached only 500 kHz before encountering a scenario in which every ADC reading returned zero, despite the MCU detecting no explicit errors. To ensure accuracy in sampling, an MCU timer was employed to trigger SPI communications at fixed intervals. However, any attempt to increase this interval to achieve 1 MHz or 2 MHz sampling resulted in null data. Consequently, the active sensing signals could only be captured at a lower sampling rate than anticipated, thereby limiting the resolution of the measurements.

A further constraint emerged from the need to define multiple SPI transfer functions that need to be triggered by an MCU timer. In the experiment, separate timers were employed for the ADC and DAC to enable periodic operations. However, the SPI hardware allowed only one transfer function to be defined at any given time. The most recently configured SPI transfer would overwrite the previous one. Moreover, the system had to complete the current SPI transfer fully before initializing a new one, preventing seamless switching between devices. As a result, much of the incoming sensing signal was missed during the transitions from DAC

actuation to ADC sampling. These constraints reduce the overall effectiveness of active sensing by limiting both the sampling frequency and the concurrency of actuation and data acquisition.

6.5 Conclusions

This work presented the design, implementation, and characterization of a miniaturized IAPS system for enhanced SHM in composite aerostructures. By merging active and passive sensing within a single platform, the system addresses the existing limitations associated with bulky hardware, insufficient flexibility in traditional wireless SHM solutions. The developed architecture demonstrates multi-channel functionality (4 channels) for distributed monitoring, accommodates both guided wave–based active inspections and impact-induced passive signals, and provides wireless data transmission via Bluetooth LE.

The hardware implementation was achieved on a compact 4-layer PCB in which careful layer stack-up, placement of components, and electromagnetic isolation strategies minimized signal interference between the digital and analog domains. The system includes an external ADC to acquire guided waves and impact events, an external DAC to generate actuation signals, and versatile switching circuits to alternate between active and passive sensing modes. Tests on a composite panel demonstrated that the developed passive sensing system reliably detects impact events across multiple channels, with adjustable attenuation levels. Active sensing experiments confirmed the effectiveness of generation of actuation signals to excite the composite panel. However, in practice, capturing the corresponding wave propagation data was constrained by a relatively low sampling rate, resulting in limited resolution. The achievable sampling rate was bounded by serial communication capabilities, highlighting the need for future improvements in parallel data acquisition and higher SPI clock speeds.

In summary, the proposed integrated solution enables a unified approach to SHM by accommodating both scheduled inspections and spontaneous impact detections in real time. This integration improves data acquisition for both active and passive sensing applications and reduces the overall mass and complexity of the wiring on aircraft structures. Although the current prototype faced practical constraints, particularly in achieving higher sampling rates

under active sensing conditions, it introduces a framework for advanced structural monitoring systems. Future work would explore optimized sampling strategies, potentially involving parallel communication buses. The findings confirm that the miniaturized IAPS system can serve as an important step towards more robust, low-power, and multifunctional SHM capabilities for the aviation industry.

Chapter 7

Conclusions and Future Work

This thesis has explored the design, development and validation of four complementary wireless SHM platforms for on-board aircraft applications, with a particular emphasis on miniaturization, energy efficiency, and accurate sensing of composite structures. The motivation behind this work resulted from the critical need to address various practical limitations of conventional SHM approaches, such as heavy wiring, inadequate scalability, lack of multi-sensor capabilities, or insufficient synchronization, in the context of composite structures. Across the four systems introduced, each prototype addressed a unique aspect of these challenges, resulting in a set of multifunctional solutions for real-time monitoring of structural health.

The first developed platform introduced the concept of a ZigBee-based SHM system. By integrating a miniaturized DAQ unit, a WSN, and a user-friendly GUI, the proposed system established a fundamental architecture that balanced hardware and software requirements to achieve real-time, multi-stage condition monitoring. A compact multi-layer PCB accommodated the core electronics, while the wireless network, based on ZigBee communication, provided reliable data exchange among sensor nodes and a central coordinator. This approach demonstrated ease of deployment compared to conventional wired systems, with significantly reduced weight and cable-management needs. The associated GUI software further enabled flexible data collection, visualization, and handling, all within a single environment.

Building upon early insights in DAQ miniaturization, the second developed platform, called PSN, was designed to detect and localize impact events on composite panels. Recognizing

the importance of immediate response to sudden and unplanned impacts such as collisions or dropped tools, the PSN featured an event-triggered comparator for energy-efficient operation. Its architecture allowed it to remain inactive until a dynamic response exceeded a specified threshold, at which point an ultra-low-power RF microcontroller immediately sampled and transmitted the detected signal over Bluetooth LE. This system addressed critical aerospace requirements of small form factor and low added weight by using a coin-cell battery power supply, ultra-compact PCB layout (28.4 mm in diameter). Comparative tests against standard oscilloscopes demonstrated that the PSN accurately captured the essential features of impact signals while allowing multiple nodes to operate in a synchronized wireless network. Furthermore, the system achieved reliable impact localization with the ML-based kNN model. Hence, the PSN highlighted the feasibility of an affordable and practical approach to real-time impact detection in weight-sensitive structures.

The third developed system expanded the scope of SHM by incorporating several different sensor types (PZT, strain gauge, accelerometer, and environmental sensor) onto a flexible 3×3 cm PCB weighing approximately 0.5 grams. This Multi-Sensor SHM System addressed the reality that composite structures experience various loading scenarios and environmental variations, all of which can influence damage initiation or progression. Integrating multiple sensing approaches into a single node and providing robust wireless data transfer through Bluetooth LE, the MSS provided a more comprehensive view of structural conditions than single-sensor systems. Through various experiments performed, its ability to capture impact-induced signal (via the PZT), acceleration data (via the accelerometer), strain variations (via the quarter-Wheatstone bridge circuit), and ambient parameters (temperature, humidity, and pressure) was validated. In addition, a calibration routine was developed to handle offset voltages in the strain gauge channel, increasing accuracy even in large deformation conditions. Through star-topology networking and real-time synchronization, the MSS can be distributed across aircraft surfaces to support multi-parameter diagnostics, enabling early actions based on combined mechanical and environmental data.

Finally, the fourth prototype, the Integrated Active–Passive Sensing system, merged two key SHM strategies (actively induced guided waves and spontaneously recorded impact signals)

within a single, multi-channel device. Implementing external ADC and DAC units on the same PCB, and carefully managing the switching of operational amplifiers, the IAPS could generate actuation signals such as tone-burst and capture the response of the structure in the active mode. Furthermore, the proposed system could also detect unforeseen impact events in the passive mode. This dual functionality substantially enlarges the diagnostic envelope, allowing sensitive wave-based inspections of internal defects along with on-demand alerting to unexpected damage. The tests confirmed that the system could reliably record impact-induced signals from multiple PZT channels along with the feature of adjustable attenuation level. Although higher sampling rates were constrained by SPI transfer limitations (restricting complete use of the ADC potential), the actuation signal was successfully generated through the DAC to excite the composite panel. Hence, the IAPS system represents an important milestone in the development of a fully integrated SHM platform designed for minimal cabling, reduced weight, and adaptable detection strategies along with wireless data transmission.

When considered as a whole, these four systems comprehensively address the objectives specified in the thesis: miniaturization, wireless communication, energy efficiency, time synchronization for accurate damage localization, and user-friendly implementation for real-world feasibility. First, the ZigBee-based SHM system introduced an integrated hardware–software architecture for remote structural monitoring. Second, the PSN demonstrated how ultra-compact, event-triggered sensing nodes could be used to capture impact signals with minimal power. Third, MSS extended coverage to multiple sensor types for a richer dataset for comprehensive health monitoring of composite structures. Finally, the IAPS combined active and passive wave-based strategies in a single device. Each prototype was tested on composite specimens or aluminium beams, showing reliable performance, minimal weight, and straightforward installation.

Overall, this thesis validates the feasibility and benefits of using low-cost, miniaturized, and wirelessly networked SHM devices for the purpose of SHM applications under service condition. Through improving fundamental aspects of compact system design, sensor circuitry, wireless communication, and user-friendly data handling, it delivers practical solutions to monitor and maintain composite structures. These prototypes are promising systems for the aerospace industry that require reduced weight, improved safety, and real-time insight into structural

conditions. Consequently, they represent a significant contribution in advancing miniaturized wireless SHM systems for reliable on-board aircraft applications.

Contributions to knowledge:

- Development of four distinct wireless SHM platforms tailored for composite structures. Each has been optimized for specific SHM challenges:
  - A ZigBee-based system for real-time multi-channel signal acquisition and processing for active sensing applications.
  - A low-power Passive Sensing Node for event-triggered impact detection with kNN-based ML.
  - A Multi-Sensor System integrating mechanical and environmental sensing with different sensor types, built on a flexible PCB.
  - An Integrated Active–Passive Sensing system unifying wave actuation and passive monitoring.
- Design and implementation of miniaturized, lightweight, and wireless SHM nodes:
  - The systems presented demonstrate effective miniaturization (e.g., 28.4 mm diameter PCBs, about 0.5 grams sensor nodes) using compact PCB layouts and lightweight components.
- Low-Power architectures for long-term deployment:
  - Comparator-based event-driven wireless impact detection and sleep modes significantly extend operational lifetimes and enable maintenance-free deployment over long periods.
- Custom, standalone software platforms for data acquisition and visualization:
  - All systems include fully customized GUIs developed independently from commercial tools (e.g., LabView or Matlab), ensuring portability, modularity, and full control over SHM workflows.

- A scalable architecture for SHM in aircraft structures:
  - The systems demonstrate a scalable architecture through modular node design, Bluetooth LE/ZigBee wireless communication, ensuring suitability for deployment over large aircraft surfaces.
- Contribution to embedded SHM system design methodology:
  - The thesis contributes a practical and replicable methodology for designing embedded SHM systems from sensor interface design and embedded processing to wireless networking and low-power strategies.

7.1 System Enhancements and Future Research Directions for Advanced Wireless SHM

7.1.1 System Enhancements

A critical approach for further advancement involves evaluating the developed SHM platforms under real operational conditions, where factors such as temperature fluctuations and humidity variations impose additional complexities. While current validation experiments have demonstrated the effectiveness of the proposed systems under controlled laboratory settings, real-world deployments introduce environmental influences that may affect sensor performance, data integrity, and wireless communication stability. Conducting experimental investigations in an aerospace-relevant environment, such as a composite fuselage section subjected to thermal cycling or a representative wing structure exposed to vibratory loading, would provide valuable insights into the robustness and long-term reliability of the proposed SHM solutions.

In addition to environmental testing, future advances should focus on evaluating the developed systems in real-time applications on large-scale composite structures, such as full-scale aircraft components. While the current validation has primarily relied on flat specimens or small-scale structures, structural complexities inherent to aerospace designs, including stiffeners, riveted joints, or bonded reinforcements, can introduce wave scattering, mode conversion, and non-

uniform strain distributions, all of which influence SHM sensor responses. Testing the proposed platforms on a representative stiffened panel would enable a more realistic assessment of their capabilities, providing key insights into how signal propagation characteristics change in complex geometries.

Another key aspect requiring further investigation is the improvement and optimization of the IAPS system, which integrates active and passive sensing in a single platform. While the current prototype successfully demonstrated dual-mode functionality, certain limitations, such as the restricted ADC sampling rate due to SPI transfer limitation and constraints on simultaneous actuation and sensing, require targeted improvements. Future work should explore hardware modifications, such as the incorporation of high-speed DAQ interfaces to overcome sampling limitations and enable more precise wave-based diagnostics. Addressing these challenges would not only enhance the reliability of the system, but also enable more effective application in impact monitoring and guided wave inspections within structures.

7.1.2 Future Research Directions

A promising direction for further research and development involves the establishment of a unified ecosystem in which all developed platforms operate cohesively. As with contemporary large-scale technology companies that develop mutually compatible devices for seamless integration, SHM systems can similarly benefit from a common framework that regulates hardware, software, and communication protocols. Currently, each prototype offers different functionalities and employs varying wireless standards (ZigBee, Bluetooth LE, and others). However, moving towards a single overarching architecture would allow every device to interoperate more effectively within a shared infrastructure.

In addition to simplifying DAQ, synchronization, and storage, a central device connected to a PC could accommodate multiple wireless interfaces, thereby enabling simultaneous communication with heterogeneous sensor nodes. Integrating system-level protocols and data-handling procedures, future development of new sensor nodes with DAQ modules would become a straightforward process. This modular approach aligns with modern engineering practice, in which compatible components can be easily integrated to expand functionalities without extensive

re-engineering.

This architecture would encourage an ecosystem-based design philosophy. Rather than developing each new SHM platform in isolation, future prototypes could adopt standardized hardware and software interfaces that allow plug-and-play integration with the central device. For instance, the proposed PSN and the ZigBee-based SHM systems could communicate with the same hub if designed to include two communication protocols (Bluetooth LE and ZigBee), thereby removing the need to implement an entirely new hardware and software development. Each development essentially becomes a targeted contribution to the overarching SHM framework, minimizing duplication of effort and promoting robust interactions amongst diverse sensing nodes.

Moreover, the framework would promote end-to-end coverage of the entire SHM cycle. Components for DAQ, wireless communication, and GUI would be developed and enhanced as part of an ecosystem. This not only simplifies the design process and shortens the path from concept to deployment, but also ensures consistent performance metrics across all system elements. By structuring the system architecture in this aspect, individual research contributions, whether introducing new sensors or improving energy-efficiency strategies, would directly strengthen the comprehensive ecosystem.

Ultimately, the establishment of a unified and flexible ecosystem is essential to achieve the long-term vision of a fully integrated, lightweight, and easy-to-deploy SHM environment for composite aerostructures. Adopting this strategy will enable scalability, reduce repetitive design work, and enable the community to collectively drive innovation in wireless SHM systems for the aerospace industry.

A second promising direction for future work is the integration of energy harvesting techniques, which are of particular interest for wireless sensor nodes operating in remote or hard-to-access areas of an aircraft structure. Traditional battery-powered solutions inevitably face limitations with respect to operational lifetime and maintenance requirements, as batteries must either be replaced or recharged at regular intervals. In contrast, energy harvesting offers the potential to capture ambient energy, such as vibration, thermal gradients, or solar radiation, and convert it into electrical power for continuous operation.

For passive sensing in particular, energy harvesting aligns well with the relatively low power demands of event-triggered or low-frequency sampling processes. Passive sensing systems, which mainly detect and record occasional impact events, can remain in deep sleep mode for extended periods and wake only when critical thresholds are exceeded. As a result, such platforms could be powered largely by the energy harvested from structural vibrations or temperature variations. This is in opposition to systems that engage in active sensing, which typically drive high-frequency actuation signals and, therefore, require comparatively greater power resources.

Incorporating energy harvesting into future SHM platforms not only extends operational lifetime but also reduces difficulties associated with battery replacement or recharging. In addition, implementing harvested energy sources can support more widespread deployment of wireless sensor nodes in aerospace applications, enabling real-time coverage over large areas without causing significant weight penalties. By combining efficient power management strategies, ultra-low-power electronics, and carefully selected harvesting transducers, future SHM devices can become increasingly self-sustaining, enabling longer-term, autonomous monitoring of safety-critical composite structures.

7.2 List of Publications

The research presented in this thesis has led to the following journal and conference publications:

1. Published:

    - Fatih Dagsever, Zahra Sharif Khodaei, M. H. Aliabadi. Development of a cyber-physical SHM system for composite structures. AIP Conf. Proc. 12 June 2023, 2848 (1): 020048.
    - Fatih Dagsever, Zahra Sharif Khodaei, and M H Aliabadi. Miniaturized wireless sensor solution for passive sensing through Bluetooth LE. Smart Materials and Structures. 34(5):55029, 2025.

2. Under Review:

- Fatih Dagsever, Zahra Sharif Khodaei and M. H. Aliabadi. Multi-Sensor SHM System. Submitted to MDPI Sensors Journal.

References

[1] Mohammed Abdulkarem, Khairulmizam Samsudin, Fakhrul Zaman Rokhani, and Mohd Fadlee A Rasid. Wireless sensor network for structural health monitoring: A contemporary review of technologies, challenges, and future direction. *Structural Health Monitoring*, 19(3):693–735, 2020.

[2] Analog Devices. CN-0350: 12-Bit, 1 MSPS, Single-Supply, Two-Chip Data Acquisition System for Piezoelectric Sensors. Technical report, 2017.

[3] Bruno Ando, Salvatore Castorina, Salvatore Graziani, Danilo Greco, Mattia Manenti, and Antonio Pistorio. An Embedded Multi-Sensor Architecture for Applications in Structural Health Monitoring. In *2023 IEEE Sensors Applications Symposium, SAS 2023 - Proceedings*, pages 1–5. IEEE, 2023.

[4] Ali M. Ay and Ying Wang. Structural damage identification based on self-fitting ARMAX model and multi-sensor data fusion. *Structural Health Monitoring*, 13(4):445–460, 2014.

[5] Bengi Aygün and Vehbi Cagri Gungor. Wireless sensor networks for structure health monitoring: Recent advances and future research directions. *Sensor Review*, 31(3):261–276, 2011.

[6] Mohsen Azimi, Armin Dadras Eslamlou, and Gokhan Pekcan. Data-driven structural health monitoring and damage detection through deep learning: State-ofthe- art review. *Sensors (Switzerland)*, 20(10), 2020.

[7] António Barrias, Joan R. Casas, and Sergi Villalba. A review of distributed optical fiber sensors for civil engineering applications. *Sensors (Switzerland)*, 16(5), 2016.

[8] Dimitrios G. Bekas, Zahra Sharif-Khodaei, and M. H. Ferri Aliabadi. An innovative diagnostic film for structural health monitoring of metallic and composite structures. *Sensors*, 2018.

[9] Md Zakirul Alam Bhuiyan, Jiannong Cao, and Guojun Wang. Deploying wireless sensor networks with fault tolerance for structural health monitoring. *Proceedings - IEEE International Conference on Distributed Computing in Sensor Systems, DCOSS 2012*, pages 194–202, 2012.

[10] Bosch Sensortec. BME280 Datasheet, 2018.

[11] Bosch Sensortec. BMA400 Datasheet, 2023.

[12] Agnes A.R. Broer, Rinze Benedictus, and Dimitrios Zarouchas. The Need for Multi-Sensor Data Fusion in Structural Health Monitoring of Composite Aircraft Structures. *Aerospace*, 9(4):1–26, 2022.

[13] Viechtbauer C., Schröder K.-U., and Schagerl M. Structural Health Control - A comprehensive concept for observation and assessment of damages applied on a Darrieus wind turbine. In *9th International Workshop on Structural Health Monitoring: A Roadmap to Intelligent Structures, IWSHM 2013*, pages 2431 – 2439, Stanford, CA, USA, 2013.

[14] Lorenzo Capineri and Andrea Bulletti. Ultrasonic guided-waves sensors and integrated structural health monitoring systems for impact detection and localization: A review. *Sensors*, 2021.

[15] Peter C. Chang, Alison Flatau, and S. C. Liu. Review Paper: Health Monitoring of Civil Infrastructure. *Structural Health Monitoring*, 2(3):257–67, 2003.

[16] M. Choi and B. Sweetman. Efficient calculation of statistical moments for structural health monitoring. *Structural Health Monitoring*, 9(1):13–24, 2010.

[17] Mario Collotta and Giovanni Pau. A solution based on bluetooth low energy for smart home energy management. *Energies*, 8(10):11916–11938, 2015.

[18] M J Cunningham and G L Bibby. Electrical Measurement. In *Electrical Engineer's Reference Book*, chapter 11, pages 11–1. Elsevier Ltd, 16th edition, 2003.

[19] Fatih Dagsever, Zahra Sharif Khodaei, and M. H. Aliabadi. Development of a cyber-physical SHM system for composite structures. *AIP Conference Proceedings*, 2848(1):20048, 2023.

[20] Swagato Das, P. Saha, and S. K. Patro. Vibration-based damage detection techniques used for health monitoring of structures: a review. *Journal of Civil Structural Health Monitoring*, 6(3):477–507, 2016.

[21] Sylvie Delepine-Lesoille, Jean Marie Henault, Gautier Moreau, Sylvain Blairon, Jean Salin, Jean Robert Courivaud, Frédéric Taillade, Erick Merliot, Jean Philippe Dubois, Johan Bertrand, Stéphane Buschaert, and Stefan Mayer. Truly distributed optical fiber sensors for structural health monitoring: From the telecommunication optical fiber drawling tower to water leakage detection in dikes and concrete structure strain monitoring. *Advances in Civil Engineering*, 2010.

[22] Sean Detwiler, Erik Barbosa, Kristen Steudel, Jeffery Tippmann, Christian Ward, and Brian West. Multi-Sensor Collaborative Sampling Schemes to Reconstruct Undersampled Mechanical System Signals for Machinery Fault Detection. In *A Conference and Exposition on Structural Dynamics*, pages 51–60, 2023.

[23] K. Diamanti and C. Soutis. Structural health monitoring techniques for aircraft composite structures. *Progress in Aerospace Sciences*, 46(8):342–352, 2010.

[24] DIGI Company. XBee ZigBee Mesh Kit User Guide, 2015.

[25] Digi International Inc. Digi XBee 3 ZigBee User Guide, 2020.

[26] Joshua F. Ensworth and Matthew S. Reynolds. BLE-Backscatter: Ultralow-Power IoT Nodes Compatible with Bluetooth 4.0 Low Energy (BLE) Smartphones and Tablets. *IEEE Transactions on Microwave Theory and Techniques*, 65(9):3360–3368, 2017.

[27] K. M. Farinholt, G. Park, and C. R. Farrar. Energy harvesting and wireless energy transmission for powering SHM sensor nodes. *Structural Health Monitoring*, 1(3):894–900, 2009.

[28] Charles R. Farrar and Keith Worden. *Structural Health Monitoring: A Machine Learning Perspective*. John Wiley and Sons, 11 2012.

[29] Federal Aviation Administration (FAA). FAA AC 20-184: Guidance on Testing and Installation of Rechargeable Lithium Batteries and Battery Systems on Aircraft, 2015.

[30] Federal Aviation Administration (FAA). FAA AC 91.21-1D: Use of Portable Electronic Devices Aboard Aircraft, 2017.

[31] Qian Feng and Yabin Liang. Development of piezoelectric-based technology for application in civil structural health monitoring. *Earthquake Research Advances*, 3(2):100154, 2023.

[32] Eric B. Flynn and Michael D. Todd. A Bayesian approach to optimal sensor placement for structural health monitoring with application to active sensing. *Mechanical Systems and Signal Processing*, 24(4):891–903, 2010.

[33] Ada Fort, Elia Landi, Marco Mugnaini, Lorenzo Parri, and Valerio Vignoli. Performance Evaluation of an IoT Sensor Node for Health Monitoring of Artwork and Ancient Wooden Structures. *Sensors*, 22(24), 2022.

[34] Hailing Fu, Zahra Sharif-Khodaei, and M. H. Ferri Aliabadi. An energy-efficient cyber-physical system for wireless on-board aircraft structural health monitoring. *Mechanical Systems and Signal Processing*, 128:352–368, 2019.

[35] Hailing Fu, Zahra Sharif Khodaei, and M. H. Ferri Aliabadi. An Event-Triggered Energy-Efficient Wireless Structural Health Monitoring System for Impact Detection in Composite Airframes. *IEEE Internet of Things Journal*, 6(1):1183–1192, 2019.

[36] M. Ghajari, Z. Sharif-Khodaei, M. H. Aliabadi, and A. Apicella. Identification of impact force for smart composite stiffened panels. *Smart Materials and Structures*, 22(8), 2013.

[37] Victor Giurgiutiu. *Structural Health Monitoring with Piezoelectric Wafer Active Sensors*. Elsevier, second edition, 2014.

[38] Carles Gomez, Joaquim Oller, and Josep Paradells. Overview and Evaluation of Bluetooth Low Energy: An Emerging Low-Power Wireless Technology. *Sensors*, 12(9), 2012.

[39] Rahim Gorgin, Ying Luo, and Zhanjun Wu. Environmental and operational conditions effects on Lamb wave based structural health monitoring systems: A review. *Ultrasonics*, 105(November 2019):106114, 2020.

[40] Jayavardhana Gubbi, Rajkumar Buyya, Slaven Marusic, and Marimuthu Palaniswami. Internet of Things (IoT): A vision, architectural elements, and future directions. *Future Generation Computer Systems*, 29(7):1645–1660, 2013.

[41] T. Harms, B. Banks, S. Sedigh Sarvestani, and F. Bastianini. Design and testing of a low-power wireless sensor network for structural health monitoring of bridges. In *Sensors and Smart Structures Technologies for Civil, Mechanical, and Aerospace Systems 2009*, San Diego, California, United States, 2009.

[42] Sahar Hassani and Ulrike Dackermann. A Systematic Review of Optimization Algorithms for Structural Health Monitoring and Optimal Sensor Placement. *Sensors*, 23(6), 2023.

[43] Mengyue He, Karthik Ram Ramakrishnan, Yishou Wang, Zhifang Zhang, and Jiyang Fu. A combined global-local approach for delamination assessment of composites using vibrational frequencies and FBGs. *Mechanical Systems and Signal Processing*, 167(PB):108577, 2022.

[44] Jilin Hou, Łukasz Jankowski, and Jinping Ou. Structural health monitoring based on combined structural global and local frequencies. *Mathematical Problems in Engineering*, 2014, 2014.

[45] Qingqing Huang, Baoping Tang, and Lei Deng. Development of high synchronous acquisition accuracy wireless sensor network for machine vibration monitoring. *Measurement: Journal of the International Measurement Confederation*, 66:35–44, 2015.

[46] Linsheng Huo, Hao Cheng, Qingzhao Kong, and Xuemin Chen. Bond-slip monitoring of concrete structures using smart sensors—A review. *Sensors (Switzerland)*, 19(5), 2019.

[47] Jeong Beom Ihn and Fu Kuo Chang. Pitch-catch active sensing methods in structural health monitoring for aircraft structures. *Structural Health Monitoring*, 7(1):5–19, 2008.

[48] Devaka Jayawardana, Ranjith Liyanapathirana, and Xinqun Zhu. RFID-Based Wireless Multi-Sensory System for Simultaneous Dynamic Acceleration and Strain Measurements of Civil Infrastructure. *IEEE Sensors Journal*, 19(24):12389–12397, 2019.

[49] Shao Fei Jiang, Chun Ming Zhang, and C. G. Koh. Structural damage detection by integrating data fusion and probabilistic neural network. *Advances in Structural Engineering*, 9(4):445–457, 2006.

[50] Ayoub Keshmiry, Sahar Hassani, Mohsen Mousavi, and Ulrike Dackermann. Effects of Environmental and Operational Conditions on Structural Health Monitoring and Non-Destructive Testing: A Systematic Review. *Buildings*, 13(4), 2023.

[51] Seth S Kessler, S Mark Spearing, and Constantinos Soutis. Damage Detection in Composite Materials Using Lamb Wave Methods. *Smart Materials and Structures*, 11(2):269, 2002.

[52] Z. Sharif Khodaei and M. H. Ferri Aliabadi. Impact detection and identification with piezoceramic sensors: Passive sensing. *Structural Health Monitoring for Advanced Composite Structures*, pages 215–265, 2017.

[53] Junhee Kim and Jerome P. Lynch. Autonomous Decentralized System Identification by Markov Parameter Estimation Using Distributed Smart Wireless Sensor Networks. *Journal of Engineering Mechanics*, 138(5):478–490, 2012.

[54] Sukun Kim, Shamim Pakzad, David Culler, James Demmel, Gregory Fenves, Steven Glaser, and Martin Turon. Health monitoring of civil infrastructures using wireless sensor networks. *IPSN 2007: Proceedings of the Sixth International Symposium on Information Processing in Sensor Networks*, pages 254–263, 2007.

[55] Y.J. Kim and L. Jofre. 3D microwave tomographic array for damage detection of civil structures. *IEEE Transactions on Antennas and Propagation*, 51(11):3022–32, 2003.

[56] J. M. Ko and Y. Q. Ni. Technology developments in structural health monitoring of large-scale bridges. *Engineering Structures*, 27(12 SPEC. ISS.):1715–1725, 2005.

[57] Christoph Kralovec and Martin Schagerl. Review of structural health monitoring methods regarding a multi-sensor approach for damage assessment of metal and composite structures. *Sensors (Switzerland)*, 20(3):1–25, 2020.

[58] Capineri L., Bulletti A., Calzolai M., and Francesconi D. A real-time electronic system for automated impact detection on aircraft structures using piezoelectric transducers. In *28th European Conference on Solid-State Transducers, EUROSENSORS 2014*, pages 1243–46, Brescia, 2014. Procedia Engineering.

[59] Huy Viet Le, Tae Uk Kim, Suleman Khan, Jun Young Park, Jong Woong Park, Seung Eock Kim, Jang Yun, and Dong Joo Kim. Development of low-cost wireless sensing system for smart ultra-high performance concrete. *Sensors*, 21(19):1–20, 2021.

[60] Yann Lecieux, Emmanuel Rozière, Virginie Gaillard, Cyril Lupi, Dominique Leduc, Johann Priou, Romain Guyard, Mathilde Chevreuil, and Franck Schoefs. Monitoring of a reinforced concrete wharf using structural health monitoring system and material testing. *Journal of Marine Science and Engineering*, 7(4):1–26, 2019.

[61] Akos Ledeczi, Peter Völgyesi, Eric Barth, Andras Nadas, Alexander Pedchenko, Thomas Hay, and Subash Jayaraman. Self-sustaining Wireless Acoustic Emission Sensor System for Bridge Monitoring. In *New Developments in Sensing Technology for Structural Health Monitoring*, pages 15–39. Springer, 2011.

[62] Jian Li, Kirill A. Mechitov, Robin E. Kim, and Billie F. Spencer. Efficient time synchronization for structural health monitoring using wireless smart sensor networks. *Structural Control and Health Monitoring*, 23(3):470 – 486, 2016.

[63] Jing Lin, Fei Gao, Zhi Luo, and Liang Zeng. High-Resolution Lamb Wave Inspection in Viscoelastic Composite Laminates. *IEEE Transactions on Industrial Electronics*, 63(11):6989–6998, 2016.

[64] José Miguel López-Higuera, Luis Rodriguez Cobo, Antonio Quintela Incera, and Adolfo Cobo. Fiber optic sensors in structural health monitoring. *Journal of Lightwave Technology*, 29(4):587–608, 2011.

[65] Gaël Loubet, Alassane Sidibe, Alexandru Takacs, and Daniela Dragomirescu. Battery-Free Bluetooth Low Energy Sensing Nodes for Structural Health Monitoring of Concretes. In *Structural Health Monitoring 2021: Enabling Next-Generation SHM for Cyber-Physical Systems - Proceedings of the 13th International Workshop on Structural Health Monitoring, IWSHM 2021*, pages 117–124, 2021.

[66] Guangtao Lu, Yourong Li, Tao Wang, Han Xiao, Linsheng Huo, and Gangbing Song. A multi-delay-and-sum imaging algorithm for damage detection using piezoceramic transducers. *Journal of Intelligent Material Systems and Structures*, 28(9):1150–1159, 2017.

[67] Jerome Peter Lynch. *Decentralization of wireless monitoring and control technologies for smart civil structures*. PhD thesis, Stanford University, Stanford, CA., 2002.

[68] Jerome Peter Lynch. An overview of wireless structural health monitoring for civil structures. *Royal Society of London Transactions Series A*, 365(1851):345–72, 2006.

[69] Fatemeh Mansourkiaie, Loay Sabry Ismail, Tarek Mohamed Elfouly, and Mohamed H. Ahmed. Maximizing Lifetime in Wireless Sensor Network for Structural Health Monitoring with and Without Energy Harvesting. *IEEE Access*, 5:2383–2395, 2017.

[70] David D.L. Mascarenas, Eric B. Flynn, Michael D. Todd, Timothy G. Overly, Kevin M. Farinholt, Gyuhae Park, and Charles R. Farrar. Development of capacitance-based and impedance-based wireless sensors and sensor nodes for structural health monitoring applications. *Journal of Sound and Vibration*, 329(12):2410–2420, 2010.

[71] Lykomidis Mastroleon, Anne S. Kiremidjian, Ed Carryer, and Kincho Law. Design of A New Power-Efficient Wireless Sensor System for Structural Health Monitoring. In *Nondestructive Detection and Measurement for Homeland Security II*, volume 5395, pages 51–60, 2004.

[72] Maxim Integrated. Datasheet of MAX11129-MAX11132.

[73] Hanfei Mei, Mohammad Faisal Haider, Roshan Joseph, Asaad Migot, and Victor Giurgiutiu. Recent advances in piezoelectric wafer active sensors for structural health monitoring applications. *Sensors (Switzerland)*, 2019.

[74] Mohammed Moness and Ahmed Mahmoud Moustafa. A Survey of Cyber-Physical Advances and Challenges of Wind Energy Conversion Systems: Prospects for Internet of Energy. *IEEE Internet of Things Journal*, 3(2):134–145, 2016.

[75] V. M. Murukeshan, P. Y. Chan, L. S. Ong, and L. K. Seah. Cure monitoring of smart composites using Fiber Bragg Grating based embedded sensors. *Sensors and Actuators, A: Physical*, 79(2):153–161, 2000.

[76] Samir Mustapha, Ye Lu, Ching Tai Ng, and Pawel Malinowski. Sensor Networks for Structures Health Monitoring: Placement, Implementations, and Challenges—A Review. *Vibration*, 4(3):551–585, 2021.

[77] Adam B. Noel, Mohamed Hossam Ahmed, Ahmed Badawy, and Mohamed S. Shehata. Structural health monitoring using wireless sensor networks: A Comprehensive Survey. *IEEE Communications Surveys and Tutorials*, 19(3):1403–1423, 2017.

[78] Gyuhae Park, Charles R. Farrar, Francesco Lanza Di Scalea, and Stefano Coccia. Performance assessment and validation of piezoelectric active-sensors in structural health monitoring. *Smart Materials and Structures*, 15(6):1673–1683, 2006.

[79] Xinlin P. Qing, Shawn J. Beard, Amrita Kumar, Teng K. Ooi, and Fu Kuo Chang. Built-in sensor network for structural health monitoring of composite structure. *Journal of Intelligent Material Systems and Structures*, 18(1):39–49, 2007.

[80] Anders Rytter. *Vibrational Based Inspection of Civil Engineering Structures*. PhD thesis, Aalborg University, 1993.

[81] O. S. Salawu. Detection of structural damage through changes in frequency: A review. *Engineering Structures*, 19(9):718–723, 1997.

[82] Raffaella Di Sante. Fibre Optic Sensors for Structural Health Monitoring of Aircraft Composite Structures: Recent Advances and Applications. *Sensors*, 15:18666–18713, 2015.

[83] João P. Santos, André D. Orcesi, Christian Crémona, and Paulo Silveira. Baseline-free real-time assessment of structural changes. *Structure and Infrastructure Engineering*, 11(2):145–161, 2015.

[84] Edward Sazonov, Vidya Krishnamurthy, and Robert Schilling. Wireless intelligent sensor and actuator network - A scalable platform for time-synchronous applications of structural health monitoring. *Structural Health Monitoring*, 9(5):465–476, 2010.

[85] Aldyandra Hami Seno and M H Ferri Aliabadi. A novel method for impact force estimation in composite plates under simulated environmental and operational conditions. *Smart Materials and Structures*, 29(11):115029, 2020.

[86] Aldyandra Hami Seno, Zahra Sharif Khodaei, and M. H.Ferri Aliabadi. Passive sensing method for impact localisation in composite plates under simulated environmental and operational conditions. *Mechanical Systems and Signal Processing*, 129:20–36, 2019.

[87] Rama Shanker, Suresh Bhalla, and Ashok Gupta. Integration of electro-mechanical impedance and global dynamic techniques for improved structural health monitoring. *Journal of Intelligent Material Systems and Structures*, 21(3):285–295, 2010.

[88] Z. Sharif-Khodaei, M. Ghajari, and M. H. Aliabadi. Determination of impact location on composite stiffened panels. *Smart Materials and Structures*, 21(10), 2012.

[89] Alassane Sidibe, Gaël Loubet, Alexandru Takacs, and Daniela Dragomirescu. A Multi-functional Battery-Free Bluetooth Low Energy Wireless Sensor Node Remotely Powered by Electromagnetic Wireless Power Transfer in Far-Field. *Sensors*, 22(11), 2022.

[90] Divya Sinha, Kavish Doshi, and M. Rajasekhara Babu. An efficient approach to civil structures health monitoring using fog computing as clusters through 5G network environment. *Advances in Systems Science and Applications*, 18(3):123–144, 2018.

[91] Joel Smithard, Nik Rajic, Stephen van der Velden, Patrick Norman, Cedric Rosalie, Steve Galea, Hanfei Mei, Bin Lin, and Victor Giurgiutiu. An advanced multi-sensor acousto-ultrasonic structural health monitoring system Development and aerospace demonstration. *Materials*, 10(7):832, 2017.

[92] A. Sofi, J. Jane Regita, Bhagyesh Rane, and Hieng Ho Lau. Structural health monitoring using wireless smart sensor network – An overview. *Mechanical Systems and Signal Processing*, 163(April 2021):108113, 2022.

[93] G. Song, H. Gu, Y. L. Mo, T. T.C. Hsu, and H. Dhonde. Concrete structural health monitoring using embedded piezoceramic transducers. *Smart Materials and Structures*, 16(4):959–968, 2007.

[94] STMicroelectronics. STM32L476ZE Ultra-low-power with FPU Arm Cortex-M4 MCU 80 MHz with 512 Kbytes of Flash memory, LCD, USB OTG, DFSDM, 2019.

[95] R Andrew Swartz, Deokwoo Jung, Jerome P Lynch, Yang Wang, Dan Shi, and Michael P Flynn. Design of a wireless sensor for scalable distributed in-network computation in a structural health monitoring system. In *Proceedings of the 5th International Workshop on Structural Health Monitoring*, Stanford, CA, USA, 2005.

[96] Iuliana Tabian, Hailing Fu, and Zahra Sharif Khodaei. A convolutional neural network for impact detection and characterization of complex composite structures. *Sensors (Switzerland)*, 19(22):1–25, 2019.

[97] C. Jr. Arcadius Tokognon, Bin Gao, Gui Yun Tian, and Yan Yan. Structural Health Monitoring Framework Based on Internet of Things: A Survey. *IEEE INTERNET OF THINGS JOURNAL*, 4(3):619–635, 2017.

[98] Jacopo Tosi, Fabrizio Taffoni, Marco Santacatterina, Roberto Sannino, and Domenico Formica. Performance evaluation of bluetooth low energy: A systematic review. *Sensors (Switzerland)*, 17(12):1–34, 2017.

[99] U-blox. ANNA-B4 Series System Integration Manual, 2022.

[100] U-blox. ANNA-B402 Datasheet, 2022.

[101] U-blox. ANNA-B402 module Product Summary, 2022.

[102] Chun H. Wang, James T. Rose, and Fu Kuo Chang. A synthetic time-reversal imaging method for structural health monitoring. *Smart Materials and Structures*, 13(2):415–423, 2004.

[103] Furui Wang, Linsheng Huo, and Gangbing Song. A piezoelectric active sensing method for quantitative monitoring of bolt loosening using energy dissipation caused by tangential damping based on the fractal contact theory. *Smart Materials and Structures*, 27(1), 2018.

[104] Yang Wang, Jerome P. Lynch, and Kincho H. Law. A wireless structural health monitoring system with multithreaded sensing devices: Design and validation. *Structure and Infrastructure Engineering*, 3(2):103–120, 2007.

[105] G. T. Webb, P. J. Vardanega, and C. R. Middleton. Categories of SHM Deployments: Technologies and Capabilities. *Journal of Bridge Engineering*, 20(11), 2015.

[106] K. Worden, G. Manson, and D. Allman. EXPERIMENTAL VALIDATION OF A STRUCTURAL HEALTH MONITORING METHODOLOGY: PART I. NOVELTY DETECTION ON A LABORATORY STRUCTURE. *Journal of Sound and VibrationVibration*, 259(2):323–343, 2003.

[107] Haiqing Yao, Heng Cao, and Jin Li. Design and Implementation of a Portable Wireless System for Structural Health Monitoring. *Measurement and Control (United Kingdom)*, 49(1):23–32, 2016.

[108] Jae Yoon, David He, and Brandon Van Hecke. On the Use of a Single Piezoelectric Strain Sensor for Wind Turbine Planetary Gearbox Fault Diagnosis. *IEEE Transactions on Industrial Electronics*, 62(10):6585–6593, 2015.

[109] Haofan Yu, Aldyandra Hami Seno, Zahra Sharif Khodaei, and M. H.Ferri Aliabadi. Structural Health Monitoring Impact Classification Method Based on Bayesian Neural Network. *Polymers*, 14(19), 2022.

[110] Quanpeng Yu, Shiyuan Zhou, Yuhan Cheng, and Yao Deng. Research on Delamination Damage Quantification Detection of CFRP Bending Plate Based on Lamb Wave Mode Control. *Sensors*, 24(6), 2024.

[111] Liang Zeng, Jing Lin, and Liping Huang. A modified lamb wave time-reversal method for health monitoring of composite structures. *Sensors (Switzerland)*, 17(5):1–15, 2017.

[112] Jicheng Zhang, Yongshui Huang, and Yu Zheng. A feasibility study on timber damage detection using piezoceramic-transducer-enabled active sensing. *Sensors (Switzerland)*, 18(5), 2018.

[113] Xiaoliang Zhao, Huidong Gao, Guangfan Zhang, Bulent Ayhan, Fei Yan, Chiman Kwan, and Joseph L. Rose. Active health monitoring of an aircraft wing with embedded piezoelectric sensor/actuator network: I. Defect detection, localization and growth monitoring. *Smart Materials and Structures*, 16(4):1208–1217, 2007.

[114] Yongteng Zhong, Jiawei Xiang, Xiaoyu Chen, Yongying Jiang, and Jihong Pang. Multiple signal classification-based impact localization in composite structures using optimized ensemble empirical mode decomposition. *Applied Sciences (Switzerland)*, 8(9), 2018.

[115] Li Zhu, Yuguang Fu, Raymond Chow, Billie F. Spencer, Jong Woong Park, and Kirill Mechitov. Development of a high-sensitivity wireless accelerometer for structural health monitoring. *Sensors (Switzerland)*, 18(1):1–16, 2018.

Appendix A

Reproducing Permissions

CCC Marketplace

This is a License Agreement between Fatih Dagsever ("User") and Copyright Clearance Center, Inc. ("CCC") on behalf of the Rightsholder identified in the order details below. The license consists of the order details, the Marketplace Permissions General Terms and Conditions below, and any Rightsholder Terms and Conditions which are included below.

All payments must be made in full to CCC in accordance with the Marketplace Permissions General Terms and Conditions below.

Order Date	11-Feb-2025	**Type of Use**	Republish in a thesis/dissertation
Order License ID	1577394-1		
ISSN	0888-3270	**Publisher**	ACADEMIC PRESS
		Portion	Image/photo/illustration

LICENSED CONTENT

Publication Title	Mechanical systems and signal processing	**Rightsholder**	Elsevier Science & Technology Journals
Article Title	An energy-efficient cyber-physical system for wireless on-board aircraft structural health monitoring	**Publication Type**	Journal
		Start Page	352
		End Page	368
		Volume	128
Date	01/01/1987		
Language	English		
Country	United Kingdom of Great Britain and Northern Ireland		

REQUEST DETAILS

Portion Type	Image/photo/illustration	**Distribution**	Worldwide
Number of Images / Photos / Illustrations	1	**Translation**	Original language of publication
Format (select all that apply)	Electronic	**Copies for the Disabled?**	No
		Minor Editing Privileges?	No
Who Will Republish the Content?	Academic institution	**Incidental Promotional Use?**	No
Duration of Use	Life of current edition	**Currency**	GBP
Lifetime Unit Quantity	Up to 499		
Rights Requested	Main product		

NEW WORK DETAILS

Title	Miniaturized IoT-based Systems for Structural Integrity and Health Monitoring	**Institution Name**	Imperial College London
		Expected Presentation Date	2025-04-01
Instructor Name	Fatih Dagsever		

ADDITIONAL DETAILS

Order Reference Number	N/A	**The Requesting Person / Organization to Appear on the License**	Fatih Dagsever

Figure A.1: Reproducing permission 1

CCC Marketplace

This is a License Agreement between Fatih Dagsever ("User") and Copyright Clearance Center, Inc. ("CCC") on behalf of the Rightsholder identified in the order details below. The license consists of the order details, the Marketplace Permissions General Terms and Conditions below, and any Rightsholder Terms and Conditions which are included below.

All payments must be made in full to CCC in accordance with the Marketplace Permissions General Terms and Conditions below.

Order Date	15-Feb-2025	**Type of Use**	Republish in a thesis/dissertation
Order License ID	1578752-1		
ISSN	1741-3168	**Publisher**	SAGE PUBLICATIONS LTD
		Portion	Image/photo/illustration

LICENSED CONTENT

Publication Title	Structural health monitoring	**Publication Type**	e-Journal
		Start Page	465
Article Title	Wireless Intelligent Sensor and Actuator Network - A Scalable Platform for Time-synchronous Applications of Structural Health Monitoring	**End Page**	476
		Issue	5
		Volume	9
		URL	http://firstsearch.oclc.org
Date	01/01/2002		
Language	English		
Country	United Kingdom of Great Britain and Northern Ireland		
Rightsholder	SAGE Publications Ltd. Journals		

REQUEST DETAILS

Portion Type	Image/photo/illustration	**Distribution**	Worldwide
Number of Images / Photos / Illustrations	1	**Translation**	Original language of publication
Format (select all that apply)	Electronic	**Copies for the Disabled?**	No
		Minor Editing Privileges?	No
Who Will Republish the Content?	Academic institution	**Incidental Promotional Use?**	No
Duration of Use	Life of current edition	**Currency**	GBP
Lifetime Unit Quantity	Up to 499		
Rights Requested	Main product		

NEW WORK DETAILS

Title	Miniaturized IoT-based Systems for Structural Integrity and Health Monitoring	**Institution Name**	Imperial College London
		Expected Presentation Date	2025-04-01
Instructor Name	Fatih Dagsever		

ADDITIONAL DETAILS

Figure A.2: Reproducing permission 2

Marketplace

This is a License Agreement between Fatih Dagsever ("User") and Copyright Clearance Center, Inc. ("CCC") on behalf of the Rightsholder identified in the order details below. The license consists of the order details, the Marketplace Permissions General Terms and Conditions below, and any Rightsholder Terms and Conditions which are included below.

All payments must be made in full to CCC in accordance with the Marketplace Permissions General Terms and Conditions below.

Order Date	12-Feb-2025	Type of Use	Republish in a thesis/dissertation
Order License ID	1577615-1	Publisher	American Society of Civil Engineers
ISSN	1943-7889	Portion	Image/photo/illustration

LICENSED CONTENT

Publication Title	Journal of Energy Engineering : Mechanics	Publication Type	e-Journal
Article Title	Autonomous Decentralized System Identification by Markov Parameter Estimation Using Distributed Smart Wireless Sensor Networks	Start Page	478
		End Page	490
		Issue	5
		Volume	138
		URL	http://www.intute.ac.uk/sciences/cgi-bin/fullrecord.pl?handle=agnes.933257385
Author / Editor	American Society of Civil Engineers.		
Date	01/01/1983		
Language	English		
Country	United States of America		
Rightsholder	American Society of Civil Engineers		

REQUEST DETAILS

Portion Type	Image/photo/illustration	Distribution	Worldwide
Number of Images / Photos / Illustrations	1	Translation	Original language of publication
Format (select all that apply)	Electronic	Copies for the Disabled?	No
		Minor Editing Privileges?	No
Who Will Republish the Content?	Academic institution	Incidental Promotional Use?	No
Duration of Use	Life of current edition	Currency	GBP
Lifetime Unit Quantity	Up to 499		
Rights Requested	Main product		

NEW WORK DETAILS

Title	Miniaturized IoT-based Systems for Structural Integrity and Health Monitoring	Institution Name	Imperial College London
		Expected Presentation Date	2025-04-01
Instructor Name	Fatih Dagsever		

ADDITIONAL DETAILS

Figure A.3: Reproducing permission 3

Marketplace

This is a License Agreement between Fatih Dagsever ("User") and Copyright Clearance Center, Inc. ("CCC") on behalf of the Rightsholder identified in the order details below. The license consists of the order details, the Marketplace Permissions General Terms and Conditions below, and any Rightsholder Terms and Conditions which are included below.

All payments must be made in full to CCC in accordance with the Marketplace Permissions General Terms and Conditions below.

Order Date	12-Feb-2025	**Type of Use**	Republish in a thesis/dissertation
Order License ID	1577657-1		
ISSN	0263-2241	**Publisher**	ELSEVIER BV
		Portion	Image/photo/illustration

LICENSED CONTENT

Publication Title	Measurement : journal of the International Measurement Confederation	**Rightsholder**	Elsevier Science & Technology Journals
		Publication Type	Journal
Article Title	Development of high synchronous acquisition accuracy wireless sensor network for machine vibration monitoring	**Start Page**	35
		End Page	44
		Volume	66
Author / Editor	INTERNATIONAL MEASUREMENT CONFEDERATION., INSTITUTE OF MEASUREMENT AND CONTROL.		
Date	01/01/1983		
Language	Dutch		
Country	Netherlands		

REQUEST DETAILS

Portion Type	Image/photo/illustration	**Distribution**	Worldwide
Number of Images / Photos / Illustrations	1	**Translation**	Original language of publication
Format (select all that apply)	Electronic	**Copies for the Disabled?**	No
		Minor Editing Privileges?	No
Who Will Republish the Content?	Academic institution	**Incidental Promotional Use?**	No
Duration of Use	Life of current edition	**Currency**	GBP
Lifetime Unit Quantity	Up to 499		
Rights Requested	Main product		

NEW WORK DETAILS

Title	Miniaturized IoT-based Systems for Structural Integrity and Health Monitoring	**Institution Name**	Imperial College London
		Expected Presentation Date	2025-04-01
Instructor Name	Fatih Dagsever		

Figure A.4: Reproducing permission 4

Marketplace

This is a License Agreement between Fatih Dagsever ("User") and Copyright Clearance Center, Inc. ("CCC") on behalf of the Rightsholder identified in the order details below. The license consists of the order details, the Marketplace Permissions General Terms and Conditions below, and any Rightsholder Terms and Conditions which are included below.

All payments must be made in full to CCC in accordance with the Marketplace Permissions General Terms and Conditions below.

Order Date	12-Feb-2025	Type of Use	Republish in a thesis/dissertation
Order License ID	1577661-1		
ISSN	1876-1100	Publisher	Springer Netherlands
		Portion	Image/photo/illustration

LICENSED CONTENT

Publication Title	Lecture notes in electrical engineering	Rightsholder	Springer Nature BV
		Publication Type	Monographic Series
Article Title	Self-sustaining wireless acoustic emission sensor system for bridge monitoring	Start Page	15
		End Page	39
		Volume	96
Date	01/01/2008		
Language	English		
Country	Netherlands		

REQUEST DETAILS

Portion Type	Image/photo/illustration	Distribution	Worldwide
Number of Images / Photos / Illustrations	1	Translation	Original language of publication
Format (select all that apply)	Electronic	Copies for the Disabled?	No
		Minor Editing Privileges?	No
Who Will Republish the Content?	Academic institution	Incidental Promotional Use?	No
Duration of Use	Life of current edition	Currency	GBP
Lifetime Unit Quantity	Up to 499		
Rights Requested	Main product		

NEW WORK DETAILS

Title	Miniaturized IoT-based Systems for Structural Integrity and Health Monitoring	Institution Name	Imperial College London
		Expected Presentation Date	2025-04-01
Instructor Name	Fatih Dagsever		

ADDITIONAL DETAILS

The Requesting Person / Organization to Appear on the License	Fatih Dagsever

REQUESTED CONTENT DETAILS

Figure A.5: Reproducing permission 5